NOTICE

The quality of this microform is heavily dependent upon the quality of the original thesis submitted for microfilming. Every effort has been made to ensure the highest quality of reproduction possible.

If pages are missing, contact the university which granted the degree.

Some pages may have indistinct print especially if the original pages were typed with a poor typewriter ribbon or if the university sent us an inferior photocopy.

Reproduction in full or in part of this microform is governed by the Canadian Copyright Act, R.S.C. 1970, c. C-30, and subsequent amendments.

AVIS

La qualité de cette microforme dépend grandement de la qualité de la thèse soumise au microfilmage. Nous avons tout fait pour assurer une qualité supérieure de reproduction.

S'il manque des pages, veuillez communiquer avec l'université qui a conféré le grade.

La qualité d'impression de certaines pages peut laisser à désirer, surtout si les pages originales ont été dactylographiées à l'aide d'un ruban usé ou si l'université nous a fait parvenir une photocopie de qualité inférieure.

La reproduction, même partielle, de cette microforme est soumise à la Loi canadienne sur le droit d'auteur, SRC 1970, c. C-30, et ses amendements subséquents.

ISBN 0-315-55599-8

THE UNIVERSITY OF ALBERTA

Effects of Resin Shrinkage on Stresses in Fiberglass

by

Christina M. Boyko

A THESIS

SUBMITTED TO THE FACULTY OF GRADUATE STUDIES AND RESEARCH

IN PARTIAL FULFILMENT OF THE REQUIREMENTS FOR THE DEGREE

OF Master of Science

IN

Metallurgical Engineering

Department of Mining, Metallurgical and Petroleum

Engineering

EDMONTON, ALBERTA

Fall, 1989

THE UNIVERSITY OF ALBERTA

RELEASE FORM

NAME OF AUTHOR Christina M. Boyko

TITLE OF THESIS Effects of Resin Shrinkage on Stresses in Fiberglass

DEGREE FOR WHICH THESIS WAS PRESENTED Master of Science

YEAR THIS DEGREE GRANTED Fall, 1989

Permission is hereby granted to THE UNIVERSITY OF ALBERTA LIBRARY to reproduce single copies of this thesis and to lend or sell such copies for private, scholarly or scientific research purposes only.

The author reserves other publication rights, and neither the thesis nor extensive extracts from it may be printed or otherwise reproduced without the author's written permission.

(SIGNED) C.M. Boyko

PERMANENT ADDRESS:
10748 - 79 AVENUE
EDMONTON, ALBERTA
T6E - 1S3

DATED SEPTEMBER 29, 1989

THE UNIVERSITY OF ALBERTA

FACULTY OF GRADUATE STUDIES AND RESEARCH

The undersigned certify that they have read, and recommend to the Faculty of Graduate Studies and Research, for acceptance, a thesis entitled Effects of Resin Shrinkage on Stresses in Fiberglass submitted by Christina M. Boyko in partial fulfilment of the requirements for the degree of Master of Science in Metallurgical Engineering.

Reg Eadie
.....
Supervisor

L. Douglas Lloyd
.....

T. Lindsay
.....

John Vanderkooy
.....

Date..... Aug. 22, 1989

Abstract

Curing of fiberglass components involves processes during which the polyester matrix shrinks, both chemically and thermally, significantly more than the glass reinforcement or the mold. Early in the development of fiberglass, research efforts focussed on the discovery of coatings for the glass fibers which maintained the integrity of the glass-matrix interface in spite of this shrinkage.

The characterization of differential shrinkage and its effects has been a central problem in understanding composite materials. The present status of understanding this problem is reviewed in the thesis. Most of the literature is found to concentrate upon thermal shrinkage effects, which are of particular concern in aerospace applications. The role of chemical shrinkage has not been fully rationalized.

This thesis endeavors to investigate the magnitude of chemical shrinkage effects both analytically and experimentally. Such a study is particularly appropriate in fiberglass, where the polyester resin undergoes of the order of 9 v/o shrinkage during curing.

Computer codes for predicting the macro stresses caused by differential shrinkage were acquired or developed from the literature. Codes based on Classical Lamination Theory and more rigorous elasticity solutions are compared. The experimental work consisted of strain measurements on the

inside of aluminum mandrels over which fairly thick hoop-oriented fiberglass layers were filament wound and cured. Strain measurements were compared with "thermal analogy" predictions. In the thermal analogy, chemical shrinkage is simulated by removing the thermal shrinkage capacity of all parts of a composite except the resin. A temperature change consistent with a given amount of resin shrinkage is applied, and the response of the system is calculated.

As an additional exercise, a preliminary study of microstresses within a layer of fiberglass was attempted using the finite element program SAPIV. (Bathe et al., 1974) Results were compared with the results of photoelasticity studies presented in the literature.

The most signiticant finding of this investigation was that the large predicted macroscopic mandrel strains were not present. A number of possible explanations are considered. Crazing of the matrix, debonding of the aluminum and composite, and a macroscopic stress relief mechanism due to non-uniform curing are thought to be the most probable causes of the observed results. Suggestions for further confirming investigations are made.

Table of Contents

Chapter — Page

Abstract iv

List of Tables viii

List of Figures ix

Nomenclature xi

Glossary of Terms xiv

1. Introduction 1

1.1 Context of the Problem 2

1.2 Polymer-Based Composite Materials 7

2. Residual Stresses in Polymeric Composites 12

2.1 Micromechanical Analysis of Residual Stresses 12

2.2 Macromechanical Treatment of Residual Stresses 25

2.2.1 Classical Lamination Theory 25

2.2.2 Elasticity Approach 37

2.3 The Importance of Moisture Effects 42

3. Experimental Work 43

3.1 Neat Resin Curing Shrinkage: Archimedean Density Tests 51

3.2 Micromechanical Analysis of Curing Shrinkage Using the Finite Element Method 64

3.3 Macro Shrinkage Analysis: Strain Gaging Experiments 81

3.4 Discussion and Conclusions 108

3.5 Recommendations 118

Bibliography 123

Appendix A: Classical Lamination Theory 128

Appendix B: The Importance of Moisture Effects 131

Appendix C: Finite Element Analysis Data Files and SAPIV Outputs 136

Appendix D: Thermal Analogy Program Descriptions, Listings, and Outputs 221

Appendix E: Application of Strain Gages to an Aluminum Mandrel 258

Appendix F: Strain Calculations 261

Appendix G: Burn-off Tests and Resin Density Measurements 263

Appendix H: The Technique of Impulse Viscoelasticity for Characterizing Mechanical Properties and Time-Dependent Curing Behavior of Thermosetting Polymers 266

Appendix I: Material Properties 269

List of Tables

Table 1: Shrinkage Results Using Vibrin 1030.....61

Table 2: Thermal Analogy Strains at Inside of Mandrel.....83

Table 3: Thermally-Induced Strains at Inside of Mandrel.....84

Table 4: Thermal Analogy Strains Plus Thermally-Induced Strains.....85

Table 5: Strain Data for Filament-Wound Tubes 102

Table 6: Strain Data for 100% Polyester Tubes 103

Table 7: Resin Density Results 106

List of Figures

Figure 1: Temperature and Relative End Displacement Versus Time During Curing for a Polyester Resin Casting 2

Figure 2: Appearance of a Figerglass Pipe Containing Small Internal Cracks..... 5

Figure 3: Magnified View of a Single Crack in the Pipe Section of Figure 2..... 6

Figure 4: Schematic of the Interphase.....11

Figure 5: The Evolution of Longitudinal Residual Stresses Between Glass and Polyester 14

Figure 6: A Square Array of Fibers in Resin 18

Figure 7: Schematic Cure Cycles for Epoxy- and Polyester-Based Composites 24

Figure 8: Tensile Stress-Strain Curves 27

Figure 9: Schematic of Changes in Neat Polyester During Curing.....45

Figure 10: Anton-Paar Densitometer 54

Figure 11: Apparatus for Archimedean Density Tests 59

Figure 12: Apparent Mass Versus Time Curve for Neat Polyester Resin.....60

Figure 13: Geometric Details for Finite Element Analysis.....67

Figure 14: Discretized Finite Element Mesh 68

Figure 15: Free Shrinkage Displacement Profile of Edge 3.....75

Figure 16: Stresses Along Edge 1 for an Imposed Displacement of -0.1717×10^{-6} m Along Edge 3 76

Figure 17: Stresses Along Edge 2 for an Imposed Displacement of -0.1717×10^{-6} m Along Edge 3 77

Figure 18: Stresses in the Vicinity of the Fiber-Matrix Interface for an Imposed Displacement of -0.1717×10^{-6} m Along Edge 3 78

Figure 19: Tube Geometry for Thermal Analogy Runs 86

Figure 20: Hoop Winding Schematic 90

Figure 21: Experimental Filament-Winding Apparatus for Hoop-Wound Tubes.....92

Figure 22: Experiment 1: Hoop-Wound Tube, Chart Recorder, and Amplifier-Conditioner Unit.....93

Figure 23: Cardboard Enclosure of the Type Used for Neat Resin Tubes in Experiments 4 and 5..... 95

Figure 24: Experiments 2 - 5: Recorder, Amplifier-Conditioner Unit, and Furnace Used to Test Temperature Response of Instrumented Mandrels.....98

Figure 25: Strain and Temperature Versus Time for Experiment 1.....101

Figure 26: Strain and Temperature Versus Time for Experiment 4.....104

Figure 27: Cross-Sectional View of Polyester Resin Between Fibers.....110

Figure 28: Assumed Temperature Profile in Fiberglass Tube Wall.....115

Nomenclature

1. Symbols

[A] or A	extensional stiffness matrix
α	coefficient of thermal expansion (CTE)
[B] or B	coupling stiffness matrix
β	coefficient of moisture expansion
[D] or D	bending stiffness matrix
E	Young's modulus
e	tensor strains
ϵ, γ	engineering normal and shear strains
$\{\epsilon\}$	engineering strains
$\{\epsilon^0\}$	total laminate midplane strains
f	fabrication strain components
G	shear modulus
$\{\kappa^0\}$	column vector of laminate midplane curvatures
{M} or M	moment resultants per unit length (width)
m	weight fraction moisture
%	percentage by mass
{N} or N	force resultants per unit length (width)
ν	Poisson's ratio
[Q] or Q	reduced stiffness matrix
[R] or R	Reuter's matrix
ρ	density
[S] or S	compliance matrix
S	shear failure stress/strain (in 12 direction)
σ, τ	normal and shear stresses
$\{\sigma\}$	stresses
[T] or T	transformation matrix
T	temperature
t	thickness
v/o	percentage by volume
X	failure stress/strain in 1-direction
x, y	in-plane laminate structural axes

X	volume fraction
Y	failure stress/strain in 2-direction
Z	through-the-thickness coordinate of a laminate (equivalent to the 3-direction in principal material direction space)

2. Superscripts

°	indicates a quantity which applies to the midplane of a laminate
T	indicates that quantity is due to thermal effects
-	(overbar) indicates a tranformed quantity in the cases of Q and S; indicates a total quantity in the case of {N}

3. Subscripts

a	indicates the axial direction
c	indicates compression or composite
f	indicates a final value or the fiber component of a composite
g	indicates glass (as in glass transition temperature)
h	indicates the hoop direction
ij	indicates the dimensions of a matrix (that is, 'i' rows by 'j' columns)
k	indicates a quantity which applies to the k'th lamina within a laminate
m	indicates the matrix component of a composite
o	indicates an original (time zero) value
r	indicates resin or matrix
R.M.	indicates reference material

R.T.	indicates room temperature
t	indicates tension
w	indicates wire used to suspend samples in Archimedean density tests
x, y, xy	indicate quantities in a tranformed coordinate system's directions (e.g., the structural axes)
1, 2, 12	indicate quantities in principal material directions; 1 indicates longitudinal direction; 2 indicates in-plane transverse direction
θ	indicates the hoop direction

Glossary of Terms

Angle-plied: Adjective indicating that the unidirectional reinforcement of a lamina is at some angle to the laminate or structural axes.

Apparent mass: The mass of a body as measured in a buoyant fluid more dense than air.

Boundary element: Spring-like element applied to the exterior of a finite element mesh to regulate displacements (or forces).

Catalyst: A substance which increases the rate of a chemical reaction. The catalyst is used in small amounts and does not itself undergo a permanent change in composition. (Scwartz, 1984) MEKP (methyl ethyl ketone hydroperoxide) is commonly used to catalyze polyester resin.

Chemical shrinkage: Shrinkage due to crosslinking.

Coefficient of thermal expansion (CTE): Usually, the linear CTE is given in the literature. This is the amount of expansion or contraction undergone by a material for each degree the material is heated or cooled.

Composite (material): Two or more different materials, combined on a macroscopic scale, to provide a material having superior properties to defined criteria. (Powell, 1983)

Coupling agent: A chemical which reacts with the matrix and reinforcement to provide a strong interface bond in a composite material. (Schwartz, 1984)

Crazing: Microcracking of a composite which gives rise to macroscale opacity.

Cross-plied: Refers to a laminate in which the unidirectional laminae are arranged with the fibers of one layer perpendicular to those of the next (that is, an angle-plied laminate with all angles equal to 0° or 90°).

Curing: The process by which a liquid resin becomes a solid. In polyester, this involves crosslinking of styrene monomers among polyester polymers.

Curing temperature: The maximum temperature reached during curing.

Drawing (process): The movement of molten glass through platinum bushings to produce glass filaments.

Failure criterion: A rule for predicting when a lamina or laminate will fail.

Failure envelope/surface: A surface in stress or strain space which contains all the stress or strain states for which a material or lamina behaves linear elastically. (Jones, 1975)

Fiber: A hairlike piece or filament (as of glass), usually of the order of 10 micrometres in diameter.

Fiberglass: 1. Glass fibers. 2. A composite material in which the reinforcement is made up of glass fibers and the matrix is (commonly) polymeric.

Filament: A fiber.

Filament-wound: Describing a body which has been produced by wrapping resin-impregnated strands of fibers (or prepreg tapes) around a form or mandrel. Strand tension, winding rate, and winding angle are closely controlled.

Finish: A material applied to fibrous reinforcements to improve the physical performance of composites. A finish usually contains coupling agents. (Schwartz, 1984)

Finite element method: Technique for analyzing continuous media. A body is subdivided into small sections or elements. Each element is described by a number of nodes at which certain degrees of freedom are defined. In the finite element analysis of Section 3.2, simple two-dimensional constant strain triangles are used. The nodal displacements are determined using linear elastic matrix methods and the nodal stresses and strains are then calculated from the nodal displacements.

Force resultant (per unit width): For a laminate, a stress term multiplied by the thickness of the laminate. Mathematically,

$$N_i = \int \sigma_i \, dz$$

where N_i is the force resultant, σ_i is the corresponding stress, and z is the through-the-thickness coordinate of the laminate. The bounds on the integral are from

the lower surface of the laminate to the top surface of the laminate. (Powell, 1983)

Gel point (or gel time): Point of inflection in the viscosity versus time curve of a curing resin. The gel point corresponds to the time when a resin first exhibits a non-zero stiffness. (Schwartz, 1984)

High-performance composite: A composite designed to provide maximum stiffness and strength in the directions of the greatest in-service loads.

Homogeneous: Uniform in composition.

Hoop-wound: Describing a composite in which the reinforcement is oriented perpendicular to the axis of the body.

Hydrostatic tension: Tension in all 3 principal directions.

Interface: Boundary between reinforcement and matrix.

Interlaminar: Between layers.

Interphase: Phase between the interface and the bulk matrix which contains a mixture of matrix and coupling agent.

Interply: Between plies.

Isotropic: Having properties which are equal in all directions.

Lamina(e): Layer or ply of a composite material. A lamina may contain unidirectional (in-plane) reinforcement or reinforcement which is randomly arranged in the plane.

Laminar: Describing a composite material or body which is made up of layers or laminae.

Laminate: An assemblage of laminae, in the form of a flat plate or a cylinder, for example.

Linear shrinkage: Shrinkage in one of the principal directions. For shrinkage of an isotropic body subjected to a uniform temperature change, the linear shrinkage is one third of the volumetric shrinkage.

Longitudinal (direction, strain, stress): Describing a property or quantity parallel to the unidirectional reinforcement. (That is, in the 1-direction in principal material

coordinate space.) It should be noted that the subscripts 1 and 2 for stresses and strains in composite materials always refer to principal material coordinates and do not imply principal stresses and strains.

Macromechanics: The study, at the structural level, of the stress and strain behavior of a composite material subjected to a load. For purposes of a macromechanical analysis, a lamina is regarded as being "...homogeneous from an engineering point of view, but having different stiffnesses and strengths in different directions." (Powell, p. 179, 1983)

Mandrel: Tubular form or structure on which a filament wound laminate is laid-up. May be made of plaster or metal; may be coated with a release agent or cardboard or be collapsible for easy removal subsequent to fabrication. "Poor mandrel design can result in... excessive residual stresses." (Schwartz, p. 4.58, 1984)

Micellular (structures): In polyester, these are highly crosslinked crystalline regions. Surrounding the micelles are somewhat amorphous regions having much lower crosslink density. (Selley, 1987)

Microcracks: Cracks whose dimensions are on the scale of the fiber diameter in a fiber-reinforced composite. They may run along the fiber-matrix interface or through the matrix.

Micromechanics: The "...study of...internal stresses {in composite materials} and the mechanics of internal reactions and interactions of the constituent parts due to imposed forces." (Marloff and Daniel, p. 156, 1969) The equations of micromechanics are used to calculate the properties of a composite based on the properties, geometry, relative proportions, and orientations of the constituents.

Microstresses: Stresses between the reinforcement and the matrix.

Moment resultant (per unit width): Defined similarly to the force resultant, above, only the integrand also contains the through-the-thickness coordinate. That is,
$M_i = \int(\sigma_i z)dz$
M_i is the moment resultant. The bounds of the

integral are the same as for the force resultant. (Powell, 1983)

Nodal points: Points delineating finite elements.

Orthotropic: "Having 3 mutually perpendicular planes of elastic symmetry." (Schwartz, p. G.19, 1984)

Photoelasticity: Technique whereby the distribution of stresses in a material subjected to a load can be determined from the appearance of the material under polarized light. (Hendry, 1964) In photoelastic models of composite materials, the refractive indices of the matrix and inclusion materials must be equal.

Polymerization: "A chemical reaction in which the molecules of a monomer are linked together to form large molecules...." (Oberholtzer, p. 32, 1988)

Plasticized: Describing a polymer to which has been added a "...material of lower molecular weight to reduce stiffness and brittleness, resulting in a lower glass transition temperature for the polymer." (Oberholtzer, p. 30, 1988)

Ply: Lamina.

Pot life: Time span during which catalyzed resin remains fluid enough to be used in filament winding.

Radial stresses and strains: 1. On the micro scale, these are stresses and strains perpendicular to the axis of the reinforcement. 2. On the macro scale, these are stresses and strains perpendicular to the axis of a tubular body.

Residual stresses and strains: Stresses and strains present in a body as a result of fabrication. They are due to chemical, thermal, and perhaps other effects (such as tension in the reinforcement) and are additional to the stresses and strains due to in-service loads.

Resin: "A solid, semisolid, or pseudo-solid organic material which has an indefinite (often high) molecular weight, exhibits a tendency to flow when subjected to stress, usually has a softening or melting range, and usually fractures conchoidally. Most resins are polymers. In reinforced plastics the material

used to bind together the reinforcement material, the matrix." (Schwartz, p. G.23, 1984)

Roving: "In filament winding a collection of bundles of continuous filaments either as untwisted strands or as twisted yarns....Glass rovings are predominantly used in filament winding." (Schwartz, p. G.23, 1984)

Self-temperature-compensated (strain gage): A gage in which (for some temperature range) the CTE of the backing material is closely matched to the CTE of the substrate to which the gage is applied

Sigmoidal: S-shaped.

Specific (strength, stiffness): A property normalized to density. For example, the specific modulus of glass fibers is the modulus divided by the density of glass.

Stacked rosette (strain gage): Several strain gages, one upon the other, each of which measures strain in a different direction. In Section 3.3, a 2-gage rosette, with the gages oriented at right angles to one another (one in the hoop direction and one in the axial direction), was used.

Stacking sequence: The order in which the laminae within a laminate are assembled. For example, when a laminate is assembled such that "...the laminae and properties are symmetric about the midplane...." (Powell, p. 165, 1983), a symmetric laminate results. The stacking sequence of a laminate influences the type of behavior exhibited. For example, a symmetric laminate made up of unidirectional orthotropic layers will not exhibit coupling between bending and extensional deformations. (Jones, 1975)

Thermoplastic: A plastic which may be formed, melted, reformed, and remelted repeatedly.

Thermoset: A plastic that cannot be melted down and reformed once it is chemically or thermally cured. In addition to being infusible, it is also "substantially insoluble." (Schwartz, p. G.28, 1984)

Transverse (strain, strength): A property pertaining to a plane perpendicular to the axis of the

reinforcement in a unidirectional lamina or laminate (Also, pertaining to the 2- and 3-directions in a unidirectional lamina or laminate.)

Transversely isotropic: Isotropic in a plane perpendicular to the reinforcement in a unidirectional lamina or laminate.

Viscoelastic: Describing time-dependent elastic (recoverable) material behavior. Viscoelastic behavior of a polymer reflects the ability of the molecules to uncoil and recoil when a load is applied and later released.

Viscous: Describing permanent (plastic) deformations. Viscous behavior of a polymer during the application of a load involves molecular chains sliding past one another. The molecules do not return to their original positions when the load is released.

Void: "Air or gas that has been trapped and cured into a laminate. Porosity is an aggregate of microvoids. Voids are essentially incapable of transmitting structural stresses or nonradiative energy fields." (Oberholtzer, p. 45, 1988)

Volumetric shrinkage: True volumetric shrinkage is the natural logarithm of the quotient of the volume at any point in time and the original volume. Engineering volumetric shrinkage is the quotient of the change in volume and the original volume.

1. Introduction

During the past several decades, composite materials have infiltrated many niches previously dominated by traditional engineering materials. The growing use of composites in aircraft provides a typical example. Consider the McDonnell Douglas Harrier jump jet, where the substitution of fiber composites for metal parts led to a doubling of load bearing capacity and range. (Jewett, 1987) Chemical plant piping, storage tanks, automobiles, sports equipment, and even musical instruments have felt the impact of the growing use of composites in design. (Schwartz, 1984) Depending upon the application, composites can provide significant advantages over traditional materials in terms of specific strength and stiffness, corrosion resistance, fatigue resistance, cosmetic appearance, vibration damping, and thermal properties. (Jones, 1975)

Despite the vast amount of ongoing research in the field, the complexities frequently associated with composite materials behavior prediction mean that, in many ways, composites are less well understood than their traditional counterparts. Because man-made composites afford the unique opportunity to engineer both the material and the structure or component into which it is incorporated, there is much incentive for continued research aimed at expanding the capabilities and possibilities of composite materials.

1.1 Context of the Problem

One aspect of composite materials research which has been the focus of considerable attention is the characterization of residual stresses and strains. Mr. Al Osborne, the Engineering Applications Manager of Fiberglas Canada's Technical Research Centre in Guelph, Ontario, has extensively observed and studied apparent manifestations of residual stresses in fiberglass.

Figure 1

Temperature and Relative End Displacement Versus Time During Curing for a Polyester Resin Casting

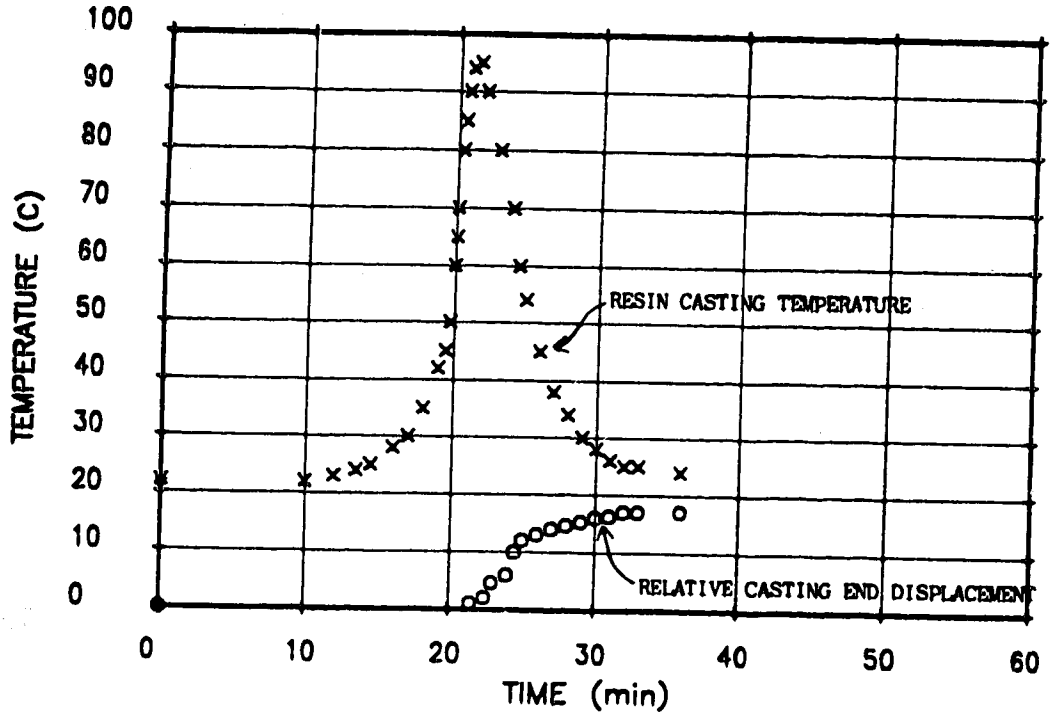

Figure 1 is taken from work done by Fiberglas Canada on a typical polyester resin used in filament-wound fiberglass products. The resin was catalysed and then cast into a bar shape. The upper curve of Figure 1 is the temperature versus time curve for the curing process of the neat resin. The lower curve represents the linear shrinkage of the resin casting during curing. From these plots, most of the shrinkage in this experiment is seen to occur in the vicinity of the maximum temperature. During this same portion of the curing cycle, bubbles, cracks, and blisters are reported to begin to form in filament-wound fiberglass products. Such flaws have been recognized for many years and have been thought to arise as a result of curing shrinkage and thermal contraction effects.

On a macro scale, some imperfections in fiberglass are identified as regions of opacity in otherwise translucent products. "Opacity is due to crazes in the resin, or debonding at the interface due to shrinkage stresses....In general, the mechanical performance of the laminate with a given resin is roughly proportional to the translucency of the finished fiberglass-resin composite." (Erickson and Plueddemann, 1974) However, Osborne (1987i) suggests that opacity is more of a cosmetic problem than an engineering concern in Fiberglas Canada products. The properties important to in-service applications do not appear to be affected in products showing opacity compared with similar, but more translucent, products.

Figure 2, following, is a section of a filament-wound, low-pressure water pipe. The whitish areas indicate small internal cracks, or crazing. Figure 3 shows a blow-up of a single crack. The crack is confined to the darker, weaker material. Microflaws such as those shown in Figures 2 and 3 occur in an unpredictable manner. It has been speculated that such microflaws are an inherent feature of fiberglass (whether they are macroscopically evident or not) and that such flaws are responsible for governing the practical attainable strength of fiberglass. The empirical transverse tensile strain limit (0.15%) governs the design of much corrosion-resistant fiberglass equipment. If residual fabrication stresses and strains are responsible for confining this strain limit to its small value, there is obviously a great deal of incentive to better understand and eventually control residual stresses. (Osborne, 1987i) It was within this framework of understanding that the program of research described in this thesis was undertaken.

The US space program has served as the impetus for concerted efforts at characterizing residual stress effects in high-performance epoxy-matrix composites. By comparison, little academic work has focussed on ubiquitous polyester-based commercial composites, such as fiberglass. Because the proportion of thermal to chemical shrinkage is greater in graphite-epoxy than in fiberglass, it is possible that the development and effects of curing stresses differ between the two system. This points out the need for

Figure 2

Appearance of a Fiberglass Pipe Containing Small Internal Cracks

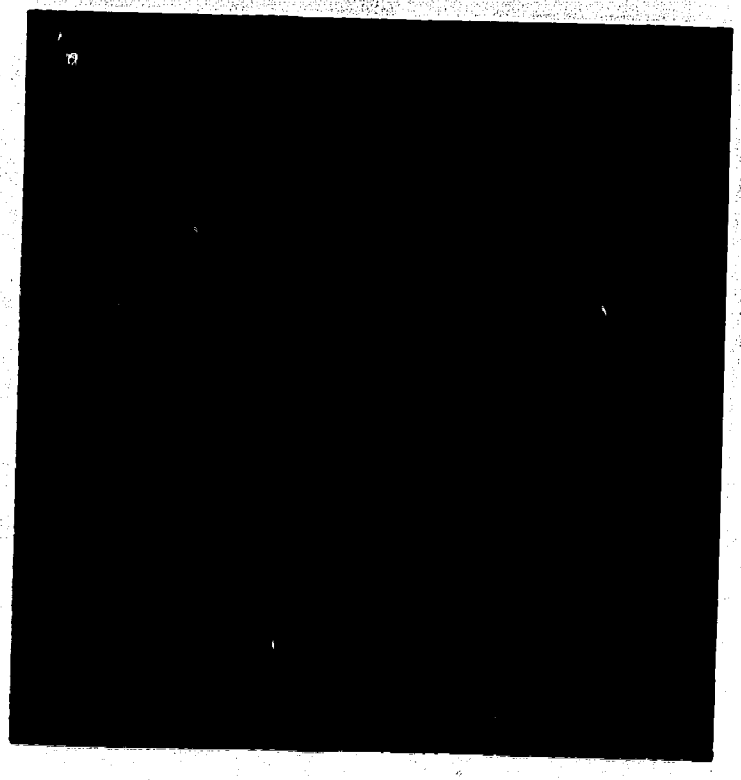

(Internal pipe diameter is approximately 0.46 m.)

Figure 3

Magnified View of a Single Crack
in the Pipe Section of Figure 2

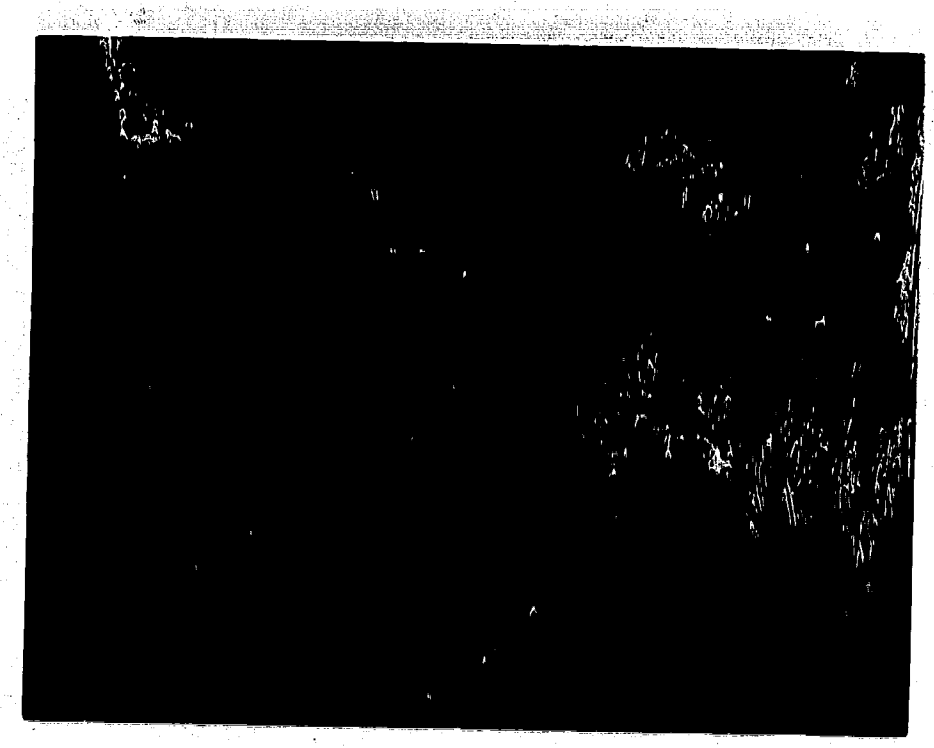

(Lamina thickness is approximately 0.5 mm;
fibers are the paler constituent.)

critical examination of the residual stress problem in fiberglass.

Current methods for analysing composite materials are sometimes based on the assumption that the material is free of stresses and strains until it is physically or thermally loaded. However, the nature of the fabrication process for fiberglass means that stresses due to chemical and thermal shrinkage may be present before the material is actually put into service. "In some cases curing stresses have been sufficiently large to cause fracture of layers within a laminate, even at room temperature." (Pagano and Hahn, 1977) Since residual stresses can significantly affect the strength of a composite, it would be useful to have a comprehensive mathematical model for predicting the three-dimensional pattern of stresses and strains from the cure cycle variables and the measured characteristics of the constituent materials. (Osborne, 1986) This thesis addresses some aspects of providing this model.

1.2 Polymer-Based Composite Materials

A composite material is any one in which two or more different materials are combined on a macroscopic scale to provide a material having superior properties to defined criteria. (Powell, 1983) Some of the possible combinations include ceramic plus metal, ceramic plus ceramic, organic plus plastic, and glass plus plastic. The constituents in the latter category may be combined in a number of ways.

Glass may be present either as chopped strands or as continuous fibers and the glass fibers may be randomly or purposefully oriented. Oriented continuous fibers within a given lamina are usually unidirectional, but a bidirectional arrangement may be achieved by using woven cloth or lightly pre-bound cross-laid roving. (Perratt, 1972) A number of types of glass fibers are available (electrical, or E glass, and high strength, or S glass, for example), and there are many polymer systems which can make up the plastic matrix. In this study, fiberglass (crosslinked polyester resin reinforced with E glass fibers) will be the system upon which most attention is focussed. Mention of other systems will be made from time to time for illustrative purposes. Furthermore, in this study, the morphology of greatest interest is a laminated structure consisting of plies containing long, oriented fibers. A filament-wound tube is used as a test piece.

Less strong than S glass is E glass, a low alkali, alumina borosilicate glass. It is less expensive, displays good chemical resistance, and is well behaved during the drawing process. E glass is drawn through holes in electrically heated platinum bushings or cisterns to produce fibers 3 to 20 x 10^{-6} m diameter. Typically, 204 or more fibers result from a single bushing; these are gathered together to form a strand, or "end". Roving used in filament winding consists of a number of parallel ends. In 1980, E glass reinforcing fibers sold for $0.84/kg to $0.95/kg (US).

The tensile yield strength of the material is about 830 MPa and the ultimate strength is of the order of 1.7 GPa. Young's modulus in tension is approximately 70 GPa. (Schwartz, 1984)

Commercially-available polyester resin is a syrupy solution of polyester polymers dissolved in an unsaturated coreactant. The polyester polymers derive from a stoichiometric mixture of unsaturated or saturated dibasic acids (or anhydrides) and dihydric alcohols (or oxides). As dictated by cost and performance criteria, styrene is the most common coreactant; it accounts for 35% to 45% by weight of the liquid resin so as to provide a ratio of two styrene monomers to each fumarate group present in the polyester polymer chains. Polymerization is free-radical initiated. The most frequently used initiator system is a mixture of methyl ethyl ketone peroxide (MEKP) catalyst plus a multivalent metal activator, such as cobalt octoate or cobalt naphthenate. This initiator system is intended for use between 25°C and 35°C. Other systems are available for use within the range from 0°C to 175°C. (Selley, 1985)

Fumarate groups and styrene monomers crosslink to produce three-dimensional, overlapping micellular structures with amorphous boundary regions of low crosslink density. The activation energy for gelation and crosslinking is estimated to be about 50 kJ/mole and the overall reaction rate constant is $2.7 \times 10^{9} \exp(-17{,}000/RT)\ min^{-1}$. (Selley, 1985) Glassy, crosslinked solid polyester has a tensile

strength of 40 to 90 MPa and a Young's modulus of around 2 to 4.5 GPa. (Parratt, 1972)

Fiber-matrix debonding due to interlaminar shear stresses is exacerbated by the low shear strength of the resin (of the order of 100 MPa or less) in addition to imperfect adhesion and the stress-concentrating effects of fibers and voids. For this reason, coupling agents, such as silanes or chromium vinyl, are employed to link oxide layers on glass fibers to organic groups in the resin. "Good adhesion of polymers to minerals often requires...100 monolayer equivalents, or more, of silanes on the surface." (Plueddemann, 1988) Coupling agents aid in bond strength retention (even in the presence of water at the bond interface) and in the enhancement of flexural strength. (Parratt, 1972) It has also been observed that silane coupling agents aid in preserving translucence during composite fabrication. (Plueddemann, 1974) Several theories have been advanced to explain how silane coupling agents might help a composite adjust to curing stresses.

The "deformable layer" theory suggested that a silane finish facilitates the development of a flexible resin layer at the fiber-matrix interface. By some mechanism, this layer might provide for relaxation of curing stresses. However, this early theory did "...not appear to be tenable in glass-reinforced composites because of the known sensitivity of rubbery polymers on glass to the debonding action of water...." (Erickson and Plueddemann, 1974) The

interdiffusion model for the microscale structure of the composite interface was suggested by Plueddemann (1988). This model, which is applicable to glass-reinforced composites, suggests that a chemically-bonded interface of covalent oxane bonds lies adjacent to a diffused interphase region of polymer plus coupling agent, as shown in Figure 4. The nature of the interphase controls composite performance. The capacity for bond reformation following bond breakage is one way in which the interface and interphase regions could accommodate resin shrinkage strains and thereby allow for the relaxation of curing stresses.

Figure 4

Schematic of the Interphase
(Adapted from Plueddemann, 1988)

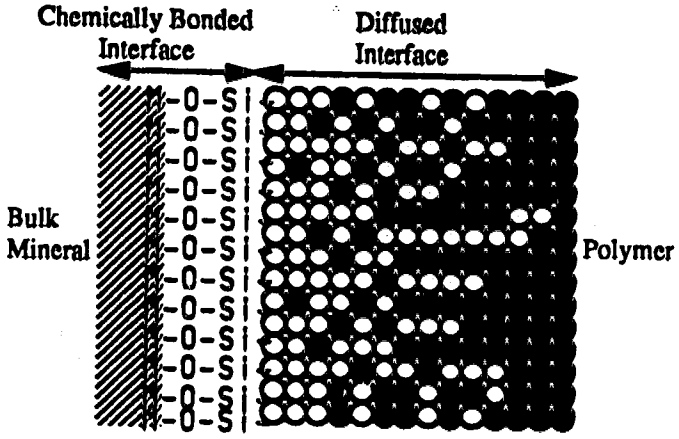

Open circles indicate regions of coupling agent.
Filled circles indicate regions of polymer.

2. Residual Stresses in Polymeric Composites

Residual stresses in polymeric composites are commonly characterized and analysed on two different levels. Micromechanical analysis is useful for developing a background understanding of the types and distributions of strains and displacements experienced by individual fibers and the matrix surrounding them. A more general macro-mechanical treatment, in which the disparity between the properties of the matrix and fibers is "smeared out" within each lamina in order to simplify the mathematics, is suited to considering the performance of engineering structures made of composite materials.

2.1 Micromechanical Analysis of Residual Stresses

The residual stresses present in an unloaded polymer composite originate during and following cure. The first curing stress component is believed to be due to resin shrinkage. The density increase of polyester resin during crosslinking results from linear shrinkage of about 2% to 3%. Most of the styrene solvent in which the polyester resin is dissolved crosslinks into the structure during curing. (Osborne, 1987i) However, any mass loss, due to chemicals being driven off by the curing exotherm, for example, will contribute to the overall volumetric shrinkage of the resin. "Polyesters are available with dissolved thermoplastic additives which precipitate during cure to minimize shrinkage and give smooth, fibre-free surfaces on

laminates." (Parratt, 1972) That is, with less shrinkage of the resin, the fibers are less likely to stand out in relief on the surface of a laminate. Despite this, polyester systems tend to display more shrinkage than other thermosetting resins. This is likely accepted due to the comparatively low price and adequate stiffness characteristics of polyester.

Epoxy and polyester are the two most widely used polymeric matrix materials. The volumetric shrinkage of epoxy upon curing ranges from 1% to 3%, while that for polyester ranges from 4% to 8%. (Powell, 1983; Schwartz, 1984; Hull, 1981) In 1987, general purpose epoxy cost $3.30/kg (US) (Puglisi and Chaudhari, 1988) while general purpose polyester sold for $1.10/kg (US). (Dudgeon, 1988)

Both external loads and internal residual stresses contribute to the total state of stress of a laminated composite. Curing "...microstresses are often sufficient to produce microcracking even in the absence of external loads." (Hull, 1981) The portion of the curing shrinkage which occurs while the resin is liquid does not lead to stress build-up. However, if a strong resin-to-fiber interfacial bond exists, both longitudinal and radial stresses will develop during later stages of curing.

Figure 5

The Evolution of Longitudinal Residual Stresses Between Glass and Polyester

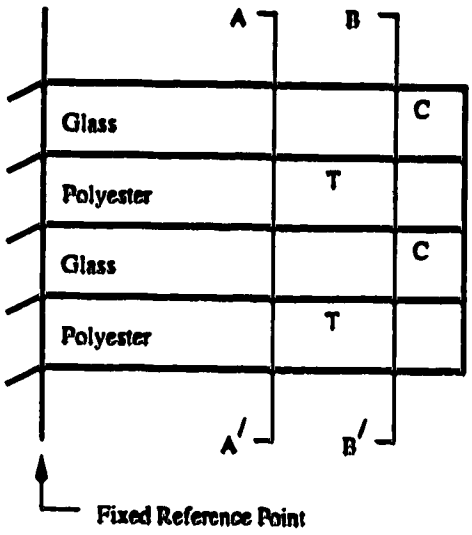

The evolution of longitudinal residual stresses is easily visualized. Consider several adjacent parallel fibers and the surrounding resin in a unidirectional fiberglass composite as shown in side view in Figure 5. Further consider only chemical shrinkage of the resin in the absence of thermal effects. Assume that the left-hand side of the above model is fixed. The resin would tend to shrink back to plane "A" in the absence of external constraints. The presence of the glass fibers means that the resin will displace less than if it were allowed to shrink freely. For illustrative purposes, assume that the resin shrinks to plane "B". If the bond between the glass and resin is

strong, then the glass will also be forced to displace to plane "B". That is, compatibility between the matrix and reinforcement is maintained. The net result is that the glass is put into compression along the length of the fibers while the resin is put into tension.

From the above example, it may be appreciated that resin shrinkage under the constraint of adjacent fibers and laminae leads to a state of tension in the matrix. Concurrently, the fibers are subjected to axial compression and shear stresses are induced in the resin parallel to the fiber-matrix interfaces. According to the classical mechanical model of the state of stress under an applied load of a long fiber within a resin matrix, the shear stress attains its maximum value near the ends of the fiber and diminishes to zero in the center. Shear-type curing microstresses would be of particular concern in short fiber composites (which contain a higher proportion of fiber ends than continuous fiber composites) and this must be recognized when interpreting the results of mechanical properties tests. (Scola, 1974)

In addition to longitudinal stresses, radial stresses are induced by resin shrinkage. Photoelastic studies performed by Koufopoulos and Theocaris (1969), Marloff and Daniel (1969), Daniel and Durelli (1962), and others have revealed that both tensile and compressive radial stresses may result from thermal and curing effects. Furthermore, the sign and magnitude of these radial stresses are strongly

dependent upon fiber size, the volume fraction of fibers, the arrangement of fibers, the total amount of shrinkage subsequent to gelation, and the relative Young's moduli and coefficients of thermal expansion (CTE's) of the fibers and matrix. (Hull, 1981) Some limiting cases pertaining to a single lamina are summarized below.

Begin by considering the case of minimum packing density of fibers within a resin matrix. This may be represented by a single fiber embedded in a large volume of resin. In this scenario, constraints to resin shrinkage are minimal. As it shrinks, the resin squeezes onto the fiber, creating radial compression across the fiber-matrix interface. Concurrently, tensile hoop stresses are developed in the matrix adjacent to the fiber.

Next, consider the theoretical configuration in which fibers assume the maximum possible packing density. Here, each pocket of resin is constrained by stiff boundaries. Since the fibers touch, the resin is unable to pull the fibers any closer together as it shrinks. As a result of curing, a tensile stress will develop, both in the resin and at the fiber-matrix interface. (Hull, 1981)

Real systems fall somewhere between these two extremes and are characterized by fibers randomly distributed throughout the matrix. The nature of the curing stresses developed depends on the local fiber configurations and the values of the parameters listed above. For example, consider adjacent fibers which are packed in a square array. This

configuration was the subject of a photoelasticity study performed by Koufopoulos and Theocaris (1969).

In this study, it was assumed that the thermal expansion coefficients of the inclusion material (unplasticized epoxy) and the matrix material (plasticized epoxy) were the same. No reference was cited to support this assumption. In general the plasticized form of a particular resin would be expected to display a higher coefficient of thermal expansion than the unplasticized form. For example, consider polyvinyl chloride where $\alpha_{rigid} = 50 - 100 \times 10^{-6}$ m/m/K and $\alpha_{flexible} = 70 - 250 \times 10^{-6}$ m/m/K. (Juran, 1989) Similar data were not found for epoxy. However, if the thermal expansion coefficients of Koufopoulos and Theocaris' plasticized and unplasticized epoxies had overlapping ranges similar to PVC, then it is possible that Koufopoulos and Theocaris did remove the differential thermal contraction effects from their experimental set up. In any case, we cannot be sure that the stresses they describe are due solely to chemical shrinkage.

Koufopoulos and Theocaris' results suggest that tension or compression can exist normal to the interface at point 'C' in Figure 6, below. A low volume fraction of fibers and a high E_f/E_m ratio favor a state of tension. Hydrostatic tension exists at point 'O' and radial compressive stress prevails between 'A' and 'B'. The magnitude of the compressive stress increases as the volume fraction of fibers increases. (Hull, 1981)

Figure 6

A Square Array of Fibers in Resin

(Adapted from Hull, 1981)

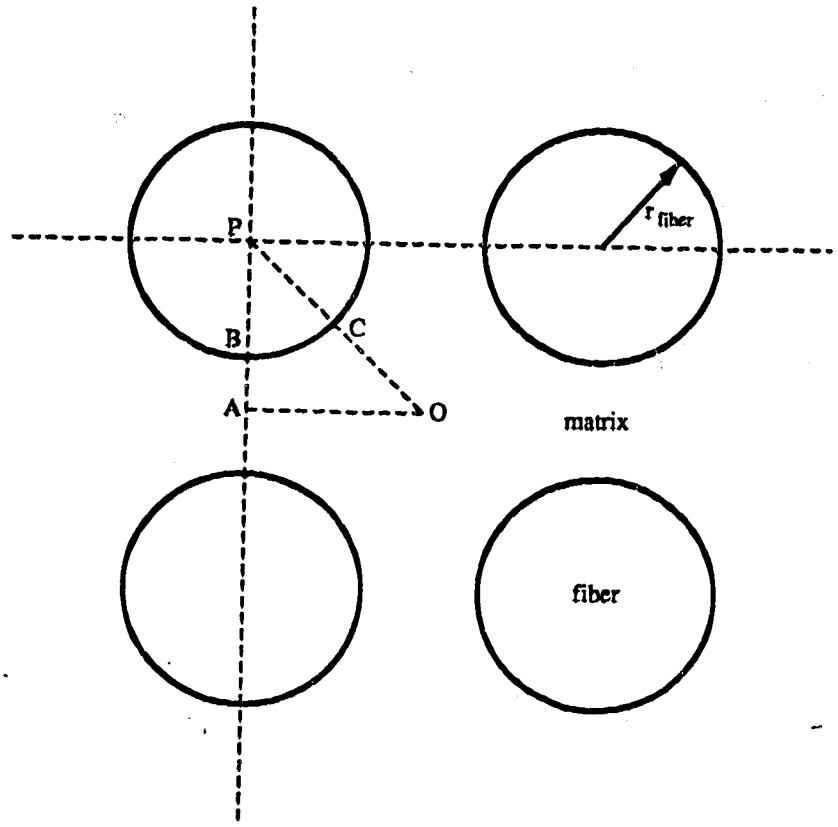

The additional constraints imposed when laminae are bonded together to form a laminate lead to a more complicated residual stress pattern than that suggested above. As well, the incorporation of the free-edge boundary condition introduces additional complications. The influence of free edges was not dealt with in the above-mentioned models but will be discussed in connection with the second type of curing microstresses.

The differential thermal contraction which occurs after the peak exotherm in the curing cycle of a typical polyester resin gives rise to the second set of stresses associated with curing. The linear CTE's of E glass and crosslinked polyester are, respectively, 5×10^{-6} m/m/K and 55 to 100 x 10^{-6} m/m/K according to Plueddemann (1974). In the Superlam program, Osborne (1986ii) provides an expansion coefficient of 63×10^{-6} m/m/K for the Vibrin resin used in this work. Hull (1981) cites a value of 150×10^{-6} m/m/K for the CTE of polyester and points out that upon cooling between the post-curing temperature of 120°C and ambient, a "...differential strain of the order of 1.5% which is about 75% of the strain to failure of resin in uniaxial tension...." (Hull, 1981) is produced, giving rise to a complicated stress state in a three-dimensional array of fibers. On the macro scale, the CTE's of the laminae comprising a laminate depend upon the volume fraction of fibers, the fiber arrangement, and the E_f/E_m ratio. Formulae based on the physical properties of the constituent

materials have been proposed for a number of possible lamina configurations. The CTE's for a laminate may then be calculated using Classical Lamination Theory (CLT) and a knowledge of the CTE's of the constituent laminae. See, for example, Jones (1975) and Tsai and Hahn (1980).

Rohwer and Jiu (1986) analysed the "...self equilibrating stresses..." developed between fibers and an epoxy matrix upon cooling to room temperature from the curing temperature. They assumed that the curing temperature represented the unstrained condition of the composite. This same assumption was used by Tsai and Hahn (1980), who explained that epoxy systems undergo most of their crosslinking at the peak curing temperature where the epoxy can be "...viscous enough to allow complete relaxation of the residual stresses." They reasoned that, so long as most of the chemical shrinkage occurred at the curing temperature, the curing temperature may be taken to be the stress free state.

Using the finite element method to analyse regular hexagonal and square arrays of carbon fibres in epoxy matrix, Rohwer and Jiu (1986) predicted the room-temperature thermomechanical stress distribution. In all cases, material behavior was assumed to be linear elastic, the fibers were assumed to be transversely isotropic, and the matrix was taken to be isotropic. Of primary interest were the stress and displacement fields near free edges, especially in the vicinity of fiber to matrix interfaces. Due to the large

difference between the stiffnesses of the fibers and the matrix, high interfacial stresses had been anticipated. Accordingly, the results showed significant radial and tangential interfacial stresses on free edges and large interfacial shear stress gradients in this region. In addition, high tangential and axial stresses were found to occur in the matrix at some distance from fiber matrix interfaces. (Rohwer and Jiu, 1986)

As with the example presented above, many resin shrinkage studies in the literature focus on epoxy. In order to be able to sort out which data and assumptions regarding epoxy pertain to polyester, it would be useful to compare some of the differences in curing behavior between the two resins.

Firstly, the temperature and pressure excursions are closely regulated for epoxy systems while, for general-purpose polyester systems, the temperature increases freely due to the exothermic curing reaction and the entire process occurs at atmospheric pressure. As illustrated in the schematic of Figure 7.a, the usual cure cycle for epoxy involves bringing the temperature up to the maximum, or curing, temperature and then holding for several hours. The natural curing exotherm of epoxy does not bear much relation to the imposed curing conditions. For the types of fiberglass products of interest in this study, the temperature climbs due to the chemically-induced curing exotherm, reaches a peak, and then decreases. The exotherm

temperature may vary within the volume of material, with the center of thick sections becoming hotter than portions exposed to air or mold materials. The temperature curve for polyester is shown in Figure 7.b. For epoxy composites, the peak curing temperature is typically of the order of 70°C to 150°C above room temperature. For general-purpose polyester composites, the pertinent temperature difference is between 40°C and 100°C. The actual temperature difference, which may vary within a lamina, is influenced by the chemistry of the resin and catalyst formulations, by the thickness of and position within the laminate, and by the thickness and material of the mold or mandrel. (Schwartz, 1984)

The first portion of Figure 7.b corresponds to polyester in the syrupy liquid state. According to Hull (1981), "much of resin shrinkage occurs while it is still liquid so that stresses do not develop." Shrinkage of the liquid polyester resin is not indicated by the results presented in Figure 1. However, in the experimental scenario associated with Figure 1, any densification of the liquid or gel would have been counteracted, to some extent, by thermal expansion effects prior to the peak exotherm. This example underscores the need to separate the thermal and chemical components of resin shrinkage for analysis.

Between time zero and the time of the peak exotherm of Figure 7.b, polyester becomes a gel. If the gel can flow viscously, shrinkage stresses would be able to relax away. By the time the peak exotherm is reached, the polyester is a

solid (with a modulus lower than the room temperature value). Physical data for polyester in the gel state are rare in the literature. Statistical distributions for molecular weight and degree of crosslinking, for example, are not readily available. If the polyester solid, as it exists in the vicinity of the peak exotherm temperature, cannot flow viscously, shrinkage occurring in this regime will lead to built-in stresses.

In contrast, most of the crosslinking (and hence curing shrinkage) in epoxy is known to occur at the maximum temperature. As mentioned above, the viscous behavior of epoxy at the curing temperature allows almost all of the chemical shrinkage stresses to relax away. This was not thought to be the case with glass-reinforced polyester.

Figure 7

Schematic Cure Cycles for Epoxy- and Polyester-Based Composites

a. Epoxy Matrix (Adapted from Tsai and Hahn, 1980),

b. Polyester Matrix

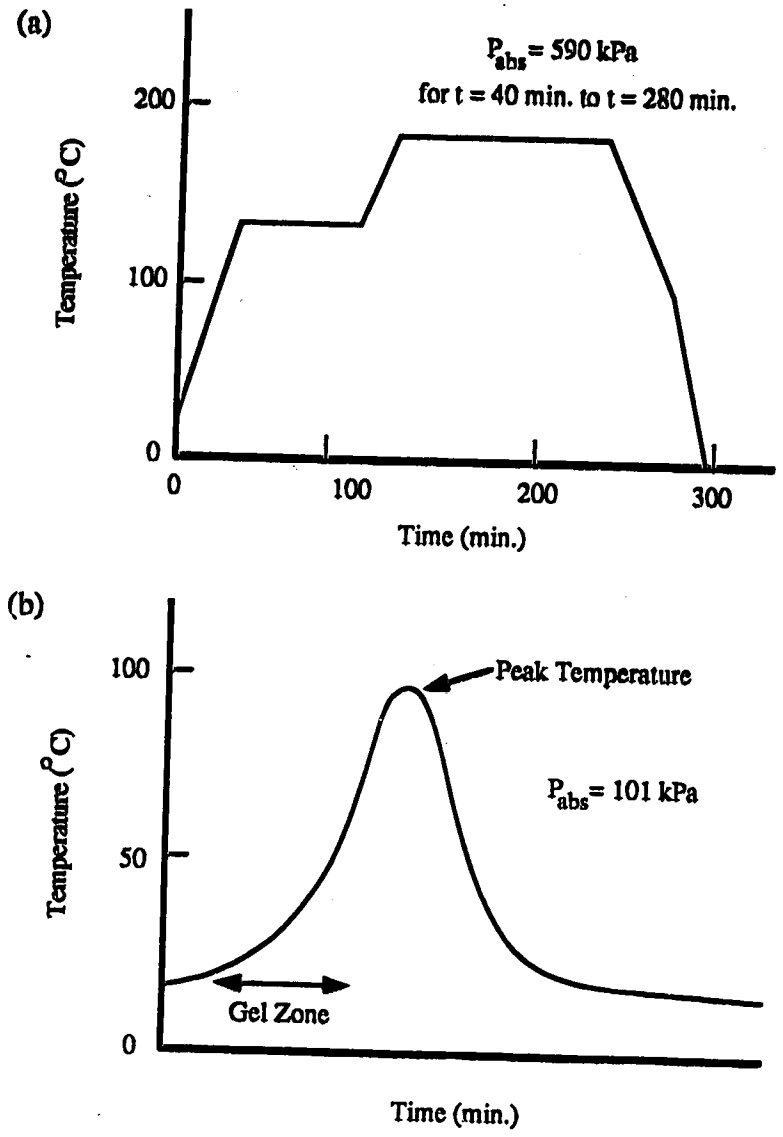

2.2 Macromechanical Treatment of Residual Stresses

There are two main mathematical approaches for dealing with macromechanical residual stresses. The first is based on Classical Lamination Theory (CLT), while the other is based on elasticity theory. A brief summary of the nature and limitations of each follows. Some of the basic mathematics of CLT are reviewed in Appendix A.

2.2.1 Classical Lamination Theory

Stiffness

Stiffness analysis using CLT presupposes linear elastic material behavior and small strains. The applicability of these stipulations varies from system to system. For fiberglass, the literature frequently employs the linear elasticity assumption. In addition, the range of deformations likely to be experienced in service falls within the classification of small deflections.

Figure 8.a, below, shows tensile stress-strain curves for several polyester resins of varying flexibility. Beyond a few percent elongation, the most flexible resin, C, shows marked nonlinearity. Tensile stress-strain curves for several different fibers are given in Figure 8.b. In all cases, the behavior is linear until failure. It should be noted that the figures in 8.b are illustrative in that a range of breaking stresses exists for any particular type of fiber. The strength of long fibers tends to be less than

that of short fibers because the existence of flaws becomes more probable the greater the gage length. (Hull, 1981) However, long fibers are much more effective at imparting strength to a composite due to the deleterious end effects associated with short-fiber reinforcements. Figure 8.c depicts transverse tension stress-strain curves of unidirectional laminae comprising E glass fibers and the resins of Figure 8.a. Lamina behavior is nearly linear even in the case of the lamina based on resin C. When considering laminae composed of glass and polyester, deviations from linearity are usually attributable to resin behavior, especially in shear loading. (Hull, 1981) It will be assumed that the polyester matrix behaves linearly throughout the entire range of curing phenomena. As seen in Figure 8, this assumption is a satisfactory one for the matrix in the solid state. However, during part of the curing history, the resin is a viscous liquid. Subsequent to gelation, resin behavior is likely viscoelastic.

Figure 8

Tensile Stress-Strain Curves

a. Polyesters, b. Fiber Materials, c. Fiberglass Laminae

(Adapted from Hull, 1981)

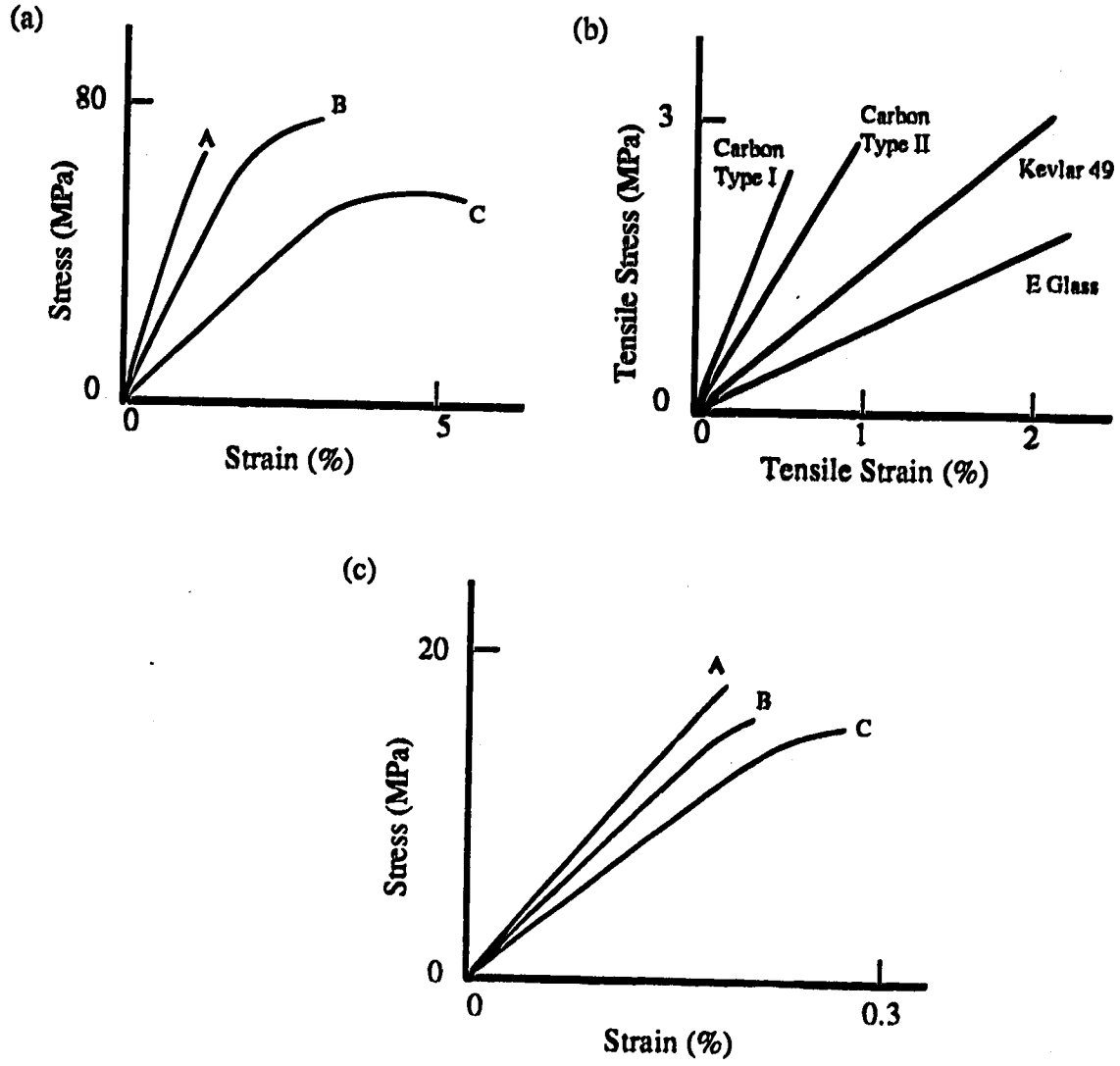

According to the Kirchhoff Hypothesis for plates (or, equivalently, the Kirchhoff-Love Hypothesis for shells), laminae comprising a laminate are assumed to be perfectly bonded. Furthermore, the bond interfaces are assumed to be very narrow and non-shear-deformable. Consequently, laminae are assumed not to slip with respect to one another and displacements are assumed to be continuous across bond interfaces. A further consequence of the Kirchhoff Hypothesis is that shear strain terms involving the through-thickness coordinate of the laminate, z, are assumed to be zero. (That is, $\gamma_{xz} = \gamma_{yz} = 0.$) (Jones, 1975) The remaining strains are assumed to vary linearly through the thickness of a laminate while the nature of the through-thickness stresses depends on the relative mechanical properties of adjacent layers. To simplify the kinematics, ϵ_z is usually assumed to be negligible.

Resultant Expressions for Laminates

Expressions for the strain and stress distributions for a lamina and the force and moment resultants for a laminate appear in Appendix A. Use of these expressions is greatly simplified when the terms of the material stiffness matrix are constant within each lamina. That is, when the individual stiffness terms do not vary with location or temperature. In the general case, however, the temperature dependence of the material properties must be recognized. Thus, suitable functions describing moduli, CTE's, and

Poisson's ratios are incorporated into the integrated expressions for force and moment resultants. As indicated in Appendix A, the extensional strains in the principal directions are suitably adjusted by the addition of terms involving CTE's and temperature differences when thermal effects must be accounted for.

Curing Shrinkage

Based on CLT, curing shrinkage effects in an unloaded laminate are sometimes modeled simply as thermal strains due to cooling from the curing temperature to the operating temperature. The fact that the chemical shrinkage component is frequently disregarded in the literature was discussed in a previous section.

In a study of graphite-epoxy laminates, Hahn and Pagano (1975) assumed that low resin stiffness and the viscous nature of polymer resins during crosslinking at high temperature combine to yield a stress-free laminate at the end of the first (crosslinking) stage of fabrication. They developed a method of assessing residual thermal stresses and strains based on total stress-strain-temperature relations. Incremental relations may readily be derived once a total relation has been formulated. An incremental relation derived from a total relation includes a stress-dependent term that is not considered by authors who begin with an incremental approach.

The total stress-strain-temperature relations proposed by Pagano and Hahn (1975, 1977) are based on a decomposition of strain into mechanical and thermal components.

$$\epsilon_i = \epsilon_i^{\sigma} + \epsilon_i^{T} \quad \ldots\ldots[1]$$

In the general case, the mechanical strain component depends upon both stress and temperature while the thermal strain is a function of temperature alone. That is,

$$\epsilon_i^{\sigma} = g_i(\sigma_i, T) \text{ and } \epsilon_i^{T} = f_i(T) \quad \ldots\ldots[2]$$

Thus, when considering a small change in strain, $d\epsilon$, instantaneous coupling expansion coefficients (the partial of mechanical strain with respect to temperature) as well as familiar CTE's (the partial of the thermal strain with respect to temperature) are invoked.

$$d\epsilon_i = (\partial g_i/\partial \sigma_j)d\sigma_j + (\partial g_i/\partial T)dT + (df_i/dT)dT \quad \ldots[3]$$

For the simple case in which the mechanical strains are linear in stress (i.e., $\epsilon_i^{\sigma} = S_{ij}(T)\ \sigma_j$) the error in neglecting the coupling expansion term (i.e., $\partial g_i/\partial T = d\epsilon_i^{\sigma}/dT = (dS_{ij}/dT)\ \sigma_j$) can be quite significant when the difference between the curing and operating temperatures is large. Still considering this simple case, when the stiffnesses are not temperature dependent, the total strain theory reduces to the incremental strain theory. In practice, the material properties required for stress analysis are temperature dependent and the inclusion of the coupling expansion term is necessary. (Hahn and Pagano,

1975)

The above comments may be elucidated by considering a brief numerical example such as that presented by Hahn and Pagano (1975). Consider a boron/epoxy laminate having a transverse modulus which varies linearly with temperature according to

$$E = E_o - aT \quad \text{.....[4]}$$

$E_o = 20.26$ GPa, $a = 63.67$ MPa/°C

The transverse CTE of this material is 29.2×10^{-6} m/m/K.

Further consider the case where the total strain is zero. That is, the mechanical strain is equal and opposite to the thermal strain. If the coupling expansion term discussed above is neglected, then substituting in the above expression for the transverse Young's modulus and replacing (df_i/dT) with α gives the following solution for the transverse stress:

$$\sigma = -\alpha(T - T_o)\ (E_o - a/2\ (T + T_o)) \quad \text{.....[5]}$$

The inclusion of the coupling expansion term leads to the following formulation

$$\sigma = -\alpha(T - T_o)(E_o - aT) \quad \text{.....[6]}$$

For a curing temperature of $T_o = 177$°C and an operating temperature of $T = 24$°C, the transverse stresses calculated in the two instances are, respectively, 61.9 MPa and 83.7 MPa. That is, the error due to neglecting the coupling expansion term is approximately 26%. (Hahn and Pagano, 1975)

The Inclusion of Fabrication Effects in CLT

In the standard thermomechanical CLT development, the in-plane principal material direction stresses for a particular lamina can be expressed as follows:

$$\{\sigma_i\} = [Q_{ij}]\ \{\epsilon_j\} \quad \text{.....[7]}$$

where i,j = 1,2,3 and

$$\epsilon_1 = e_1 - \alpha_1 \Delta T \quad \text{.....[7.a]}$$

$$\epsilon_2 = e_2 - \alpha_2 \Delta T \quad \text{.....[7.b]}$$

$$\epsilon_3 = \gamma_{12} \quad \text{.....[7.c]}$$

Above, ϵ represents mechanical strain, e represents total strain, γ represents shear strain, and $\alpha\Delta T$ represents thermal strain.

In their work on residual stresses in composite shells, Morozov and Popkova (1986) experimentally determined the magnitude of fabrication-induced residual strains in unidirectional glass-epoxy laminae after curing. These strain terms were factored into their CLT analysis in the same fashion as thermal strain terms. Thus, the formulae for ϵ_1 and ϵ_2 become

$$\epsilon_1 = e_1 - \alpha_1 \Delta T - f_1 \quad \text{.....[8.a]}$$

$$\epsilon_2 = e_2 - \alpha_2 \Delta T - f_2 \quad \text{.....[8.b]}$$

The shearing strain, γ_{12}, is not affected.

Based on work by Brivmanis (1966), the longitudinal fabrication strain component, f_1, was said to be due solely to the pretensioning of the reinforcement, with no contribution from resin shrinkage. The transverse

fabrication strain component, f_2, was found by Morozov and Popkova (1986) to arise from both chemical and thermal shrinkage effects. Both quantities must be determined experimentally for a particular material system and set of fabrication parameters. Note that for this epoxy-based system, the resin shrinkage is hypothesized to be anisotropic. This is the only reference cited which suggests this possibility.

Strength

Once the stiffness analysis of a laminate has been formalized, the next task is to be able to predict the strength of a laminate based on the strengths of the individual laminae. In order to do this, the state of stress in each lamina must be known; residual stresses must be incorporated when either the operating temperature of a laminated composite is far below the curing temperature or when significant resin shrinkage stresses are present.

In general, a phenomenological approach is pursued. That is, laminate behavior is studied without having a detailed knowledge of the cause of the observed effects. (Jones, 1975) The interplay of modes and mechanisms of laminate failure are very subtle and complex and as yet not completely understood. Thus, any analysis must necessarily involve a good deal of simplification. The major parameters which must be accounted for in laminate strength analysis are laminae strength, stiffness, and thermal properties; orientation and stacking sequence of the layers; and the curing temperature. (Jones, 1975)

Regardless of the failure criterion employed, the procedure for strength analysis and failure prediction involves mathematically raising the load applied to a laminate until one of the layers fails. At this point, stresses in the remaining layers are recalculated and the possibility of additional lamina failures is assessed. When no other lamina failures are predicted based on the original

load applied, the load is increased and the procedure is repeated. Laminate failure ensues after a sufficient fraction of the laminae have failed. The proportion of lamina failures which leads to laminate failure will, in turn, depend on the type of composite and the type of application for which the composite is designed.

Several "biaxial strength theories for an orthotropic lamina" (Jones, 1975) are documented below. The simplest possible criteria to employ are the maximum stress criterion and the maximum strain criterion. These assume no interaction between the failure modes and so axial, shear, and transverse failure are assumed to occur independently of one another. The Tsai-Hill criterion is slightly more complex than either of the preceding two and, in certain cases, the predictions match observations quite closely. This relates to the fact that the variation in strength with angle of orientation is smooth (rather than cusped) and that interaction among the failure modes is accounted for. The Tsai-Wu criterion is yet more general. It offers better curve-fitting capability than any of the preceding and may be readily incorporated into a computer program due to its tensor format.

According to the maximum stress failure criterion, failure occurs when the stresses in the principal material directions exceed the strengths in those directions. That is, failure occurs if one or more of the following inequalities is not satisfied:

$$\sigma_1 < X_t;\ \sigma_2 < Y_t;\ |\tau_{12}| < S \text{ (Tension)} \quad [9]$$

$$\sigma_1 > X_c;\ \sigma_2 > Y_c \text{ (Compression)} \quad [10]$$

This criterion assumes no interaction between failure modes and, thus, is actually three subcriteria (one for axial failure, one for shear failure, and one for transverse failure). The above comments also apply to the maximum strain failure criterion, where failure is predicted if one or more of the following is not satisfied:

$$\epsilon_1 < X_{\epsilon t};\ \epsilon_2 < Y_{\epsilon t};\ |\tau_{12}| < S_\epsilon \text{ (Tension)} \quad [11]$$

$$\epsilon_1 > X_{\epsilon c};\ \epsilon_2 > Y_{\epsilon c} \text{ (Compression)} \quad [12]$$

The Tsai-Hill criterion stated in Equation 13, below, reveals interaction among the failure strengths, X, Y, and S. In addition, strength varies smoothly with angle as the angle of orientation of the x-y axes with respect to the principal axes grows beyond zero. This is more realistic than the assumed behavior of the two preceding criteria, where the strength versus angle curves are cusped. (See Jones, 1975, pp. 71-83)

$$(\sigma_1/X)^2 - (\sigma_1\sigma_2/X^2) + (\sigma_2/Y)^2 + (\tau_{12}/S)^2 = 1 \quad [13]$$

Finally, the Tsai-Wu tensor theory (or quadratic failure criterion) takes the following form:

$$F_i\sigma_i + F_{ij}\sigma_i\sigma_j = i \quad [14]$$

For the general case, $i,j = 1,2,\ldots,6$

For an orthotropic material, $i,j = 1,2,6$

The presence of additional terms beyond those present in the

Tsai-Hill theory increases both the complexity and the curve-fitting ability of this criterion. Standard tensor transformation laws are valid. Also, the same symmetry properties which apply to the stiffness and compliance tensors also apply to the Tsai-Wu failure criterion. (Jones, 1975)

Interlaminar Stresses

A major shortcoming of CLT is its failure to adequately deal with interlaminar stresses. Contrary to physical evidence, such as debonding at free edges, the shearing stresses on the z-plane in both the x- and y-directions are assumed to be zero. Secondly, Jones (1975) points out that when a symmetric angle-plied laminate is subjected to an extensional force in the x-direction, CLT suggests the existence of non-zero shearing strains (γ_{12}) in the laminae. "The shearing stresses that correspond to such shearing strains are not physically possible at the [free] edge of a lamina...." Finally, CLT does not predict extensional stiffness changes due to alteration of a laminate's stacking sequence. Observed extensional stiffness effects are thought to be due to interlaminar normal stresses, which are not accounted for in CLT. (Jones, 1975)

2.2.2 Elasticity Approach

In general, an elasticity problem involves the solution of 15 partial differential equations in 15 unknowns. The

equations are of three types: equilibrium, constitutive (or stress-strain), and kinematic (or strain-displacement); the unknowns are stresses, strains, and displacements. Although it is more complicated than the CLT approach, the elasticity approach to the residual stress problem does offer certain advantages. A three-dimensional stress state which includes through-thickness interlaminar stresses may be calculated. As previously mentioned, a tubular geometry is of particular interest in this study. For thick-walled tubes, interlaminar stresses become increasingly important since they contribute to the delamination problems associated with the free edges of such tubes. The elasticity approach also accommodates important curvature effects and allows for the inclusion of through-thickness expansion effects. (Hyer and Cohen, 1984)

Hyer and Cohen (1984) studied cross-ply graphite-epoxy tubes subjected to a spatially uniform temperature below the cure temperature. By employing a number of simplifications, they were able to reduce the elasticity equations to ordinary differential equations. These were solved ply-by-ply and the results were used to assess the effects of stacking arrangement on the distribution of residual stresses. The elasticity results were then compared to CLT results.

It should be noted that only thermal effects were considered. That is, densification residual stresses were assumed to be negligible. As well, material properties were assumed to be independent of temperature due to the

unavailability of data for the variation of elastic properties with temperature. Some further assumptions employed by Hyer and Cohen (1984i) are as follows:

1. Stresses and strains were taken to be invariant along the axis of the tube. (i.e., the problem was reduced to a planar elasticity problem.)
2. Derivatives of all stresses, strains, and displacements with respect to the circumferential coordinate were taken to be zero due to the axisymmetric nature of the problem.
3. Circumferential displacements were set to zero due to the simple cross-ply arrangement considered.

The usual types of boundary conditions were applied. Continuity of tractions and displacements between successive layers' cylindrical surfaces was enforced as was the condition that free surfaces are stress-free. Following application of the boundary conditions, the resulting system of algebraic equations was solved for $\Delta T = -278°C$ and an outer radius to wall thickness ratio of 12.5. A total of three configurations was considered by Hyer and Cohen (1984i): $(0/90/0/90)_t$, $(90/0/90/0)_t$, and $(90_4)_t$. Additional results for different configurations were provided by Hyer and Cohen (1984ii).

For axial stresses, the agreement between the CLT and elasticity solutions was quite good. For hoop stresses, however, CLT predicted a constant stress within the 90° plies while the elasticity solution showed a linear variation of stress in these layers. Consequently, the

elasticity approach predicted the existence of compressive hoop stresses of much greater magnitude at the ply interfaces. From the CLT results, the maximum and minimum hoop stresses were of the order of 80 MPa and -80 MPa while the elasticity solution hoop stress results ranged from about 80 MPa down to about -160 MPa. (Hyer and Cohen, 1984)

CLT assumes that no radial stresses are present in the tube. The elasticity solution, however, predicted the existence of radial stresses having a magnitude of several MPa. Furthermore, the radial stress distribution was found to be quite sensitive to the stacking sequence. Depending upon the stacking arrangement, either tensile or compressive interply stresses were predicted. (Cohen and Hyer, 1984), (Hyer and Cohen, 1984)

Rousseau, Hyer, and Tompkins (1987) extended the generalized plane strain elasticity solution of Cohen and Hyer (1984) to include angle-plied lamination sequences and temperature-dependent material properties. Axisymmetric, thermally-induced stresses and strains were studied in graphite-epoxy tubes proposed for use as truss elements in the US/International Space Station. The cure temperature of the composite was taken to be the stress-free state. Residual stresses due to chemical shrinkage were not accounted for. Analytically, it was predicted that even tubes with a balanced, symmetric wall construction would exhibit thermally-induced hoop-axial shearing deformations ("due to the radial difference in location of off-axis

[angle-] plies.") (Rousseau et al., 1987) A shell-like approach would not have revealed this phenomenon due to the way in which the stiffnesses of the laminae are "lumped" together at the midplane coordinate of the laminate. (See, for example, Appendix A which illustrates how laminate force and moment resultants are expressed in terms of midplane strains and curvatures in CLT.)

Other significant results for the tube geometries and lamination sequences considered by these researchers include the following:

1. The predicted thermal twist was slightly lessened by the inclusion of temperature-dependent material properties while the predicted axial strain was 25% higher.
2. The stresses predicted in 51 x 10^{-6} m thick aluminum coatings on the inner and outer surfaces of the graphite-epoxy tubes exceeded the yield strength (approximately 75 MPa) of the aluminum alloy 6061. Metallic coatings were being considered for use in protecting against radiation, free-atomic oxygen, and excessive thermal gradients. Stresses in the coatings were due to axial and hoop deformations of the graphite-epoxy tubes considered.
3. The presence of aluminum coatings affected the sign and magnitude of stresses within the composite. Radial stresses were changed from tensile to compressive due to the coatings. Although the predicted radial stresses were small, radial compression could help deter propagation of delamination cracks.

Due to the seriousness of the thermal fatigue problem that could result from thermal twist of the tubular truss members, the experimental work of Rousseau et al. (1987) focussed mainly on this phenomenon. Eighteen specimens were tested in an environmental chamber. Using electromechanical transducers, fairly good agreement between predicted and measured twist responses was achieved. However, thermally-induced axial deformations, measured both with displacement transducers and with strain gages, were found to exceed predicted levels by a factor of three. Further investigation is required to explain this finding.

2.3 The Importance of Moisture Effects

Thus far, primary emphasis has been focussed on how thermal effects influence the residual stress state in laminated composites. In practice, moisture effects may also be of considerable importance in predicting lamina and laminate properties and behavior. Farley and Herakovich (1977) found that small, uniform moisture concentrations were beneficial in alleviating the effects of residual thermal curing stresses. Chamis et al. (1977) treated moisture and thermal effects in a mathematically similar fashion in a computer program for predicting the hygrothermomechanical response of laminated composites. Further comments are found in Appendix B.

3. Experimental Work

Setting the Context

Curing shrinkage of polyester resin in a fiberglass composite is often described as comprising two main components. The first is chemical shrinkage. This is a natural consequence of the exothermic process whereby styrene monomers crosslink among polyester molecules. The second, thermal shrinkage, occurs as polyester resin cools from the peak exotherm temperature to ambient temperature. In all of the discussions which follow, ambient temperature (25°C) will be used as the reference temperature.

The ultimate goal to which this experimental work is aimed is to be able to quantitatively describe and predict the stresses and strains induced in a fiberglass body due to the curing shrinkage of the polyester resin. The first step in accomplishing this goal is to acquire a comprehensive understanding of the changes undergone by the neat resin as it cures. Following this, the second step would be to develop a picture of the effects of resin curing shrinkage on a composite material composed of resin plus reinforcement. Here, the *in situ* effects of liquid resin transforming to a solid in the presence of obstacles (stiff reinforcing fibers) would have to be considered. Finally, the third step would involve calculating the behavior of a structure with a given geometry and composition from information on material behavior. This information is

summarized below. Possible means of addressing the various points are noted in parentheses. Several of these approaches are pursued in the body of the thesis.

Pieces of the Resin Shrinkage Puzzle

I. Behavior of the resin alone (Archimedean Density Measurements)

II. Microscopic view of the behavior of resin surrounding a regular array of fibers (Finite Element Models, Photoelasticity)

III. Macroscopic description of curing shrinkage of a laminate of a given geometry and subject to specific boundary conditions (Strain Gaging an Aluminum Mandrel Overwrapped by Fiberglass; Thermal Analogy using the computer codes CYLAN (Whitney et al., 1987), ELAS2 (Rousseau et al., 1987), and Superlam (Osborne, 1986ii))

Each of these points will be discussed in subsequent sections, but, first, it would be useful to review some of the fundamental changes which occur in neat resin during curing. Refer to Figure 9, following. It should be noted that the plots are representative of the effects which occur but do not pertain to a specified grade of polyester or to a specific volume and geometry of material.

Figure 9

Schematic of Changes in Neat Polyester During Curing
a. Temperature versus Time, b. Volume Shrinkage versus Time,
c. Stiffness Development versus Time

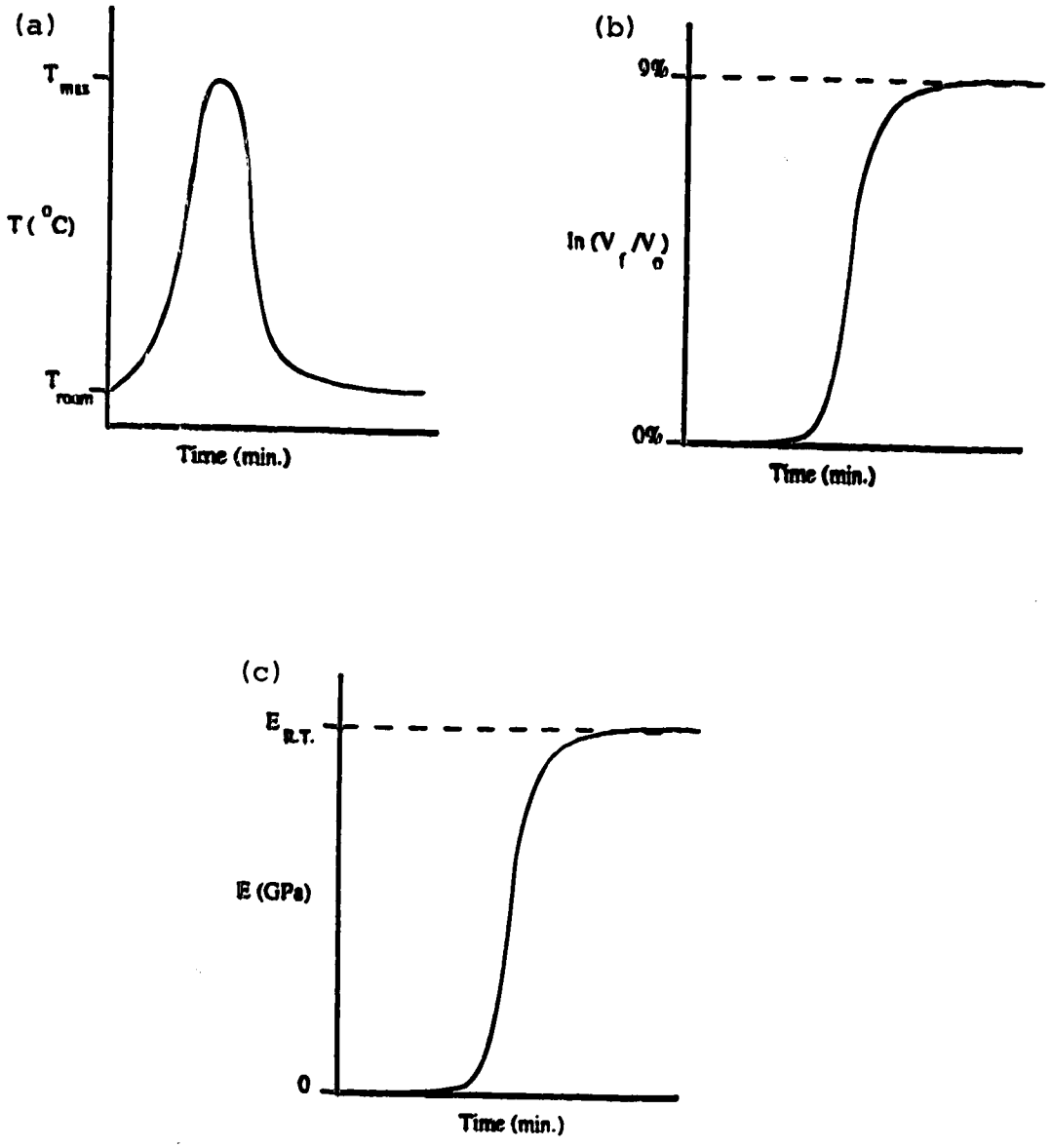

As revealed in Figure 9.a, a temperature versus resin curing time curve for polyester has a characteristic peaked shape with the maximum denoted as the peak curing temperature or as the peak exotherm. As the percentage of catalyst is increased, a shift in the curve to a higher peak exotherm and a shorter curing time is expected. The slope of the curve on the ascent towards the maximum also increases as the amount of catalyst is increased. That is, the curing reaction occurs more rapidly. Curing is essentially complete a short time after the peak exotherm is reached.

Figure 9.b shows the possible appearance of the trend in cumulative volumetric shrinkage of resin as a function of time and of percentage of catalyst. The curve has a sigmoidal shape. Very little if any shrinkage occurs prior to the onset of rapid crosslinking. Cumulative shrinkage is not arrested once crosslinking is complete due to the existence of the thermal component which comes into play as the resin cools to ambient temperature. A simple method for determining the magnitude of total volumetric shrinkage derives from the fact that a density increase accompanies the increase in degree of crosslinking. This density measurement technique is documented in a subsequent section.

Figure 9.c illustrates the development of stiffness as a function of time and percentage of catalyst. By definition, a liquid is unable to withstand shearing stresses. The first portion of the curve indicates a Young's modulus of zero and corresponds to resin in the liquid

state. As curing progresses and the resin begins to gel, its ability to resist shear stress develops. Vratsanos and Farris (1986) equate the gel point with the attainment of a non-zero modulus value. During crosslinking, the modulus increases concurrently with the increasing effective molecular weight. As the fully solidified polyester cools to ambient temperature, the stiffness increases in accordance with the observation that modulus increases with decreasing temperature.

Assuming that the temperature, shrinkage, and modulus versus time trends had been mapped out for a particular set of variables (i.e., type of polyester resin, proportion of catalyst, heating rate, and cure temperature) one would next require a scaling criterion. That is, one would need to know how information regarding a small test sample could be related to the sorts of volumes of resin that would be required in the production of a particular commercial product. In a small sample, the peak exotherm temperature would be less than in a large body where the outer portions effectively insulate the inner parts.

For a dynamic analysis of the problem, it would be necessary to carefully delineate the transient portions of the curves in Figure 9. For a static analysis, only the steady state values of the solid polyester's total volumetric shrinkage and Young's modulus are required. These data would be required to calculate the original (that is, post curing) stress state of a control volume of composite

material. To describe the relationship between the volumetric shrinkage of neat resin and the volumetric shrinkage of resin when it is part of a composite material, the composite material must be fully characterized. That is, the fraction and distribution of the reinforcement must be known and the moduli, Poisson's ratios, and thermal expansion coefficients of the composite material must be measurable or calculable. The critical issue is to discover rules for combining data on resin shrinkage with the geometric and physical data on the glass fibers and the polyester resin so as to determine how the composite material responds when the resin cures.

As a first approximation, resin shrinkage might be assumed to be isotropic. Successive developments of the resin shrinkage problem will have to address the distribution of shrinkage strains throughout a control volume and also the issue of what proportion of the shrinkage strain is stress-inducing. The analysis of the thermal component of the curing shrinkage is well-documented in the literature. It remains to separate out the chemical shrinkage component.

Appendix A shows how thermal effects may be included in CLT. Laminate midplane strains and curvatures are calculated by multiplying the inverted laminate stiffness matrix by the thermal force and moment resultants. The total strain for each layer is calculated from the midplane quantities. The residual strain is found by subtracting the free thermal

strains from the total strains. The simplest approach to dealing with the chemical shrinkage effects has been to draw an analogy with the thermal shrinkage component of curing shrinkage. This technique was suggested by Osborne (1987i).

The Thermal Analogy

The thermal analogy on the microscale (as exemplified by the finite element analysis of a single fiber and surrounding resin in Section 3.2) must be differentiated from the thermal analogy on the macroscale (as used to predict experimental strain values in Section 3.3). On the microscale, the thermal analogy involves setting the CTE of the fiber reinforcement to zero and leaving the CTE of the resin as it is. A temperature change consistent with a given amount of resin shrinkage is applied and the response of the matrix plus reinforcement is observed. The fiber and resin retain their identities, thereby preserving the microscale inhomogeneity of the composite.

In macromechanical analyses of unidirectional fiber-reinforced composites, the distinction between the matrix and fibers is "smeared out" to simplify the mathematics. Properties of the reinforcement and the matrix are averaged using the equations of micromechanics (see, for example, program INPUT in Appendix D), and the composite is treated as a homogeneous, orthotropic body. When the thermal expansion properties are averaged, the contribution of the fibers is set to zero for purposes of the thermal analogy.

The standard linear elastic thermomechanical stress and strain analysis is then carried out using the modified lamina thermal properties. As a simple illustration, consider a unidirectional planar lamina composed of 50 v/o glass and 50 v/o polyester. In a two-dimensional analysis, the CTE's for the principal material directions of the lamina are calculated as follows: (Powell, 1983)

$$\alpha_1 = (V_f E_f \alpha_f + V_m E_m \alpha_m)/ (V_f E_f + V_m E_m) \quad [15]$$

$$\alpha_2 = V_f \alpha_f + V_m \alpha_m + V_f \nu_f \alpha_f + V_m \nu_m \alpha_m - (V_f \nu_f + V_m \nu_m)\alpha_1 \quad [16]$$

The pertinent data for this example are

$$V_f = V_m = 0.5$$

$$E_f = 72 \text{ GPa and } E_m = 3.4 \text{ GPa}$$

$$\nu_f = 0.25 \text{ and } \nu_m = 0.35$$

$$\alpha_f = 5 \times 10^{-6} \text{ m/m/K and } \alpha_m = 63 \times 10^{-6} \text{ m/m/K}$$

Therefore, $\alpha_1 = 7.6 \times 10^{-6}$ m/m/K and $\alpha_2 = 44.5 \times 10^{-6}$ m/m/K That is, if the lamina is subjected to a uniform temperature change, the ratio of transverse thermal strain to longitudinal thermal strain is 5.9:1. In executing a thermal analogy, the CTE of the fiber material is set to zero and the resulting lamina strain for an imposed temperature change is taken to be resin densification strain. To simulate the effect of, for example, 3 linear % shrinkage of the matrix, a temperature change of -476 K (i.e., $(-0.03 \text{ m/m})/(63 \times 10^{-6} \text{ m/m/K})$) would be applied to the composite. The densification coefficients in the principal lamina directions, as calculated from the above data are

$f_1 = 2.8 \times 10^{-6}$ m/m/K and $f_2 = 42.1 \times 10^{-6}$ m/m/K.

In a CLT analysis, these quantities receive the same mathematical treatment as CTE's. The ratio of the transverse to the longitudinal curing strain is 15:1. That is, the thermal analogy for the above example suggests that 94% (15/16 x 100%) of the free chemical shrinkage will occur in the transverse directions within the unidirectional lamina.

The complications associated with describing and predicting chemical curing effects are the incentives to use a thermal analogy as a first approximation. However, the assumptions implicit in the analysis techniques used will be carried through into the thermal analogy. For example, linear elastic material behavior was assumed in all of the computer programs used. This is a very rough approximation, for, as we have seen, some densification occurs while the resin is semi-solid. The possibility that some of the chemical shrinkage-induced residual stresses are able to relax away means that perhaps only a fraction of the total volumetric shrinkage will ultimately lead to stresses.

3.1 Neat Resin Curing Shrinkage: Archimedean Density Tests

The preliminary characterization of the curing behavior of neat polyester resin comprised a series of resin shrinkage tests. The objectives of the tests were to determine the volumetric shrinkage of polyester resin as a function of time and to determine whether gelation of the resin occurred prior to the peak curing exotherm. Since the

preceding data may be influenced by the amount of catalyst used, this parameter was held between 0.25% and 0.28% for all of the experimental work.

Total volumetric curing shrinkage derives primarily from density changes of resin during curing but is also affected by mass loss (due to volatilization, for example). In the present work, attention focussed on the time-dependent density change. This was easily determined by suspending a small quantity of catalysed resin in a liquid of known density and by following the change in the apparent mass of the resin during the curing reaction. Hence the term "Archimedean" to describe this series of tests.

Raw Materials

Two types of polyester resin, both of which are Fiberglas Canada products, were studied. The first, Vibrin 1029, is a general-purpose commercially-available laminating polyester. Although the formulation is proprietary, it is known that Vibrin 1029 contains 35% to 45% styrene; the balance is made up of maleic anhydride, propylene glycol, promoters, and other additives. The second, Vibrin 1030, is chemically similar to Vibrin 1029 except for the addition of a small quantity (less than 0.2%) of wax. The wax migrates to exposed surfaces during curing. By suppressing oxygen inhibition of crosslinking, a monomolecular layer of wax prevents tacky, undercured surfaces. (Selley, 1987) MEKP was used to catalyse both types of resin. Fiberglas Canada

indicates that their work has shown no difference in shrinkage behavior between Vibrin 1029 and Vibrin 1030. (Osborne, 1989)

The density of Vibrin 1029 at 22°C as measured using an Anton-Paar densitometer is 1110 kg/m^3. The Anton-Paar densitometer is shown, following, in Figure 10. Due to the difficulties associated with removing wax from the densitometer, the density of Vibrin 1030 at 22°C was determined by weighing an accurately known volume of resin. Three different vessels were used to provide the known volume: a 10 mL syringe, a 50 mL volumetric flask, and a 50 mL pycnometer. The average density from these determinations is 1100 kg/m^3. These density values agree with the expectation that chemically similar resin solutions should have similar densities.

Figure 10

Anton-Paar Densitometer

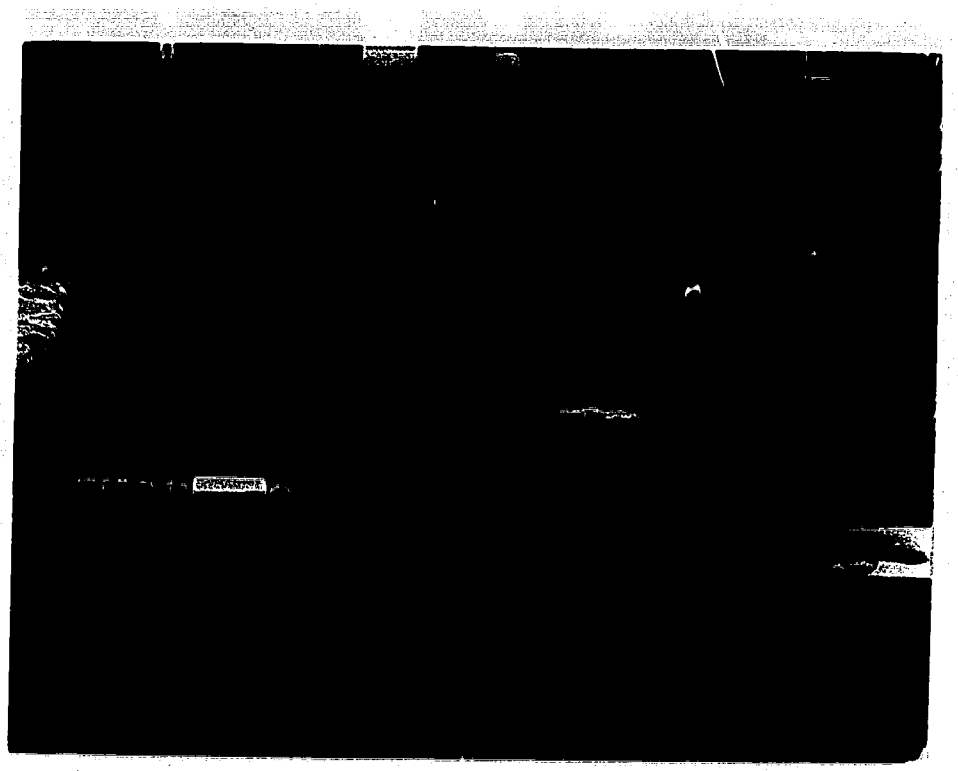

Apparatus and Techniques

The first set of tests began with the determination of the apparent mass of Vibrin 1029. In the first trial, the resin was held within a small glass container. This proved satisfactory for keeping the mass of the system constant, but shrinkage of the resin away from the sides of the container during curing made it difficult to determine the apparent mass of the polyester resin as a function of time. In subsequent trials, both with Vibrin 1029 and Vibrin 1030, small, polyethylene Zip Lock bags were used to contain the resin. Although such bags could act as semi-permeable membranes, thereby allowing mass to enter or leave the system, the problem of gaps opening up between the resin and its container was eliminated.

In the Vibrin 1029 trials, the bags were suspended from the hook of a Sartorius 2003 MP1 digital electronic balance. The suspended pan was removed from the balance in order to accommodate the water bath within the balance enclosure. A small weight was used to replace the mass of the pan.

Using Archimedes' principle, the expected mass of a bag containing freshly catalysed resin is given by

$$m_a = m_s - \rho_l V \qquad [17]$$

m_a = the apparent mass of the resin, bag, and wire

m_s = the mass of the resin, bag, and wire

ρ_l = the density of the suspending liquid

V = the volume of the resin, bag, and wire

$$V = m_{res}/\rho_{res} + m_{bag}/\rho_{bag} + m_{wire}/\rho_{wire} \quad \ldots\ldots\ldots [18]$$

In general, the volume of the submerged wire was negligible compared with the volumes of the resin and plastic bag. Comparing the calculated and measured apparent masses at the start of each run, it was found that the measured value was 1.5% to 1.8% smaller than expected. Entrainment of air in the bag along with the resin would increase the submerged volume of the system, thereby lowering its apparent mass. However, even with close attention paid to minimizing the amount of air, the above mentioned discrepancy persisted.

A second set of shrinkage tests was pursued using a different apparatus to determine if the systematic errors could be eliminated. The waxed version of the all-purpose polyester resin was used for the second set of tests.

Four trials were completed using the Vibrin 1030 resin. A Sartorius E 5500 S digital electronic balance was mounted on bricks and bags of resin were hung from a hook attached to the underside of the balance. This is shown, following, in Figure 11. The buoyant medium, an ethanol-methanol-water mixture (ρ = 810 kg/m^3, as measured using an Anton-Paar densitometer), was situated in a one-litre container beneath the balance. This mixture was chosen over water due to its lower density. Increasing the spread between the density of the resin and that of the liquid bath resulted in larger apparent masses. In the four trials using Vibrin 1030, the error in the original apparent mass ranged from -0.2% to

-0.7%. This range of error was deemed more acceptable than the previous range. Thus, only qualitative observations on the Vibrin 1029 runs will be presented, following. Both qualitative and quantitative results will be presented for the Vibrin 1030 runs.

Results

In the trials using Vibrin 1029, the apparent mass began to climb rapidly about one hour after the resin was catalyzed. In the Vibrin 1030 trials, the apparent mass began to increase rapidly about 120 minutes to 150 minutes after catalysis of the resin. One possible cause of the difference between these time ranges could stem from the different heat transfer coefficients between resin and water and between resin and alcohol. For each of the Vibrin 1030 trials, the final resin density (as determined 24 hours to 72 hours after the resin was catalysed) was 1200 kg/m^3. See Table 1, following.

Figure 12 illustrates the sigmoidal shape of the change of apparent mass with time curve. Control samples held in alcohol were observed to gel and become rubbery well in advance of the steeply sloped portion of the curve. For example, gelation was observed in the Vibrin 1030 control samples between 110 minutes and 120 minutes. By the time the middle of the oblique portion of the curve was reached, the control samples were rigid to the touch. The curve shown in Figure 12 is based on data from Run 3 using Vibrin 1030.

Data for all of the runs plot up in the same basic shape.

The apparent mass drops slightly between 50 minutes and 150 minutes in Figure 12. Chemical and thermal effects oppose one another during the heating portion of the curing cycle. The drop in apparent mass could reflect the thermally-induced drop in density temporarily overriding the increase in density due to crosslinking. It should be noted that, over the course of the experiment, the drop in density due to thermal expansion of the crosslinking resin is offset by the increase in density due to thermal contraction of the fully crosslinked resin. The two effects would exactly cancel one another if the CTE did not vary as the resin changed state and temperature. In addition to the above, thermal effects are small in these experiments as compared to thermal effects encountered in fabricating fiberglass composites. This is due to the heat capacity of the liquid medium in which the curing resin was suspended and the improved heat removal provided by the set up. Typically, the alcohol temperature fluctuated only 4°C between time zero and the time of the peak exotherm. Because of the above, any thermal component of the densification shrinkages listed in Table 1 is assumed to be negligible.

For the run of Figure 12, the peak exotherm was attained on the range of 150 minutes to 200 minutes. Temperature measurements were taken by periodically stirring the liquid in which the control samples were placed and then measuring the temperature of the liquid. It would be

preferable, in subsequent work, to know the actual resin temperature during curing. This could be accomplished by inserting a thermocouple into the control sample subsequent to gelation, or by sealing a thermocouple within the sample prior to immersion in the alcohol bath.

Figure 11

Apparatus for Archimedean Density Tests

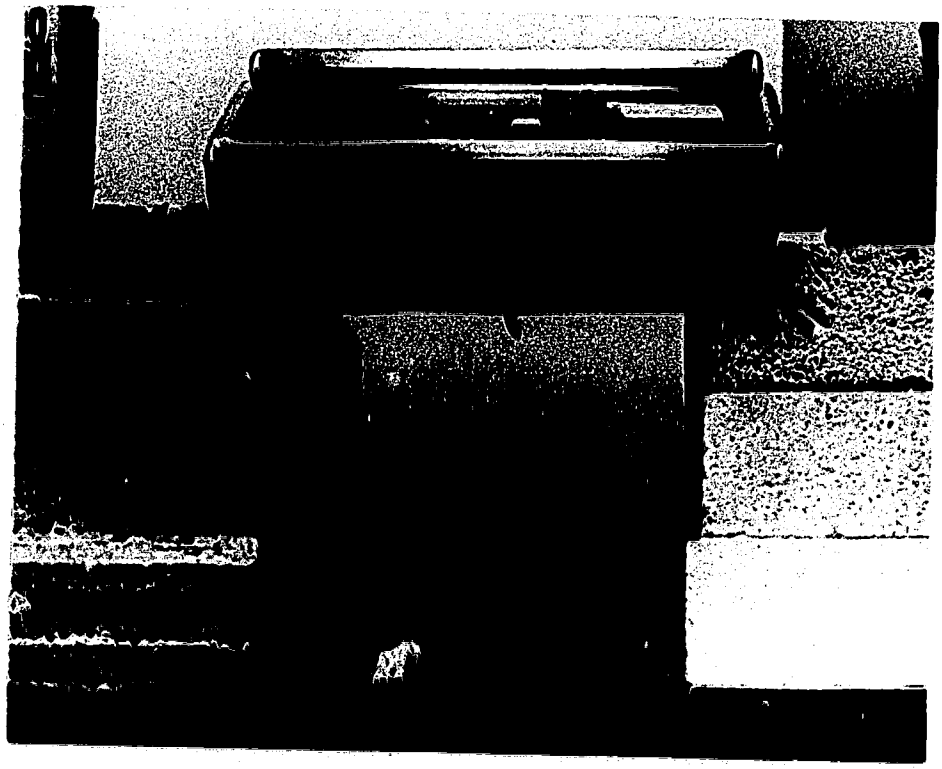

Figure 12

Apparent Mass Versus Time Curve for Neat Resin

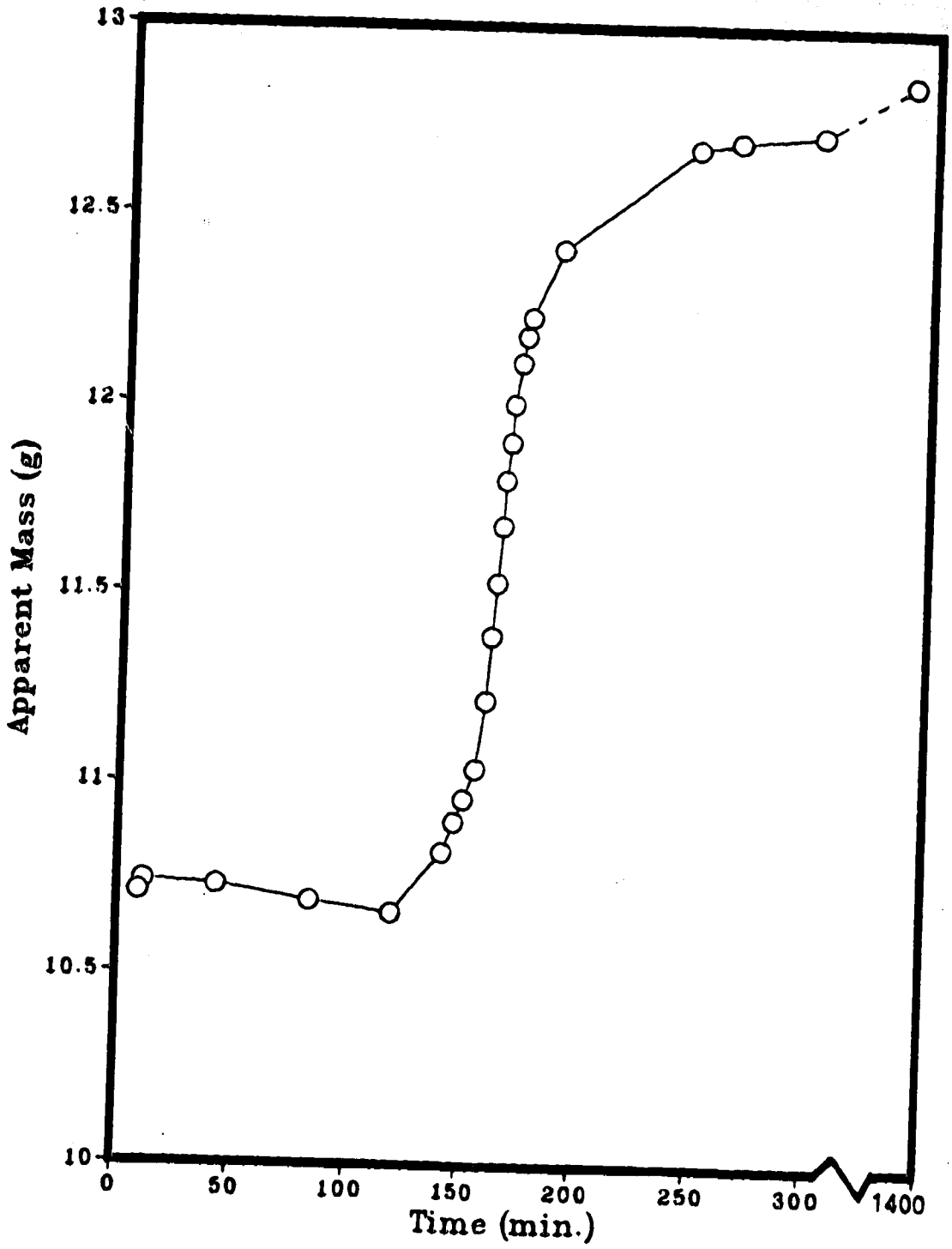

Table 1

Shrinkage Results Using Vibrin 1030

Trial	$m_{o,res}$	$m_{f,res}$	% catalyst	ρ_f	Densification Shrinkage
1	40.37	38.74	0.25	1200	8.7%
2	44.51	43.25	0.25	1200	8.7%
3	40.09	39.01	0.27	1200	8.7%
4	46.71	45.79	0.27	1200	8.7%

Whether control samples were placed in air, water, or alcohol, some loss of resin was observed. From the above table, between 2% and 2.5% mass loss was typical. Judging from the odor of the specimens, it would appear that styrene accounts for a portion of the lost mass. The density of the alcohol was tested after a specimen had been submerged in it for 24 hours and no significant change was noted. This is likely due to the fact that of the order of a gram of resin was lost in a litre (810 g) or more of alcohol. Some stickiness remained in the extremities of the sample bags even after a day or two. The curing reaction may have been much slower in the corners of the resin mass. Some incompletely cured resin would have been lost when the solid resin chunk was removed for the final density determination. Still, the resin caught along the seams of the bags was typically only a few tenths of a gram.

Since the mass of resin lost due to natural curing process effects was not explicitly determined from the experiments, the densification component of true volumetric shrinkage is given in the above table. The mass loss

component can be calculated as $\ln(m_f/m_o)$. This would be added to the densification component in Table 1 to find total true volumetric curing shrinkage, according to the following formula:

$$\ln(V_f/V_o) = \ln(m_f/m_o) - \ln(\rho_f/\rho_o) \quad [19]$$

(By contrast, the engineering volumetric shrinkage is calculated as shown below:

$$\Delta V/V = (m_f\rho_o/m_o\rho_f) - 1 \quad [20]$$

The engineering densification component is -8.3% for all trials using Vibrin 1030.)

Figure 12 presents the relationship between apparent mass and time during the curing of Vibrin resin. Ideally, the plot of cumulative volume shrinkage versus time would also be available. If the resin temperature, average alcohol temperature, and resin mass were known for each point in time, the apparent mass versus time curve could be transformed to a true shrinkage versus time curve using the following formulae:

$$\rho(t,T) = \rho_{alc}(T)/(1-m_a(t)/m(t)) \quad [21]$$

$\rho(t,T)$ is the density of the resin at a given time and temperature

ρ_{alc} is the density of the alcohol at a given temperature

m and m_a are the mass and apparent mass of the resin at a given time. These

quantities are determined from the measured mass and apparent mass of the resin, bag, and wire.

Having calculated resin density for each point in time, true volumetric shrinkage could be obtained from the following:

$$\ln(V(t, T)/V_o) = -\ln(\rho(t,T)/\rho_o) + \ln(m(t)/m_o)...[22]$$

As the resin densified and shrank in volume, a gap tended to develop below the seam of the bag. Over time, alcohol was drawn into the bag through imperfections in the closure. To avoid this, the apparent mass in alcohol was monitored for three to four hours, after which the bag was removed and allowed to complete its cure in air. It should be noted that by the time the bag was withdrawn from the alcohol bath, the resin was solid and cool to the touch and its density had reached 1190 kg/m^3 (almost the maximum value). To perform a final measurement, the polyester pellet was removed from the polyethylene bag. Wire was used to suspend the solid pellet in the alcohol. The mass of the pellet was easily and directly measured. The density of the polyester was calculated by dividing the mass by the volume as calculated using the following formula:

$$V_{res} = (1/\rho_{alc})\ (m_{res} - m_a + m_{wire})\text{.....}[23]$$

3.2 Micromechanical Analysis of Curing Shrinkage Using the Finite Element Method

Having considered the magnitude of the chemical curing shrinkage of Vibrin resin in the absence of constraints, attention will next focus upon the development of microresidual stresses which evolve as Vibrin resin crosslinks in the presence of stiff glass fibers. "Knowledge of the internal state of stress...contributes to the evaluation of average (macroscopic) response and...provides the basis for understanding failure modes and establishing failure criteria." (Marloff and Daniel, 1969)

Photomicrographs reveal that the microcracks responsible for the characteristic opaque appearance of filament-wound composites run predominantly transverse to the fibers within a lamina. (Fiber-direction cracks caused by high shearing stresses at fiber ends are not significant in continuous-fiber composites.) Osborne (1987), Hull (1981), and Plueddemann (1974) all present photomicrographs showing transverse cracks. (See, for example, Figure 3.) Tensile hoop stresses within the matrix and strain magnification effects in the matrix are instrumental in producing such cracks. It is interesting to note that the cracks caused by curing shrinkage (as in Figure 3) closely resemble those due to loading a fiberglass sample to failure (as is the case for the photos presented by Hull, p. 152, 1981).

Establishing the Parameters for the Analysis

The most suitable scale for studying resin shrinkage cracks is of the order of the size of the microconstituents, namely the fiber diameter and the resin pocket size. The fiber diameter is typically of the order of 10×10^{-6} m while the extent of the resin-rich zones is sensitive to manufacturing variables and can reach several fiber diameters in commercial composites.

Early photoelastic studies of arrays of fibers in a thermosetting resin matrix attempted to characterize the magnitude and distribution of curing shrinkage stresses on a micro scale. Due to the mathematical and statistical complexities associated with trying to analyse a truly random array of fibers, such studies tended to concentrate on idealized arrangements such as square and hexagonal arrays. A portion of a regular square array is shown in Figure 13.a. In addition, a portion of a single, uni-directional lamina was usually considered so as to avoid introducing complicated boundary conditions. Small strains, linear elastic behavior of both fibers and matrix, and temperature independence of elasticity constants were assumed.

SAPIV, a simple finite element package, (Bathe et al., 1974) was chosen to execute an analysis of a regular square array within a fiber composite. It was hoped that the use of the thermal analogy in a finite element analysis would

generate results similar to the photoelastic results presented by Koufopoulos and Theocaris (1969) and also provide information to tie in the results of the experimental work with the objective of developing a mathematical tool for predicting the effects of chemical curing shrinkage. It should be noted that this is a stiffness analysis. Failure mechanisms and processes were not addressed in this work.

The fundamental element in a square array consists of a single fiber and surrounding resin, as shown in Figure 13.b, following. As a simplification, strains in the y-z plane were considered and the x-direction strains were assumed to be negligible. The motivation for pursuing this plane strain analysis is twofold. Firstly, it was desired to formulate a two dimensional problem for the first attempt at the analysis. Secondly, based on the nature of the material, plane strain is a reasonable first approximation. Logically, localized curing shrinkage deformations should be most pronounced in resin-rich directions. The high axial stiffness of the glass fibers relative to the matrix suggests that the strains in the fiber direction will be small compared with transverse (y- and z- direction) strains. It is recognized that, in practice, compressive axial curing stresses can lead to detrimental effects such as fiber buckling.

Figure 13

Geometric Details for Finite Element Analysis

a. Cross Sectional View of a Square Array of Fibers in Resin

b. Blow-up of an Individual Cell in the Square Array Showing One Symmetry Element

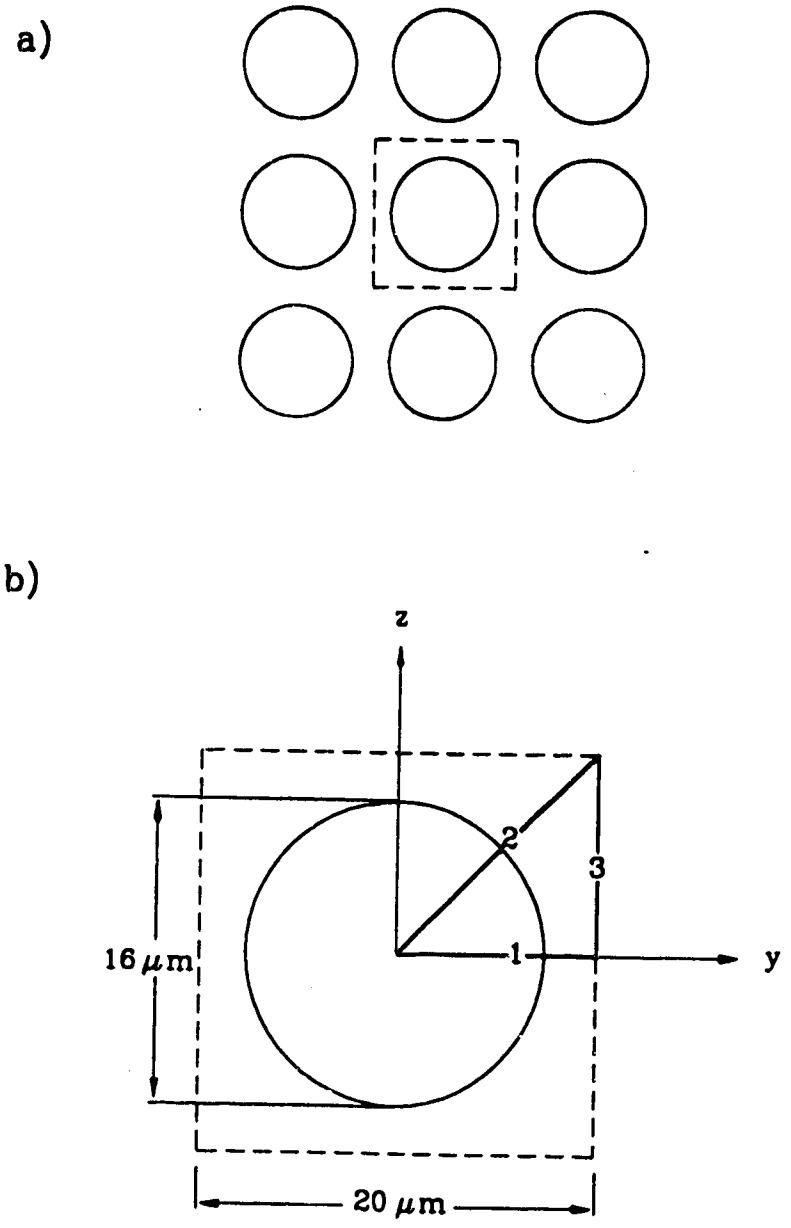

Figure 14

Discretized Finite Element Mesh of a Symmetry Element

a. Showing Element Numbering,

b. Showing Boundary Element Numbering

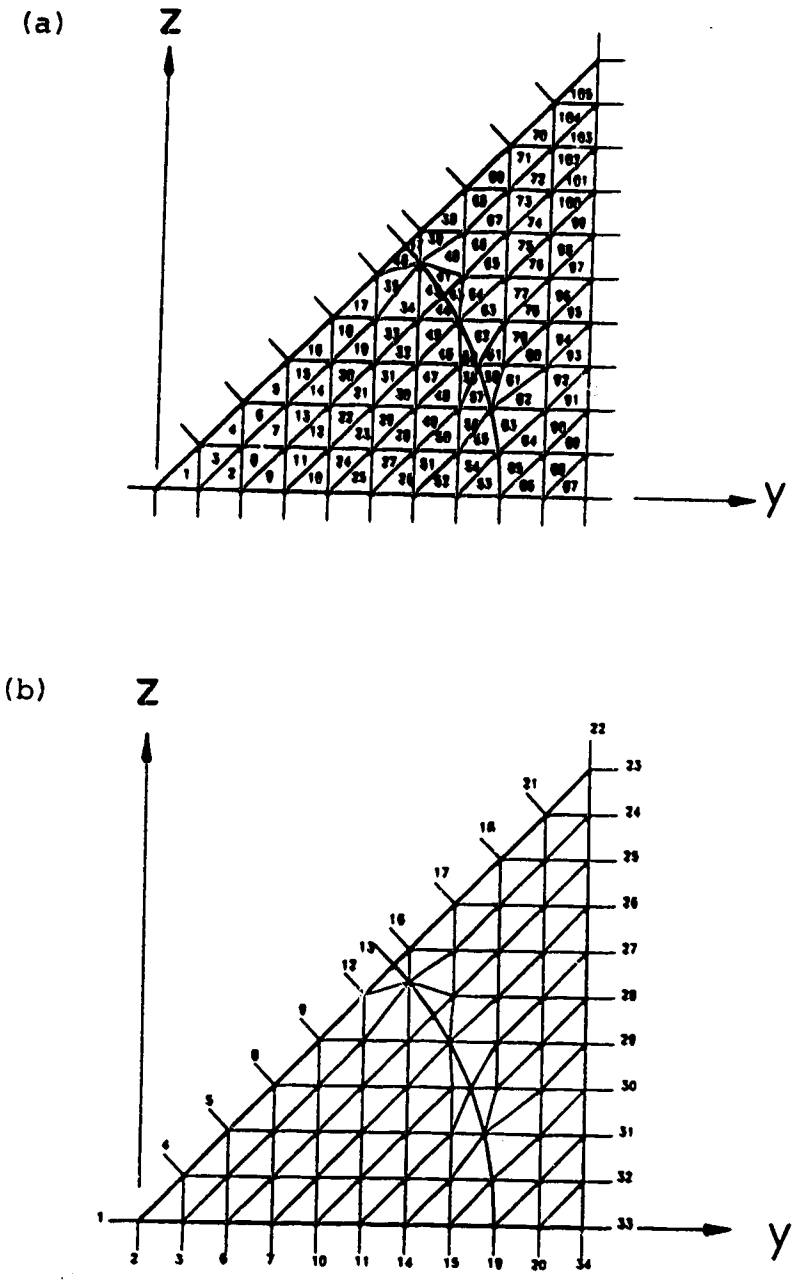

A fiber diameter of 16×10^{-6} m and a cell dimension of 20×10^{-6} m were chosen. This geometry, as illustrated in Figure 13.b, results in a fiber volume fraction of about 0.5 and yields convenient units for inputs to the computer program. As well, a fiber volume fraction of 0.5 falls within the range of typical values for filament-wound fiberglass products.

The basic square array element may be subdivided by lines of symmetry into 8 portions. The analysis of one such subsection is mathematically equivalent to analysis of an entire square array element. The wedge shown in Figure 13.b was discretized to produce a finite element mesh having 103 nodes. A total of 105 triangular elements and 34 boundary elements resulted. Figures 14.a and 14.b show the numbering of the triangular and boundary elements, respectively. The boundary elements' stiffnesses were taken to be about a million times the magnitude of the largest term in the element stiffness matrix for glass.

The boundary elements were supplied along the edges labelled 1, 2, and 3 in Figure 13.b in order to enforce the required boundary conditions. Edges 1 and 2 are roller-type boundaries coincident with the symmetry lines used to subdivide the original square array element. No forces are permitted parallel to edges 1 and 2 and no displacements are permitted perpendicular to these edges.

The boundary conditions to be supplied along edge 3 are somewhat more complicated than the above. Referring to the

three-dimensional finite element analysis pursued by Rohwer and Jiu in their study of edge effects in fiber composites (1986), the necessary conditions for edge 3 are as follows. The edge must remain straight (and parallel to its original orientation), displacements normal to the edge must not be prevented, and the normal force resultant along the edge must be zero. The first two conditions were met by specifying equal applied displacements for each nodal point along edge 3. The final integral condition was satisfied iteratively by perturbing the edge 3 displacement until the sum of the y-forces along edge three was equal to zero.

Details of the Computer Runs

A preliminary analysis of this finite element problem comprises several computer runs. Appendix C contains sample data files and a listing of the outputs for which graphical results are presented, following, in Figures 15 through 18. The first run constitutes a test case to be used for comparison purposes. In the test case, the physical division of the mesh was retained, but only one material was specified. A uniform temperature change was applied, as was an arbitrary uniform displacement (-0.125×10^{-6} m) along edge 3. From the nature of the inputs, uniform stress outputs were expected. The uniformity of the stresses throughout the mesh is a measure of the confidence which can be placed in the results of the other runs. Severe stress gradients, which are most likely to occur in the vicinity of

the fiber matrix interface, would indicate that the mesh is not sufficiently refined.

As expected, the results of the test run show fairly uniform stresses, except in the vicinity of the fiber-matrix interface, where the division of the mesh becomes less regular. The centroidal in-plane principal stresses ranged from 234.77 MPa to 234.98 MPa, while the stress acting on the y-z plane ranged from 266.33 MPa to 266.44 MPa. The lowest stress levels were present in element 36 and the highest levels were present in element 39.

The second run is analogous to a shrink fit situation. No boundary elements are employed to restrain the elements along edge 3. The resin is allowed to shrink freely onto the glass fiber under the imposed temperature change. The output from this run shows the position the resin would assume if it were not influenced by surrounding material. The resin displacement profile along edge 3 shows a smooth gradation from -0.224×10^{-6} m at the top right hand corner of the mesh to -0.127×10^{-6} m at the lower right hand corner of the mesh. This is shown in Figure 15, following.

The average displacement corresponding to the free shrinkage displacement profile was determined by calculating $\int \Delta_y dz / \int dz$ along edge 3 using Simpson's rule. This value, -0.181×10^{-6} m, was used as the imposed displacement for the third run. In run 4, an imposed displacement of -0.17×10^{-6} m was applied to edge 3.

For runs 3 and 4, the stresses at the 11 nodes defining edge 3 were calculated by averaging the y-direction centroidal stresses of the "nearest neighbor" elements of each node. Then, using Simpson's rule, the y-direction stresses along edge 3 were integrated with respect to the z-coordinate. (The mesh is of unit thickness in the x-direction.) The values of the integral were -164 N/m and 33 N/m for runs 3 and 4, respectively. Linear interpolation between these two results suggests that -0.1718×10^{-6} m should be used as the next trial displacement. Eventually, a displacement of -0.1717×10^{-6} m (which yielded a force resultant of -2 N/m) was chosen as the required displacement to approximately satisfy the integrated boundary condition along edge 3.

In Section 3.1, polyester resin was found to shrink approximately 9% by volume upon curing. If a body composed wholly of resin shrinks 9%, then a body containing half polyester and half glass would be expected to shrink 4.5%. This assumes that the glass fibers do not alter the total shrinkage of the crosslinking resin and that no external constraints are operative.

If shrinkage is uniform, then 4.5% volume shrinkage corresponds to 1.5% shrinkage in each principal direction. If a condition of plane strain exists, 2.25% shrinkage would be expected in each of the principal in-plane directions. The average displacement from the shrink fit case mentioned above corresponds to 1.81% linear shrinkage in the square

array element. This indicates that the presence of reinforcement provides an internal constraint to resin shrinkage. Since one of the boundary conditions requires that a uniform net displacement occur on edge 3 of the mesh, it is natural to choose a displacement value on the range of zero to -0.181×10^{-6} m. The closer the value is to zero, the greater the degree of external constraint to resin shrinkage which is built into the analysis. An imposed displacement of zero indicates total restraint and would lead to the prediction of very large tensile stresses in the resin elements. However, the preceding discussion revealed that all of the stated boundary conditions are met for only one displacement (approximately -0.1717×10^{-6} m) within the range of possible displacements.

Figures 16 and 17 show stresses along edges 1 and 2 of the wedge-shaped region delineated in Figure 13.b. For the most part, compressive stresses exist within the fiber elements and tensile stresses are present in the matrix elements. The radial stress along edge 1, however, becomes increasingly compressive towards the matrix end. In Figure 17, the hoop stress curve shows a sharp jump in the stress level upon moving from the glass into the polyester elements.

The tensile strength of general purpose polyester ranges from 40 to 90 MPa; the compressive strength ranges from 90 to 250 MPa. The shear strength is typically less than 100 MPa. The tensile strength of E glass is typically

within the range of 1400 to 2500 MPa. (Hull, 1981) All of the predicted stresses are well below the strength of E glass. Thus, attention will be focussed on the weaker matrix material. The shear stress levels within the matrix elements are below 100 MPa in all of the figures. The hoop stresses within the polyester elements along edges 1 and 2 approach or exceed the tensile strength of the material. As well, the matrix compressive stresses along edge 1 fall within the failure stress range quoted above. Stress levels are especially high along the radial ray in which the fibers have the highest linear density (that is, along edge 1). This direction also happens to be that in which the finite element mesh is stiffest.

Figure 15

Free Shrinkage Displacement Profile of Edge 3

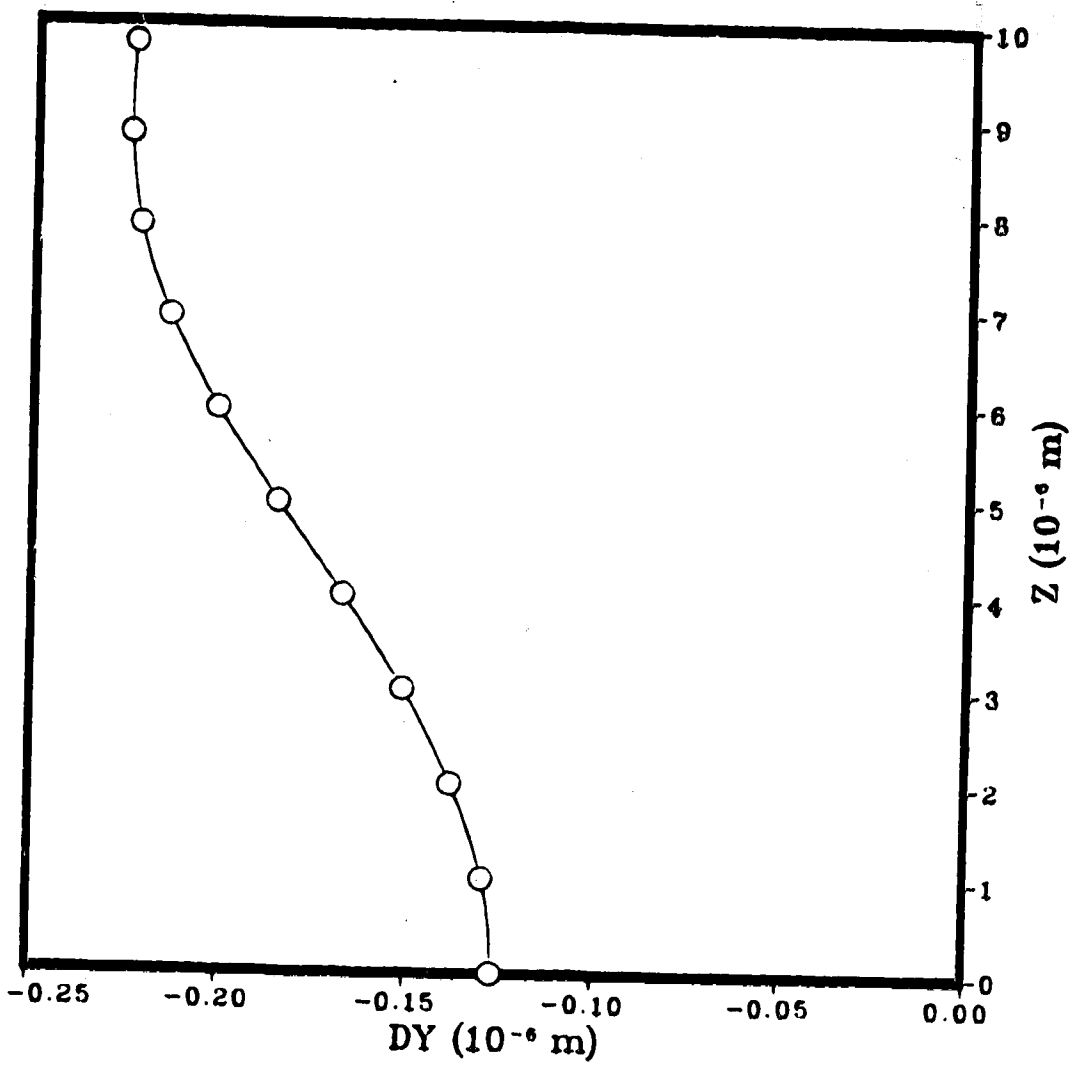

Figure 16

Stresses Along Edge 1 for an Applied Displacement of -0.1717×10^{-6} m Along Edge 3

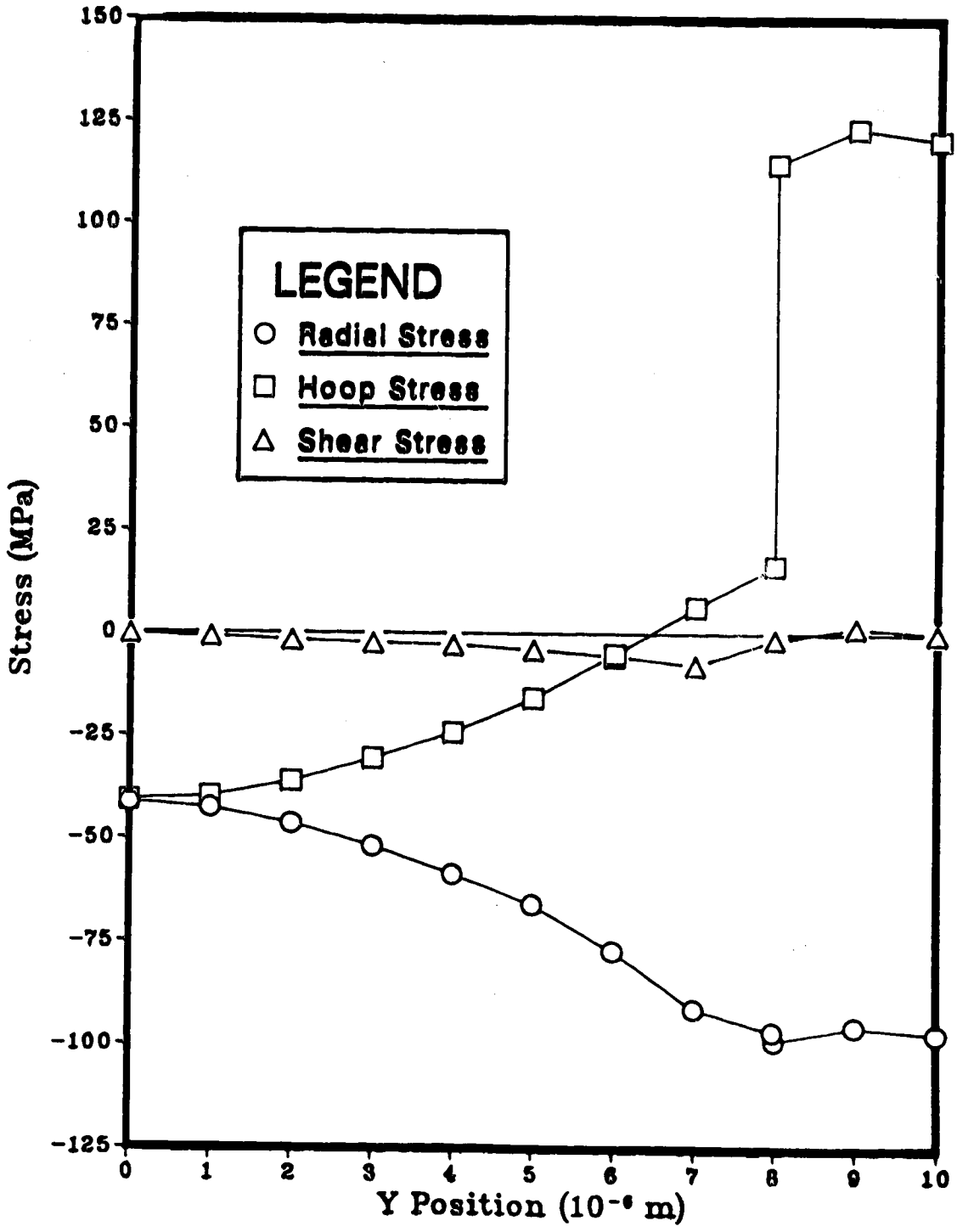

Figure 17

Stresses Along Edge 2 for an Applied Displacement of -0.1717×10^{-6} m Along Edge 3

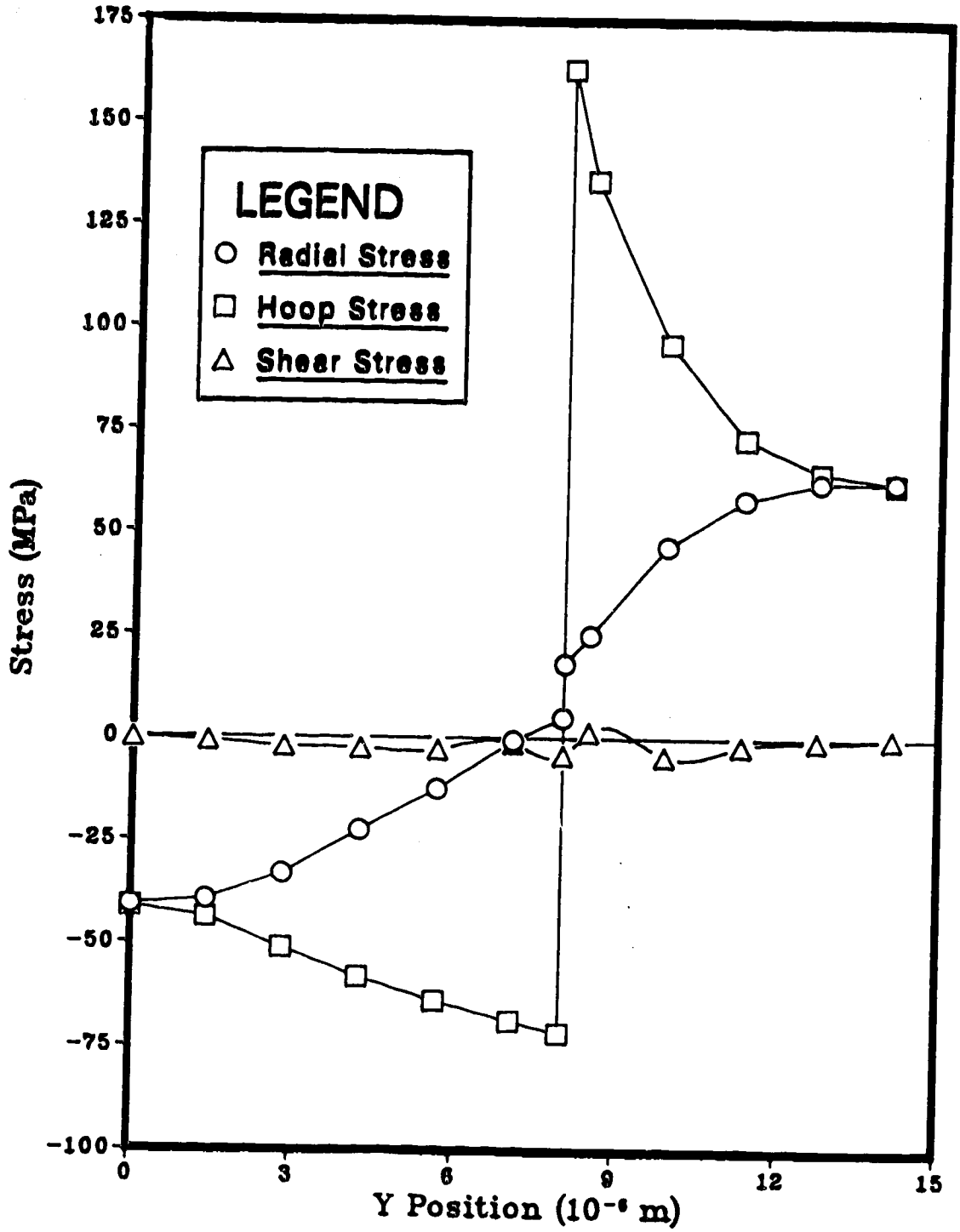

Figure 18

Stresses in the Vicinity of the Fiber-Matrix Interface for an Applied Displacement of -0.1717×10^{-6} m Along Edge 3

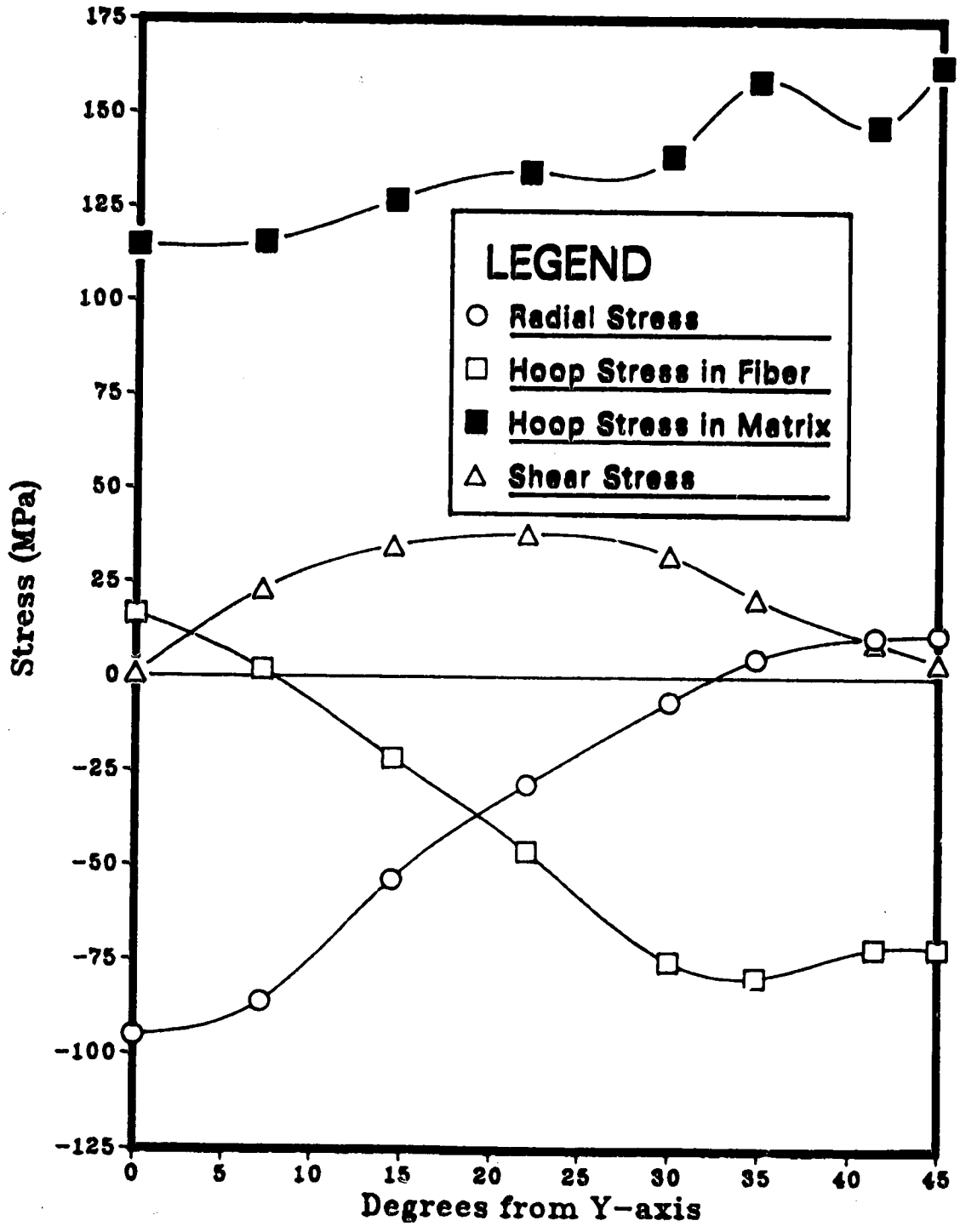

The stresses acting within the reinforcement and matrix elements near the interface are shown in Figure 18. Again, predominantly compressive stresses persist in the reinforcement. Radial stresses in the matrix change character from tensile near edge 2 to compressive near edge 1. The matrix hoop stresses are tensile along the whole of the interface. As well, it should be noted that shear stresses assume much higher levels than in the preceding plots, both in the matrix and in the reinforcement.

Comparison with Literature Results

The literature contains many studies of microresidual stresses in regular arrays of fibers in thermosetting resin matrices (e.g., Marloff and Daniel, 1969) Unfortunately, few studies look beyond thermal effects. By comparison, Koufopoulos and Theocaris (1969) attempted to remove differential thermal contraction effects in their study of curing shrinkage stresses in a square array of unplasticized epoxy fibers in a plasticized epoxy matrix. They suggested that it is the amount of resin shrinkage and the ratio of the fiber modulus to the changing resin modulus which controls the residual stress distribution in a square array.

Figure 6 shows the geometry of the test region considered by Koufopoulos and Theocaris. Segments PBA and PCO and arc BC in Figure 6 are equivalent to edges 1 and 2 and the interface, respectively, in the preceding finite element analysis. Koufopoulos and Theocaris found

compressive radial stresses between points A and B and tensile or compressive radial stresses at point C. Tensile stresses were more likely for low V_f and high E_f/E_m. The magnitudes of these stresses increased with increasing fiber content and modulus ratio until the stresses were large enough to initiate cracking. In the finite element analysis, compressive radial stresses were found in the resin along edge 1, and these were sufficiently large to initiate interface cracks. From Figure 17, it may be seen that the hoop stress curve shows a sharp jump into the tensile regime at a location equivalent to point C in Figure 6. Tensile hoop stresses were also predicted for point C by the finite element analysis.

The stress state at point O in Figure 6 (or, equivalently, the final data points of the curves in Figure 17) is biaxial tension according to Koufopoulos and Theocaris. The finite element result show that both the hoop and radial stresses are of the order of 60 MPa and the shear stress is negligible at point O.

3.3 Macro Shrinkage Analysis: Strain Gaging Experiments

Only when constrained do chemical and thermal shrinkage lead to stresses. Constraint can exist both on the micro scale (due to the presence of stiff reinforcing fibers, for example) and on the macro scale (due to geometric factors, such as the presence of an underlying layer, for example). Both micro and macro effects are invoked in the fabrication of filament-wound fiberglass tubes. The regions of opacity caused by curing shrinkage effects often become apparent prior to removal of the finished product from the mandrel.

Thus, the motivation for studying filament-wound fiberglass tubes is due not only to the wide range of applications for such structures, but also to the fact that the fabrication process interacts with the resin shrinkage phenomena we wish to study. The experimental scenario in experiments 1 and 2 was therefore taken to consist of a number of hoop windings of fiberglass on an aluminum mandrel. This scenario is readily amenable to analysis by three available computer programs. (Further details on these programs are available in Appendix D.) The exclusive use of hoop windings greatly simplified the nature of the apparatus required to produce lab-scale filament-wound tubes. For balance and comparison, Experiments 4 and 5 focussed on cast polyester tubes. Experiment 3 was also an all-polyester run but has been deleted. Leakage of resin from the enclosure rendered the strain gage readings void. The raw materials and experimental apparatus for each set of experiments will

be outlined, in turn, after discussing the expected results.

Thermal Analogy Predictions

Neat resin shrinkage tests (detailed in Section 3.1) indicated that Vibrin resin catalysed at a rate of 0.25% to 0.27% displays on the order of 9 v/o shrinkage. Since linear shrinkage in one of the three principal coordinate directions is a third of the volumetric shrinkage, the thermal analogy for this system involves applying to the laminate a temperature change corresponding to 3% linear resin shrinkage. For polyester resin having a CTE of 63 X 10^{-6} m/m/K (35 X 10^{-6} in/in/°F) the pertinent temperature change is -476°C (-857°F).

Table 2, below, is a compilation of mandrel surface strains predicted by the three available computer programs for tubes having wall thicknesses of 7.62 mm (0.3 in). The first set of strains relates to a hoop-wound laminate laid up on an aluminum mandrel while the second set of strains derives from the scenario of an unreinforced resin tube cast surrounding an aluminum mandrel. Since the thermal analogy is intended to explore the effects of chemical curing shrinkage, only the shrinkage capacity of the resin was retained. That is, the CTE's of both the aluminum mandrel and the fiber reinforcement were set to zero in executing this macro scale thermal analogy.

Table 2

Thermal Analogy Strains at Inside of Mandrel

* Resin-containing layer thickness = 7.62 mm (0.3 inches)
** Strains are given in microstrains

Program	Fiberglass, V_f=0.50		Pure Resin	
	ϵ_x	ϵ_θ	ϵ_x	ϵ_θ
CYLAN	-8700	- 700	-8800	-6900
ELAS2	-8200	400	-7800	-6200
Superlam	-9500	-1100	-4200	-4300

The predicted hoop-axial shear strains for each case in the preceding table are zero. In addition to the in-plane strains, ELAS2 also provided radial strains. For the two cases presented above, the predicted radial strains are 3900 and 6900 microstrains, respectively. The details of tube geometry for the above results are given in Figure 19, following. It should be noted that the ratio of radius to wall thickness is less than 10; thus, a condition of plane stress in the fiberglass tube cannot reasonably be expected. Both CYLAN and Superlam are based on a plane stress analysis; their results are included for comparison but must be interpreted with this limitation in mind.

Compared with thermal analogy predictions of chemical residual strains, it was anticipated that thermal residual strains would be small. Table 3, following, contains predicted thermal residual strains due to cooling from the peak exotherm to room temperature. Except for the hoop strain in the composite tube, the strains in Table 3 are significantly smaller than those in Table 2. The two

temperature differences (-40 K and -80 K) employed in modelling the thermal curing strains are reasonable values for laminates and pure resin, respectively. (Compare with the experimental peak exotherm temperatures for composite and neat resin tubes in Tables 5 and 6.) To obtain the results of Table 3, the shrinkage capacity of the aluminum mandrel was retained and the temperature difference was applied uniformly over the mandrel and resin-containing layer. All values quoted below are mechanical strains (total strain minus free thermal expansion or contraction).

Table 3

Thermally-Induced Strains at Inside of Mandrel

* Resin-containing layer thickness = 7.62 mm (0.3 inches)
** Strains are given in microstrains
*** ΔT for fiberglass = -40 K; ΔT for pure resin = -80 K

Program	Fiberglass, V_f=0.50		Pure Resin	
	ϵ_x	ϵ_θ	ϵ_x	ϵ_θ
CYLAN	- 200	500	- 200	- 900
ELAS2	- 400	600	- 800	- 700
Superlam	- 400	600	- 700	- 700

If predicted thermal analogy strains and predicted thermal strains are superposed, the net strain values are as shown in Table 4, below. The thermal analogy strains dominate all responses except the predicted hoop strain for the mandrel overlain by the composite tube.

Table 4

Thermal Analogy (Polymerization) Strains
Plus Thermally-Induced Strains

* Resin-containing layer thickness = 7.62 mm (0.3 inches)
** Strains are given in microstrains
*** ΔT for fiberglass = -40 K; ΔT for pure resin = -80 K
for calculation of the thermal component of net strain

Program	Fiberglass, V_f=0.50		Pure Resin	
	ϵ_x	ϵ_θ	ϵ_x	ϵ_θ
CYLAN	-8900	- 200	-9000	-7800
ELAS2	-8600	1000	-8600	-6900
Superlam	-9900	- 500	-4900	-5000

It was hoped that by recreating the above scenario experimentally, hoop and axial strains could be measured on the inside surface of the aluminum mandrel during and following curing of the hoop-wound fiberglass layers. A comparison of the strain level after curing with the predicted results, above, was expected to provide some insight into the applicability of the thermal analogy.

Figure 19

Tube Geometry for Thermal Analogy Runs

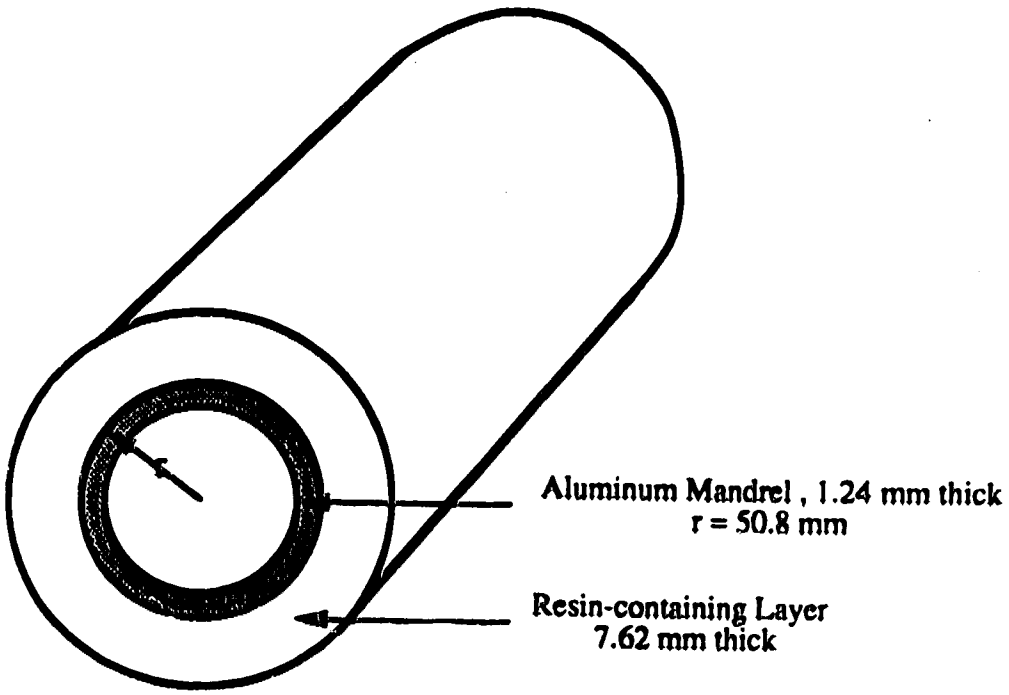

The Raw Materials

In Experiments 1 through 5, the aluminum mandrels used were nominally 0.102 m (4 in) outside diameter and 1.24 mm (0.049 in) wall thickness alloy 6063 cut to 0.304 m (1 ft) lengths. The mandrels were precipitation heat treated at 177°C (350°F) for 8 hours to achieve "T6" condition, a fully-hard state in which the tubular mandrel possessed its maximum yield strength. Alloy 6063 contains approximately 0.7% magnesium and 0.4% silicon. At room temperature, alloy 6063-T6 has a tensile strength of 240 MPa (35 ksi) and a yield strength of 212 MPa (31 ksi). (Lyman, 1961) Linear elastic material behavior can be expected of this alloy up to about 0.3% strain.

Several criteria were important in selecting the mandrel geometry and material. First, the internal diameter had to be large enough to permit placement of strain gages. The internal diameter could not be too large, however, as this would increase the amount of material required to wind a laminate of a given thickness. The greater the amount of fiberglass involved, the larger the apparatus required and the longer the production time. Second, the wall thickness had to be large enough to give the mandrel adequate structural stiffness yet small enough to serve as an effective window through which curing strains could be monitored and measured. Third, the mandrel had to be long enough so that strain gages mounted at the center of the

tube would not be influenced by end effects. A length of three times the tube's outside diameter was thought suitable to accomplish this goal. A well-characterized material, such as an isotropic metal, was deemed most suitable. Of all such materials, aluminum alloys used in aircraft applications were the only ones commonly used in tubes meeting the desired geometric criteria.

In Experiments 1 and 2, E glass roving of designation P30-2200-475 was chosen as the reinforcement. P30 indicates that the strands comprising the E glass roving are untwisted; 2200 is the tex, or weight of the roving in grams per kilometre. 475 is Fiberglas Canada's product style number. This fairly heavy roving was chosen to help keep winding times and material handling problems to a minimum. The spool of roving used in the experiments can be seen in Figure 21. The polyester resin used for all of the runs was Vibrin 1029, a multi-purpose grade; MEKP catalyst was used at a rate of between 0.26% and 0.28%. As previously noted, the density of the liquid resin, as measured by an Anton-Paar densitometer, was 1110 kg/m^3 at 22°C.

Apparatus

In an industrial filament-winding operation, strands of glass fibers are fed through a resin bath and subsequently wound onto a rotating mandrel at a feed rate which produces the desired wind angle in the product. The various production parameters are usually computer controlled. The glass fibers may be pretensioned upon removal from the supply spool or just prior to application to the workpiece. The glass fibers are made to travel over bends of sufficiently small radius of curvature and from sufficiently steep angles of approach to cause the sizing to crack. This allows full separation of the glass filaments and enhances wetting of the glass by the resin. A simple schematic of hoop winding appears in Figure 20.

Figure 20

Hoop Winding Schematic

(Adapted from Schwartz, 1984)

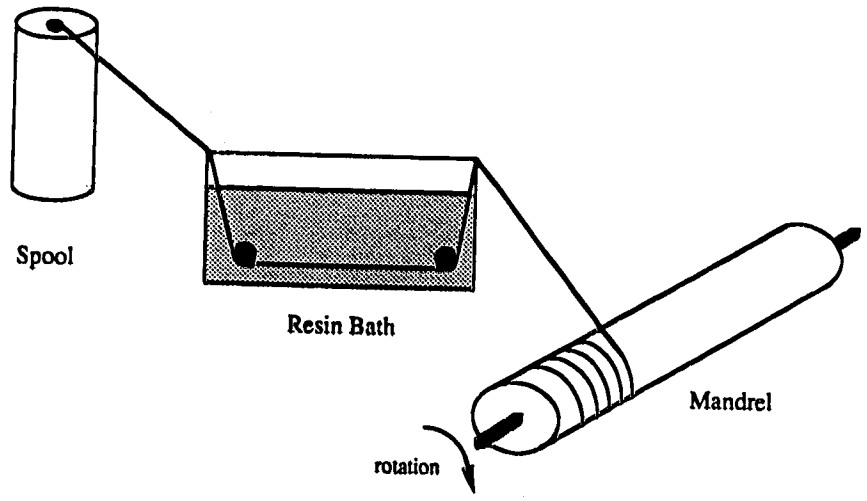

Once catalysed, a pool of polyester resin has a finite pot life (time span during which it is fluid enough to be used in laying up a laminate). Thus, industrial scale products tend to be produced in a step-wise fashion. A number of closures (+/- θ° layers) are wound and allowed to set. Subsequently, more layers are applied using a new batch of resin if a thick-walled product is to be produced. This piecemeal production strategy also prevents too great an exotherm building up (as would be the case if a large number of layers were applied at one time).

The laboratory-scale apparatus used in the resin shrinkage Experiments 1 and 2 is an analog of its more elaborate industrial counterparts. Roving was fed from the supply spool over the edge of the white polyethylene basin containing the resin and then threaded beneath two 25.4 mm (1 inch) diameter polyethylene rollers separated by 120 mm (4.72 inches). This was the "wet-out" section of the assembly. Next, the saturated glass was distributed by a rotating acrylic screw of 31.8 mm (1.25 inch) diameter and having 276 threads/m (7 threads/inch). After passing over the screw, the glass was wound onto an aluminum mandrel rotating at the same angular speed as the threaded rod. The actual winding rate varied during the production cycle due to the manual nature of the operation. The average rate was about one hertz. Several views of the experimental apparatus are shown in Figure 21, following, and the filament-wound tube from Experiment 1 is shown in Figure 22.

Figure 21

Experimental Filament-Winding Apparatus for Hoop-Wound Tubes

(Length of aluminum mandrel is 0.304 m.)

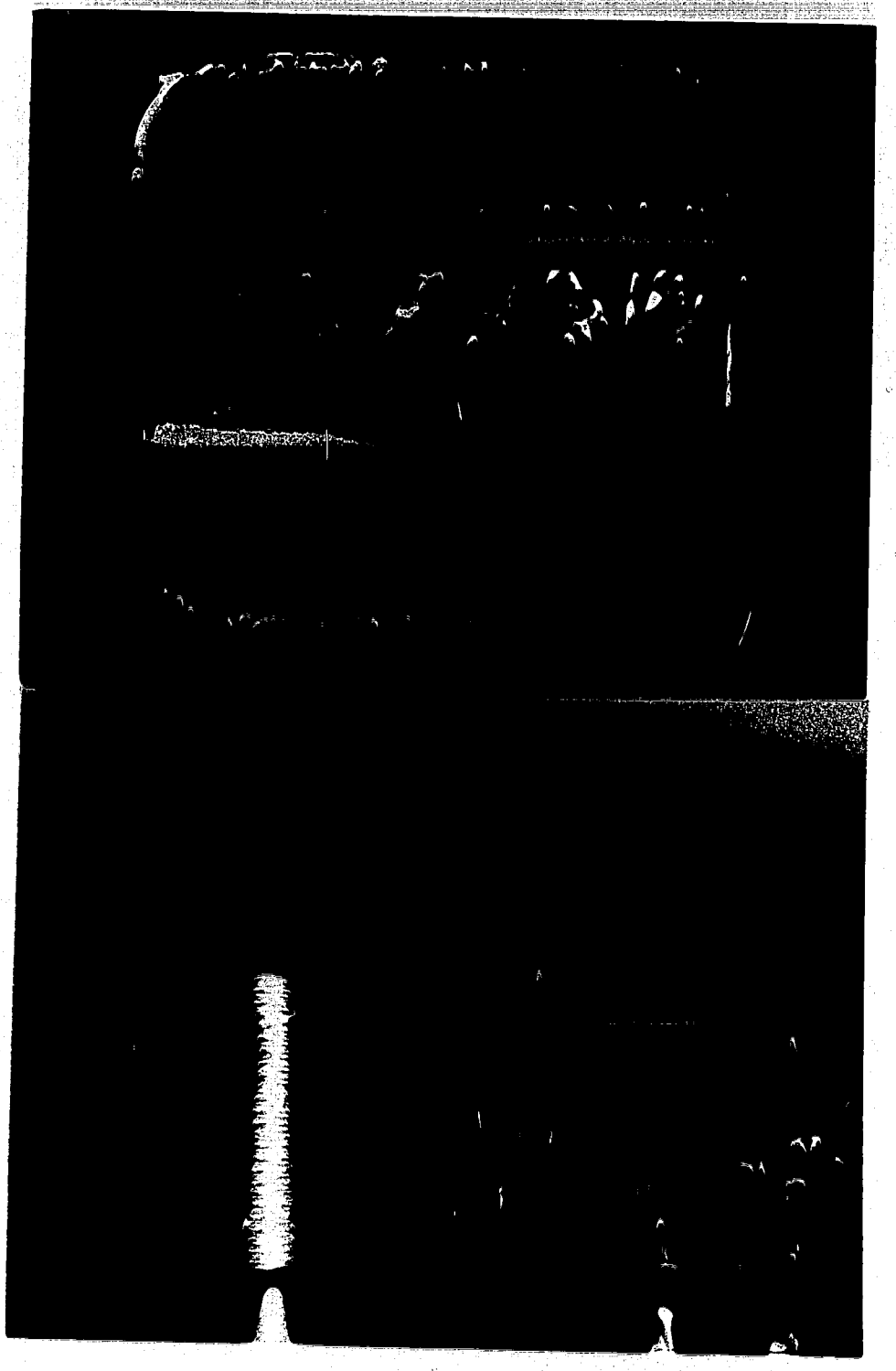

Figure 22

Experiment 1: Hoop-Wound Tube, Chart Recorder, and Amplifier-Conditioner Unit

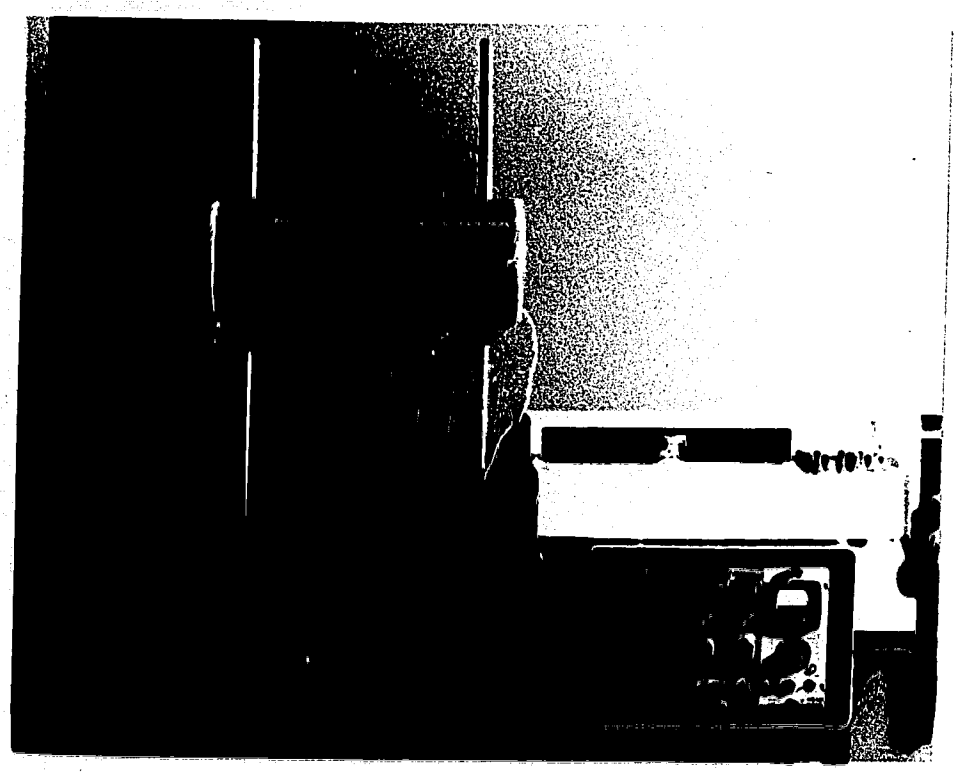

A filament-winding apparatus was not required in Experiments 3 through 5 where the objective was to measure strains induced in an aluminum mandrel due to curing of an unreinforced (100% polyester) tube. To produce such a tube, liquid resin was cast into an annulus surrounding the instrumented mandrel. The outer portion of the enclosure to contain the resin consisted of 3.8 mm (0.15 in)-thick corrugated cardboard. In Experiment 3, the cardboard was impregnated with wax to resin-proof the sides and to seal the enclosure against resin leakage. In Experiments 4 and 5, the cardboard was coated with a thin layer of polyester resin catalysed at 0.25%. In Experiment 3, the bottom of the annulus was closed off with a torus of cardboard and a wax seal. Due to problems with leakage, the bottom closure was modified in the last two runs. There, a rubber gasket sealed with silicone RTD was wound around the mandrel and the cardboard enclosure was held against the gasket with the aid of a hose clamp. This latter type of enclosure is shown, following, in Figure 23.

Since minimal stiffness was desired, cardboard was chosen as the enclosure material. Ideally, it was hoped that the enclosure would be flexible enough to follow the curing displacements of the resin without greatly influencing the strains that the shrinking resin would impart on the inside surface of the mandrel.

Figure 23

Cardboard Enclosure of the Type Used for Neat Resin Tubes in Experiments 4 and 5

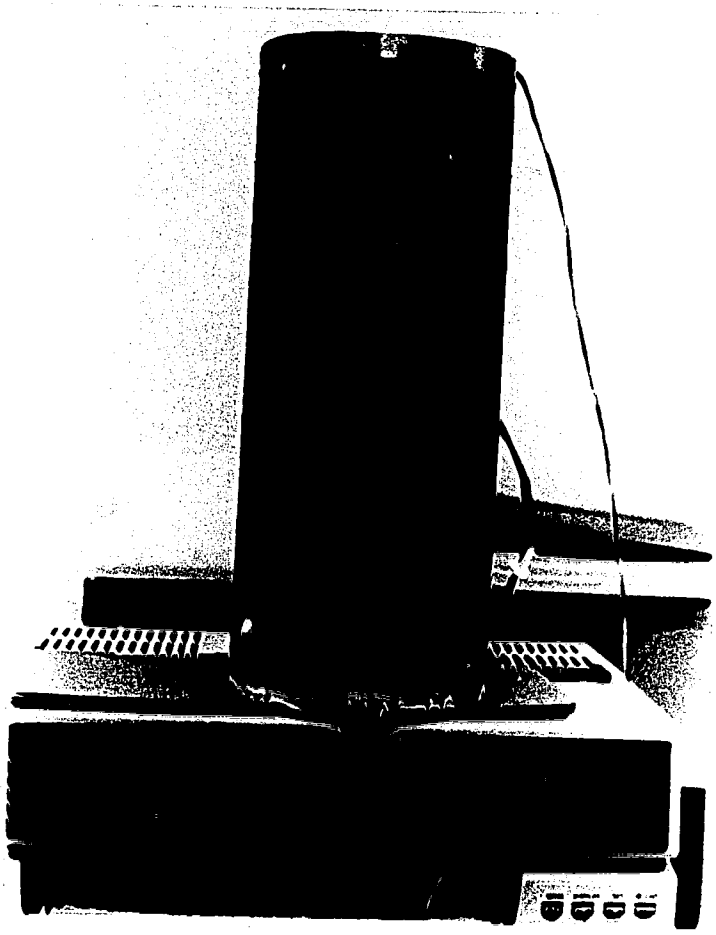

From the computer programs used in Tables 2 through 4, it was found that doubling the thickness of the resin tube augments predicted strains by a similar factor. However, it should be noted that a balance must be struck between the magnitude of the strain signal and the cracking tendency of the tube. A thick-walled resin tube is more susceptible to cracking than its thin-walled counterpart due to a more severe curing exotherm and the less ready dissipation of heat from a thicker body. Cracking relieves built-up curing stresses and strains. This would tend to cause a smaller strain signal from a thick-walled cracked tube than from a thin-walled tube which remains intact following curing. Massive cracking resulted when a 15.24 mm (0.6 in) thick tube was cast in Experiment 3. Thus, in Experiment 4 the annulus thickness was reduced by a factor of 2.

Instrumentation

In Experiment 1, Micro-Measurements stacked rosette gages of designation CEA-13-125WT-350 were mounted in the hoop and axial orientations at the center of the aluminum mandrel. Some details of strain gage application are included in Appendix E. A two-wire assembly was employed in the first run.

In Experiment 2, two stacked rosettes were mounted on the outside of the aluminum mandrel. These were separated by 90° around the circumference of the tube. A three-wire assembly was employed to help minimize spurious temperature

effects. Prior to winding the second tube, the second mandrel, with its externally mounted gages, was taken through several temperature excursions similar to those which might be undergone during curing. The furnace used for this procedure is shown, following, in Figure 24. This exercise served as a check of the use of a 3-wire assembly in reducing spurious temperature effects. The decision to use two stacked rosettes situated 90° apart stemmed from the concern that the wall thickness of the mandrel was not uniform. The eccentricity of the aluminum mandrel is typical of extruded products. The fattest portions of the mandrel wall (about 1.42 mm or 0.056 in thick) were located roughly 90° from the thinnest portions (about 1.19 mm or 0.047 in thick).

The external gages on mandrel 2 served merely as calibration gages and were removed prior to winding tube 2. Four single (unstacked) gages (two each in the hoop and axial orientations) were mounted inside mandrel 2 using a 3-wire assembly. Single gages were chosen over stacked gages to help minimize self-heating of the gages. The use of these CEA-13-062UT-350 gages was continued in Experiments 3 and 4, but only two gages were used in each of these runs. The decision to use but a single hoop and a single axial gage in these runs arose because it was found that the strain signals at the thick and thin locations of the mandrel were not very different.

Figure 24

Experiments 2 - 5: Recorder, Amplifier-Conditioner Unit, and Furnace Used to Test Temperature Response of Instrumented Mandrels

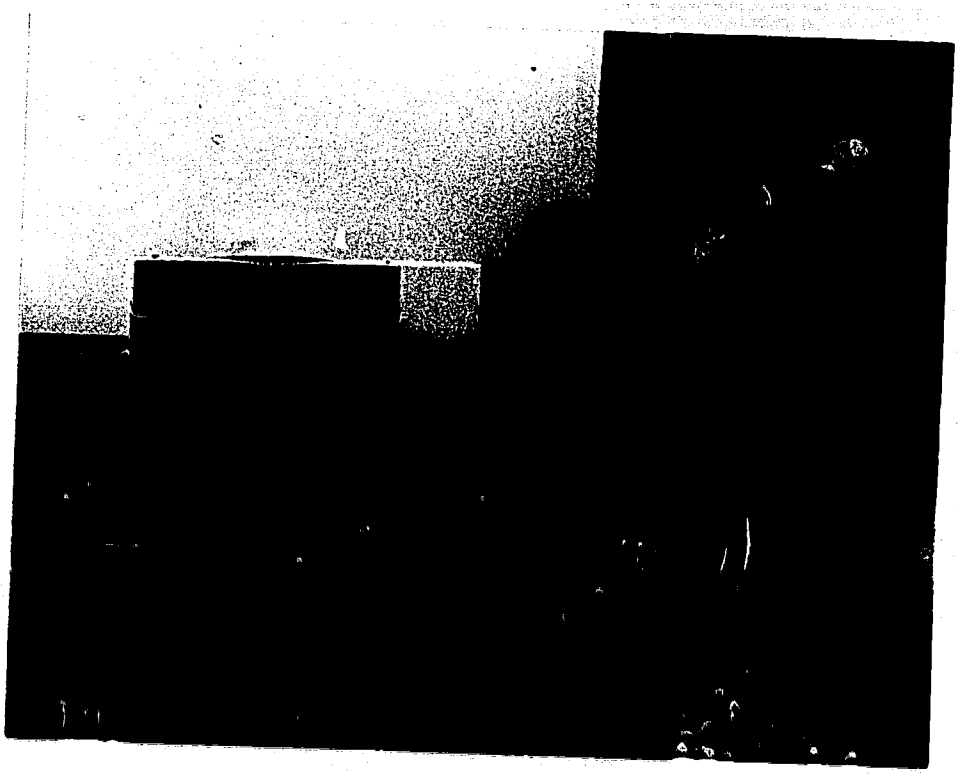

In Experiments 1 and 2, the strain gage lead wires were tucked inside the mandrel and secured in place using masking tape prior to winding the fiberglass tubes. After completion of the tubes, excess resin was allowed to drip off and the tubes were slowly rotated to keep resin from pooling along the bottom seam of the horizontally-disposed tubes. The tubes were then removed from the filament-winding apparatus and supported on steel ring stands before the gages were connected to the signal-measuring equipment. In Experiments 3 and 4, the strain gage input plugs were connected to the Vishay 2120 strain gage conditioner and amplifier before the resin was cast into the annulus surrounding the mandrel. The signal conditioner/amplifier unit employed a Vishay 2110 power supply.

In Experiment 1, output was fed to a Cole-Parmer 8376-30 2-pen chart recorder, as shown in Figure 22, and temperature readings at the mandrel surface in the vicinity of the gages were relayed using a Cole-Parmer digi-sense thermocouple, Model 8529-00. In all subsequent work, the strain gage signals and the temperature signal from a K-type thermocouple were sent to a 13-channel Yew portable hybrid recorder, Model 3087. The Yew recorder is shown in Figure 24.

Results

The two hoop-wound fiberglass tube samples caused very small mandrel strains compared to those predicted. In fact, the final strain values are more than an order of magnitude smaller than the thermal strain component of the net curing strain. The measured strains were predominantly tensile hoop strains and compressive axial strains on the inside surface of the aluminum mandrels. The strain and temperature versus time curves for Experiment 1 are shown in Figure 25. Note that time zero corresponds to the point at which the resin was catalyzed. Qualitatively similar strain behavior was shown in Experiment 2.

Several distinguishing features of the hoop-wound tube results warrant scrutiny. Firstly, prior to the attainment of the peak exotherm, both the hoop and axial strain responses show a rapid increase in the magnitude of strain levels culminating in several closely-spaced peaks. These are, perhaps, a macro scale manifestation of a micro scale stress relief mechanism. The average of the strain levels at these peaks and the range of times over which the peaks occurred are tabulated below. The magnitude of the hoop strain response is approximately double that of the axial response in both experiments.

Secondly, the strain levels at the times of the maximum temperatures (as measured on the inside surface of the mandrels) were much lower than the peak strains listed above. This reflects the fact that strain levels had begun

Figure 25

Strain and Temperature Versus Time

For Experiment 1

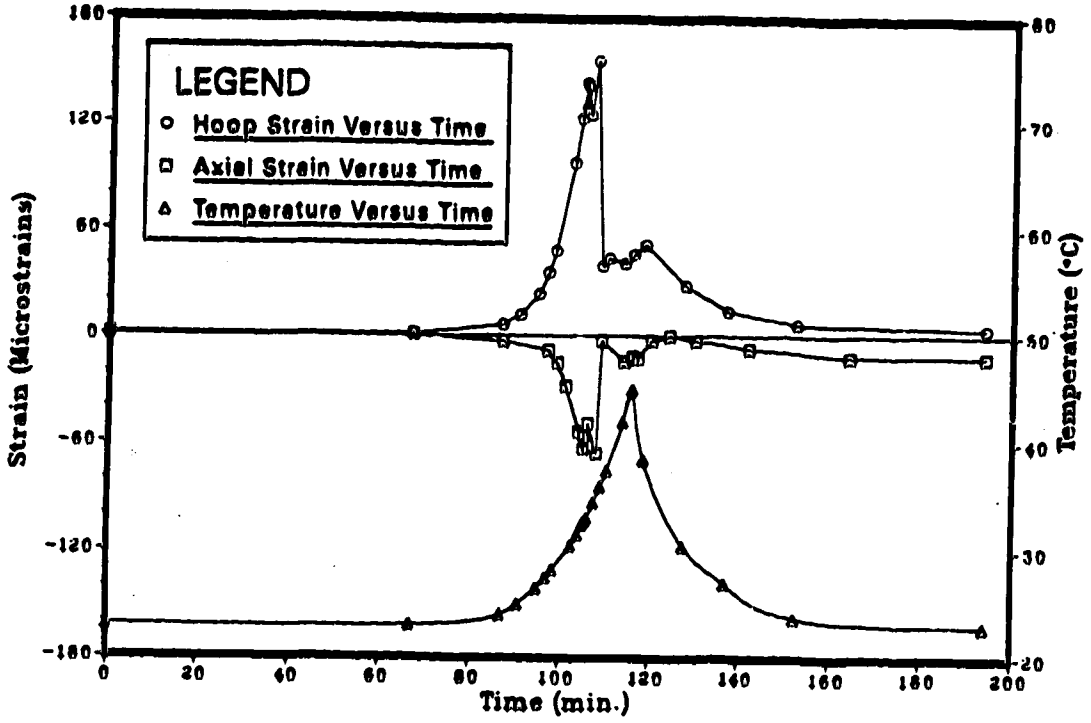

to decay towards their final values prior to the attainment of the peak exotherm. See Table 5, below.

Thirdly, both hoop and axial final strains were negligibly small. Final hoop and axial strains in Experiment 1 were 4 microstrains and -13 microstrains, respectively, at 1440 minutes and in Experiment 2 were 10 microstrains and -5 microstrains, respectively, at 1232 minutes.

Table 5

Strain Data for Filament-Wound Tubes

* Strains are given in microstrains

Exp't	Time to Peaks (min.)	ϵ_θ	ϵ_x	Time (min.)	T_{max} (°C)	ϵ_θ	ϵ_x
1	105 to 107.5	156	-67	116	45	49	-13
2	97.5 to 106	88	-50	110	52	23	-3

Experiments 4 and 5 considered 100% polyester tubes cured surrounding an instrumented mandrel. The strain and temperature versus time curves for Experiment 4 are shown, following, in Figure 26. As in the first two experiments, the hoop strain response exceeded the axial response. Hoop strains were predominantly negative, while axial strains wavered back and forth between low positive levels and low negative ones before finally settling at negative values. Several strain peaks occurred in the vicinity of the maximum temperature. In Experiment 4, the average peak hoop strain is -179 microstrains and the average peak axial strain is 22 microstrains. These peaks occurred between 100 minutes and

113 minutes. It should be noted that the peak hoop strains are not extrema of the hoop strain curves, only noticeable discontinuities. Strain levels at the peak exotherm as well as final strain values are given in Table 6.

Table 6

Strain Data for 100% Polyester Tubes

* Strains are given in microstrains

Exp't	Time (min.)	Temp. (°C)	ϵ_θ	ϵ_x	Time (min.)	ϵ_θ	ϵ_x
4	104.5	109	-105	11	1253	-298	-20
5	85.5	106	-29	32	1091	-69	-24

The final experimental hoop and axial mandrel strains are, respectively, 4 and 30 times smaller than the predicted thermal curing strains listed in Table 3. In turn, the predicted thermal interaction strains are an order of magnitude smaller than the predicted strains due to resin densification.

Figure 26

Strain and Temperature Versus Time

For Experiment 4

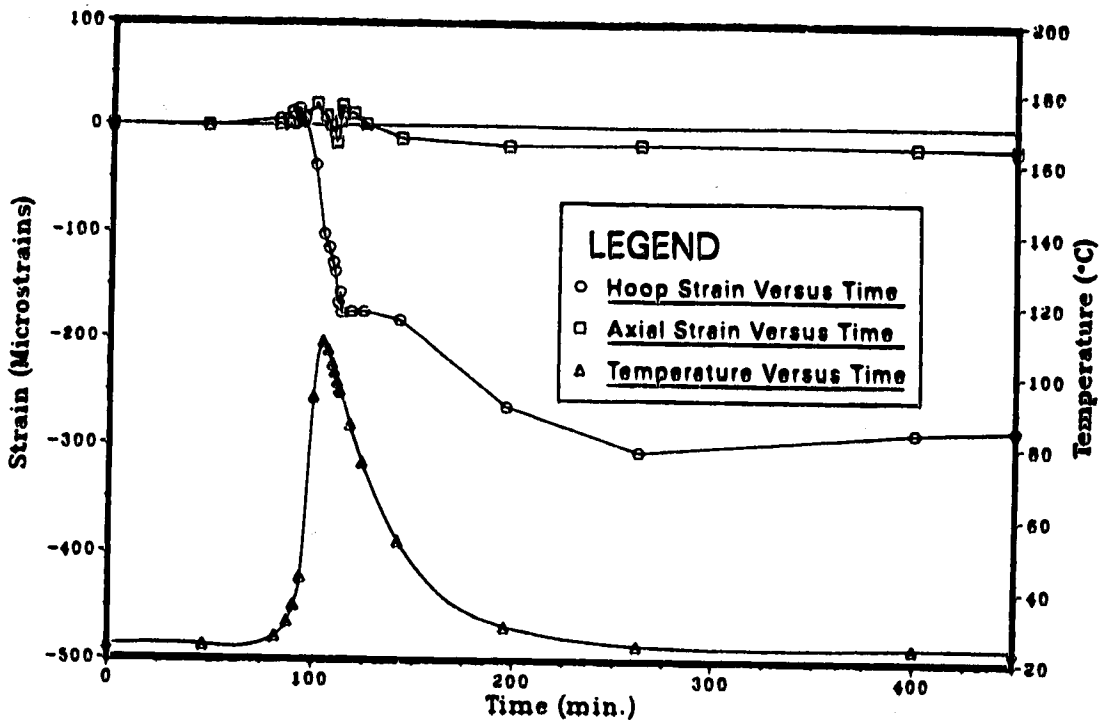

In-Situ Density of Resin in a Composite

The results of the thermal analogy runs presented earlier suggested that sizeable strains would be present on the inside surface of the mandrel during and after curing. In all of the experimental trials, however, the measured strains were considerably smaller than the predicted values. In investigating the reasons for the discrepancy, one possibility which was considered was that the magnitude of the shrinkage displayed by the resin in the composite tubes could be different from the amount displayed by neat resin. The density of cured resin is an inferential measure of the amount of chemical shrinkage which took place.

Thus, a series of measurements were undertaken in order to ascertain whether the total volumetric shrinkage of resin within a composite differed from that observed in the neat resin. These tests were performed by determining the mass and volume of composite samples. After burning off the resin, the mass and volume of the glass were determined. By difference, the mass and volume of the resin, and hence the density, were calculated. Further details of the measurements and calculations for the burn-off tests are found in Appendix G. For comparison, the densities of neat resin tube samples are also included below. The standard deviations for the density values tabulated below are 0.3% to 1.1% for experiments 1 and 2 and 0.1% to 0.2% for experiments 3 to 5.

Table 7

Resin Density Results

Exp't	% Catalyst	T_{max}(°C)	t_{wall}(mm)	V_f	ρ_{resin}(kg/m^3)
1	0.27	45	7.6	0.55	1260
2	0.28	52	6.4	0.51	1240
3	0.26	64	7.6	0.00	1210
4	0.26	109	15.	0.00	1210
5	0.27	106	7.6	0.00	1210

The resin densification shrinkages consistent with the resin densities given in Table 7 are 12.7 v/o, 11.1 v/o, and 8.6 v/o for experiments 1, 2, and 3 through 5, respectively. This suggests that at least as much resin densification took place in the composite as in the neat resin. Various sources of experimental error could contribute to the values being larger than those for the neat resin. More measurements were required to calculate the density of resin within the composite as compared with the density of neat resin and there is a possibility that some glass was carried away by air currents in the furnace during burn-off. In addition, the mass of the glass fibers may have been reduced as a result of removal of the coating. Thomason and Morsink (1988) found that coatings on epoxy-compatible E glass rovings could account for 0.2% to 1.0% of the mass of the rovings. An artificially low mass (or volume) of glass will lead to an inflated resin density and, hence, an overestimation of the amount of resin shrinkage. Resin density is calculated as

$$\rho_r = (\rho_c - \chi_g \rho_g)/\chi_r \quad \text{.....[24]}$$

or, equivalently,

$$\rho_r = (\rho_c - m_g/V_c)/ (V_r/V_c) \quad \text{.....[25]}$$

where the density of the composite (ρ_c) is determined from the apparent mass; the volume of the composite (V_c) is determined from the mass and density of the composite; the density of the glass (ρ_g) is known; and the mass of the glass (m_g) is found from the burn-off test. x is the volume fraction of either glass or resin. Note that $x_g + x_r = 1$.

3.4 Discussion and Conclusions

Since this thesis serves as a critical investigation and assessment of the thermal analogy's utility in gaining a better understanding of the mathematical manipulations of resin curing stresses and strains, it is worthwhile to highlight some merits and potential pitfalls of the thermal analogy.

Both thermal and chemical curing shrinkage can lead to complex microresidual stress and strain distributions in composite materials. The complexity of the effects is certainly of interest, but so, too, is the identification and description of the relationship between the causes and the effects. Three points which differentiate thermal and chemical shrinkage warrant discussion.

Firstly, chemical shrinkage of the resin is less clearly amenable to succint mathematical description than thermal shrinkage. Consider the calculation of total strains in a homogeneous mass of polyester. The total thermal strain is simply the product of the change in temperature and the tendency of the material to expand or contract. This tendency, the coefficient of thermal expansion of the material, is tabulated in the literature for a wide range of materials. In general, the CTE depends on temperature.

The amount of chemical shrinkage at any location in a body of resin changes with time during the curing process. If coefficients of chemical shrinkage were available in the literature, they would likely be complicated functions of

chemical composition (e.g., percent catalyst, percent monomer), reaction rate, and temperature. For a given cure cycle, reaction rate, the degree of crosslinking, and temperature change are time-dependent. The time-dependent chemical shrinkage is complicated by the fact that the resin undergoes a change of state from liquid to gel to solid during crosslinking. In any case, the magnitude of chemical shrinkage stresses locked into a mass of polyester resin depends on the nature of the material behavior at the time the shrinkage occurred. If the resin undergoes viscous flow, the stresses induced by densification strains could relax away. Since the calculation of total chemical shrinkage has not been formalized, this quantity may be determined by experimental measurements for a given chemical composition and set of curing variables. In addition to stress relief by viscous flow, other stress relief mechanisms could become operative during or following curing (e.g., crazing).

Secondly, the mathematics for calculating the fraction of total thermal strain which induces residual stresses in a composite is well-established for simple cases, both on the micro- and macro-scale.

Thirdly, the inherent nature of the shrinkage process may differ between thermal and chemical shrinkage. Consider the cross-sectional view of circular fibers embedded in polyester resin, as shown in Figure 27, below.

Figure 27

Cross Sectional View of Polyester Matrix between Fibers

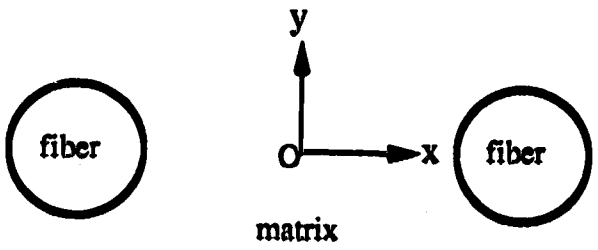

The CTE of the resin at point "O" is the same in both the x- and y-directions. Thermal shrinkage thus tends to be isotropic within the plane at point "O". (Overall, the thermal strains in a control volume of the composite are not uniform due to the mismatch in mechanical properties between the matrix and the fibers.) It is not known whether the tendency towards chemical shrinkage is the same in both the x- and y-directions at point "O". Fluid flow in the resin, micro stress fields due to prestress in the fibers, and stress fields as they develop during curing might influence a "preferred orientation for crosslinking", leading to anisotropic densification. This point requires further investigation.

Utility of the Thermal Analogy on the Micro Scale

The finite element analysis of Section 3.2 was a simplified look at the utility of the thermal analogy on the micro scale.

The high resin stress levels predicted by the finite element analyses suggest that widespread microcracking would occur in a fiberglass composite (based on a square array of fibers and a volume fraction of 0.5). In addition, the finite element analysis considered only local boundary conditions. Long-range effects of adjacent laminae or of a particular structural geometry would likely compound the stresses predicted. In any case, a composite which behaved as predicted would be unlikely to have sufficient integrity to be a useful engineering material.

To reconcile the knowledge of the driving force for the development of large microstresses with the observation that fiberglass is a useful material, there must be an internal mechanism to soften the effects of curing shrinkage. The role of an interphase region of modified resin in providing microresidual stress relaxation has been mentioned by Plueddemann (1974, 1988). Within the present finite element analysis, a modified resin layer having properties intermediate between those of glass and polyester could help smooth out the the variation of curing stresses across the fiber-matrix interface. The introduction of temperature- and time-dependent material properties and responses are logical

further improvements.

A further criticism of the present use of the thermal analogy on the micro scale is that a temperature change corresponding to the full amount of curing shrinkage observed in the neat resin was employed. This is similar to stipulating that all of the resin shrinkage occurs subsequent to gelation. In fact, some of the shrinkage may occur while the resin is liquid, that is, when the shrinkage has no potential to induce stresses. The use of room temperature properties in a static analysis exacerbated the above problem. Obviously, a detailed characterization of resin behavior during crosslinking would be useful in delineating the gel point and the resin properties at, and subsequent to, gelation. Vratsanos and Farris (1986) suggested the technique of impulse viscoelasticity for monitoring the property changes in thermosetting resins during curing. Further comments on their work appear in Appendix H.

Utility of the Thermal Analogy on the Macro Scale

In the Archimedean density tests, bags of Vibrin 1030 resin were, more or less, able to shrink without outside hindrance during curing. 8.7 v/o densification shrinkage was measured in all the neat resin samples in Section 3.1. The Vibrin 1029 tube samples produced in experiments 3 to 5 in Section 3.3 showed 8.6 v/o densification shrinkage. Extensive cracking was observed in the neat resin tubes. In

turn, the cracking probably contributed to the resin shrinkage achieving the same value in the tubes as well as in the unconstrained bags of resin.

The polyester matrix within the hoop-wound fiberglass tubes of experiments 1 and 2 in Section 3.3 experienced both external geometric constraints (due to the tubular mandrel) and also internal constraints (due to the presence of stiff reinforcing fibers). The greater degree of resistance to shrinkage, as compared with that in the experiments involving unreinforced resin, would suggest a reduced level of net shrinkage. (Recall Figure 5, where the fibers were forced into compression and the matrix into tension because the resin was unable to shrink to its equilibrium state.) However, if all of the chemical shrinkage occurred while the resin was fluid, then a reduced net shrinkage would be unlikely in the fiberglass tubes compared with the neat resin. As well, cracking of the neat resin tubes would not have occurred due to chemical shrinkage, but could could have been caused by differential thermal contraction. The fact that cracks were observed in the neat resin tubes in the vicinity of the peak exotherm contradicts the possibility of cracking being due soley to thermal effects.

Contrary to expectations, the resin in the fiberglass tubes was found to display at least as much densification as the neat resin. Concomitant with this were an absence of macro scale cracks and negligibly small mandrel strains (see Table 5) at the conclusion of the experiments. Even the peak

mandrel strains were several orders of magnitude smaller than those predicted by the thermal analogy. Despite the large amount of cracking in the tubes of Experiments 4 and 5, the final hoop strain levels were higher for these neat resin tubes than for the composite tubes!

Based on the Archimedean density tests, it was expected that most of the chemical shrinkage effects would present themselves prior to the peak exotherm. In agreement with this expectation, the largest measured strain responses for the filament-wound tubes occurred just before the peak exotherm. See Figure 25. The strain response prior to the peak exotherm is much smaller than the thermal analogy predictions would suggest. Failure to attain higher levels might be ascribed to a macroscopic stress relief mechanism. The basis of the proposed mechanism is non-uniform curing due to temperature gradients through the thickness of the body.

Figure 28

Assumed Temperature Profile in Fiberglass Tube Wall

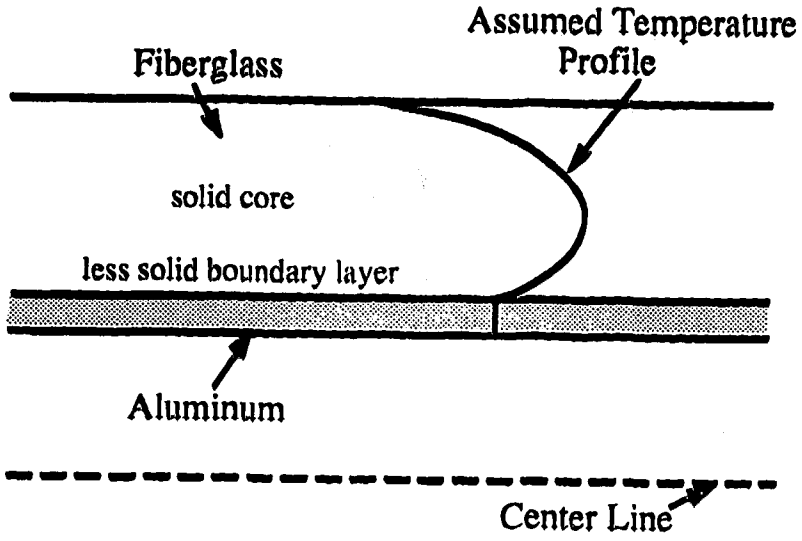

In a fairly thick-walled tube whose exterior (as well as the inner surface of the aluminum mandrel) is exposed to air currents, the maximum temperature at some time during curing would occur in the insulated interior as shown in Figure 28. The interior would thus tend to solidify sooner than the cooler outer portions of the composite tube. Shrinkage deformations of the core would exert pressure on the more fluid resin at the boundary layer, thereby causing the resin to flow. Less stress would be transferred to the mandrel under these circumstances than if the entirety of the composite cured at once. Several limitations of this stress-relief mechanism include the fact that the curing resin is quite friable (Selley, 1987) and the fact that resin flow is restricted by the presence of the fibers.

Thermal expansion effects, which oppose chemical shrinkage effects during the ascent to the peak exotherm, would tend to further reduce mandrel strains compared with thermal analogy predictions.

Just prior to the peak exotherm in Figure 25, the magnitudes of both the hoop and axial mandrel strains drop suddenly. Perhaps this reflects the onset of crazing. The thermal analogy results from ELAS2 (See Appendix D) show tensile axial strains through the composite wall and tensile hoop strains in the composite near the mandrel. It is conceivable that, upon reaching a critical tensile strain, the resin underwent localized microcracking to relieve the tension. This would help to explain the sudden change in

mandrel strain levels. Another possibility is that the drop in strain levels just prior to the peak exotherm was influenced by a momentary release of the bond between the composite and the mandrel. The stipulation of "momentary" debonding is necessary because it was found that the fiberglass and mandrel were well-bonded when tubes 1 and 2 were sectioned for the burn-off tests of Section 3.3. The tubes were cut into rings, and then the rings were cut up before the composite and aluminum layers could be pried apart. Only if the bond between the fiberglass and the mandrel had momentarily relaxed and then reformed could the strong adhesion between the two materials be explained.

The change in measured mandrel strains between the peak exotherm and the conclusion of the experiment does not agree well with the predicted thermally-induced mandrel strains as given in Table 3. The existence of microcracks in the resin is not accounted for in the model. This fact might contribute to the observed discrepancy.

In contrast to the fiberglass tube trials, there is no parallel occurrence of significant strain levels prior to the peak exotherm in the 100% resin tube trials. See Figure 26. Perhaps this result obtains due to the factors which tend to produce severe microcracking of the resin during the early stages of curing. The two main factors are the large disparity between the modulus of the aluminum and that of the rubbery crosslinking resin and the geometric constraints to resin shrinkage.

As well, a macroscopic stress relief mechanism, similar to that suggested for the filament wound tubes, is not likely tenable in the all-resin tubes. The pure resin within the annulus between a cardboard enclosure and a mandrel sealed to prevent resin leaks was much more insulated than the fiberglass tubes, which were exposed to air currents as they cooled. Thus, the temperature gradient through the all-resin tube walls was probably smaller, even so the measured peak curing temperature was higher.

The final compressive mandrel strains are likely caused by cooling of the assembly after the peak exotherm. Even so, the final strains do not approach levels suggested by the thermal analyses.

In connection with the filament-wound tubes, it should be noted that any microresidual stress relief mechanisms (due to viscous flow of the curing resin, for example) do not prevent overall shrinkage of the resin. The presence of geometric and material constraints would thus lead to macroscale interaction strains.

3.5 Recommendations

In subsequent work, it will be necessary to establish the relative significance of chemical and thermal residual stresses in fiberglass (both on the micro and macro scales) and to identify the factors which control the proportions. In determining the significance of thermal effects, it might be worthwhile to investigate whether consideration of

transient temperature gradients and time- and temperature-dependent material properties and responses improves the agreement between observations and predictions. Some more specific suggestions for the finite element analyses and instrumented mandrel experiments are presented below.

Finite Element Analyses

Mesh refinement might be useful in improving the quality of the results obtained from the micro scale thermal analogy analysis. For some regions (for example, a traverse across edge 1, which involves only two matrix elements) too few matrix elements exist in the trial mesh to produce a good stress profile plot. Sharp changes in hoop stress were noted in the vicinity of the fiber matrix interface for traverses along edges 1 and 2 of the region of analysis. Mesh refinement could elucidate the character of stress functions in these regions. In addition to (or in place of) mesh refinement, further work might employ a different type of element with more complex interpolation functions to encourage convergence of the finite element solution to the exact solution. For example, quadratic serendipity elements could be used.

Subsequent work might focus on different geometric configurations. Beyond regular arrays, random arrangements of fibers and matrix could be considered. A useful example would be to model a region containing a microcrack within a

material whose curing history is well-characterized. The parameters of the thermal analogy (magnitude of temperature change, magnitude of effective *in situ* thermal expansion coefficients, etc.) could be perturbed until agreement between the predicted stress distribution and the observed state of the material is obtained.

Plane strain was chosen as a reasonable two-dimensional solution to model resin shrinkage, as the axial stiffness of the reinforcement suggests that curing shrinkage effects will manifest themselves primarily in the resin-rich transverse directions. A generalized plane strain solution, in which the material is afforded the capacity to undergo a uniform strain parallel to the fiber direction, might be considered in future work. If generalized plane strain is found to be inadequate to model fiber-direction effects (due to pretensioning of the reinforcement, for example), then the merits of a truly three-dimensional analysis will have to be weighed against greater complexity, labor, storage requirements, and computation time.

Instrumented Mandrel Experiments

Several causes for the small observed strains in the hoop-wound tube experiments (Section 3.3) were suggested in the preceding section. One of the stress relief mechanisms proposed is based on non-uniform curing of the composite. This could be investigated in a number of ways. Two instrumented mandrel experiments are suggested below. Both

experiments are designed to minimize the likelihood of a fluid resin layer adjacent to the mandrel. Without a mechanism to relieve stresses induced by the first part of the composite to set up, larger strains would be anticipated on the inside surface of the mandrel.

One technique involves winding a thick-walled fiberglass tube on an insulating ceramic mandrel. During curing, the highest temperatures would be expected in the composite nearest the mandrel. Thermocouples could be embedded at various locations within the composite tube wall to characterize the temperature distribution. If the material adjacent to the mandrel cures first, then larger strain signals (compared with those in Section 3.3) should be observed on the inside of the mandrel prior to the peak exotherm.

It might also be useful to wind a very thin laminate onto an aluminum mandrel. If the wall thickness of the composite is such that the temperature is quite uniform throughout at any given time during curing, then larger mandrel surface strains would be expected.

Finally, in any subsequent instrumented mandrel experiments, it is suggested that reference gages be used to correct measured strains for thermal effects. (Rousseau et al., 1987) A reference gage would be mounted on a material having a well-characterized CTE and would be located proximal to the mandrel gages so as to experience the same change in temperature. Measured total strain would then be

corrected for thermal effects as shown below:

$$\epsilon_{true} = \epsilon_{total} - (\epsilon_{total,\ R.M.} - \alpha_{R.M.} \Delta T_{R.M.}) \quad .[26]$$

Bibliography

Bathe, Klaus-Jurgen, Edward L. Wilson, and Fred E. Peterson, SAP IV: A Structural Analysis Program for Static and Dynamic Response of Linear Systems, College of Engineering, University of California, Berkeley, CA, 1974.

Brivmanis, R.E., "Experimental Determination of Residual Stresses in Wound Unidirectional Glass-Reinforced Plastics", Mekhanika Polimerov, Vol. 2, No. 1, pp. 123-129, 1966.

Chamis, C.C., "Mechanics of Load Transfer at the Interface", pp. 31-77, Composite Materials, Volume 6: Interfaces in Polymer Matrix Composites, Academic Press, New York, 1974.

Chamis, C.C., R.F. Lark, and J.H. Sinclair, "Integrated Theory for Predicting the Hygrothermomechanical Response of Advanced Composite Structural Components", pp. 160-192, Advanced Composite Materials-Environmental Effects, ASTM PCN 658, American Society for Testing and Materials, Philadelphia, PA, 1977.

Cohen, D. and M.W. Hyer, Residual Stresses in Cross-Ply Composite Tubes, Virginia Polytechnic Institute and State University, Blacksburg, VA, 1984.

Daniel, I.M. and A.J. Durelli, "Shrinkage Stresses around Rigid Inclusions" Experimental Mechanics, Vol. 2, pp. 240-244, 1962.

Dudgeon, Charles D., "Unsaturated Polyesters", pp. 246-251, Engineered Materials Handbook, Volume 2, Engineering Plastics, (Cyril A. Dostal, Ed.), ASM International, Metals Park, OH, 1988.

Erickson, Porter W. and Edwin P. Plueddemann, "Historical Background of the Interface - Studies and Theories", pp. 1-29, Theories", Composite Materials, Volume 6: Interfaces in Polymer Matrix Composites, (Edwin P. Plueddemann, Ed.), Academic Press, New York, 1974.

Farley, G.L. and C.T. Herakovich, "Influence of TwoDimensional Hygrothermal Gradients on Interlaminar Stresses Near Free Edges", pp. 143-192, Advanced Composite Materials-Environmental Effects, ASTM PCN 658, American Society for Testing and Materials, Philadelphia, PA, 1977.

Hahn, H.T. and N.J. Pagano, "Curing Stresses in Composite Laminates" J. Comp. Mater., Vol. 9, January, pp. 91-106, 1975.

Hendry, A.W., Elements of Experimental Stress Analysis, Pergamon Press Ltd., Oxford, 1964.

Hull, Derek, An Introduction to Composite Materials, Cambridge University Press, Cambridge, 1981.

Hyer, M.W. and D. Cohen, "Residual Thermal Stresses in Cross-Ply Graphite-Epoxy Tubes", pp. 87-93, 1984 Advances in Aerospace Sciences and Engineering: Structures, Dynamics and Space Station Propulsion (Proceedings of the Annual Winter Meeting), New Orleans, LA, December, 1984.

Jewett, G.A., Structural Materials Technology Challenges and Opportunities for Canada, G.A. Jewett and Associates Inc., Toronto, Canada, January, 1987.

Jones, Robert M., Mechanics of Composite Materials, McGraw-Hill Book Company, New York, 1975.

Juran, Rosalind, Ed., Modern Plastics Encyclopedia, McGraw-Hill, New York, 1989.

Koufopoulos, T. and P.S. Theocaris, "Shrinkage Stresses in Two-Phase Materials" J. Comp. Mater., Vol. 3, pp. 308-320, April, 1969.

Kriz, R.D. and W.W. Stinchcomb, "Effects of Moisture, Residual Thermal Curing Stresses, and Mechanical Load on the Damage Development in Quasi-Isotropic Laminates", pp. 63-80, Damage in Composite Materials: Basic Mechanisms, Accumulation, Tolerance, and Characterization, ASTM PCN 775, American Society for Testing and Materials, Philadelphia, PA, 1982.

Loos, Alfred C. and G.S. Springer, "Moisture Absorption of Polyester E Glass Composites", pp. 51-62, Environmental Effects on Composite Materials, Technomic Publishing Co., Inc., Westport, CT, 1981.

Lyman, Taylor, Ed., Metals Handbook, 8th Edition, Volume 1, Properties and Selection of Metals, American Society for Metals, Metals Park, OH, 1961.

Marloff, R.H. and I.M. Daniel, "Three-dimensional Photoelastic Analysis of a Fiber-reinforced Composite Model" Experimental Mechanics, Vol. 4, pp. 156-162, 1969.

Morozov, E.V., and L.K. Popkova, "Combined Theoretical and Experimental Method of Determining Residual Stresses in Wound Composite Shells", Mekhanika Kompozitnykh Materialov, No. 6, pp. 1105-1110, November-December, 1987.

Oberholtzer, L.C. Roy, "General Design Considerations", pp. 1-47, Volume 2, Engineered Materials Handbook, Engineering Plastics, (Cyril A. Dostal, Ed.), ASM International, Metals Park, OH, 1988.

Osborne, Al, Personal Correspondence, May 21, 1986.

Osborne, Al, Superlam Laminate Analysis Program, Fiberglas Canada Inc., Guelph, Ontario, 1986.

Osborne, Al, Private Communication, May, 1987.

Osborne, Al, Superlam Laminate Analysis Program - 3D Version, (under development), Fiberglas Canada Inc., Guelph, Ontario, 1987.

Osborne, Al, Private Communication, May, 1989.

Pagano, N.J. and H.T. Hahn, "Evaluation of Composite Curing Stresses", pp. 317-329, Composite Materials: Testing and Design (Fourth Conference), ASTM STP 617, American Society for Testing and Materials, Philadelphia, PA, 1977.

Parratt, N. J., Fiber Reinforced Materials Technology, Van Nostrand Reinhold Company, London, 1972.

Plueddemann, Edwin P., "Mechanisms of Adhesion through Silane Coupling Agents", pp. 174-216, Composite Materials, Volume 6: Interfaces in Polymer Matrix Composites, (Edwin P. Plueddemann, Ed.), Academic Press, New York, 1974.

Plueddemann, Edwin P., "Present Status and Research Needs in Silane Coupling", pp. 17-33, Interfaces in Polymer, Ceramic, and Metal Matrix Composites, (Hatsuo Ishida, Ed.), Elsevier Science Publishing Co., Inc., New York, 1988.

Powell, Peter C., Engineering with Polymers, Chapman and Hall Ltd., 1983.

Puglisi, Joseph S. and Mohammad A. Chaudhari, "Epoxies (EP)", pp. 240-241, Engineered Materials Handbook, Volume 2, Engineering Plastics, (Cyril A. Dostal, Ed.), ASM International, Metals Park, OH, 1988.

Rohwer, Klaus and Xie Ming Jiu, "Micromechanical Curing Stresses in CFRP", Composites Science and Technology, Vol. 25, pp. 169-186, 1986.

Rousseau, C.Q., M.W. Hyer, and S.S. Tompkins, Stresses and Deformations in Angle-Ply Composite Tubes, Virginia Polytechnic Institute and State University, Blacksburg, VA, 1987.

Schwartz, Mel M., Composite Materials Handbook, McGraw-Hill Book Company, New York, 1984.

Selley, Jeffrey, "Polyester Resins", pp. 256-274, Encyclopedia of Polymer Science and Engineering, Volume 12, John Wiley and Sons, New York, 1987.

Springer, George S., Barbara A. Sanders, and Randy W. Tung, "Environmental Effects on Glass Fiber Reinforced Polyester and Vinylester Composites", pp. 126-144, Environmental Effects on Composite Materials, Technomic Publishing Co., Inc., Westport, CT, 1981.

Thomason, J.L., and J.B.W. Morsink, "Investigation of the Interphase in Glass Fiber Reinforced Epoxy Composites", pp. 503-512, Interfaces in Polymer, Ceramic, and Metal Matrix Composites, (Hatsuo Ishida, Ed.), Elsevier Science Publishing Co., Inc., New York, 1988.

Vratsanos, Menas S. and Richard J. Farris, "A New Method for Determining Shrinkage Stresses and Properties of Curing Thermosets", pp. 71-80, Composite Interfaces, (Hatsuo Ishida and Jack L. Koenig, Eds.), Elsevier Science Publishing Co., Inc., New York, 1986.

Whitney, J.M., J.W. Gillespie, Jr., L. Biggs, J. Snowden, and J.J. Garrett, CYLAN: Cylinder Analysis, (Computer Program), University of Delaware Engineering Research Center for Composites Manufacturing Science and Engineering, Technomic Publishing Co., Inc., Lancaster, PA, 1987.

Appendix A: Classical Lamination Theory

Classical Lamination Theory is a plane stress solution. Mathematically,

$$\sigma_x = \sigma_x(x,y)$$

$$\sigma_y = \sigma_x(x,y)$$

$$\tau_{xy} = \tau_{xy}(x,y)$$

$$\sigma_z = \tau_{xz} = \tau_{yz} = \gamma_{xz} = \gamma_{yz} = \varepsilon_z = 0$$

$$\gamma_{xy} = \gamma_{xy}(\sigma_x,\sigma_y)$$

Begin with an assumed form of the strain distribution (linear in the through-the thickness coordinate of the laminate):

$$\{\varepsilon\} = \{\varepsilon^0\} + z\{K^0\}$$

$$\{\varepsilon^0\} = \begin{Bmatrix} u_{,x} \\ v_{,y} \\ u_{,y} + v_{,x} \end{Bmatrix}$$

$$\{K^0\} = \begin{Bmatrix} w_{,xx} \\ w_{,yy} \\ 2w_{,xy} \end{Bmatrix}$$

Stress is expressed in terms of strain as follows:

$$\{\sigma\}_k = [\overline{Q}_{ij}]_k \{\varepsilon\}_k$$

$$\overline{Q}_{ij} = T^{-1} Q_{ij} RTR^{-1}$$

$$[T] = \begin{bmatrix} c^2 & s^2 & 2cs \\ s^2 & c^2 & -2cs \\ -sc & sc & c^2 - s^2 \end{bmatrix}$$

$$c = \cos(\theta) \text{ and } s = \sin(\theta)$$

$$[Q_{ij}] = \frac{1}{1-\nu_{12}\nu_{21}} \begin{bmatrix} E_1 & -\nu_{21}E_2 & 0 \\ -\nu_{21}E_2 & E_2 & 0 \\ 0 & 0 & (1-\nu_{12}\nu_{21})G_{12} \end{bmatrix}$$

$$[R] = \begin{bmatrix} 1 & 0 & 0 \\ 0 & 1 & 0 \\ 0 & 0 & 2 \end{bmatrix}$$

Force and moment resultants are expressed as follows (in the structural x-y axes):

$$\{N\}, \{M\} = \sum_{k=1}^{N} \int_{z_{k-1}}^{z_k} \{\sigma\}_k (1, z)\, dz$$

$$\begin{Bmatrix} N \\ M \end{Bmatrix} = \begin{bmatrix} A & B \\ B & D \end{bmatrix} \begin{Bmatrix} \varepsilon^0 \\ \kappa^0 \end{Bmatrix}$$

$$A_{ij}, B_{ij}, D_{ij} = \left(1, \frac{1}{2}, \frac{1}{3}\right) \sum_{k=1}^{N} [\overline{Q}_{ij}](z, z^2, z^3) \Big|_{z_{k-1}}^{z_k}$$

To account for thermal strains,

$$\{\sigma\} = Q_{ij} \begin{Bmatrix} \varepsilon_1 - \alpha_1 \Delta T \\ \varepsilon_2 - \alpha_1 \Delta T \\ \gamma_{12} \end{Bmatrix}$$

$$\{\sigma\} = \overline{Q}_{ij} \begin{Bmatrix} \varepsilon_x - \alpha_x \Delta T \\ \varepsilon_y - \alpha_y \Delta T \\ \gamma_{xy} - \alpha_{xy} \Delta T \end{Bmatrix}$$

$$\{N\} = [A]\{\varepsilon^0\} + [B]\{K^0\} - \{N^T\}$$

$$\{M\} = [B]\{\varepsilon^0\} + [D]\{K^0\} - \{M^T\}$$

$$\{N^T\}, \{M^T\} = \int_{z=-\frac{h}{2}}^{z=\frac{h}{2}} [\overline{Q}_{ij}]_k \begin{Bmatrix} \alpha_x \\ \alpha_y \\ \alpha_{xy} \end{Bmatrix}_k \Delta T(1, z)\, dz = \sum_{k=1}^{N} \int_{z_{k-1}}^{z_k} [\overline{Q}]_k \{\alpha\}_k \Delta T(1, z)\, dz$$

Replace $\{N\}$ by $\{N^T\} + \{N\}$ in the preceding relationships

Appendix B: The Importance of Moisture Effects

Kriz and Stinchcomb (1982) found that moisture absorption leads to the degradation of the matrix and of fiber-matrix interfaces. This results in a drop in lamina properties. Loos (1981) and Springer (1981) measured weight and property changes in polyester-E glass and vinylester-E glass composites as a function of time spent in various media. Humid air, distilled water, salt water, and a number of types of fuel served as the test environments. The nature of the material tested, the temperature of the environment, and the type of environment were found to influence the weight change and mechanical properties. Furthermore, it was found that the effects of temperature and environment on mechanical properties were particularly significant. Clearly, the results indicated that moisture absorption was related to the change in mechanical properties, but no clear-cut correlation between the two could be established from the results.

The specimens described above were analysed as-is following completion of the tests. Other specimens were held under the test conditions for 6 months after which they were dried for 3 weeks at 66°C before being tested. Drying did not lead to a complete restoration of strength or of modulus from the levels observed in the first group of samples to the original levels. Thus, changes in material properties were concluded to be (to some extent) permanent. (Springer

et al., 1981)

In their studies, Springer et al. assumed that moisture absorption was goverened by Fick's law. Agreement between theory and experiment was fairly good until the predicted maximum weight change was attained. The development of internal and surface microcracks was thought to be responsible for matrix material losses and ultimately for the deviation from Fickian behavior. In regions where the process of moisture absorption can not be described by Fick's law, the authors suggest that test data is necessary to establish long-term material behavior. (Springer et al., 1981)

Chamis et al. (1977) presented an integrated theory for predicting the hygrothermomechanical (HGTM) response of laminated fiber-reinforced composite materials and for predicting the effects of hygro and thermal factors on mechanical properties. Graphite-epoxy was the system considered. It was assumed that only the HGTM properties of the resin were affected by moisture and that these effects could be expressed in terms of the laminate's operating temperature and the reduced glass transition temperature of the wet resin.

Micromechanical relationships for volume, density, elastic constants, coefficients of thermal expansion, coefficients of moisture expansion, and strengths of wet resin were summarized. Magnification factors to account for the presence of voids and residual strains were included.

The resin was modelled as being essentially incompressible (i.e., no volume expansion of the resin as the composite expands due to the influx of moisture) and resin behavior was classified as being either viscoelastic or viscoplastic. Good agreement between predicted and measured micromechanical properties was achieved. (Chamis et al., 1977)

The macromechanical behavior of a lamina was described as

$$\{\epsilon_l\} = [E_l]^{-1}\{\sigma_l\} + \Delta T_l\{\alpha_l\} + m_l\{\beta_l\}$$

The similarities between the last two terms allowed the authors to lump the thermal and moisture effects and to use a pre-existing computer program which dealt only with thermal effects. It should be noted that a CLT approach was employed. The results of the study showed that voids present in the resin matrix tended to collapse at moisture contents of ≥1% and that nonuniform through-thickness moisture profiles caused severe laminate warpage. (Chamis et al., 1977)

Farley and Herakovich (1977), recognizing the inability of CLT to predict interlaminar effects, employed an elasticity approach to study the influence of temperature and moisture gradients on interlaminar shear stresses near free edges of a composite laminate. In earlier studies, these authors had found that free edge boundary layer regions were especially likely to contain transverse and lateral moisture gradients. For simplicity, a long,

finite-width planar laminate comprising homogeneous, isotropic layers and displaying linear elastic material behavior was chosen as the test configuration. Uniform axial mechanical loads and gradient hygrothermal loads were considered using the displacement formulation of the Finite Element Method. It was found that moisture-induced stresses could be larger than those due to mechanical and thermal loads and that slight changes in moisture gradients had significant effects upon the calculated stress distributions. Interface morphology, material properties, and laminate stacking sequence were also found to influence the results.

Under conditions of uniform hygrothermal and mechanical loading, a uniform moisture content of 0.5% was found to cancel out the effects of the residual thermal curing stresses associated with a curing to operating temperature difference of 82.5 K. Thus, small, uniform moisture concentrations were found to be beneficial in alleviating the effects of residual curing stresses. At higher moisture contents (e.g., 1%) however, hygral stresses were found to far exceed the thermal curing stresses. (Farley and Herakovich, 1977)

In comparing temperature and moisture effects, it was pointed out that the relatively high coefficient of thermal diffusivity of graphite-polyimide composites enables them to reach a uniform temperature quite quickly. In contrast, the attainment of a uniformly saturated moisture condition may

require several years at ambient temperature. The implication of this is that a gradient-type analysis is frequently appropriate, even under controlled laboratory conditions.

Farley and Herakovich (1977) compared the stress effects due to various moisture gradients to the stress state in a uniformly saturated composite. A uniform moisture gradient was found to cause a stress distribution similar to that of the base case except in the boundary layer region. For two-dimensional moisture gradients, the interlaminar normal stress distribution was significantly affected by the location of the gradient while interlaminar shearing stresses were less affected as compared to the base case. It was also noted that once steep moisture gradients had passed through a boundary layer (i.e., near the free edges of a laminate) the interlaminar stresses attained a state like that in the base case.

Farley and Herakovich (1977) recommended that hygrothermal loading be considered in addition to mechanical loading for any stress analysis of composite structures with free edges. They also pointed out that it would be desirable to have results which reflect nonlinear material behavior and also which include the variations in material properties due to hygrothermal effects.

Appendix C: Finite Element Analysis Data Files and SAPIV Outputs

The first section of this appendix contains listings of the data files used to perform the analysis documented in Section 3.2. The data files pertain to the following four cases, respectively:

1. The "test case" using a uniform material; used to assess the suitability of the mesh for the analysis.
2. The data corresponding to free shrinkage of the resin onto the fiber.
3. The data corresponding to an imposed displacement of -0.181×10^{-6} m along edge 3 of the region of analysis.
4. The data corresponding to an imposed displacement of -0.1717×10^{-6} m along edge 3 of the region of analysis.

The second section of this appendix contains a listing of the SAP IV output corresponding to case 4, above.

Data File for Case 1

```
Plane Strain Solution using 2D Elements
  103     2     1     0     0     0     0     0
    1     1     0     0     1     1     1           0           0           0     0    25
    2     1     0     0     1     1     1           0           1           0     0    25
    3     1     0     0     1     1     1           0           1           1     0    25
    4     1     0     0     1     1     1           0           2           2     0    25
    5     1     0     0     1     1     1           0           2           1     0    25
    6     1     0     0     1     1     1           0           2           0     0    25
    7     1     0     0     1     1     1           0           3           0     0    25
    8     1     0     0     1     1     1           0           3           1     0    25
    9     1     0     0     1     1     1           0           3           2     0    25
   10     1     0     0     1     1     1           0           3           3     0    25
   11     1     0     0     1     1     1           0           4           4     0    25
   12     1     0     0     1     1     1           0           4           3     0    25
   13     1     0     0     1     1     1           0           4           2     0    25
   14     1     0     0     1     1     1           0           4           1     0    25
   15     1     0     0     1     1     1           0           4           0     0    25
   16     1     0     0     1     1     1           0           5           0     0    25
   17     1     0     0     1     1     1           0           5           1     0    25
   18     1     0     0     1     1     1           0           5           2     0    25
   19     1     0     0     1     1     1           0           5           3     0    25
   20     1     0     0     1     1     1           0           5           4     0    25
   21     1     0     0     1     1     1           0           5           5     0    25
   22     1     0     0     1     1     1           0   5657E-3     5657E-3     0    25
   23     1     0     0     1     1     1           0           6     5292E-3     0    25
   24     1     0     0     1     1     1           0           6           4     0    25
   25     1     0     0     1     1     1           0           6           3     0    25
   26     1     0     0     1     1     1           0           6           2     0    25
   27     1     0     0     1     1     1           0           6           1     0    25
   28     1     0     0     1     1     1           0           6           0     0    25
   29     1     0     0     1     1     1           0           7           0     0    25
   30     1     0     0     1     1     1           0           7           1     0    25
   31     1     0     0     1     1     1           0           7           2     0    25
   32     1     0     0     1     1     1           0           7           3     0    25
```

33	1	0	0	1	1	1	0	6928E-3	4	0	25
34	1	0	0	1	1	1	0	6568E-3	4568E-3	0	25
35	1	0	0	1	1	1	0	7	5	0	25
36	1	0	0	1	1	1	0	7	6	0	25
37	1	0	0	1	1	1	0	6	6	0	25
38	1	0	0	1	1	1	0	7	7	0	25
39	1	0	0	1	1	1	0	8	8	0	25
40	1	0	0	1	1	1	0	8	7	0	25
41	1	0	0	1	1	1	0	8	6	0	25
42	1	0	0	1	1	1	0	8	5	0	25
43	1	0	0	1	1	1	0	8	4	0	25
44	1	0	0	1	1	1	0	7416E-3	3	0	25.
45	1	0	0	1	1	1	0	8	3	0	25
46	1	0	0	1	1	1	0	7746E-3	2	0	25
47	1	0	0	1	1	1	0	7937E-3	1	0	25
48	1	0	0	1	1	1	0	8	0	0	25
49	1	0	0	1	1	1	0	9	0	0	25
50	1	0	0	1	1	1	0	9	1	0	25
51	1	0	0	1	1	1	0	9	2	0	25
52	1	0	0	1	1	1	0	9	3	0	25
53	1	0	0	1	1	1	0	9	4	0	25
54	1	0	0	1	1	1	0	9	5	0	25
55	1	0	0	1	1	1	0	9	6	0	25
56	1	0	0	1	1	1	0	9	7	0	25
57	1	0	0	1	1	1	0	9	8	0	25
58	1	0	0	1	1	1	0	9	9	0	25
59	1	0	0	1	1	1	0	10	10	0	25
60	1	0	0	1	1	1	0	10	9	0	25
61	1	0	0	1	1	1	0	10	8	0	25
62	1	0	0	1	1	1	0	10	7	0	25
63	1	0	0	1	1	1	0	10	6	0	25
64	1	0	0	1	1	1	0	10	5	0	25
65	1	0	0	1	1	1	0	10	4	0	25
66	1	0	0	1	1	1	0	10	3	0	25
67	1	0	0	1	1	1	0	10	2	0	25
68	1	0	0	1	1	1	0	10	1	0	25

69	1	0	0	1	1	1	0	10	0	0	25	
70	1	1	1	1	1	1	0	11	0	0	25	
71	1	1	1	1	1	1	0	11	1	0	25	
72	1	1	1	1	1	1	0	11	2	0	25	
73	1	1	1	1	1	1	0	11	3	0	25	
74	1	1	1	1	1	1	0	11	4	0	25	
75	1	1	1	1	1	1	0	11	5	0	25	
76	1	1	1	1	1	1	0	11	6	0	25	
77	1	1	1	1	1	1	0	11	7	0	25	
78	1	1	1	1	1	1	0	11	8	0	25	
79	1	1	1	1	1	1	0	11	9	0	25	
80	1	1	1	1	1	1	0	11	10	0	25	
81	1	1	1	1	1	1	0	10	11	0	25	
82	1	1	1	1	1	1	0	82929E-4	97071E-4	0	25	
83	1	1	1	1	1	1	0	72929E-4	87071E-4	0	25	
84	1	1	1	1	1	1	0	62929E-4	77071E-4	0	25	
85	1	1	1	1	1	1	0	52929E-4	67071E-4	0	25	
86	1	1	1	1	1	1	0	49498E-4	63639E-4	0	25	
87	1	1	1	1	1	1	0	42929E-4	57071E-4	0	25	
88	1	1	1	1	1	1	0	32929E-4	47071E-4	0	25	
89	1	1	1	1	1	1	0	22929E-4	37071E-4	0	25	
90	1	1	1	1	1	1	0	12929E-4	27071E-4	0	25	
91	1	1	1	1	1	1	0	2929E-4	17071E-4	0	25	
92	1	1	1	1	1	1	0	-1	0	0	25	
93	1	1	1	1	1	1	0	0	-1	0	25	
94	1	1	1	1	1	1	0	1	-1	0	25	
95	1	1	1	1	1	1	0	2	-1	0	25	
96	1	1	1	1	1	1	0	3	-1	0	25	
97	1	1	1	1	1	1	0	4	-1	0	25	
98	1	1	1	1	1	1	0	5	-1	0	25	
99	1	1	1	1	1	1	0	6	-1	0	25	
100	1	1	1	1	1	1	0	7	-1	0	25	
101	1	1	1	1	1	1	0	8	-1	0	25	
102	1	1	1	1	1	1	0	9	-1	0	25	
103	1	1	1	1	1	1	0	10	-1	0	25	
4	105	2	1	1	1							

```
1    1          1.          1.          0.
      25.     3400E6      3400E6      3400E6     350E-3      350E-3      350E-3      126E7
    63E-6       63E-6       63E-6
2    1          1.          1.          0.
      25.     7200E7      7200E7      7200E7     250E-3      250E-3      250E-3      288E8
    50E-7       50E-7       50E-7
    10E-1          0.          0.          0.          0.
         0          0.          0.          0.          0.
         0          0.          0.          0.          0.
         0          0.          0.          0.          0.
1    1    2    3    3    1      501.          0.    16    0      1.
2    2    6    5    5    1      501.          0.    16    0      1.
3    2    5    3    3    1      501.          0.    16    0      1.
4    3    5    4    4    1      501.          0.    16    0      1.
5    4    9   10   10    1      501.          0.    16    0      1.
6    5    9    4    4    1      501.          0.    16    0      1.
7    5    8    9    9    1      501.          0.    16    0      1.
8    6    8    5    5    1      501.          0.    16    0      1.
9    6    7    8    8    1      501.          0.    16    0      1.
10   7   15   14   14    1      501.          0.    16    0      1.
11   7   14    8    8    1      501.          0.    16    0      1.
12   8   14   13   13    1      501.          0.    16    0      1.
13   8   13    9    9    1      501.          0.    16    0      1.
14   9   13   12   12    1      501.          0.    16    0      1.
15   9   12   10   10    1      501.          0.    16    0      1.
16  10   12   11   11    1      501.          0.    16    0      1.
17  11   20   21   21    1      501.          0.    16    0      1.
18  12   20   11   11    1      501.          0.    16    0      1.
19  12   19   20   20    1      501.          0.    16    0      1.
20  13   19   12   12    1      501.          0.    16    0      1.
21  13   18   19   19    1      501.          0.    16    0      1.
22  14   18   13   13    1      501.          0.    16    0      1.
23  14   17   18   18    1      501.          0.    16    0      1.
24  15   17   14   14    1      501.          0.    16    0      1.
25  15   16   17   17    1      501.          0.    16    0      1.
26  16   28   27   27    1      501.          0.    16    0      1.
```

27	16	27	17	17	1	501.	0.	16	0	1.
28	17	27	26	26	1	501.	0.	16	0	1.
29	17	26	18	18	1	501.	0.	16	0	1.
30	18	26	25	25	1	501.	0.	16	0	1.
31	18	25	19	19	1	501.	0.	16	0	1.
32	19	25	24	24	1	501.	0.	16	0	1.
33	19	24	20	20	1	501.	0.	16	0	1.
34	20	24	23	23	1	501.	0.	16	0	1.
35	20	23	21	21	1	501.	0.	16	0	1.
36	21	23	22	22	1	501.	0.	16	0	1.
37	22	23	37	37	1	501.	0.	16	0	1.
38	37	36	38	38	1	501.	0.	16	0	1.
39	23	36	37	37	1	501.	0.	16	0	1.
40	23	35	36	36	1	501.	0.	16	0	1.
41	23	34	35	35	1	501.	0.	16	0	1.
42	23	24	34	34	1	501.	0.	16	0	1.
43	34	33	35	35	1	501.	0.	16	0	1.
44	24	33	34	34	1	501.	0.	16	0	1.
45	25	33	24	24	1	501.	0.	16	0	1.
46	25	32	33	33	1	501.	0.	16	0	1.
47	25	26	32	32	1	501.	0.	16	0	1.
48	26	31	32	32	1	501.	0.	16	0	1.
49	26	27	31	31	1	501.	0.	16	0	1.
50	27	30	31	31	1	501.	0.	16	0	1.
51	27	28	30	30	1	501.	0.	16	0	1.
52	28	29	30	30	1	501.	0.	16	0	1.
53	29	48	47	47	1	501.	0.	16	0	1.
54	29	47	30	30	1	501.	0.	16	0	1.
55	30	47	46	46	1	501.	0.	16	0	1.
56	30	46	31	31	1	501.	0.	16	0	1.
57	31	46	44	44	1	501.	0.	16	0	1.
58	31	44	32	32	1	501.	0.	16	0	1.
59	46	45	44	44	1	501.	0.	16	0	1.
60	32	44	33	33	1	501.	0.	16	0	1.
61	44	45	43	43	1	501.	0.	16	0	1.
62	44	43	33	33	1	501.	0.	16	0	1.

63	33	43	42	42	1	501.	0.	16	0	1.
64	33	42	35	35	1	501.	0.	16	0	1.
65	35	42	41	41	1	501.	0.	16	0	1.
66	35	41	36	36	1	501.	0.	16	0	1.
67	36	41	40	40	1	501.	0.	16	0	1.
68	36	40	38	38	1	501.	0.	16	0	1.
69	38	40	39	39	1	501.	0.	16	0	1.
70	39	57	58	58	1	501.	0.	16	0	1.
71	40	57	39	39	1	501.	0.	16	0	1.
72	40	56	57	57	1	501.	0.	16	0	1.
73	41	56	40	40	1	501.	0.	16	0	1.
74	41	55	56	56	1	501.	0.	16	0	1.
75	42	55	41	41	1	501.	0.	16	0	1.
76	42	54	55	55	1	501.	0.	16	0	1.
77	43	54	42	42	1	501.	0.	16	0	1.
78	43	53	54	54	1	501.	0.	16	0	1.
79	43	45	53	53	1	501.	0.	16	0	1.
80	45	52	53	53	1	501.	0.	16	0	1.
81	46	52	45	45	1	501.	0.	16	0	1.
82	46	51	52	52	1	501.	0.	16	0	1.
83	46	47	51	51	1	501.	0.	16	0	1.
84	47	50	51	51	1	501.	0.	16	0	1.
85	47	48	50	50	1	501.	0.	16	0	1.
86	48	49	50	50	1	501.	0.	16	0	1.
87	49	69	68	68	1	501.	0.	16	0	1.
88	49	68	50	50	1	501.	0.	16	0	1.
89	50	68	67	67	1	501.	0.	16	0	1.
90	51	50	67	67	1	501.	0.	16	0	1.
91	51	67	66	66	1	501.	0.	16	0	1.
92	52	51	66	66	1	501.	0.	16	0	1.
93	52	66	65	65	1	501.	0.	16	0	1.
94	53	52	65	65	1	501.	0.	16	0	1.
95	53	65	64	64	1	501.	0.	16	0	1.
96	54	53	64	64	1	501.	0.	16	0	1.
97	54	64	63	63	1	501.	0.	16	0	1.
98	55	54	63	63	1	501.	0.	16	0	1.

99	55	63	62	62	1	501.	0.	16	0	1.
100	56	55	62	62	1	501.	0.	16	0	1.
101	56	62	61	61	1	501.	0.	16	0	1.
102	57	56	61	61	1	501.	0.	16	0	1.
103	57	61	60	60	1	501.	0.	16	0	1.
104	58	57	60	60	1	501.	0.	16	0	1.
105	58	60	59	59	1	501.	0.	16	0	1.
7	34									
	1.		0.		0.	0.				
1	92				1		0		0	1E16
1	93				1		0		0	1E16
2	94				1		0		0	1E16
3	91				1		0		0	1E16
4	90				1		0		0	1E16
6	95				1		0		0	1E16
7	96				1		0		0	1E16
10	89				1		0		0	1E16
11	88				1		0		0	1E16
15	97				1		0		0	1E16
16	98				1		0		0	1E16
21	87				1		0		0	1E16
22	86				1		0		0	1E16
28	99				1		0		0	1E16
29	100				1		0		0	1E16
37	85				1		0		0	1E16
38	84				1		0		0	1E16
39	83				1		0		0	1E16
48	101				1		0		0	1E16
49	102				1		0		0	1E16
58	82				1		0		0	1E16
59	81				1		-.1250E-0		0	1E16
59	80				1		-.1250E-0		0	1E16
60	79				1		-.1250E-0		0	1E16
61	78				1		-.1250E-0		0	1E16
62	77				1		-.1250E-0		0	1E16
63	76				1		-.1250E-0		0	1E16

64	75	1	-.1250E-0	0	1E16
65	74	1	-.1250E-0	0	1E16
66	73	1	-.1250E-0	0	1E16
67	72	1	-.1250E-0	0	1E16
68	71	1	-.1250E-0	0	1E16
69	70	1	-.1250E-0	0	1E16
69	103	1	0	0	1E16

1. 0. 0. 0.

Data File for Case 2

```
Plane Strain Solution using 2D Elements
  103     2     1     0     0     0     0     0
    1     1     0     0     1     1     1           0           0           0     0    25
    2     1     0     0     1     1     1           0           1           0     0    25
    3     1     0     0     1     1     1           0           1           1     0    25
    4     1     0     0     1     1     1           0           2           2     0    25
    5     1     0     0     1     1     1           0           2           1     0    25
    6     1     0     0     1     1     1           0           2           0     0    25
    7     1     0     0     1     1     1           0           3           0     0    25
    8     1     0     0     1     1     1           0           3           1           25
    9     1     0     0     1     1     1           0           3           2     0    25
   10     1     0     0     1     1     1           0           3           3     0    25
   11     1     0     0     1     1     1           0           4           4     0    25
   12     1     0     0     1     1     1           0           4           3     0    25
   13     1     0     0     1     1     1           0           4           2     0    25
   14     1     0     0     1     1     1           0           4           1     0    25
   15     1     0     0     1     1     1           0           4           0     0    25
   16     1     0     0     1     1     1           0           5           0     0    25
   17     1     0     0     1     1     1           0           5           1     0    25
   18     1     0     0     1     1     1           0           5           2     0    25
   19     1     0     0     1     1     1           0           5           3     0    25
   20     1     0     0     1     1     1           0           5           4     0    25
   21     1     0     0     1     1     1           0           5           5     0    25
   22     1     0     0     1     1     1           0    5657E-3     5657E-3     0    25
   23     1     0     0     1     1     1           0           6     5292E-3     0    25
   24     1     0     0     1     1     1           0           6           4     0    25
   25     1     0     0     1     1     1           0           6           3     0    25
   26     1     0     0     1     1     1           0           6           2     0    25
   27     1     0     0     1     1     1           0           6           1     0    25
   28     1     0     0     1     1     1           0           6           0     0    25
   29     1     0     0     1     1     1           0           7           0     0    25
   30     1     0     0     1     1     1           0           7           1     0    25
   31     1     0     0     1     1     1           0           7           2     0    25
   32     1     0     0     1     1     1           0           7           3     0    25
```

33	1	0	0	1	1	1	0	6928E-3	4	0	25
34	1	0	0	1	1	1	0	6568E-3	4568E-3	0	25
35	1	0	0	1	1	1	0	7	5	0	25
36	1	0	0	1	1	1	0	7	6	0	25
37	1	0	0	1	1	1	0	6	6	0	25
38	1	0	0	1	1	1	0	7	7	0	25
39	1	0	0	1	1	1	0	8	8	0	25
40	1	0	0	1	1	1	0	8	7	0	25
41	1	0	0	1	1	1	0	8	6	0	25
42	1	0	0	1	1	1	0	8	5	0	25
43	1	0	0	1	1	1	0	8	4	0	25
44	1	0	0	1	1	1	0	7416E-3	3	0	25
45	1	0	0	1	1	1	0	8	3	0	25
46	1	0	0	1	1	1	0	7746E-3	2	0	25
47	1	0	0	1	1	1	0	7937E-3	1	0	25
48	1	0	0	1	1	1	0	8	0	0	25
49	1	0	0	1	1	1	0	9	0	0	25
50	1	0	0	1	1	1	0	9	1	0	25
51	1	0	0	1	1	1	0	9	2	0	25
52	1	0	0	1	1	1	0	9	3	0	25
53	1	0	0	1	1	1	0	9	4	0	25
54	1	0	0	1	1	1	0	9	5	0	25
55	1	0	0	1	1	1	0	9	6	0	25
56	1	0	0	1	1	1	0	9	7	0	25
57	1	0	0	1	1	1	0	9	8	0	25
58	1	0	0	1	1	1	0	9	9	0	25
59	1	0	0	1	1	1	0	10	10	0	25
60	1	0	0	1	1	1	0	10	9	0	25
61	1	0	0	1	1	1	0	10	8	0	25
62	1	0	0	1	1	1	0	10	7	0	25
63	1	0	0	1	1	1	0	10	6	0	25
64	1	0	0	1	1	1	0	10	5	0	25
65	1	0	0	1	1	1	0	10	4	0	25
66	1	0	0	1	1	1	0	10	3	0	25
67	1	0	0	1	1	1	0	10	2	0	25
68	1	0	0	1	1	1	0	10	1	0	25

69	1	0	0	1	1	1	0	10	0	0	25	
70	1	1	1	1	1	1	0	11	0	0	25	
71	1	1	1	1	1	1	0	11	1	0	25	
72	1	1	1	1	1	1	0	11	2	0	25	
73	1	1	1	1	1	1	0	11	3	0	25	
74	1	1	1	1	1	1	0	11	4	0	25	
75	1	1	1	1	1	1	0	11	5	0	25	
76	1	1	1	1	1	1	0	11	6	0	25	
77	1	1	1	1	1	1	0	11	7	0	25	
78	1	1	1	1	1	1	0	11	8	0	25	
79	1	1	1	1	1	1	0	11	9	0	25	
80	1	1	1	1	1	1	0	11	10	0	25	
81	1	1	1	1	1	1	0	92929E-4	107071E-4	0	25	
82	1	1	1	1	1	1	0	82929E-4	97071E-4	0	25	
83	1	1	1	1	1	1	0	72929E-4	87071E-4	0	25	
84	1	1	1	1	1	1	0	62929E-4	77071E-4	0	25	
85	1	1	1	1	1	1	0	52929E-4	67071E-4	0	25	
86	1	1	1	1	1	1	0	49498E-4	63639E-4	0	25	
87	1	1	1	1	1	1	0	42929E-4	57071E-4	0	25	
88	1	1	1	1	1	1	0	32929E-4	47071E-4	0	25	
89	1	1	1	1	1	1	0	22929E-4	37071E-4	0	25	
90	1	1	1	1	1	1	0	12929E-4	27071E-4	0	25	
91	1	1	1	1	1	1	0	2929E-4	17071E-4	0	25	
92	1	1	1	1	1	1	0	-1	0	0	25	
93	1	1	1	1	1	1	0	0	-1	0	25	
94	1	1	1	1	1	1	0	1	-1	0	25	
95	1	1	1	1	1	1	0	2	-1	0	25	
96	1	1	1	1	1	1	0	3	-1	0	25	
97	1	1	1	1	1	1	0	4	-1	0	25	
98	1	1	1	1	1	1	0	5	-1	0	25	
99	1	1	1	1	1	1	0	6	-1	0	25	
100	1	1	1	1	1	1	0	7	-1	0	25	
101	1	1	1	1	1	1	0	8	-1	0	25	
102	1	1	1	1	1	1	0	9	-1	0	25	
103	1	1	1	1	1	1	0	10	-1	0	25	
4	105	2	1	1	1							

```
 1     1          1.          1.          0.
      25.     3400E6      3400E6      3400E6     350E-3     350E-3     350E-3     126E7
    63E-6       63E-6       63E-6
 2     1          1.          1.          0.
      25.     7200E7      7200E7      7200E7     250E-3     250E-3     250E-3     288E8
    50E-7       50E-7       50E-7
    10E-1          0.          0.          0.         0.
         0          0.          0.          0.         0.
         0          0.          0.          0.         0.
         0          0.          0.          0.         0.
 1     1     2     3     3     2        25.         0.    16     0        1.
 2     2     6     5     5     2        25.         0.    16     0        1.
 3     2     5     3     3     2        25.         0.    16     0        1.
 4     3     5     4     4     2        25.         0.    16     0        1.
 5     4     9    10    10     2        25.         0.    16     0        1.
 6     5     9     4     4     2        25.         0.    16     0        1.
 7     5     8     9     9     2        25.         0.    16     0        1.
 8     6     8     5     5     2        25.         0.    16     0        1.
 9     6     7     8     8     2        25.         0.    16     0        1.
10     7    15    14    14     2        25.         0.    16     0        1.
11     7    14     8     8     2        25.         0.    16     0        1.
12     8    14    13    13     2        25.         0.    16     0        1.
13     8    13     9     9     2        25.         0.    16     0        1.
14     9    13    12    12     2        25.         0.    16     0        1.
15     9    12    10    10     2        25.         0.    16     0        1.
16    10    12    11    11     2        25.         0.    16     0        1.
17    11    20    21    21     2        25.         0.    16     0        1.
18    12    20    11    11     2        25.         0.    16     0        1.
19    12    19    20    20     2        25.         0.    16     0        1.
20    13    19    12    12     2        25.         0.    16     0        1.
21    13    18    19    19     2        25.         0.    16     0        1.
22    14    18    13    13     2        25.         0.    16     0        1.
23    14    17    18    18     2        25.         0.    16     0        1.
24    15    17    14    14     2        25.         0.    16     0        1.
25    15    16    17    17     2        25.         0.    16     0        1.
26    16    28    27    27     2        25.         0.    16     0        1.
```

27	16	27	17	17	2
28	17	27	26	26	2
29	17	26	18	18	2
30	18	26	25	25	2
31	18	25	19	19	2
32	19	25	24	24	2
33	19	24	20	20	2
34	20	24	23	23	2
35	20	23	21	21	2
36	21	23	22	22	2
37	22	23	37	37	1
38	37	36	38	38	1
39	23	36	37	37	1
40	23	35	36	36	1
41	23	34	35	35	1
42	23	24	34	34	2
43	34	33	35	35	1
44	24	33	34	34	2
45	25	33	24	24	2
46	25	32	33	33	2
47	26	27	31	31	2
48	26	31	32	32	2
49	26	27	31	31	2
50	27	30	31	31	2
51	27	28	30	30	2
52	28	29	30	30	2
53	29	48	47	47	2
54	29	47	30	30	2
55	30	47	46	46	2
56	30	46	31	31	2
57	31	46	44	44	2
58	31	44	32	32	2
59	46	45	44	44	1
60	32	44	33	33	2
61	44	45	43	43	1
62	44	43	33	33	1

25.	0.	16	0	1.
25.	0.	16	0	1.
25.	0.	16	0	1.
25.	0.	16	0	1.
25.	0.	16	0	1.
25.	0.	16	0	1.
25.	0.	16	0	1.
25.	0.	16	0	1.
25.	0.	16	0	1.
25.	0.	16	0	1.
501.	0.	16	0	1.
501.	0.	16	0	1.
501.	0.	16	0	1.
501.	0.	16	0	1.
501.	0.	16	0	1.
25.	0.	16	0	1.
501.	0.	16	0	1.
25.	0.	16	0	1.
25.	0.	16	0	1.
25.	0.	16	0	1.
25.	0.	16	0	1.
25.	0.	16	0	1.
25.	0.	16	0	1.
25.	0.	16	0	1.
25.	0.	16	0	1.
25.	0.	16	0	1.
25.	0.	16	0	1.
25.	0.	16	0	1.
25.	0.	16	0	1.
25.	0.	16	0	1.
501.	0.	16	0	1.
25.	0.	16	0	1.
501.	0.	16	0	1.
501.	0.	16	0	1.

63	33	43	42	42	1	501.	0.	16	0	1.
64	33	42	35	35	1	501.	0.	16	0	1.
65	35	42	41	41	1	501.	0.	16	0	1.
66	35	41	36	36	1	501.	0.	16	0	1.
67	36	41	40	40	1	501.	0.	16	0	1.
68	36	40	38	38	1	501.	0.	16	0	1.
69	38	40	39	39	1	501.	0.	16	0	1.
70	39	57	58	58	1	501.	0.	16	0	1.
71	40	57	39	39	1	501.	0.	16	0	1.
72	40	56	57	57	1	501.	0.	16	0	1.
73	41	56	40	40	1	501.	0.	16	0	1.
74	41	55	56	56	1	501.	0.	16	0	1.
75	42	55	41	41	1	501.	0.	16	0	1.
76	42	54	55	55	1	501.	0.	16	0	1.
77	43	54	42	42	1	501.	0.	16	0	1.
78	43	53	54	54	1	501.	0.	16	0	1.
79	43	45	53	53	1	501.	0.	16	0	1.
80	45	52	53	53	1	501.	0.	16	0	1.
81	46	52	45	45	1	501.	0.	16	0	1.
82	46	51	52	52	1	501.	0.	16	0	1.
83	46	47	51	51	1	501.	0.	16	0	1.
84	47	50	51	51	1	501.	0.	16	0	1.
85	47	48	50	50	1	501.	0.	16	0	1.
86	48	49	50	50	1	501.	0.	16	0	1.
87	49	69	68	68	1	501.	0.	16	0	1.
88	49	68	50	50	1	501.	0.	16	0	1.
89	50	68	67	67	1	501.	0.	16	0	1.
90	51	50	67	67	1	501.	0.	16	0	1.
91	51	67	66	66	1	501.	0.	16	0	1.
92	52	51	66	66	1	501.	0.	16	0	1.
93	52	66	65	65	1	501.	0.	16	0	1.
94	53	52	65	65	1	501.	0.	16	0	1.
95	53	65	64	64	1	501.	0.	16	0	1.
96	54	53	64	64	1	501.	0.	16	0	1.
97	54	64	63	63	1	501.	0.	16	0	1.
98	55	54	63	63	1	501.	0.	16	0	1.

```
 99   55   63   62   62    1      501.          0.   16    0      1.
100   56   55   62   62    1      501.          0.   16    0      1.
101   56   62   61   61    1      501.          0.   16    0      1.
102   57   56   61   61    1      501.          0.   16    0      1.
103   57   61   60   60    1      501.          0.   16    0      1.
104   58   57   60   60    1      501.          0.   16    0      1.
105   58   60   59   59    1      501.          0.   16    0      1.
  7   23
       1.         0.         0.        0.
  1   92                     1                    0         0     1E16
  1   93                     1                    0         0     1E16
  2   94                     1                    0         0     1E16
  3   91                     1                    0         0     1E16
  4   90                     1                    0         0     1E16
  6   95                     1                    0         0     1E16
  7   96                     1                    0         0     1E16
 10   89                     1                    0         0     1E16
 11   88                     1                    0         0     1E16
 15   97                     1                    0         0     1E16
 16   98                     1                    0         0     1E16
 21   87                     1                    0         0     1E16
 22   86                     1                    0         0     1E16
 28   99                     1                    0         0     1E16
 29  100                     1                    0         0     1E16
 37   85                     1                    0         0     1E16
 38   84                     1                    0         0     1E16
 39   83                     1                    0         0     1E16
 48  101                     1                    0         0     1E16
 49  102                     1                    0         0     1E16
 58   82                     1                    0         0     1E16
 59   81                     1                    0         0     1E16
 69  103                     1                    0         0     1E16
       1.         0.         0.        0.
```

Data File for Case 3

```
Plane Strain Solution using 2D Elements
  103     2     1     0     0     0     0     0
    1     1     0     0     1     1     1          0          0          0     0        25
    2     1     0     0     1     1     1          0          1          0     0        25
    3     1     0     0     1     1     1          0          1          1     0        25
    4     1     0     0     1     1     1          0          2          2     0        25
    5     1     0     0     1     1     1          0          2          1     0        25
    6     1     0     0     1     1     1          0          2          0     0        25
    7     1     0     0     1     1     1          0          3          0     0        25
    8     1     0     0     1     1     1          0          3          1     0        25
    9     1     0     0     1     1     1          0          3          2     0        25
   10     1     0     0     1     1     1          0          3          3     0        25
   11     1     0     0     1     1     1          0          4          4     0        25
   12     1     0     0     1     1     1          0          4          3     0        25
   13     1     0     0     1     1     1          0          4          2     0        25
   14     1     0     0     1     1     1          0          4          1     0        25
   15     1     0     0     1     1     1          0          4          0     0        25
   16     1     0     0     1     1     1          0          5          0     0        25
   17     1     0     0     1     1     1          0          5          1     0        25
   18     1     0     0     1     1     1          0          5          2     0        25
   19     1     0     0     1     1     1          0          5          3     0        25
   20     1     0     0     1     1     1          0          5          4     0        25
   21     1     0     0     1     1     1          0          5          5     0        25
   22     1     0     0     1     1     1          0   5657E-3    5657E-3     0        25
   23     1     0     0     1     1     1          0          6    5292E-3     0        25
   24     1     0     0     1     1     1          0          6          4     0        25
   25     1     0     0     1     1     1          0          6          3     0        25
   26     1     0     0     1     1     1          0          6          2     0        25
   27     1     0     0     1     1     1          0          6          1     0        25
   28     1     0     0     1     1     1          0          6          0     0        25
   29     1     0     0     1     1     1          0          7          0     0        25
   30     1     0     0     1     1     1          0          7          1     0        25
   31     1     0     0     1     1     1          0          7          2     0        25
   32     1     0     0     1     1     1          0          7          3     0        25
```

33	1	0	0	1	1	1	0	6928E-3	4	0	25
34	1	0	0	1	1	1	0	6568E-3	4568E-3	0	25
35	1	0	0	1	1	1	0	7	5	0	25
36	1	0	0	1	1	1	0	7	6	0	25
37	1	0	0	1	1	1	0	6	6	0	25
38	1	0	0	1	1	1	0	7	7	0	25
39	1	0	0	1	1	1	0	8	8	0	25
40	1	0	0	1	1	1	0	8	7	0	25
41	1	0	0	1	1	1	0	8	6	0	25
42	1	0	0	1	1	1	0	8	5	0	25
43	1	0	0	1	1	1	0	8	4	0	25
44	1	0	0	1	1	1	0	7416E-3	3	0	25
45	1	0	0	1	1	1	0	8	3	0	25
46	1	0	0	1	1	1	0	7746E-3	2	0	25
47	1	0	0	1	1	1	0	7937E-3	1	0	25
48	1	0	0	1	1	1	0	8	0	0	25
49	1	0	0	1	1	1	0	9	0	0	25
50	1	0	0	1	1	1	0	9	1	0	25
51	1	0	0	1	1	1	0	9	2	0	25
52	1	0	0	1	1	1	0	9	3	0	25
53	1	0	0	1	1	1	0	9	4	0	25
54	1	0	0	1	1	1	0	9	5	0	25
55	1	0	0	1	1	1	0	9	6	0	25
56	1	0	0	1	1	1	0	9	7	0	25
57	1	0	0	1	1	1	0	9	8	0	25
58	1	0	0	1	1	1	0	9	9	0	25
59	1	0	0	1	1	1	0	10	10	0	25
60	1	0	0	1	1	1	0	10	9	0	25
61	1	0	0	1	1	1	0	10	8	0	25
62	1	0	0	1	1	1	0	10	7	0	25
63	1	0	0	1	1	1	0	10	6	0	25
64	1	0	0	1	1	1	0	10	5	0	25
65	1	0	0	1	1	1	0	10	4	0	25
66	1	0	0	1	1	1	0	10	3	0	25
67	1	0	0	1	1	1	0	10	2	0	25
68	1	0	0	1	1	1	0	10	1	0	25

69	1	0	0	1	1	1	0	10	0	0	25
70	1	1	1	1	1	1	0	11	0	0	25
71	1	1	1	1	1	1	0	11	1	0	25
72	1	1	1	1	1	1	0	11	2	0	25
73	1	1	1	1	1	1	0	11	3	0	25
74	1	1	1	1	1	1	0	11	4	0	25
75	1	1	1	1	1	1	0	11	5	0	25
76	1	1	1	1	1	1	0	11	6	0	25
77	1	1	1	1	1	1	0	11	7	0	25
78	1	1	1	1	1	1	0	11	8	0	25
79	1	1	1	1	1	1	0	11	9	0	25
80	1	1	1	1	1	1	0	11	10	0	25
81	1	1	1	1	1	1	0	10	11	0	25
82	1	1	1	1	1	1	0	82929E-4	97071E-4	0	25
83	1	1	1	1	1	1	0	72929E-4	87071E-4	0	25
84	1	1	1	1	1	1	0	62929E-4	77071E-4	0	25
85	1	1	1	1	1	1	0	52929E-4	67071E-4	0	25
86	1	1	1	1	1	1	0	49498E-4	63639E-4	0	25
87	1	1	1	1	1	1	0	42929E-4	57071E-4	0	25
88	1	1	1	1	1	1	0	32929E-4	47071E-4	0	25
89	1	1	1	1	1	1	0	22929E-4	37071E-4	0	25
90	1	1	1	1	1	1	0	12929E-4	27071E-4	0	25
91	1	1	1	1	1	1	0	2929E-4	17071E-4	0	25
92	1	1	1	1	1	1	0	-1	0	0	25
93	1	1	1	1	1	1	0	0	-1	0	25
94	1	1	1	1	1	1	0	1	-1	0	25
95	1	1	1	1	1	1	0	2	-1	0	25
96	1	1	1	1	1	1	0	3	-1	0	25
97	1	1	1	1	1	1	0	4	-1	0	25
98	1	1	1	1	1	1	0	5	-1	0	25
99	1	1	1	1	1	1	0	6	-1	0	25
100	1	1	1	1	1	1	0	7	-1	0	25
101	1	1	1	1	1	1	0	8	-1	0	25
102	1	1	1	1	1	1	0	9	-1	0	25
103	1	1	1	1	1	1	0	10	-1	0	25
4	105	2	1	1	1						

1	1		1.		1.	0.					
	25.		3400E6		3400E6	3400E6	350E-3		350E-3	350E-3	126E7
	63E-6		63E-6		63E-6						
2	1		1.		1.	0.					
	25.		7200E7		7200E7	7200E7	250E-3		250E-3	250E-3	288E8
	50E-7		50E-7		50E-7						
	10E-1		0.		0.	0.	0.				
	0		0.		0.	0.	0.				
	0		0.		0.	0.	0.				
	0		0.		0.	0.	0.				
1	1	2	3	3	2	25.	0.	16	0	1.	
2	2	6	5	5	2	25.	0.	16	0	1.	
3	2	5	3	3	2	25.	0.	16	0	1.	
4	3	5	4	4	2	25.	0.	16	0	1.	
5	4	9	10	10	2	25.	0.	16	0	1.	
6	5	9	4	4	2	25.	0.	16	0	1.	
7	5	8	9	9	2	25.	0.	16	0	1.	
8	6	8	5	5	2	25.	0.	16	0	1.	
9	6	7	8	8	2	25.	0.	16	0	1.	
10	7	15	14	14	2	25.	0.	16	0	1.	
11	7	14	8	8	2	25.	0.	16	0	1.	
12	8	14	13	13	2	25.	0.	16	0	1.	
13	8	13	9	9	2	25.	0.	16	0	1.	
14	9	13	12	12	2	25.	0.	16	0	1.	
15	9	12	10	10	2	25.	0.	16	0	1.	
16	10	12	11	11	2	25.	0.	16	0	1.	
17	11	20	21	21	2	25.	0.	16	0	1.	
18	12	20	11	11	2	25.	0.	16	0	1.	
19	12	19	20	20	2	25.	0.	16	0	1.	
20	13	19	12	12	2	25.	0.	16	0	1.	
21	13	18	19	19	2	25.	0.	16	0	1.	
22	14	18	13	13	2	25.	0.	16	0	1.	
23	14	17	18	18	2	25.	0.	16	0	1.	
24	15	17	14	14	2	25.	0.	16	0	1.	
25	15	16	17	17	2	25.	0.	16	0	1.	
26	16	28	27	27	2	25.	0.	16	0	1.	

27	16	27	17	17	2	25.	0.	16	0	1.
28	17	27	26	26	2	25.	0.	16	0	1.
29	17	26	18	18	2	25.	0.	16	0	1.
30	18	26	25	25	2	25.	0.	16	0	1.
31	18	25	19	19	2	25.	0.	16	0	1.
32	19	25	24	24	2	25.	0.	16	0	1.
33	19	24	20	20	2	25.	0.	16	0	1.
34	20	24	23	23	2	25.	0.	16	0	1.
35	20	23	21	21	2	25.	0.	16	0	1.
36	21	23	22	22	2	25.	0.	16	0	1.
37	22	23	37	37	1	501.	0.	16	0	1.
38	37	36	38	38	1	501.	0.	16	0	1.
39	23	36	37	37	1	501.	0.	16	0	1.
40	23	35	36	36	1	501.	0.	16	0	1.
41	23	34	35	35	1	501.	0.	16	0	1.
42	23	24	34	34	2	25.	0.	16	0	1.
43	34	33	35	35	1	501.	0.	16	0	1.
44	24	33	34	34	2	25.	0.	16	0	1.
45	25	33	24	24	2	25.	0.	16	0	1.
46	25	32	33	33	2	25.	0.	16	0	1.
47	26	27	31	31	2	25.	0.	16	0	1.
48	26	31	32	32	2	25.	0.	16	0	1.
49	26	27	31	31	2	25.	0.	16	0	1.
50	27	30	31	31	2	25.	0.	16	0	1.
51	27	28	30	30	2	25.	0.	16	0	1.
52	28	29	30	30	2	25.	0.	16	0	1.
53	29	48	47	47	2	25.	0.	16	0	1.
54	29	47	30	30	2	25.	0.	16	0	1.
55	30	47	46	46	2	25.	0.	16	0	1.
56	30	46	31	31	2	25.	0.	16	0	1.
57	31	46	44	44	2	25.	0.	16	0	1.
58	31	44	32	32	2	25.	0.	16	0	1.
59	46	45	44	44	1	501.	0.	16	0	1.
60	32	44	33	33	2	25.	0.	16	0	1.
61	44	45	43	43	1	501.	0.	16	0	1.
62	44	43	33	33	1	501.	0.	16	0	1.

63	33	43	42	42	1	501.	0.	16	0	1.
64	33	42	35	35	1	501.	0.	16	0	1.
65	35	42	41	41	1	501.	0.	16	0	1.
66	35	41	36	36	1	501.	0.	16	0	1.
67	36	41	40	40	1	501.	0.	16	0	1.
68	36	40	38	38	1	501.	0.	16	0	1.
69	38	40	39	39	1	501.	0.	16	0	1.
70	39	57	58	58	1	501.	0.	16	0	1.
71	40	57	39	39	1	501.	0.	16	0	1.
72	40	56	57	57	1	501.	0.	16	0	1.
73	41	56	40	40	1	501.	0.	16	0	1.
74	41	55	56	56	1	501.	0.	16	0	1.
75	42	55	41	41	1	501.	0.	16	0	1.
76	42	54	55	55	1	501.	0.	16	0	1.
77	43	54	42	42	1	501.	0.	16	0	1.
78	43	53	54	54	1	501.	0.	16	0	1.
79	43	45	53	53	1	501.	0.	16	0	1.
80	45	52	53	53	1	501.	0.	16	0	1.
81	46	52	45	45	1	501.	0.	16	0	1.
82	46	51	52	52	1	501.	0.	16	0	1.
83	46	47	51	51	1	501.	0.	16	0	1.
84	47	50	51	51	1	501.	0.	16	0	1.
85	47	48	50	50	1	501.	0.	16	0	1.
86	48	49	50	50	1	501.	0.	16	0	1.
87	49	69	68	68	1	501.	0.	16	0	1.
88	49	68	50	50	1	501.	0.	16	0	1.
89	50	68	67	67	1	501.	0.	16	0	1.
90	51	50	67	67	1	501.	0.	16	0	1.
91	51	67	66	66	1	501.	0.	16	0	1.
92	52	51	66	66	1	501.	0.	16	0	1.
93	52	66	65	65	1	501.	0.	16	0	1.
94	53	52	65	65	1	501.	0.	16	0	1.
95	53	65	64	64	1	501.	0.	16	0	1.
96	54	53	64	64	1	501.	0.	16	0	1.
97	54	64	63	63	1	501.	0.	16	0	1.
98	55	54	63	63	1	501.	0.	16	0	1.

99	.55	63	62	62	1	501.	0.	16	0	1.
100	56	55	62	62	1	501.	0.	16	0	1.
101	56	62	61	61	1	501.	0.	16	0	1.
102	57	56	61	61	1	501.	0.	16	0	1.
103	57	61	60	60	1	501.	0.	16	0	1.
104	58	57	60	60	1	501.	0.	16	0	1.
105	58	60	59	59	1	501.	0.	16	0	1.
7	34									
	1.		0.		0.	0.				
1	92				1		0		0	1E16
1	93				1		0		0	1E16
2	94				1		0		0	1E16
3	91				1		0		0	1E16
4	90				1		0		0	1E16
6	95				1		0		0	1E16
7	96				1		0		0	1E16
10	89				1		0		0	1E16
11	88				1		0		0	1E16
15	97				1		0		0	1E16
16	98				1		0		0	1E16
21	87				1		0		0	1E16
22	86				1		0		0	1E16
28	99				1		0		0	1E16
29	100				1		0		0	1E16
37	85				1		0		0	1E16
38	84				1		0		0	1E16
39	83				1		0		0	1E16
48	101				1		0		0	1E16
49	102				1		0		0	1E16
58	82				1		0		0	1E16
59	81				1		-.181		0	1E16
59	80				1		-.181		0	1E16
60	79				1		-.181		0	1E16
61	78				1		-.181		0	1E16
62	77				1		-.181		0	1E16
63	76				1		-.181		0	1E16

64	75		1		-.181	0	1E16
65	74		1		-.181	0	1E16
66	73		1		-.181	0	1E16
67	72		1		-.181	0	1E16
68	71		1		-.181	0	1E16
69	70		1		-.181	0	1E16
69	103		1		0	0	1E16
	1.	0.	0.	0.			

Data File for Case 4

```
Plane Strain Solution using 2D Elements
  103    2    1    0    0    0    0    0
    1    1    0    0    1    1    1          0          0          0    0       25
    2    1    0    0    1    1    1          0          1          0    0       25
    3    1    0    0    1    1    1          0          1          1    0       25
    4    1    0    0    1    1    1          0          2          2    0       25
    5    1    0    0    1    1    1          0          2          1    0       25
    6    1    0    0    1    1    1          0          2          0    0       25
    7    1    0    0    1    1    1          0          3          0    0       25
    8    1    0    0    1    1    1          0          3          1    0       25
    9    1    0    0    1    1    1          0          3          2    0       25
   10    1    0    0    1    1    1          0          3          3    0       25
   11    1    0    0    1    1    1          0          4          4    0       25
   12    1    0    0    1    1    1          0          4          3    0       25
   13    1    0    0    1    1    1          0          4          2    0       25
   14    1    0    0    1    1    1          0          4          1    0       25
   15    1    0    0    1    1    1          0          4          0    0       25
   16    1    0    0    1    1    1          0          5          0    0       25
   17    1    0    0    1    1    1          0          5          1    0       25
   18    1    0    0    1    1    1          0          5          2    0       25
   19    1    0    0    1    1    1          0          5          3    0       25
   20    1    0    0    1    1    1          0          5          4    0       25
   21    1    0    0    1    1    1          0          5          5    0       25
   22    1    0    0    1    1    1          0  5657E-3    5657E-3    0       25
   23    1    0    0    1    1    1          0          6    5292E-3    0       25
   24    1    0    0    1    1    1          0          6          4    0       25
   25    1    0    0    1    1    1          0          6          3    0       25
   26    1    0    0    1    1    1          0          6          2    0       25
   27    1    0    0    1    1    1          0          6          1    0       25
   28    1    0    0    1    1    1          0          6          0    0       25
   29    1    0    0    1    1    1          0          7          0    0       25
   30    1    0    0    1    1    1          0          7          1    0       25
   31    1    0    0    1    1    1          0          7          2    0       25
```

32	1	0	0	1	1	1	0	7	3	0	25	
33	1	0	0	1	1	1	0	6928E-3	4	0	25	
34	1	0	0	1	1	1	0	6568E-3	4568E-3	0	25	
35	1	0	0	1	1	1	0	7	5	0	25	
36	1	0	0	1	1	1	0	7	6	0	25	
37	1	0	0	1	1	1	0	6	6	0	25	
38	1	0	0	1	1	1	0	7	7	0	25	
39	1	0	0	1	1	1	0	8	8	0	25	
40	1	0	0	1	1	1	0	8	7	0	25	
41	1	0	0	1	1	1	0	8	6	0	25	
42	1	0	0	1	1	1	0	8	5	0	25	
43	1	0	0	1	1	1	0	8	4	0	25	
44	1	0	0	1	1	1	0	7416E-3	3	0	25	
45	1	0	0	1	1	1	0	8	3	0	25	
46	1	0	0	1	1	1	0	7746E-3	2	0	25	
47	1	0	0	1	1	1	0	7937E-3	1	0	25	
48	1	0	0	1	1	1	0	8	0	0	25	
49	1	0	0	1	1	1	0	9	0	0	25	
50	1	0	0	1	1	1	0	9	1	0	25	
51	1	0	0	1	1	1	0	9	2	0	25	
52	1	0	0	1	1	1	0	9	3	0	25	
53	1	0	0	1	1	1	0	9	4	0	25	
54	1	0	0	1	1	1	0	9	5	0	25	
55	1	0	0	1	1	1	0	9	6	0	25	
56	1	0	0	1	1	1	0	9	7	0	25	
57	1	0	0	1	1	1	0	9	8	0	25	
58	1	0	0	1	1	1	0	9	9	0	25	
59	1	0	0	1	1	1	0	10	10	0	25	
60	1	0	0	1	1	1	0	10	9	0	25	
61	1	0	0	1	1	1	0	10	8	0	25	
62	1	0	0	1	1	1	0	10	7	0	25	
63	1	0	0	1	1	1	0	10	6	0	25	
64	1	0	0	1	1	1	0	10	5	0	25	
65	1	0	0	1	1	1	0	10	4	0	25	
66	1	0	0	1	1	1	0	10	3	0	25	
67	1	0	0	1	1	1	0	10	2	0	25	

68	1	0	0	1	1	1	0	10	1	0	25
69	1	0	0	1	1	1	0	10	0	0	25
70	1	1	1	1	1	1	0	11	0	0	25
71	1	1	1	1	1	1	0	11	1	0	25
72	1	1	1	1	1	1	0	11	2	0	25
73	1	1	1	1	1	1	0	11	3	0	25
74	1	1	1	1	1	1	0	11	4	0	25
75	1	1	1	1	1	1	0	11	5	0	25
76	1	1	1	1	1	1	0	11	6	0	25
77	1	1	1	1	1	1	0	11	7	0	25
78	1	1	1	1	1	1	0	11	8	0	25
79	1	1	1	1	1	1	0	11	9	0	25
80	1	1	1	1	1	1	0	11	10	0	25
81	1	1	1	1	1	1	0	10	11	0	25
82	1	1	1	1	1	1	0	82929E-4	97071E-4	0	25
83	1	1	1	1	1	1	0	72929E-4	87071E-4	0	25
84	1	1	1	1	1	1	0	62929E-4	77071E-4	0	25
85	1	1	1	1	1	1	0	52929E-4	67071E-4	0	25
86	1	1	1	1	1	1	0	49498E-4	63639E-4	0	25
87	1	1	1	1	1	1	0	42929E-4	57071E-4	0	25
88	1	1	1	1	1	1	0	32929E-4	47071E-4	0	25
89	1	1	1	1	1	1	0	22929E-4	37071E-4	0	25
90	1	1	1	1	1	1	0	12929E-4	27071E-4	0	25
91	1	1	1	1	1	1	0	2929E-4	17071E-4	0	25
92	1	1	1	1	1	1	0	-1	0	0	25
93	1	1	1	1	1	1	0	0	-1	0	25
94	1	1	1	1	1	1	0	1	-1	0	25
95	1	1	1	1	1	1	0	2	-1	0	25
96	1	1	1	1	1	1	0	3	-1	0	25
97	1	1	1	1	1	1	0	4	-1	0	25
98	1	1	1	1	1	1	0	5	-1	0	25
99	1	1	1	1	1	1	0	6	-1	0	25
100	1	1	1	1	1	1	0	7	-1	0	25
101	1	1	1	1	1	1	0	8	-1	0	25
102	1	1	1	1	1	1	0	9	-1	0	25
103	1	1	1	1	1	1	0	10	-1	0	25

```
 4  105     2     1     1     1
 1    1          1.          1.          0.
      25.   3400E6    3400E6    3400E6    350E-3    350E-3    350E-3    126E7
    63E-6     63E-6     63E-6
 2    1          1.          1.          0.
      25.   7200E7    7200E7    7200E7    250E-3    250E-3    250E-3    288E8
    50E-7     50E-7     50E-7
    10E-1        0.          0.          0.          0.
         0       0.          0.          0.          0.
         0       0.          0.          0.          0.
         0       0.          0.          0.          0.
 1    1    2    3    3    2    25.         0.    16    0    1.
 2    2    6    5    5    2    25.         0.    16    0    1.
 3    2    5    3    3    2    25.         0.    16    0    1.
 4    3    5    4    4    2    25.         0.    16    0    1.
 5    4    9   10   10    2    25.         0.    16    0    1.
 6    5    9    4    4    2    25.         0.    16    0    1.
 7    5    8    9    9    2    25.         0.    16    0    1.
 8    6    8    5    5    2    25.         0.    16    0    1.
 9    6    7    8    8    2    25.         0.    16    0    1.
10    7   15   14   14    2    25.         0.    16    0    1.
11    7   14    8    8    2    25.         0.    16    0    1.
12    8   14   13   13    2    25.         0.    16    0    1.
13    8   13    9    9    2    25.         0.    16    0    1.
14    9   13   12   12    2    25.         0.    16    0    1.
15    9   12   10   10    2    25.         0.    16    0    1.
16   10   12   11   11    2    25.         0.    16    0    1.
17   11   20   21   21    2    25.         0.    16    0    1.
18   12   20   11   11    2    25.         0.    16    0    1.
19   12   19   20   20    2    25.         0.    16    0    1.
20   13   19   12   12    2    25.         0.    16    0    1.
21   13   18   19   19    2    25.         0.    16    0    1.
22   14   18   13   13    2    25.         0.    16    0    1.
23   14   17   18   18    2    25.         0.    16    0    1.
24   15   17   14   14    2    25.         0.    16    0    1.
25   15   16   17   17    2    25.         0.    16    0    1.
```

26	16	28	27	27	2	25.	0.	16	0	1.
27	16	27	17	17	2	25.	0.	16	0	1.
28	17	27	26	26	2	25.	0.	16	0	1.
29	17	26	18	18	2	25.	0.	16	0	1.
30	18	26	25	25	2	25.	0.	16	0	1.
31	18	25	19	19	2	25.	0.	16	0	1.
32	19	25	24	24	2	25.	0.	16	0	1.
33	19	24	20	20	2	25.	0.	16	0	1.
34	20	24	23	23	2	25.	0.	16	0	1.
35	20	23	21	21	2	25.	0.	16	0	1.
36	21	23	22	22	2	25.	0.	16	0	1.
37	22	23	37	37	1	501.	0.	16	0	1.
38	37	36	38	38	1	501.	0.	16	0	1.
39	23	36	37	37	1	501.	0.	16	0	1.
40	23	35	36	36	1	501.	0.	16	0	1.
41	23	34	35	35	1	501.	0.	16	0	1.
42	23	24	34	34	2	25.	0.	16	0	1.
43	34	33	35	35	1	501.	0.	16	0	1.
44	24	33	34	34	2	25.	0.	16	0	1.
45	25	33	24	24	2	25.	0.	16	0	1.
46	25	32	33	33	2	25.	0.	16	0	1.
47	26	27	31	31	2	25.	0.	16	0	1.
48	26	31	32	32	2	25.	0.	16	0	1.
49	26	27	31	31	2	25.	0.	16	0	1.
50	27	30	31	31	2	25.	0.	16	0	1.
51	27	28	30	30	2	25.	0.	16	0	1.
52	28	29	30	30	2	25.	0.	16	0	1.
53	29	48	47	47	2	25.	0.	16	0	1.
54	29	47	30	30	2	25.	0.	16	0	1.
55	30	47	[illegible]	46	2	25.	0.	16	0	1.
56	30	46	[illegible]	31	2	25.	0.	16	0	1.
57	31	46	[illegible]	44	2	25.	0.	16	0	1.
58	31	44	[illegible]	32	2	25.	0.	16	0	1.
59	46	[illegible]	[illegible]	44	1	501.	0.	16	0	1.
60	32	44	33	33	2	25.	0.	16	0	1.
61	44	45	43	43	1	501.	0.	16	0	1.

62	44	43	33	33	1	501.	0.	16	0	1.
63	33	43	42	42	1	501.	0.	16	0	1.
64	33	42	35	35	1	501.	0.	16	0	1.
65	35	42	41	41	1	501.	0.	16	0	1.
66	35	41	36	36	1	501.	0.	16	0	1.
67	36	41	40	40	1	501.	0.	16	0	1.
68	36	40	38	38	1	501.	0.	16	0	1.
69	38	40	39	39	1	501.	0.	16	0	1.
70	39	57	58	58	1	501.	0.	16	0	1.
71	40	57	39	39	1	501.	0.	16	0	1.
72	40	56	57	57	1	501.	0.	16	0	1.
73	41	56	40	40	1	501.	0.	16	0	1.
74	41	55	56	56	1	501.	0.	16	0	1.
75	42	55	41	41	1	501.	0.	16	0	1.
76	42	54	55	55	1	501.	0.	16	0	1.
77	43	54	42	42	1	501.	0.	16	0	1.
78	43	53	54	54	1	501.	0.	16	0	1.
79	43	45	53	53	1	501.	0.	16	0	1.
80	45	52	53	53	1	501.	0.	16	0	1.
81	46	52	45	45	1	501.	0.	16	0	1.
82	46	51	52	52	1	501.	0.	16	0	1.
83	46	47	51	51	1	501.	0.	16	0	1.
84	47	50	51	51	1	501.	0.	16	0	1.
85	47	48	50	50	1	501.	0.	16	0	1.
86	48	49	50	50	1	501.	0.	16	0	1.
87	49	69	68	68	1	501.	0.	16	0	1.
88	49	68	50	50	1	501.	0.	16	0	1.
89	50	68	67	67	1	501.	0.	16	0	1.
90	51	50	67	67	1	501.	0.	16	0	1.
91	51	67	66	66	1	501.	0.	16	0	1.
92	52	51	66	66	1	501.	0.	16	0	1.
93	52	66	65	65	1	501.	0.	16	0	1.
94	53	52	65	65	1	501.	0.	16	0	1.
95	53	65	64	64	1	501.	0.	16	0	1.
96	54	53	64	64	1	501.	0.	16	0	1.
97	54	64	63	63	1	501.	0.	16	0	1.

98	55	54	63	63	1	501.	0.	16	0	1.
99	55	63	62	62	1	501.	0.	16	0	1.
100	56	55	62	62	1	501.	0.	16	0	1.
101	56	62	61	61	1	501.	0.	16	0	1.
102	57	56	61	61	1	501.	0.	16	0	1.
103	57	61	60	60	1	501.	0.	16	0	1.
104	58	57	60	60	1	501.	0.	16	0	1.
105	58	60	59	59	1	501.	0.	16	0	1.
7	34									
	1.		0.		0.	0.				
1	92				1		0		0	1E16
1	93				1		0		0	1E16
2	94				1		0		0	1E16
3	91				1		0		0	1E16
4	90				1		0		0	1E16
6	95				1		0		0	1E16
7	96				1		0		0	1E16
10	89				1		0		0	1E16
11	88				1		0		0	1E16
15	97				1		0		0	1E16
16	98				1		0		0	1E16
21	87				1		0		0	1E16
22	86				1		0		0	1E16
28	99				1		0		0	1E16
29	100				1		0		0	1E16
37	85				1		0		0	1E16
38	84				1		0		0	1E16
39	83				1		0		0	1E16
48	101				1		0		0	1E16
49	102				1		0		0	1E16
58	82				1		0		0	1E16
59	81				1		-.1717		0	1E16
59	80				1		-.1717		0	1E16
60	79				1		-.1717		0	1E16
61	78				1		-.1717		0	1E16
62	77				1		-.1717		0	1E16

63	76	1	-.1717	0	1E16
64	75	1	-.1717	0	1E16
65	74	1	-.1717	0	1E16
66	73	1	-.1717	0	1E16
67	72	1	-.1717	0	1E16
68	71	1	-.1717	0	1E16
69	70	1	-.1717	0	1E16
69	103	1	0	0	1E16

1. 0. 0. 0.

Output for Case 4

Plane Strain Solution using 2D Elements

C O N T R O L I N F O R M A T I O N

```
    NUMBER OF NODAL POINTS    =  103
    NUMBER OF ELEMENT TYPES   =    2
    NUMBER OF LOAD CASES      =    1
    NUMBER OF FREQUENCIES     =    0
    ANALYSIS CODE (NDYN)      =    0
      EQ.0.  STATIC
      EQ.1.  MODAL EXTRACTION
      EQ.2.  FORCED RESPONSE
      EQ.3.  RESPONSE SPECTRUM
      EQ.4.  DIRECT INTEGRATION
    SOLUTION MODE (MODEX)     =    0
      EQ.0.  EXECUTION
      EQ.1.  DATA CHECK
    NUMBER OF SUBSPACE
    ITERATION VECTORS (NAD)   =    0
    EQUATIONS PER BLOCK       =    0
    TAPE10 SAVE FLAG (N10SV)  =    0
```

NODAL POINT INPUT DATA

NODE	BOUNDARY CONDITION CODES						NODAL POINT COORDINATES				
NUMBER	X	Y	Z	XX	YY	ZZ	X	Y	Z		T
1	1	0	0	1	1	1	0.000	0.000	0.000	0	25.000
2	1	0	0	1	1	1	0.000	1.000	0.000	0	25.000
3	1	0	0	1	1	1	0.000	1.000	1.000	0	25.000
4	1	0	0	1	1	1	0.000	2.000	2.000	0	25.000
5	1	0	0	1	1	1	0.000	2.000	1.000	0	25.000
6	1	0	0	1	1	1	0.000	2.000	0.000	0	25.000

7	1	0	0	1	1	1	0.000	3.000	0.000	0	25.000
8	1	0	0	1	1	1	0.000	3.000	1.000	0	25.000
9	1	0	0	1	1	1	0.000	3.000	2.000	0	25.000
10	1	0	0	1	1	1	0.000	3.000	3.000	0	25.000
11	1	0	0	1	1	1	0.000	4.000	4.000	0	25.000
12	1	0	0	1	1	1	0.000	4.000	3.000	0	25.000
13	1	0	0	1	1	1	0.000	4.000	2.000	0	25.000
14	1	0	0	1	1	1	0.000	4.000	1.000	0	25.000
15	1	0	0	1	1	1	0.000	4.000	0.000	0	25.000
16	1	0	0	1	1	1	0.000	5.000	0.000	0	25.000
17	1	0	0	1	1	1	0.000	5.000	1.000	0	25.000
18	1	0	0	1	1	1	0.000	5.000	2.000	0	25.000
19	1	0	0	1	1	1	0.000	5.000	3.000	0	25.000
20	1	0	0	1	1	1	0.000	5.000	4.000	0	25.000
21	1	0	0	1	1	1	0.000	5.000	5.000	0	25.000
22	1	0	0	1	1	1	0.000	5.657	5.657	0	25.000
23	1	0	0	1	1	1	0.000	6.000	5.292	0	25.000
24	1	0	0	1	1	1	0.000	6.000	4.000	0	25.000
25	1	0	0	1	1	1	0.000	6.000	3.000	0	25.000
26	1	0	0	1	1	1	0.000	6.000	2.000	0	25.000
27	1	0	0	1	1	1	0.000	6.000	1.000	0	25.000
28	1	0	0	1	1	1	0.000	6.000	0.000	0	25.000
29	1	0	0	1	1	1	0.000	7.000	0.000	0	25.000
30	1	0	0	1	1	1	0.000	7.000	1.000	0	25.000
31	1	0	0	1	1	1	0.000	7.000	2.000	0	25.000
32	1	0	0	1	1	1	0.000	7.000	3.000	0	25.000
33	1	0	0	1	1	1	0.000	6.928	4.000	0	25.000
34	1	0	0	1	1	1	0.000	6.568	4.568	0	25.000
35	1	0	0	1	1	1	0.000	7.000	5.000	0	25.000
36	1	0	0	1	1	1	0.000	7.000	6.000	0	25.000
37	1	0	0	1	1	1	0.000	6.000	6.000	0	25.000
38	1	0	0	1	1	1	0.000	7.000	7.000	0	25.000
39	1	0	0	1	1	1	0.000	8.000	8.000	0	25.000
40	1	0	0	1	1	1	0.000	8.000	7.000	0	25.000
41	1	0	0	1	1	1	0.000	8.000	6.000	0	25.000
42	1	0	0	1	1	1	0.000	8.000	5.000	0	25.000

43	1	0	0	1	1	1	0.000	8.000	4.000	0	25.000
44	1	0	0	1	1	1	0.000	7.416	3.000	0	25.000
45	1	0	0	1	1	1	0.000	8.000	3.000	0	25.000
46	1	0	0	1	1	1	0.000	7.746	2.000	0	25.000
47	1	0	0	1	1	1	0.000	7.937	1.000	0	25.000
48	1	0	0	1	1	1	0.000	8.000	0.000	0	25.000
49	1	0	0	1	1	1	0.000	9.000	0.000	0	25.000
50	1	0	0	1	1	1	0.000	9.000	1.000	0	25.000
51	1	0	0	1	1	1	0.000	9.000	2.000	0	25.000
52	1	0	0	1	1	1	0.000	9.000	3.000	0	25.000
53	1	0	0	1	1	1	0.000	9.000	4.000	0	25.000
54	1	0	0	1	1	1	0.000	9.000	5.000	0	25.000
55	1	0	0	1	1	1	0.000	9.000	6.000	0	25.000
56	1	0	0	1	1	1	0.000	9.000	7.000	0	25.000
57	1	0	0	1	1	1	0.000	9.000	8.000	0	25.000
58	1	0	0	1	1	1	0.000	9.000	9.000	0	25.000
59	1	0	0	1	1	1	0.000	10.000	10.000	0	25.000
60	1	0	0	1	1	1	0.000	10.000	9.000	0	25.000
61	1	0	0	1	1	1	0.000	10.000	8.000	0	25.000
62	1	0	0	1	1	1	0.000	10.000	7.000	0	25.000
63	1	0	0	1	1	1	0.000	10.000	6.000	0	25.000
64	1	0	0	1	1	1	0.000	10.000	5.000	0	25.000
65	1	0	0	1	1	1	0.000	10.000	4.000	0	25.000
66	1	0	0	1	1	1	0.000	10.000	3.000	0	25.000
67	1	0	0	1	1	1	0.000	10.000	2.000	0	25.000
68	1	0	0	1	1	1	0.000	10.000	1.000	0	25.000
69	1	0	0	1	1	1	0.000	10.000	0.000	0	25.000
70	1	1	1	1	1	1	0.000	11.000	0.000	0	25.000
71	1	1	1	1	1	1	0.000	11.000	1.000	0	25.000
72	1	1	1	1	1	1	0.000	11.000	2.000	0	25.000
73	1	1	1	1	1	1	0.000	11.000	3.000	0	25.000
74	1	1	1	1	1	1	0.000	11.000	4.000	0	25.000
75	1	1	1	1	1	1	0.000	11.000	5.000	0	25.000
76	1	1	1	1	1	1	0.000	11.000	6.000	0	25.000
77	1	1	1	1	1	1	0.000	11.000	7.000	0	25.000
78	1	1	1	1	1	1	0.000	11.000	8.000	0	25.000

79	1	1	1	1	1	1	0.000	11.000	9.000	0	25.000
80	1	1	1	1	1	1	0.000	11.000	10.000	0	25.000
81	1	1	1	1	1	1	0.000	10.000	11.000	0	25.000
82	1	1	1	1	1	1	0.000	8.293	9.707	0	25.000
83	1	1	1	1	1	1	0.000	7.293	8.707	0	25.000
84	1	1	1	1	1	1	0.000	6.293	7.707	0	25.000
85	1	1	1	1	1	1	0.000	5.293	6.707	0	25.000
86	1	1	1	1	1	1	0.000	4.950	6.364	0	25.000
87	1	1	1	1	1	1	0.000	4.293	5.707	0	25.000
88	1	1	1	1	1	1	0.000	3.293	4.707	0	25.000
89	1	1	1	1	1	1	0.000	2.293	3.707	0	25.000
90	1	1	1	1	1	1	0.000	1.293	2.707	0	25.000
91	1	1	1	1	1	1	0.000	0.293	1.707	0	25.000
92	1	1	1	1	1	1	0.000	-1.000	0.000	0	25.000
93	1	1	1	1	1	1	0.000	0.000	-1.000	0	25.000
94	1	1	1	1	1	1	0.000	1.000	-1.000	0	25.000
95	1	1	1	1	1	1	0.000	2.000	-1.000	0	25.000
96	1	1	1	1	1	1	0.000	3.000	-1.000	0	25.000
97	1	1	1	1	1	1	0.000	4.000	-1.000	0	25.000
98	1	1	1	1	1	1	0.000	5.000	-1.000	0	25.000
99	1	1	1	1	1	1	0.000	6.000	-1.000	0	25.000
100	1	1	1	1	1	1	0.000	7.000	-1.000	0	25.000
101	1	1	1	1	1	1	0.000	8.000	-1.000	0	25.000
102	1	1	1	1	1	1	0.000	9.000	-1.000	0	25.000
103	1	1	1	1	1	1	0.000	10.000	-1.000	0	25.000

GENERATED NODAL DATA

NODE	BOUNDARY CONDITION CODES						NODAL POINT COORDINATES			
NUMBER	X	Y	Z	XX	YY	ZZ	X	Y	Z	T
1	1	0	0	1	1	1	0.000	0.000	0.000	25.000
2	1	0	0	1	1	1	0.000	1.000	0.000	25.000
3	1	0	0	1	1	1	0.000	1.000	1.000	25.000
4	1	0	0	1	1	1	0.000	2.000	2.000	25.000
5	1	0	0	1	1	1	0.000	2.000	1.000	25.000
6	1	0	0	1	1	1	0.000	2.000	0.000	25.000

7	1	0	0	1	1	1	0.000	3.000	0.000	25.000
8	1	0	0	1	1	1	0.000	3.000	1.000	25.000
9	1	0	0	1	1	1	0.000	3.000	2.000	25.000
10	1	0	0	1	1	1	0.000	3.000	3.000	25.000
11	1	0	0	1	1	1	0.000	4.000	4.000	25.000
12	1	0	0	1	1	1	0.000	4.000	3.000	25.000
13	1	0	0	1	1	1	0.000	4.000	2.000	25.000
14	1	0	0	1	1	1	0.000	4.000	1.000	25.000
15	1	0	0	1	1	1	0.000	4.000	0.000	25.000
16	1	0	0	1	1	1	0.000	5.000	0.000	25.000
17	1	0	0	1	1	1	0.000	5.000	1.000	25.000
18	1	0	0	1	1	1	0.000	5.000	2.000	25.000
19	1	0	0	1	1	1	0.000	5.000	3.000	25.000
20	1	0	0	1	1	1	0.000	5.000	4.000	25.000
21	1	0	0	1	1	1	0.000	5.000	5.000	25.000
22	1	0	0	1	1	1	0.000	5.657	5.657	25.000
23	1	0	0	1	1	1	0.000	6.000	5.292	25.000
24	1	0	0	1	1	1	0.000	6.000	4.000	25.000
25	1	0	0	1	1	1	0.000	6.000	3.000	25.000
26	1	0	0	1	1	1	0.000	6.000	2.000	25.000
27	1	0	0	1	1	1	0.000	6.000	1.000	25.000
28	1	0	0	1	1	1	0.000	6.000	0.000	25.000
29	1	0	0	1	1	1	0.000	7.000	0.000	25.000
30	1	0	0	1	1	1	0.000	7.000	1.000	25.000
31	1	0	0	1	1	1	0.000	7.000	2.000	25.000
32	1	0	0	1	1	1	0.000	7.000	3.000	25.000
33	1	0	0	1	1	1	0.000	6.928	4.000	25.000
34	1	0	0	1	1	1	0.000	6.568	4.568	25.000
35	1	0	0	1	1	1	0.000	7.000	5.000	25.000
36	1	0	0	1	1	1	0.000	7.000	6.000	25.000
37	1	0	0	1	1	1	0.000	6.000	6.000	25.000
38	1	0	0	1	1	1	0.000	7.000	7.000	25.000
39	1	0	0	1	1	1	0.000	8.000	8.000	25.000
40	1	0	0	1	1	1	0.000	8.000	7.000	25.000
41	1	0	0	1	1	1	0.000	8.000	6.000	25.000
42	1	0	0	1	1	1	0.000	8.000	5.000	25.000

43	1	0	0	1	1	1	0.000	8.000	4.000	25.000
44	1	0	0	1	1	1	0.000	7.416	3.000	25.000
45	1	0	0	1	1	1	0.000	8.000	3.000	25.000
46	1	0	0	1	1	1	0.000	7.746	2.000	25.000
47	1	0	0	1	1	1	0.000	7.937	1.000	25.000
48	1	0	0	1	1	1	0.000	8.000	0.000	25.000
49	1	0	0	1	1	1	0.000	9.000	0.000	25.000
50	1	0	0	1	1	1	0.000	9.000	1.000	25.000
51	1	0	0	1	1	1	0.000	9.000	2.000	25.000
52	1	0	0	1	1	1	0.000	9.000	3.000	25.000
53	1	0	0	1	1	1	0.000	9.000	4.000	25.000
54	1	0	0	1	1	1	0.000	9.000	5.000	25.000
55	1	0	0	1	1	1	0.000	9.000	6.000	25.000
56	1	0	0	1	1	1	0.000	9.000	7.000	25.000
57	1	0	0	1	1	1	0.000	9.000	8.000	25.000
58	1	0	0	1	1	1	0.000	9.000	9.000	25.000
59	1	0	0	1	1	1	0.000	10.000	10.000	25.000
60	1	0	0	1	1	1	0.000	10.000	9.000	25.000
61	1	0	0	1	1	1	0.000	10.000	8.000	25.000
62	1	0	0	1	1	1	0.000	10.000	7.000	25.000
63	1	0	0	1	1	1	0.000	10.000	6.000	25.000
64	1	0	0	1	1	1	0.000	10.000	5.000	25.000
65	1	0	0	1	1	1	0.000	10.000	4.000	25.000
66	1	0	0	1	1	1	0.000	10.000	3.000	25.000
67	1	0	0	1	1	1	0.000	10.000	2.000	25.000
68	1	0	0	1	1	1	0.000	10.000	1.000	25.000
69	1	0	0	1	1	1	0.000	10.000	0.000	25.000
70	1	1	1	1	1	1	0.000	11.000	0.000	25.000
71	1	1	1	1	1	1	0.000	11.000	1.000	25.000
72	1	1	1	1	1	1	0.000	11.000	2.000	25.000
73	1	1	1	1	1	1	0.000	11.000	3.000	25.000
74	1	1	1	1	1	1	0.000	11.000	4.000	25.000
75	1	1	1	1	1	1	0.000	11.000	5.000	25.000
76	1	1	1	1	1	1	0.000	11.000	6.000	25.000
77	1	1	1	1	1	1	0.000	11.000	7.000	25.000
78	1	1	1	1	1	1	0.000	11.000	8.000	25.000

79	1	1	1	1	1	1	0.000	11.000	9.000	25.000
80	1	1	1	1	1	1	0.000	11.000	10.000	25.000
81	1	1	1	1	1	1	0.000	10.000	11.000	25.000
82	1	1	1	1	1	1	0.000	8.293	9.707	25.000
83	1	1	1	1	1	1	0.000	7.293	8.707	25.000
84	1	1	1	1	1	1	0.000	6.293	7.707	25.000
85	1	1	1	1	1	1	0.000	5.293	6.707	25.000
86	1	1	1	1	1	1	0.000	4.950	6.364	25.000
87	1	1	1	1	1	1	0.000	4.293	5.707	25.000
88	1	1	1	1	1	1	0.000	3.293	4.707	25.000
89	1	1	1	1	1	1	0.000	2.293	3.707	25.000
90	1	1	1	1	1	1	0.000	1.293	2.707	25.000
91	1	1	1	1	1	1	0.000	0.293	1.707	25.000
92	1	1	1	1	1	1	0.000	-1.000	0.000	25.000
93	1	1	1	1	1	1	0.000	0.000	-1.000	25.000
94	1	1	1	1	1	1	0.000	1.000	-1.000	25.000
95	1	1	1	1	1	1	0.000	2.000	-1.000	25.000
96	1	1	1	1	1	1	0.000	3.000	-1.000	25.000
97	1	1	1	1	1	1	0.000	4.000	-1.000	25.000
98	1	1	1	1	1	1	0.000	5.000	-1.000	25.000
99	1	1	1	1	1	1	0.000	6.000	-1.000	25.000
100	1	1	1	1	1	1	0.000	7.000	-1.000	25.000
101	1	1	1	1	1	1	0.000	8.000	-1.000	25.000
102	1	1	1	1	1	1	0.000	9.000	-1.000	25.000
103	1	1	1	1	1	1	0.000	10.000	-1.000	25.000

EQUATION NUMBERS

N	X	Y	Z	XX	YY	ZZ
1	0	1	2	0	0	0
2	0	3	4	0	0	0
3	0	5	6	0	0	0
4	0	7	8	0	0	0
5	0	9	10	0	0	0
6	0	11	12	0	0	0
7	0	13	14	0	0	0

8	0	15	16	0	0	0
9	0	17	18	0	0	0
10	0	19	20	0	0	0
11	0	21	22	0	0	0
12	0	23	24	0	0	0
13	0	25	26	0	0	0
14	0	27	28	0	0	0
15	0	29	30	0	0	0
16	0	31	32	0	0	0
17	0	33	34	0	0	0
18	0	35	36	0	0	0
19	0	37	38	0	0	0
20	0	39	40	0	0	0
21	0	41	42	0	0	0
22	0	43	44	0	0	0
23	0	45	46	0	0	0
24	0	47	48	0	0	0
25	0	49	50	0	0	0
26	0	51	52	0	0	0
27	0	53	54	0	0	0
28	0	55	56	0	0	0
29	0	57	58	0	0	0
30	0	59	60	0	0	0
31	0	61	62	0	0	0
32	0	63	64	0	0	0
33	0	65	66	0	0	0
34	0	67	68	0	0	0
35	0	69	70	0	0	0
36	0	71	72	0	0	0
37	0	73	74	0	0	0
38	0	75	76	0	0	0
39	0	77	78	0	0	0
40	0	79	80	0	0	0
41	0	81	82	0	0	0
42	0	83	84	0	0	0
43	0	85	86	0	0	0

44	0	87	88	0	0	0
45	0	89	90	0	0	0
46	0	91	92	0	0	0
47	0	93	94	0	0	0
48	0	95	96	0	0	0
49	0	97	98	0	0	0
50	0	99	100	0	0	0
51	0	101	102	0	0	0
52	0	103	104	0	0	0
53	0	105	106	0	0	0
54	0	107	108	0	0	0
55	0	109	110	0	0	0
56	0	111	112	0	0	0
57	0	113	114	0	0	0
58	0	115	116	0	0	0
59	0	117	118	0	0	0
60	0	119	120	0	0	0
61	0	121	122	0	0	0
62	0	123	124	0	0	0
63	0	125	126	0	0	0
64	0	127	128	0	0	0
65	0	129	130	0	0	0
66	0	131	132	0	0	0
67	0	133	134	0	0	0
68	0	135	136	0	0	0
69	0	137	138	0	0	0
70	0	0	0	0	0	0
71	0	0	0	0	0	0
72	0	0	0	0	0	0
73	0	0	0	0	0	0
74	0	0	0	0	0	0
75	0	0	0	0	0	0
76	0	0	0	0	0	0
77	0	0	0	0	0	0
78	0	0	0	0	0	0
79	0	0	0	0	0	0

80	0	0	0	0	0	0
81	0	0	0	0	0	0
82	0	0	0	0	0	0
83	0	0	0	0	0	0
84	0	0	0	0	0	0
85	0	0	0	0	0	0
86	0	0	0	0	0	0
87	0	0	0	0	0	0
88	0	0	0	0	0	0
89	0	0	0	0	0	0
90	0	0	0	0	0	0
91	0	0	0	0	0	0
92	0	0	0	0	0	0
93	0	0	0	0	0	0
94	0	0	0	0	0	0
95	0	0	0	0	0	0
96	0	0	0	0	0	0
97	0	0	0	0	0	0
98	0	0	0	0	0	0
99	0	0	0	0	0	0
100	0	0	0	0	0	0
101	0	0	0	0	0	0
102	0	0	0	0	0	0
103	0	0	0	0	0	0

PLANE STRAIN ANALYSIS
INCOMPATIBLE MODES SUPPRESSED

NUMBER OF ELEMENTS = 105
NUMBER OF MATERIALS = 2
MAXIMUM TEMPERATURES
PER MATERIAL = 1
ANALYSIS CODE = 1
CODE FOR INCLUSION
OF BENDING MODES = 1
EQ.0. INCLUDE

GT.O. SUPPRESS

MATERIAL I.D. NUMBER	=	1
NUMBER OF TEMPERATURES	=	1
WEIGHT DENSITY	=	0.1000E+01
MASS DENSITY	=	0.1000E+01
BETA ANGLE	=	0.000

TEMP	E(N)	E(S)	E(T)	NU(NS)	NU(NT)	NU(ST)	G(NS)	ALPHA(N)	ALPHA(S)	ALPHA(T)
25.0	0.3400E+10	0.3400E+10	0.3400E+10	0.3500	0.3500	0.3500	0.1260E+10	0.6300E-04	0.6300E-04	0.6300E-04

MATERIAL I.D. NUMBER = 2
NUMBER OF TEMPERATURES = 1
WEIGHT DENSITY = 0.1000E+01
MASS DENSITY = 0.1000E+01
BETA ANGLE = 0.000

TEMP	E(N)	E(S)	E(T)	NU(NS)	NU(NT)	NU(ST)	G(NS)	ALPHA(N)	ALPHA(S)	ALPHA(T)
25.0	0.7200E+11	0.7200E+11	0.7200E+11	0.2500	0.2500	0.2500	0.2880E+11	0.5000E-05	0.5000E-05	0.5000E-05

ELEMENT LOAD MULTIPLIERS

LOAD CASE	TEMPERATURE	PRESSURE	X-GRAVITY	Y-GRAVITY	Z-GRAVITY
A	1.000	0.000	0.000	0.000	0.000
B	0.000	0.000	0.000	0.000	0.000
C	0.000	0.000	0.000	0.000	0.000
D	0.000	0.000	0.000	0.000	0.000

ELEMENT NUMBER	I	J	K	L	MATL TYPE	REFERENCE TEMPERATURE	I-J FACE PRESSURE	STRESS OPTION	KG	THICKNESS
1	1	2	3	3	2	25.000	0.000E+00	16	1	1.0000
2	2	6	5	5	2	25.000	0.000E+00	16	1	1.0000
3	2	5	3	3	2	25.000	0.000E+00	16	1	1.0000
4	3	5	4	4	2	25.000	0.000E+00	16	1	1.0000
5	4	9	10	10	2	25.000	0.000E+00	16	1	1.0000
6	5	9	4	4	2	25.000	0.000E+00	16	1	1.0000
7	5	8	9	9	2	25.000	0.000E+00	16	1	1.0000
8	6	8	5	5	2	25.000	0.000E+00	16	1	1.0000

9	6	7	8	8	2	25.000	0.000E+00	16	1	1.0000
10	7	15	14	14	2	25.000	0.000E+00	16	1	1.0000
11	7	14	8	8	2	25.000	0.000E+00	16	1	1.0000
12	8	14	13	13	2	25.000	0.000E+00	16	1	1.0000
13	8	13	9	9	2	25.000	0.000E+00	16	1	1.0000
14	9	13	12	12	2	25.000	0.000E+00	16	1	1.0000
15	9	12	10	10	2	25.000	0.000E+00	16	1	1.0000
16	10	12	11	11	2	25.000	0.000E+00	16	1	1.0000
17	11	20	21	21	2	25.000	0.000E+00	16	1	1.0000
18	12	20	11	11	2	25.000	0.000E+00	16	1	1.0000
19	12	19	20	20	2	25.000	0.000E+00	16	1	1.0000
20	13	19	12	12	2	25.000	0.000E+00	16	1	1.0000
21	13	18	19	19	2	25.000	0.000E+00	16	1	1.0000
22	14	18	13	13	2	25.000	0.000E+00	16	1	1.0000
23	14	17	18	18	2	25.000	0.000E+00	16	1	1.0000
24	15	17	14	14	2	25.000	0.000E+00	16	1	1.0000
25	15	16	17	17	2	25.000	0.000E+00	16	1	1.0000
26	16	28	27	27	2	25.000	0.000E+00	16	1	1.0000
27	16	27	17	17	2	25.000	0.000E+00	16	1	1.0000
28	17	27	26	26	2	25.000	0.000E+00	16	1	1.0000
29	17	26	18	18	2	25.000	0.000E+00	16	1	1.0000
30	18	26	25	25	2	25.000	0.000E+00	16	1	1.0000
31	18	25	19	19	2	25.000	0.000E+00	16	1	1.0000
32	19	25	24	24	2	25.000	0.000E+00	16	1	1.0000
33	19	24	20	20	2	25.000	0.000E+00	16	1	1.0000
34	20	24	23	23	2	25.000	0.000E+00	16	1	1.0000
35	20	23	21	21	2	25.000	0.000E+00	16	1	1.0000
36	21	23	22	22	2	25.000	0.000E+00	16	1	1.0000
37	22	23	37	37	1	501.000	0.000E+00	16	1	1.0000
38	37	36	38	38	1	501.000	0.000E+00	16	1	1.0000
39	23	36	37	37	1	501.000	0.000E+00	16	1	1.0000
40	23	35	36	36	1	501.000	0.000E+00	16	1	1.0000
41	23	34	35	35	1	501.000	0.000E+00	16	1	1.0000
42	23	24	34	34	2	25.000	0.000E+00	16	1	1.0000
43	34	33	35	35	1	501.000	0.000E+00	16	1	1.0000
44	24	33	34	34	2	25.000	0.000E+00	16	1	1.0000

45	25	33	24	24	2	25.000	0.000E+00	16	1	1.0000
46	25	32	33	33	2	25.000	0.000E+00	16	1	1.0000
47	26	27	31	31	2	25.000	0.000E+00	16	1	1.0000
48	26	31	32	32	2	25.000	0.000E+00	16	1	1.0000
49	26	27	31	31	2	25.000	0.000E+00	16	1	1.0000
50	27	30	31	31	2	25.000	0.000E+00	16	1	1.0000
51	27	28	30	30	2	25.000	0.000E+00	16	1	1.0000
52	28	29	30	30	2	25.000	0.000E+00	16	1	1.0000
53	29	48	47	47	2	25.000	0.000E+00	16	1	1.0000
54	29	47	30	30	2	25.000	0.000E+00	16	1	1.0000
55	30	47	46	46	2	25.000	0.000E+00	16	1	1.0000
56	30	46	31	31	2	25.000	0.000E+00	16	1	1.0000
57	31	46	44	44	2	25.000	0.000E+00	16	1	1.0000
58	31	44	32	32	2	25.000	0.000E+00	16	1	1.0000
59	46	45	44	44	1	501.000	0.000E+00	16	1	1.0000
60	32	44	33	33	2	25.000	0.000E+00	16	1	1.0000
61	44	45	43	43	1	501.000	0.000E+00	16	1	1.0000
62	44	43	33	33	1	501.000	0.000E+00	16	1	1.0000
63	33	43	42	42	1	501.000	0.000E+00	16	1	1.0000
64	33	42	35	35	1	501.000	0.000E+00	16	1	1.0000
65	35	42	41	41	1	501.000	0.000E+00	16	1	1.0000
66	35	41	36	36	1	501.000	0.000E+00	16	1	1.0000
67	36	41	40	40	1	501.000	0.000E+00	16	1	1.0000
68	36	40	38	38	1	501.000	0.000E+00	16	1	1.0000
69	38	40	39	39	1	501.000	0.000E+00	16	1	1.0000
70	39	57	58	58	1	501.000	0.000E+00	16	1	1.0000
71	40	57	39	39	1	501.000	0.000E+00	16	1	1.0000
72	40	56	57	57	1	501.000	0.000E+00	16	1	1.0000
73	41	56	40	40	1	501.000	0.000E+00	16	1	1.0000
74	41	55	56	56	1	501.000	0.000E+00	16	1	1.0000
75	42	55	41	41	1	501.000	0.000E+00	16	1	1.0000
76	42	54	55	55	1	501.000	0.000E+00	16	1	1.0000
77	43	54	42	42	1	501.000	0.000E+00	16	1	1.0000
78	43	53	54	54	1	501.000	0.000E+00	16	1	1.0000
79	43	45	53	53	1	501.000	0.000E+00	16	1	1.0000
80	45	52	53	53	1	501.000	0.000E+00	16	1	1.0000

81	46	52	45	45	1	501.000	0.000E+00	16	1	1.0000
82	46	51	52	52	1	501.000	0.000E+00	16	1	1.0000
83	46	47	51	51	1	501.000	0.000E+00	16	1	1.0000
84	47	50	51	51	1	501.000	0.000E+00	16	1	1.0000
85	47	48	50	50	1	501.000	0.000E+00	16	1	1.0000
86	48	49	50	50	1	501.000	0.000E+00	16	1	1.0000
87	49	69	68	68	1	501.000	0.000E+00	16	1	1.0000
88	49	68	50	50	1	501.000	0.000E+00	16	1	1.0000
89	50	68	67	67	1	501.000	0.000E+00	16	1	1.0000
90	51	50	67	67	1	501.000	0.000E+00	16	1	1.0000
91	51	67	66	66	1	501.000	0.000E+00	16	1	1.0000
92	52	51	66	66	1	501.000	0.000E+00	16	1	1.0000
93	52	66	65	65	1	501.000	0.000E+00	16	1	1.0000
94	53	52	65	65	1	501.000	0.000E+00	16	1	1.0000
95	53	65	64	64	1	501.000	0.000E+00	16	1	1.0000
96	54	53	64	64	1	501.000	0.000E+00	16	1	1.0000
97	54	64	63	63	1	501.000	0.000E+00	16	1	1.0000
98	55	54	63	63	1	501.000	0.000E+00	16	1	1.0000
99	55	63	62	62	1	501.000	0.000E+00	16	1	1.0000
100	56	55	62	62	1	501.000	0.000E+00	16	1	1.0000
101	56	62	61	61	1	501.000	0.000E+00	16	1	1.0000
102	57	56	61	61	1	501.000	0.000E+00	16	1	1.0000
103	57	61	60	60	1	501.000	0.000E+00	16	1	1.0000
104	58	57	60	60	1	501.000	0.000E+00	16	1	1.0000
105	58	60	59	59	1	501.000	0.000E+00	16	1	1.0000

B O U N D A R Y E L E M E N T S

ELEMENT TYPE = 7
NUMBER OF ELEMENTS = 34

ELEMENT LOAD CASE MULTIPLIERS

CASE(A) CASE(B) CASE(C) CASE(D)

1.0000	0.0000	0.0000	0.0000	

ELEMENT NUMBER	NODE (N)	NODES DEFINING CONSTRAINT DIRECTION (NI)	(NJ)	(NK)	(NL)	CODE KD	CODE KR	GENERATION CODE (KN)	SPECIFIED DISPLACEMENT	SPECIFIED ROTATION	SPRING RATE
1	1	92	0	0	0	1	0	0	0.0000E+00	0.0000E+00	0.1000E+17
2	1	93	0	0	0	1	0	0	0.0000E+00	0.0000E+00	0.1000E+17
3	2	94	0	0	0	1	0	0	0.0000E+00	0.0000E+00	0.1000E+17
4	3	91	0	0	0	1	0	0	0.0000E+00	0.0000E+00	0.1000E+17
5	4	90	0	0	0	1	0	0	0.0000E+00	0.0000E+00	0.1000E+17
6	6	95	0	0	0	1	0	0	0.0000E+00	0.0000E+00	0.1000E+17
7	7	96	0	0	0	1	0	0	0.0000E+00	0.0000E+00	0.1000E+17
8	10	89	0	0	0	1	0	0	0.0000E+00	0.0000E+00	0.1000E+17
9	11	88	0	0	0	1	0	0	0.0000E+00	0.0000E+00	0.1000E+17
10	15	97	0	0	0	1	0	0	0.0000E+00	0.0000E+00	0.1000E+17
11	16	98	0	0	0	1	0	0	0.0000E+00	0.0000E+00	0.1000E+17
12	21	87	0	0	0	1	0	0	0.0000E+00	0.0000E+00	0.1000E+17
13	22	86	0	0	0	1	0	0	0.0000E+00	0.0000E+00	0.1000E+17
14	28	99	0	0	0	1	0	0	0.0000E+00	0.0000E+00	0.1000E+17
15	29	100	0	0	0	1	0	0	0.0000E+00	0.0000E+00	0.1000E+17
16	37	85	0	0	0	1	0	0	0.0000E+00	0.0000E+00	0.1000E+17
17	38	84	0	0	0	1	0	0	0.0000E+00	0.0000E+00	0.1000E+17
18	39	83	0	0	0	1	0	0	0.0000E+00	0.0000E+00	0.1000E+17
19	48	101	0	0	0	1	0	0	0.0000E+00	0.0000E+00	0.1000E+17
20	49	102	0	0	0	1	0	0	0.0000E+00	0.0000E+00	0.1000E+17
21	58	82	0	0	0	1	0	0	0.0000E+00	0.0000E+00	0.1000E+17
22	59	81	0	0	0	1	0	0	-0.1717E+00	0.0000E+00	0.1000E+17
23	59	80	0	0	0	1	0	0	-0.1717E+00	0.0000E+00	0.1000E+17
24	60	79	0	0	0	1	0	0	-0.1717E+00	0.0000E+00	0.1000E+17
25	61	78	0	0	0	1	0	0	-0.1717E+00	0.0000E+00	0.1000E+17
26	62	77	0	0	0	1	0	0	-0.1717E+00	0.0000E+00	0.1000E+17
27	63	76	0	0	0	1	0	0	-0.1717E+00	0.0000E+00	0.1000E+17
28	64	75	0	0	0	1	0	0	-0.1717E+00	0.0000E+00	0.1000E+17
29	65	74	0	0	0	1	0	0	-0.1717E+00	0.0000E+00	0.1000E+17

30	66	73	0	0	0	1	0	0	-0.1717E+00	0.0000E+00	0.1000E+17
31	67	72	0	0	0	1	0	0	-0.1717E+00	0.0000E+00	0.1000E+17
32	68	71	0	0	0	1	0	0	-0.1717E+00	0.0000E+00	0.1000E+17
33	69	70	0	0	0	1	0	0	-0.1717E+00	0.0000E+00	0.1000E+17
34	69	103	0	0	0	1	0	0	0.0000E+00	0.0000E+00	0.1000E+17

E Q U A T I O N P A R A M E T E R S

TOTAL NUMBER OF EQUATIONS = 138
BANDWIDTH = 42
NUMBER OF EQUATIONS IN A BLOCK = 79
NUMBER OF BLOCKS = 2

N O D A L L O A D S (S T A T I C) O R M A S S E S (D Y N A M I C)

NODE NUMBER	LOAD CASE	X-AXIS FORCE	Y-AXIS FORCE	Z-AXIS FORCE	X-AXIS MOMENT	Y-AXIS MOMENT	Z-AXIS MOMENT

STRUCTURE LOAD CASE	ELEMENT LOAD MULTIPLIERS A	B	C	D
1	1.000	0.000	0.000	0.000

N O D E D I S P L A C E M E N T S / R O T A T I O N S

NODE NUMBER	LOAD CASE	X-TRANSLATION	Y-TRANSLATION	Z-TRANSLATION	X-ROTATION	Y-ROTATION	Z-ROTATION
103	1	0.00000E+00	0.00000E+00	0.00000E+00	0.00000E+00	0.00000E+00	0.00000E+00
102	1	0.00000E+00	0.00000E+00	0.00000E+00	0.00000E+00	0.00000E+00	0.00000E+00
101	1	0.00000E+00	0.00000E+00	0.00000E+00	0.00000E+00	0.00000E+00	0.00000E+00
100	1	0.00000E+00	0.00000E+00	0.00000E+00	0.00000E+00	0.00000E+00	0.00000E+00

99	1	0.00000E+00	0.00000E+00	0.00000E+00	0.00000E+00	0.00000E+00	0.00000E+00
98	1	0.00000E+00	0.00000E+00	0.00000E+00	0.00000E+00	0.00000E+00	0.00000E+00
97	1	0.00000E+00	0.00000E+00	0.00000E+00	0.00000E+00	0.00000E+00	0.00000E+00
96	1	0.00000E+00	0.00000E+00	0.00000E+00	0.00000E+00	0.00000E+00	0.00000E+00
95	1	0.00000E+00	0.00000E+00	0.00000E+00	0.00000E+00	0.00000E+00	0.00000E+00
94	1	0.00000E+00	0.00000E+00	0.00000E+00	0.00000E+00	0.00000E+00	0.00000E+00
93	1	0.00000E+00	0.00000E+00	0.00000E+00	0.00000E+00	0.00000E+00	0.00000E+00
92	1	0.00000E+00	0.00000E+00	0.00000E+00	0.00000E+00	0.00000E+00	0.00000E+00
91	1	0.00000E+00	0.00000E+00	0.00000E+00	0.00000E+00	0.00000E+00	0.00000E+00
90	1	0.00000E+00	0.00000E+00	0.00000E+00	0.00000E+00	0.00000E+00	0.00000E+00
89	1	0.00000E+00	0.00000E+00	0.00000E+00	0.00000E+00	0.00000E+00	0.00000E+00
88	1	0.00000E+00	0.00000E+00	0.00000E+00	0.00000E+00	0.00000E+00	0.00000E+00
87	1	0.00000E+00	0.00000E+00	0.00000E+00	0.00000E+00	0.00000E+00	0.00000E+00
86	1	0.00000E+00	0.00000E+00	0.00000E+00	0.00000E+00	0.00000E+00	0.00000E+00
85	1	0.00000E+00	0.00000E+00	0.00000E+00	0.00000E+00	0.00000E+00	0.00000E+00
84	1	0.00000E+00	0.00000E+00	0.00000E+00	0.00000E+00	0.00000E+00	0.00000E+00
83	1	0.00000E+00	0.00000E+00	0.00000E+00	0.00000E+00	0.00000E+00	0.00000E+00
82	1	0.00000E+00	0.00000E+00	0.00000E+00	0.00000E+00	0.00000E+00	0.00000E+00

81	1	0.00000E+00	0.00000E+00	0.00000E+00	0.00000E+00	0.00000E+00	0.00000E+00
80	1	0.00000E+00	0.00000E+00	0.00000E+00	0.00000E+00	0.00000E+00	0.00000E+00
79	1	0.00000E+00	0.00000E+00	0.00000E+00	0.00000E+00	0.00000E+00	0.00000E+00
78	1	0.00000E+00	0.00000E+00	0.00000E+00	0.00000E+00	0.00000E+00	0.00000E+00
77	1	0.00000E+00	0.00000E+00	0.00000E+00	0.00000E+00	0.00000E+00	0.00000E+00
76	1	0.00000E+00	0.00000E+00	0.00000E+00	0.00000E+00	0.00000E+00	0.00000E+00
75	1	0.00000E+00	0.00000E+00	0.00000E+00	0.00000E+00	0.00000E+00	0.00000E+00
74	1	0.00000E+00	0.00000E+00	0.00000E+00	0.00000E+00	0.00000E+00	0.00000E+00
73	1	0.00000E+00	0.00000E+00	0.00000E+00	0.00000E+00	0.00000E+00	0.00000E+00
72	1	0.00000E+00	0.00000E+00	0.00000E+00	0.00000E+00	0.00000E+00	0.00000E+00
71	1	0.00000E+00	0.00000E+00	0.00000E+00	0.00000E+00	0.00000E+00	0.00000E+00
70	1	0.00000E+00	0.00000E+00	0.00000E+00	0.00000E+00	0.00000E+00	0.00000E+00
69	1	0.00000E+00	-0.17170E+00	0.60296E-08	0.00000E+00	0.00000E+00	0.00000E+00
68	1	0.00000E+00	-0.17170E+00	0.41631E-02	0.00000E+00	0.00000E+00	0.00000E+00
67	1	0.00000E+00	-0.17170E+00	0.68672E-02	0.00000E+00	0.00000E+00	0.00000E+00
66	1	0.00000E+00	-0.17170E+00	0.43062E-02	0.00000E+00	0.00000E+00	0.00000E+00
65	1	0.00000E+00	-0.17170E+00	-0.55698E-02	0.00000E+00	0.00000E+00	0.00000E+00
64	1	0.00000E+00	-0.17170E+00	-0.22958E-01	0.00000E+00	0.00000E+00	0.00000E+00

63	1	0.00000E+00	-0.17170E+00	-0.46730E-01	0.00000E+00	0.00000E+00	0.00000E+00
62	1	0.00000E+00	-0.17170E+00	-0.74919E-01	0.00000E+00	0.00000E+00	0.00000E+00
61	1	0.00000E+00	-0.17170E+00	-0.10604E+00	0.00000E+00	0.00000E+00	0.00000E+00
60	1	0.00000E+00	-0.17170E+00	-0.13859E+00	0.00000E+00	0.00000E+00	0.00000E+00
59	1	0.00000E+00	-0.17170E+00	-0.17170E+00	0.00000E+00	0.00000E+00	0.00000E+00
58	1	0.00000E+00	-0.13873E+00	-0.13873E+00	0.00000E+00	0.00000E+00	0.00000E+00
57	1	0.00000E+00	-0.13793E+00	-0.10620E+00	0.00000E+00	0.00000E+00	0.00000E+00
56	1	0.00000E+00	-0.13596E+00	-0.75133E-01	0.00000E+00	0.00000E+00	0.00000E+00
55	1	0.00000E+00	-0.13203E+00	-0.46993E-01	0.00000E+00	0.00000E+00	0.00000E+00
54	1	0.00000E+00	-0.12613E+00	-0.23538E-01	0.00000E+00	0.00000E+00	0.00000E+00
53	1	0.00000E+00	-0.11749E+00	-0.61820E-02	0.00000E+00	0.00000E+00	0.00000E+00
52	1	0.00000E+00	-0.10735E+00	0.41179E-02	0.00000E+00	0.00000E+00	0.00000E+00
51	1	0.00000E+00	-0.97732E-01	0.67856E-02	0.00000E+00	0.00000E+00	0.00000E+00
50	1	0.00000E+00	-0.90840E-01	0.48272E-02	0.00000E+00	0.00000E+00	0.00000E+00
49	1	0.00000E+00	-0.89342E-01	0.12559E-07	0.00000E+00	0.00000E+00	0.00000E+00
48	1	0.00000E+00	-0.57824E-02	0.61186E-08	0.00000E+00	0.00000E+00	0.00000E+00
47	1	0.00000E+00	-0.54629E-02	0.63491E-03	0.00000E+00	0.00000E+00	0.00000E+00
46	1	0.00000E+00	-0.46322E-02	0.10691E-02	0.00000E+00	0.00000E+00	0.00000E+00

45	1	0.00000E+00	-0.42367E-01	0.27337E-03	0.00000E+00	0.00000E+00	0.00000E+00
44	1	0.00000E+00	-0.36453E-02	0.11586E-02	0.00000E+00	0.00000E+00	0.00000E+00
43	1	0.00000E+00	-0.62647E-01	-0.75444E-02	0.00000E+00	0.00000E+00	0.00000E+00
42	1	0.00000E+00	-0.79918E-01	-0.21905E-01	0.00000E+00	0.00000E+00	0.00000E+00
41	1	0.00000E+00	-0.92557E-01	-0.44741E-01	0.00000E+00	0.00000E+00	0.00000E+00
40	1	0.00000E+00	-0.10069E+00	-0.72975E-01	0.00000E+00	0.00000E+00	0.00000E+00
39	1	0.00000E+00	-0.10467E+00	-0.10467E+00	0.00000E+00	0.00000E+00	0.00000E+00
38	1	0.00000E+00	-0.67125E-01	-0.67125E-01	0.00000E+00	0.00000E+00	0.00000E+00
37	1	0.00000E+00	-0.20306E-01	-0.20306E-01	0.00000E+00	0.00000E+00	0.00000E+00
36	1	0.00000E+00	-0.54218E-01	-0.37592E-01	0.00000E+00	0.00000E+00	0.00000E+00
35	1	0.00000E+00	-0.34690E-01	-0.14604E-01	0.00000E+00	0.00000E+00	0.00000E+00
34	1	0.00000E+00	-0.14175E-02	0.61645E-03	0.00000E+00	0.00000E+00	0.00000E+00
33	1	0.00000E+00	-0.22075E-02	0.93214E-03	0.00000E+00	0.00000E+00	0.00000E+00
32	1	0.00000E+00	-0.33050E-02	0.90865E-03	0.00000E+00	0.00000E+00	0.00000E+00
31	1	0.00000E+00	-0.38265E-02	0.71663E-03	0.00000E+00	0.00000E+00	0.00000E+00
30	1	0.00000E+00	-0.42937E-02	0.40426E-03	0.00000E+00	0.00000E+00	0.00000E+00
29	1	0.00000E+00	-0.44524E-02	0.32294E-09	0.00000E+00	0.00000E+00	0.00000E+00
28	1	0.00000E+00	-0.33835E-02	-0.88113E-09	0.00000E+00	0.00000E+00	0.00000E+00

27	1	0.00000E+00	-0.32726E-02	0.20380E-03	0.00000E+00	0.00000E+00	0.00000E+00
26	1	0.00000E+00	-0.31640E-02	0.31851E-03	0.00000E+00	0.00000E+00	0.00000E+00
25	1	0.00000E+00	-0.20599E-02	0.22129E-03	0.00000E+00	0.00000E+00	0.00000E+00
24	1	0.00000E+00	-0.15658E-02	0.23286E-03	0.00000E+00	0.00000E+00	0.00000E+00
23	1	0.00000E+00	-0.67448E-03	-0.29201E-06	0.00000E+00	0.00000E+00	0.00000E+00
22	1	0.00000E+00	-0.26178E-03	-0.26189E-03	0.00000E+00	0.00000E+00	0.00000E+00
21	1	0.00000E+00	-0.50823E-03	-0.50822E-03	0.00000E+00	0.00000E+00	0.00000E+00
20	1	0.00000E+00	-0.10998E-02	-0.25610E-03	0.00000E+00	0.00000E+00	0.00000E+00
19	1	0.00000E+00	-0.15831E-02	-0.72335E-04	0.00000E+00	0.00000E+00	0.00000E+00
18	1	0.00000E+00	-0.22637E-02	0.47941E-04	0.00000E+00	0.00000E+00	0.00000E+00
17	1	0.00000E+00	-0.24622E-02	0.20152E-04	0.00000E+00	0.00000E+00	0.00000E+00
16	1	0.00000E+00	-0.25222E-02	-0.19259E-08	0.00000E+00	0.00000E+00	0.00000E+00
15	1	0.00000E+00	-0.18234E-02	-0.26975E-08	0.00000E+00	0.00000E+00	0.00000E+00
14	1	0.00000E+00	-0.17670E-02	-0.10011E-03	0.00000E+00	0.00000E+00	0.00000E+00
13	1	0.00000E+00	-0.15781E-02	-0.21160E-03	0.00000E+00	0.00000E+00	0.00000E+00
12	1	0.00000E+00	-0.11369E-02	-0.42559E-03	0.00000E+00	0.00000E+00	0.00000E+00
11	1	0.00000E+00	-0.71841E-03	-0.71839E-03	0.00000E+00	0.00000E+00	0.00000E+00
10	1	0.00000E+00	-0.75147E-03	-0.75146E-03	0.00000E+00	0.00000E+00	0.00000E+00

9	1	0.00000E+00	-0.10484E-02	-0.44172E-03	0.00000E+00	0.00000E+00	0.00000E+00
8	1	0.00000E+00	-0.11986E-02	-0.20855E-03	0.00000E+00	0.00000E+00	0.00000E+00
7	1	0.00000E+00	-0.12423E-02	-0.32928E-08	0.00000E+00	0.00000E+00	0.00000E+00
6	1	0.00000E+00	-0.76258E-03	-0.38059E-08	0.00000E+00	0.00000E+00	0.00000E+00
5	1	0.00000E+00	-0.73658E-03	-0.29949E-03	0.00000E+00	0.00000E+00	0.00000E+00
4	1	0.00000E+00	-0.63306E-03	-0.63305E-03	0.00000E+00	0.00000E+00	0.00000E+00
3	1	0.00000E+00	-0.35104E-03	-0.35103E-03	0.00000E+00	0.00000E+00	0.00000E+00
2	1	0.00000E+00	-0.36084E-03	-0.40843E-08	0.00000E+00	0.00000E+00	0.00000E+00
1	1	0.00000E+00	-0.20643E-08	0.14106E-10	0.00000E+00	0.00000E+00	0.00000E+00

T W O - D I M E N S I O N A L F I N I T E E L E M E N T S

1. CENTROID STRESSES REFERENCED TO LOCAL Y-Z COORDINATES.
2. MID-SIDE STRESSES ARE NORMAL AND PARALLEL TO ELEMENT EDGES.

ELEMENT (1)

LOAD	LOC	S11	S22	S33	S12	S-MAX	S-MIN	ANGLE
1	CEN	-0.41286E+08	-0.40721E+08	-0.20502E+08	0.28211E+06	-0.40604E+08	-0.41403E+08	67.52
1	L-I	-0.41286E+08	-0.40721E+08	-0.20502E+08	-0.28254E+06	-0.40604E+08	-0.41403E+08	-67.48
1	J-K	-0.41286E+08	-0.40721E+08	-0.20502E+08	0.28211E+06	-0.40604E+08	-0.41403E+08	67.52
1	I-J	-0.40721E+08	-0.41286E+08	-0.20502E+08	-0.28211E+06	-0.40604E+08	-0.41403E+08	-22.48

ELEMENT (2)

LOAD	LOC	S11	S22	S33	S12	S-MAX	S-MIN	ANGLE
1	CEN	-0.43335E+08	-0.37445E+08	-0.20195E+08	0.74872E+06	-0.37352E+08	-0.43429E+08	82.87
1	L-I	-0.41139E+08	-0.39641E+08	-0.20195E+08	-0.29449E+07	-0.37352E+08	-0.43429E+08	-52.13
1	J-K	-0.43335E+08	-0.37445E+08	-0.20195E+08	0.74872E+06	-0.37352E+08	-0.43429E+08	82.87
1	I-J	-0.37445E+08	-0.43335E+08	-0.20195E+08	-0.74872E+06	-0.37352E+08	-0.43429E+08	-7.13

ELEMENT (3)

LOAD	LOC	S11	S22	S33	S12	S-MAX	S-MIN	ANGLE
1	CEN	-0.43420E+08	-0.41432E+08	-0.21213E+08	0.17668E+07	-0.40399E+08	-0.44453E+08	59.68
1	L-I	-0.43420E+08	-0.41432E+08	-0.21213E+08	0.17668E+07	-0.40399E+08	-0.44453E+08	59.68
1	J-K	-0.41432E+08	-0.43420E+08	-0.21213E+08	-0.17668E+07	-0.40399E+08	-0.44453E+08	-30.32
1	I-J	-0.44193E+08	-0.40659E+08	-0.21213E+08	-0.99388E+06	-0.40399E+08	-0.44453E+08	-75.32

ELEMENT (4)

LOAD	LOC	S11	S22	S33	S12	S-MAX	S-MIN	ANGLE
1	CEN	-0.42917E+08	-0.39923E+08	-0.20710E+08	0.44660E+07	-0.36710E+08	-0.46130E+08	54.27
1	L-I	-0.45886E+08	-0.36954E+08	-0.20710E+08	-0.14969E+07	-0.36710E+08	-0.46130E+08	-80.74
1	J-K	-0.42917E+08	-0.39923E+08	-0.20710E+08	0.44660E+07	-0.36710E+08	-0.46130E+08	54.27
1	I-J	-0.39923E+08	-0.42917E+08	-0.20710E+08	-0.44660E+07	-0.36710E+08	-0.46130E+08	-35.74

ELEMENT (5)

LOAD	LOC	S11	S22	S33	S12	S-MAX	S-MIN	ANGLE
1	CEN	-0.44808E+08	-0.38723E+08	-0.20883E+08	0.14063E+08	-0.27378E+08	-0.56154E+08	51.10
1	L-I	-0.55828E+08	-0.27703E+08	-0.20883E+08	-0.30424E+07	-0.27378E+08	-0.56154E+08	-83.90
1	J-K	-0.44808E+08	-0.38723E+08	-0.20883E+08	0.14063E+08	-0.27378E+08	-0.56154E+08	51.10
1	I-J	-0.38723E+08	-0.44808E+08	-0.20883E+08	-0.14063E+08	-0.27378E+08	-0.56154E+08	-38.90

ELEMENT (6)

LOAD	LOC	S11	S22	S33	S12	S-MAX	S-MIN	ANGLE
1	CEN	-0.45494E+08	-0.40782E+08	-0.21569E+08	0.84916E+07	-0.34326E+08	-0.51951E+08	52.75
1	L-I	-0.45494E+08	-0.40782E+08	-0.21569E+08	0.84916E+07	-0.34326E+08	-0.51951E+08	52.75
1	J-K	-0.40782E+08	-0.45494E+08	-0.21569E+08	-0.84916E+07	-0.34326E+08	-0.51951E+08	-37.25
1	I-J	-0.51630E+08	-0.34647E+08	-0.21569E+08	-0.23560E+07	-0.34326E+08	-0.51951E+08	-82.25

ELEMENT (7)

LOAD	LOC	S11	S22	S33	S12	S-MAX	S-MIN	ANGLE
1	CEN	-0.46634E+08	-0.33453E+08	-0.20022E+08	0.69441E+07	-0.30470E+08	-0.49618E+08	66.75
1	L-I	-0.46988E+08	-0.33099E+08	-0.20022E+08	-0.65908E+07	-0.30470E+08	-0.49618E+08	-68.25
1	J-K	-0.46634E+08	-0.33453E+08	-0.20022E+08	0.69441E+07	-0.30470E+08	-0.49618E+08	66.75
1	I-J	-0.33453E+08	-0.46634E+08	-0.20022E+06	-0.69441E+07	-0.30470E+08	-0.49618E+08	-23.25

ELEMENT (8)

LOAD	LOC	S11	S22	S33	S12	S-MAX	S-MIN	ANGLE
1	CEN	-0.48544E+08	-0.39182E+08	-0.21931E+08	0.33677E+07	-0.38096E+08	-0.49630E+08	72.13
1	L-I	-0.48544E+08	-0.39182E+08	-0.21931E+08	0.33677E+07	-0.38096E+08	-0.49630E+08	72.13
1	J-K	-0.39182E+08	-0.48544E+08	-0.21931E+08	-0.33677E+07	-0.38096E+08	-0.49630E+08	-17.87
1	I-J	-0.47231E+08	-0.40495E+08	-0.21931E+08	-0.46812E+07	-0.38096E+08	-0.49630E+08	-62.87

ELEMENT (9)

LOAD	LOC	S11	S22	S33	S12	S-MAX	S-MIN	ANGLE
1	CEN	-0.47452E+08	-0.31833E+08	-0.19821E+08	0.12576E+07	-0.31733E+08	-0.47552E+08	85.43
1	L-I	-0.40900E+08	-0.38385E+08	-0.19821E+08	-0.78091E+07	-0.31733E+08	-0.47552E+08	-49.57
1	J-K	-0.47452E+08	-0.31833E+08	-0.19821E+08	0.12576E+07	-0.31733E+08	-0.47552E+08	85.43
1	I-J	-0.31833E+08	-0.47452E+08	-0.19821E+08	-0.12576E+07	-0.31733E+08	-0.47552E+08	-4.57

ELEMENT (10)

LOAD	LOC	S11	S22	S33	S12	S-MAX	S-MIN	ANGLE
1	CEN	-0.53090E+08	-0.25385E+08	-0.19619E+08	0.16229E+07	-0.25290E+08	-0.53184E+08	86.66
1	L-I	-0.40860E+08	-0.37614E+08	-0.19619E+08	-0.13852E+08	-0.25290E+08	-0.53184E+08	-48.34
1	J-K	-0.53090E+08	-0.25385E+08	-0.19619E+08	0.16229E+07	-0.25290E+08	-0.53184E+08	86.66
1	I-J	-0.25385E+08	-0.53090E+08	-0.19619E+08	-0.16229E+07	-0.25290E+08	-0.53184E+08	-3.34

ELEMENT (11)

LOAD	LOC	S11	S22	S33	S12	S-MAX	S-MIN	ANGLE
1	CEN	-0.55116E+08	-0.34388E+08	-0.22376E+08	0.43804E+07	-0.33501E+08	-0.56004E+08	78.54
1	L-I	-0.55116E+08	-0.34388E+08	-0.22376E+08	0.43804E+07	-0.33501E+08	-0.56004E+08	78.54
1	J-K	-0.34388E+08	-0.55116E+08	-0.22376E+08	-0.43804E+07	-0.33501E+08	-0.56004E+08	-11.46
1	I-J	-0.49133E+08	-0.40372E+08	-0.22376E+08	-0.10364E+08	-0.33501E+08	-0.56004E+08	-56.46

ELEMENT (12)

LOAD	LOC	S11	S22	S33	S12	S-MAX	S-MIN	ANGLE
1	CEN	-0.52321E+08	-0.26002E+08	-0.19581E+08	0.85636E+07	-0.23461E+08	-0.54862E+08	73.47
1	L-I	-0.47725E+08	-0.30598E+08	-0.19581E+08	-0.13159E+08	-0.23461E+08	-0.54862E+08	-61.53
1	J-K	-0.52321E+08	-0.26002E+08	-0.19581E+08	0.85636E+07	-0.23461E+08	-0.54862E+08	73.47
1	I-J	-0.26002E+08	-0.52321E+08	-0.19581E+08	-0.85636E+07	-0.23461E+08	-0.54862E+08	-16.53

ELEMENT (13)

LOAD	LOC	S11	S22	S33	S12	S-MAX	S-MIN	ANGLE
1	CEN	-0.52479E+08	-0.35401E+08	-0.21970E+08	0.10953E+08	-0.30052E+08	-0.57828E+08	63.97
1	L-I	-0.52479E+08	-0.35401E+08	-0.21970E+08	0.10953E+08	-0.30052E+08	-0.57828E+08	63.97
1	J-K	-0.35401E+08	-0.52479E+08	-0.21970E+08	-0.10953E+08	-0.30052E+08	-0.57828E+08	-26.03
1	I-J	-0.54893E+08	-0.32987E+08	-0.21970E+08	-0.85390E+07	-0.30052E+08	-0.57828E+08	-71.03

ELEMENT (14)

LOAD	LOC	S11	S22	S33	S12	S-MAX	S-MIN	ANGLE
1	CEN	-0.51927E+08	-0.33744E+08	-0.21418E+08	0.19333E+08	-0.21471E+08	-0.64199E+08	57.59
1	L-I	-0.62168E+08	-0.23502E+08	-0.21418E+08	-0.90915E+07	-0.21471E+08	-0.64199E+08	-77.41
1	J-K	-0.51927E+08	-0.33744E+08	-0.21418E+08	0.19333E+08	-0.21471E+08	-0.64199E+08	57.59
1	I-J	-0.33744E+08	-0.51927E+08	-0.21418E+08	-0.19333E+08	-0.21471E+08	-0.64199E+08	-32.41

ELEMENT (15)

LOAD	LOC	S11	S22	S33	S12	S-MAX	S-MIN	ANGLE
1	CEN	-0.42224E+08	-0.37862E+08	-0.20022E+08	0.17937E+08	-0.21974E+08	-0.58113E+08	48.47
1	L-I	-0.42224E+08	-0.37862E+08	-0.20022E+08	0.17937E+08	-0.21974E+08	-0.58113E+08	48.47
1	J-K	-0.37862E+08	-0.42224E+08	-0.20022E+08	-0.17937E+08	-0.21974E+08	-0.58113E+08	-41.53
1	I-J	-0.57981E+08	-0.22106E+08	-0.20022E+08	-0.21811E+07	-0.21974E+08	-0.58113E+08	-86.53

ELEMENT (16)

LOAD	LOC	S11	S22	S33	S12	S-MAX	S-MIN	ANGLE
1	CEN	-0.41737E+08	-0.36399E+08	-0.19534E+08	0.21438E+08	-0.17464E+08	-0.60672E+08	48.55
1	L-I	-0.60507E+08	-0.17630E+08	-0.19534E+08	-0.26687E+07	-0.17464E+08	-0.60672E+08	-86.45
1	J-K	-0.41737E+08	-0.36399E+08	-0.19534E+08	0.21438E+08	-0.17464E+08	-0.60672E+08	48.55
1	I-J	-0.36399E+08	-0.41737E+08	-0.19534E+08	-0.21438E+08	-0.17464E+08	-0.60672E+08	-41.45

ELEMENT (17)

LOAD	LOC	S11	S22	S33	S12	S-MAX	S-MIN	ANGLE
1	CEN	-0.40210E+08	-0.32766E+08	-0.18244E+08	0.30350E+08	-0.59108E+07	-0.67066E+08	48.50
1	L-I	-0.66838E+08	-0.61382E+07	-0.18244E+08	-0.37220E+07	-0.59108E+07	-0.67066E+08	-86.50
1	J-K	-0.40210E+08	-0.32766E+08	-0.18244E+08	0.30350E+08	-0.59108E+07	-0.67066E+08	48.50
1	I-J	-0.32766E+08	-0.40210E+08	-0.18244E+08	-0.30350E+08	-0.59108E+07	-0.67066E+08	-41.50

ELEMENT (18)

LOAD	LOC	S11	S22	S33	S12	S-MAX	S-MIN	ANGLE
1	CEN	-0.41382E+08	-0.36281E+08	-0.19416E+08	0.25368E+08	-0.13336E+08	-0.64327E+08	47.87
1	L-I	-0.41382E+08	-0.36281E+08	-0.19416E+08	0.25368E+08	-0.13336E+08	-0.64327E+08	47.87
1	J-K	-0.36281E+08	-0.41382E+08	-0.19416E+08	-0.25368E+08	-0.13336E+08	-0.64327E+08	-42.13
1	I-J	-0.64199E+08	-0.13464E+08	-0.19416E+08	-0.25504E+07	-0.13336E+08	-0.64327E+08	-87.13

ELEMENT (19)

LOAD	LOC	S11	S22	S33	S12	S-MAX	S-MIN	ANGLE
1	CEN	-0.43842E+08	-0.28727E+08	-0.18142E+08	0.24094E+08	-0.11033E+08	-0.61536E+08	53.71
1	L-I	-0.60379E+08	-0.12190E+08	-0.18142E+08	-0.75574E+07	-0.11033E+08	-0.61536E+08	-81.29
1	J-K	-0.43842E+08	-0.28727E+08	-0.18142E+08	0.24094E+08	-0.11033E+08	-0.61536E+08	53.71
1	I-J	-0.28727E+08	-0.43842E+08	-0.18142E+08	-0.24094E+08	-0.11033E+08	-0.61536E+08	-36.29

ELEMENT (20)

LOAD	LOC	S11	S22	S33	S12	S-MAX	S-MIN	ANGLE
1	CEN	-0.44713E+08	-0.31339E+08	-0.19013E+08	0.22879E+08	-0.14189E+08	-0.61862E+08	53.15
1	L-I	-0.44713E+08	-0.31339E+08	-0.19013E+08	0.22879E+08	-0.14189E+08	-0.61862E+08	53.15
1	J-K	-0.31339E+08	-0.44713E+08	-0.19013E+08	-0.22879E+08	-0.14189E+08	-0.61862E+08	-36.85
1	I-J	-0.60905E+08	-0.15146E+08	-0.19013E+08	-0.66868E+07	-0.14189E+08	-0.61862E+08	-81.85

ELEMENT (21)

LOAD	LOC	S11	S22	S33	S12	S-MAX	S-MIN	ANGLE
1	CEN	-0.62696E+08	-0.30136E+08	-0.23208E+08	0.27075E+08	-0.14824E+08	-0.78008E+08	60.51
1	L-I	-0.73491E+08	-0.19342E+08	-0.23208E+08	-0.16280E+08	-0.14824E+08	-0.78008E+08	-74.49
1	J-K	-0.62696E+08	-0.30136E+08	-0.23208E+08	0.27075E+08	-0.14824E+08	-0.78008E+08	60.51
1	I-J	-0.30136E+08	-0.62696E+08	-0.23208E+08	-0.27075E+08	-0.14824E+08	-0.78008E+08	-29.49

ELEMENT (22)

LOAD	LOC	S11	S22	S33	S12	S-MAX	S-MIN	ANGLE
1	CEN	-0.62443E+08	-0.29376E+08	-0.22955E+08	0.12915E+08	-0.24930E+08	-0.66890E+08	71.00
1	L-I	-0.62443E+08	-0.29376E+08	-0.22955E+08	0.12915E+08	-0.24930E+08	-0.66890E+08	71.00
1	J-K	-0.29376E+08	-0.62443E+08	-0.22955E+08	-0.12915E+08	-0.24930E+08	-0.66890E+08	-19.00
1	I-J	-0.58825E+08	-0.32994E+08	-0.22955E+08	-0.16533E+08	-0.24930E+08	-0.66890E+08	-64.00

ELEMENT (23)

LOAD	LOC	S11	S22	S33	S12	S-MAX	S-MIN	ANGLE
1	CEN	-0.59262E+08	-0.17620E+08	-0.19220E+08	0.91809E+07	-0.15685E+08	-0.61196E+08	78.10
1	L-I	-0.47622E+08	-0.29260E+08	-0.19220E+08	-0.20821E+08	-0.15685E+08	-0.61196E+08	-56.90
1	J-K	-0.59262E+08	-0.17620E+08	-0.19220E+08	0.91809E+07	-0.15685E+08	-0.61196E+08	78.10
1	I-J	-0.17620E+08	-0.59262E+08	-0.19220E+08	-0.91809E+07	-0.15685E+08	-0.61196E+08	-11.90

ELEMENT (24)

LOAD	LOC	S11	S22	S33	S12	S-MAX	S-MIN	ANGLE
1	CEN	-0.62945E+08	-0.28670E+08	-0.22904E+08	0.50866E+07	-0.27931E+08	-0.63684E+08	81.73
1	L-I	-0.62945E+08	-0.28670E+08	-0.22904E+08	0.50866E+07	-0.27931E+08	-0.63684E+08	81.73
1	J-K	-0.28670E+08	-0.62945E+08	-0.22904E+08	-0.50866E+07	-0.27931E+08	-0.63684E+08	-8.27
1	I-J	-0.50894E+08	-0.40721E+08	-0.22904E+08	-0.17137E+08	-0.27931E+08	-0.63684E+08	-53.27

ELEMENT (25)

LOAD	LOC	S11	S22	S33	S12	S-MAX	S-MIN	ANGLE
1	CEN	-0.59799E+08	-0.18385E+08	-0.19546E+08	0.17288E+07	-0.18313E+08	-0.59871E+08	87.61
1	L-I	-0.40821E+08	-0.37363E+08	-0.19546E+08	-0.20707E+08	-0.18313E+08	-0.59871E+08	-47.39
1	J-K	-0.59799E+08	-0.18385E+08	-0.19546E+08	0.17288E+07	-0.18313E+08	-0.59871E+08	87.61
1	I-J	-0.18385E+08	-0.59799E+08	-0.19546E+08	-0.17288E+07	-0.18313E+08	-0.59871E+08	-2.39

ELEMENT (26)

LOAD	LOC	S11	S22	S33	S12	S-MAX	S-MIN	ANGLE
1	CEN	-0.68546E+08	-0.71968E+07	-0.18936E+08	0.31947E+07	-0.70309E+07	-0.68712E+08	87.03
1	L-I	-0.41066E+08	-0.34677E+08	-0.18936E+08	-0.30674E+08	-0.70309E+07	-0.68712E+08	-47.97
1	J-K	-0.68546E+08	-0.71968E+07	-0.18936E+08	0.31947E+07	-0.70309E+07	-0.68712E+08	87.03
1	I-J	-0.71968E+07	-0.68546E+08	-0.18936E+08	-0.31947E+07	-0.70309E+07	-0.68712E+08	-2.97

ELEMENT (27)

LOAD	LOC	S11	S22	S33	S12	S-MAX	S-MIN	ANGLE
1	CEN	-0.69437E+08	-0.21598E+08	-0.22759E+08	0.70178E+07	-0.20590E+08	-0.70445E+08	81.82
1	L-I	-0.69437E+08	-0.21598E+08	-0.22759E+08	0.70178E+07	-0.20590E+08	-0.70445E+08	81.82
1	J-K	-0.21598E+08	-0.69437E+08	-0.22759E+08	-0.70178E+07	-0.20590E+08	-0.70445E+08	-8.18
1	I-J	-0.52535E+08	-0.38500E+08	-0.22759E+08	-0.23920E+08	-0.20590E+08	-0.70445E+08	-53.18

ELEMENT (28)

LOAD	LOC	S11	S22	S33	S12	S-MAX	S-MIN	ANGLE
1	CEN	-0.66714E+08	-0.13428E+08	-0.20035E+08	0.84154E+07	-0.12130E+08	-0.68011E+08	81.24
1	L-I	-0.48486E+08	-0.31655E+08	-0.20035E+08	-0.26643E+08	-0.12130E+08	-0.68011E+08	-53.76
1	J-K	-0.66714E+08	-0.13428E+08	-0.20035E+08	0.84154E+07	-0.12130E+08	-0.68011E+08	81.24
1	I-J	-0.13428E+08	-0.66714E+08	-0.20035E+08	-0.84154E+07	-0.12130E+08	-0.68011E+08	-8.76

ELEMENT (29)

LOAD	LOC	S11	S22	S33	S12	S-MAX	S-MIN	ANGLE
1	CEN	-0.76990E+08	-0.23529E+08	-0.25130E+08	0.13510E+08	-0.20309E+08	-0.80210E+08	76.59
1	L-I	-0.76990E+08	-0.23529E+08	-0.25130E+08	0.13510E+08	-0.20309E+08	-0.80210E+08	76.59
1	J-K	-0.23529E+08	-0.76990E+08	-0.25130E+08	-0.13510E+08	-0.20309E+08	-0.80210E+08	-13.41
1	I-J	-0.63769E+08	-0.36750E+08	-0.25130E+08	-0.26730E+08	-0.20309E+08	-0.80210E+08	-58.41

ELEMENT (30)

LOAD	LOC	S11	S22	S33	S12	S-MAX	S-MIN	ANGLE
1	CEN	-0.80590E+08	-0.34330E+08	-0.28730E+08	0.39591E+08	-0.11608E+08	-0.10331E+09	60.15
1	L-I	-0.97051E+08	-0.17869E+08	-0.28730E+08	-0.23130E+08	-0.11608E+08	-0.10331E+09	-74.85
1	J-K	-0.80590E+08	-0.34330E+08	-0.28730E+08	0.39591E+08	-0.11608E+08	-0.10331E+09	60.15
1	I-J	-0.34330E+08	-0.80590E+08	-0.28730E+08	-0.39591E+08	-0.11608E+08	-0.10331E+09	-29.85

ELEMENT (31)

LOAD	LOC	S11	S22	S33	S12	S-MAX	S-MIN	ANGLE
1	CEN	-0.44659E+08	-0.24123E+08	-0.17196E+08	0.28056E+08	-0.45150E+07	-0.64267E+08	55.05
1	L-I	-0.44659E+08	-0.24123E+08	-0.17196E+08	0.28056E+08	-0.45150E+07	-0.64267E+08	55.05
1	J-K	-0.24123E+08	-0.44659E+08	-0.17196E+08	-0.28056E+08	-0.45150E+07	-0.64267E+08	-34.95
1	I-J	-0.62447E+08	-0.63347E+07	-0.17196E+08	-0.10268E+08	-0.45150E+07	-0.64267E+08	-79.95

ELEMENT (32)

LOAD	LOC	S11	S22	S33	S12	S-MAX	S-MIN	ANGLE
1	CEN	-0.40862E+08	-0.12732E+08	-0.13398E+08	0.22685E+08	-0.10521E+06	-0.53489E+08	60.90
1	L-I	-0.49482E+08	-0.41114E+07	-0.13398E+08	-0.14065E+08	-0.10521E+06	-0.53489E+08	-74.10
1	J-K	-0.40862E+08	-0.12732E+08	-0.13398E+08	0.22685E+08	-0.10521E+06	-0.53489E+08	60.90
1	I-J	-0.12732E+08	-0.40862E+08	-0.13398E+08	-0.22685E+08	-0.10521E+06	-0.53489E+08	-29.10

ELEMENT (33)

LOAD	LOC	S11	S22	S33	S12	S-MAX	S-MIN	ANGLE
1	CEN	-0.45561E+08	-0.29300E+08	-0.18715E+08	0.28002E+08	-0.82719E+07	-0.66589E+08	53.10
1	L-I	-0.45561E+08	-0.29300E+08	-0.18715E+08	0.28002E+08	-0.82719E+07	-0.66589E+08	-36.90
1	J-K	-0.29300E+08	-0.45561E+08	-0.18715E+08	-0.28002E+08	-0.82719E+07	-0.66589E+08	-36.90
1	I-J	-0.65433E+08	-0.94283E+07	-0.18715E+08	-0.81304E+07	-0.82719E+07	-0.66589E+08	-81.91

ELEMENT (34)

LOAD	LOC	S11	S22	S33	S12	S-MAX	S-MIN	ANGLE
1	CEN	-0.45466E+08	-0.29014E+08	-0.18620E+08	0.33951E+08	-0.23065E+07	-0.72174E+08	51.81
1	L-I	-0.72169E+08	-0.23108E+07	-0.18620E+08	0.54966E+06	-0.23065E+07	-0.72174E+08	89.55
1	J-K	-0.45466E+08	-0.29014E+08	-0.18620E+08	0.33951E+08	-0.23065E+07	-0.72174E+08	51.81
1	I-J	-0.29014E+08	-0.45466E+08	-0.18620E+08	-0.33951E+08	-0.23065E+07	-0.72174E+08	-38.19

ELEMENT (35)

LOAD	LOC	S11	S22	S33	S12	S-MAX	S-MIN	ANGLE
1	CEN	-0.36548E+08	-0.31546E+08	-0.17023E+08	0.33785E+08	-0.16984E+06	-0.67924E+08	47.12
1	L-I	-0.36548E+08	-0.31546E+08	-0.17023E+08	0.33785E+08	-0.16984E+06	-0.67924E+08	47.12
1	J-K	-0.50119E+08	-0.17975E+08	-0.17023E+08	-0.29822E+08	-0.16984E+06	-0.67924E+08	-59.16
1	I-J	-0.67380E+08	-0.71433E+06	-0.17023E+08	0.60494E+07	-0.16984E+06	-0.67924E+08	84.86

ELEMENT (36)

LOAD	LOC	S11	S22	S33	S12	S-MAX	S-MIN	ANGLE
1	CEN	-0.39065E+08	-0.27448E+08	-0.16628E+08	0.38230E+08	0.54122E+07	-0.71925E+08	49.32
1	L-I	-0.71486E+08	0.49735E+07	-0.16628E+08	-0.58083E+07	0.54122E+07	-0.71925E+08	-85.68
1	J-K	0.45391E+07	-0.71052E+08	-0.16628E+08	0.81707E+07	0.54122E+07	-0.71925E+08	6.10
1	I-J	-0.48933E+08	-0.17580E+08	-0.16628E+08	-0.35348E+08	0.54122E+07	-0.71925E+08	-56.96

ELEMENT (37)

LOAD	LOC	S11	S22	S33	S12	S-MAX	S-MIN	ANGLE
1	CEN	0.88013E+08	0.93124E+08	0.16536E+09	-0.72433E+08	0.16305E+09	0.18091E+08	-46.01
1	L-I	0.16300E+09	0.18136E+08	0.16536E+09	-0.25556E+07	0.16305E+09	0.18091E+08	-1.01
1	J-K	0.88013E+08	0.93124E+08	0.16536E+09	-0.72433E+08	0.16305E+09	0.18091E+08	-46.01
1	I-J	0.18117E+08	0.16302E+09	0.16536E+09	-0.19464E+07	0.16305E+09	0.18091E+08	-89.23

ELEMENT (38)

LOAD	LOC	S11	S22	S33	S12	S-MAX	S-MIN	ANGLE
1	CEN	0.68038E+08	0.79066E+08	0.15345E+09	-0.38042E+08	0.11199E+09	0.35112E+08	-49.12
1	L-I	0.11159E+09	0.35510E+08	0.15345E+09	-0.55143E+07	0.11199E+09	0.35112E+08	-4.12
1	J-K	0.68038E+08	0.79066E+08	0.15345E+09	-0.38042E+08	0.11199E+09	0.35112E+08	-49.12
1	I-J	0.79066E+08	0.68038E+08	0.15345E+09	0.38042E+08	0.11199E+09	0.35112E+08	40.88

ELEMENT (39)

LOAD	LOC	S11	S22	S33	S12	S-MAX	S-MIN	ANGLE
1	CEN	0.70542E+08	0.83717E+08	0.15595E+09	-0.56718E+08	0.13423E+09	0.20030E+08	-48.31
1	L-I	0.70542E+08	0.83717E+08	0.15595E+09	-0.56718E+08	0.13423E+09	0.20030E+08	-48.31
1	J-K	0.83717E+08	0.70542E+08	0.15595E+09	0.56718E+08	0.13423E+09	0.20030E+08	41.69
1	I-J	0.13281E+09	0.21444E+08	0.15595E+09	0.12629E+08	0.13423E+09	0.20030E+08	6.39

ELEMENT (40)

LOAD	LOC	S11	S22	S33	S12	S-MAX	S-MIN	ANGLE
1	CEN	0.55589E+08	0.97724E+08	0.15562E+09	-0.51464E+08	0.13227E+09	0.21047E+08	-56.13
1	L-I	0.13220E+09	0.21116E+08	0.15562E+09	-0.27740E+07	0.13227E+09	0.21047E+08	-1.43
1	J-K	0.55589E+08	0.97724E+08	0.15562E+09	-0.51464E+08	0.13227E+09	0.21047E+08	-56.13
1	I-J	0.66720E+08	0.86593E+08	0.15562E+09	0.54715E+08	0.13227E+09	0.21047E+08	50.15

ELEMENT (41)

LOAD	LOC	S11	S22	S33	S12	S-MAX	S-MIN	ANGLE
1	CEN	0.54298E+08	0.12423E+09	0.16444E+09	-0.66215E+08	0.16415E+09	0.14385E+08	-58.92
1	L-I	0.83106E+08	0.95424E+08	0.16444E+09	0.74626E+08	0.16415E+09	0.14385E+08	47.36
1	J-K	0.15548E+09	0.23050E+08	0.16444E+09	-0.34967E+08	0.16415E+09	0.14385E+08	-13.92
1	I-J	0.16631E+08	0.16190E+09	0.16444E+09	0.18202E+08	0.16415E+09	0.14385E+08	82.97

ELEMENT (42)

LOAD	LOC	S11	S22	S33	S12	S-MAX	S-MIN	ANGLE
1	CEN	-0.42243E+08	-0.27940E+08	-0.17546E+08	0.44516E+08	0.99950E+07	-0.80179E+08	49.56
1	L-I	0.64427E+07	-0.76626E+08	-0.17546E+08	0.17542E+08	0.99950E+07	-0.80179E+08	11.45
1	J-K	-0.79608E+08	0.94242E+07	-0.17546E+08	-0.71516E+07	0.99950E+07	-0.80179E+08	-85.44
1	I-J	-0.42243E+08	-0.27940E+08	-0.17546E+08	0.44516E+08	0.99950E+07	-0.80179E+08	49.56

ELEMENT (43)

LOAD	LOC	S11	S22	S33	S12	S-MAX	S-MIN	ANGLE
1	CEN	0.36819E+08	0.12241E+09	0.15769E+09	-0.63318E+08	0.15604E+09	0.31907E+07	-62.03
1	L-I	0.14293E+09	0.16296E+08	0.15769E+09	-0.42795E+08	0.15604E+09	0.31907E+07	-17.03
1	J-K	0.46331E+08	0.11290E+09	0.15769E+09	-0.68795E+08	0.15604E+09	0.31907E+07	-57.91
1	I-J	0.40877E+07	0.15514E+09	0.15769E+09	0.11675E+08	0.15604E+09	0.31907E+07	85.61

ELEMENT (44)

LOAD	LOC	S11	S22	S33	S12	S-MAX	S-MIN	ANGLE
1	CEN	-0.61989E+08	-0.26669E+08	-0.22165E+08	0.49135E+08	0.78830E+07	-0.96541E+08	54.89
1	L-I	-0.93464E+08	0.48056E+07	-0.22165E+08	-0.17660E+08	0.78830E+07	-0.96541E+08	-80.12
1	J-K	-0.74331E+07	-0.81225E+08	-0.22165E+08	0.36943E+08	0.78830E+07	-0.96541E+08	22.52
1	I-J	-0.26669E+08	-0.61989E+08	-0.22165E+08	-0.49135E+08	0.78830E+07	-0.96541E+08	-35.12

ELEMENT (45)

LOAD	LOC	S11	S22	S33	S12	S-MAX	S-MIN	ANGLE
1	CEN	-0.59404E+08	-0.18913E+08	-0.19579E+08	0.35931E+08	0.20836E+07	-0.80401E+08	59.70
1	L-I	-0.59404E+08	-0.18913E+08	-0.19579E+08	0.35931E+08	0.20836E+07	-0.80401E+08	59.70
1	J-K	-0.18913E+08	-0.59404E+08	-0.19579E+08	-0.35931E+08	0.20836E+07	-0.80401E+08	-30.30
1	I-J	-0.76499E+08	-0.18177E+07	-0.19579E+08	-0.17509E+08	0.20836E+07	-0.80401E+08	-77.44

ELEMENT (46)

LOAD	LOC	S11	S22	S33	S12	S-MAX	S-MIN	ANGLE
1	CEN	-0.10547E+09	-0.29553E+08	-0.33757E+08	0.48823E+08	-0.56695E+07	-0.12936E+09	63.93
1	L-I	-0.11903E+09	-0.15995E+08	-0.33757E+08	-0.34213E+08	-0.56695E+07	-0.12936E+09	-73.21
1	J-K	-0.98088E+08	-0.36939E+08	-0.33757E+08	0.53758E+08	-0.56695E+07	-0.12936E+09	59.81
1	I-J	-0.29553E+08	-0.10547E+09	-0.33757E+08	-0.48823E+08	-0.56695E+07	-0.12936E+09	-26.07

ELEMENT (47)

LOAD	LOC	S11	S22	S33	S12	S-MAX	S-MIN	ANGLE
1	CEN	-0.53932E+08	-0.91672E+07	-0.15775E+08	0.14592E+08	-0.48307E+07	-0.58269E+08	73.45
1	L-I	-0.91672E+07	-0.53932E+08	-0.15775E+08	-0.14592E+08	-0.48307E+07	-0.58269E+08	-16.55
1	J-K	-0.46142E+08	-0.16958E+08	-0.15775E+08	-0.22383E+08	-0.48307E+07	-0.58269E+08	-61.55
1	I-J	-0.53932E+08	-0.91672E+07	-0.15775E+08	0.14592E+08	-0.48307E+07	-0.58269E+08	73.45

ELEMENT (48)

LOAD	LOC	S11	S22	S33	S12	S-MAX	S-MIN	ANGLE
1	CEN	-0.51706E+08	-0.24880E+07	-0.13548E+08	0.26484E+08	0.90555E+07	-0.63249E+08	66.45
1	L-I	-0.53581E+08	-0.61301E+06	-0.13548E+08	-0.24609E+08	0.90555E+07	-0.63249E+08	-68.55
1	J-K	-0.51706E+08	-0.24880E+07	-0.13548E+08	0.26484E+08	0.90555E+07	-0.63249E+08	66.45
1	I-J	-0.24880E+07	-0.51706E+08	-0.13548E+08	-0.26484E+08	0.90555E+07	-0.63249E+08	-23.55

ELEMENT (49)

LOAD	LOC	S11	S22	S33	S12	S-MAX	S-MIN	ANGLE
1	CEN	-0.53932E+08	-0.91672E+07	-0.15775E+08	0.14592E+08	-0.48307E+07	-0.58269E+08	73.45
1	L-I	-0.91672E+07	-0.53932E+08	-0.15775E+08	-0.14592E+08	-0.48307E+07	-0.58269E+08	-16.55
1	J-K	-0.46142E+08	-0.16958E+08	-0.15775E+08	-0.22383E+08	-0.48307E+07	-0.58269E+08	-61.55
1	I-J	-0.53932E+08	-0.91672E+07	-0.15775E+08	0.14592E+08	-0.48307E+07	-0.58269E+08	73.45

ELEMENT (50)

LOAD	LOC	S11	S22	S33	S12	S-MAX	S-MIN	ANGLE
1	CEN	-0.79230E+08	-0.24204E+07	-0.20413E+08	0.19230E+08	0.21250E+07	-0.83776E+08	76.70
1	L-I	-0.60055E+08	-0.21595E+08	-0.20413E+08	-0.38405E+08	0.21250E+07	-0.83776E+08	-58.30
1	J-K	-0.79230E+08	-0.24204E+07	-0.20413E+08	0.19230E+08	0.21250E+07	-0.83776E+08	76.70
1	I-J	-0.24204E+07	-0.79230E+08	-0.20413E+08	-0.19230E+08	0.21250E+07	-0.83776E+08	-13.30

ELEMENT (51)

LOAD	LOC	S11	S22	S33	S12	S-MAX	S-MIN	ANGLE
1	CEN	-0.82357E+08	-0.11801E+08	-0.23539E+08	0.89680E+07	-0.10679E+08	-0.83479E+08	82.87
1	L-I	-0.11801E+08	-0.82357E+08	-0.23539E+08	-0.89680E+07	-0.10679E+08	-0.83479E+08	-7.13
1	J-K	-0.56047E+08	-0.38111E+08	-0.23539E+08	-0.35278E+08	-0.10679E+08	-0.83479E+08	-52.13
1	I-J	-0.82357E+08	-0.11801E+08	-0.23539E+08	0.89680E+07	-0.10679E+08	-0.83479E+08	82.87

ELEMENT (52)

LOAD	LOC	S11	S22	S33	S12	S-MAX	S-MIN	ANGLE
1	CEN	-0.80708E+08	0.41445E+07	-0.19141E+08	0.45695E+07	0.43899E+07	-0.80954E+08	86.93
1	L-I	-0.42851E+08	-0.33712E+08	-0.19141E+08	-0.42426E+08	0.43899E+07	-0.80954E+08	-48.07
1	J-K	-0.80708E+08	0.41445E+07	-0.19141E+08	0.45695E+07	0.43899E+07	-0.80954E+08	86.93
1	I-J	0.41445E+07	-0.80708E+08	-0.19141E+08	-0.45695E+07	0.43899E+07	-0.80954E+08	-3.07

ELEMENT (53)

LOAD	LOC	S11	S22	S33	S12	S-MAX	S-MIN	ANGLE
1	CEN	-0.96630E+08	0.16551E+08	-0.20020E+08	0.67874E+07	0.16956E+08	-0.97035E+08	86.58
1	L-I	-0.50490E+08	-0.29589E+08	-0.20020E+08	-0.56030E+08	0.16956E+08	-0.97035E+08	-50.28
1	J-K	-0.95330E+08	0.15252E+08	-0.20020E+08	0.13836E+08	0.16956E+08	-0.97035E+08	82.98
1	I-J	0.16551E+08	-0.96630E+08	-0.20020E+08	-0.67874E+07	0.16956E+08	-0.97035E+08	-3.42

ELEMENT (54)

LOAD	LOC	S11	S22	S33	S12	S-MAX	S-MIN	ANGLE
1	CEN	-0.96172E+08	-0.10099E+07	-0.24295E+08	0.11659E+08	0.39765E+06	-0.97579E+08	83.12
1	L-I	-0.96172E+08	-0.10099E+07	-0.24295E+08	0.11659E+08	0.39765E+06	-0.97579E+08	83.12
1	J-K	-0.10099E+07	-0.96172E+08	-0.24295E+08	-0.11659E+08	0.39765E+06	-0.97579E+08	-6.88
1	I-J	-0.63317E+08	-0.33865E+08	-0.24295E+08	-0.46723E+08	0.39765E+06	-0.97579E+08	-53.75

ELEMENT (55)

LOAD	LOC	S11	S22	S33	S12	S-MAX	S-MIN	ANGLE
1	CEN	-0.93955E+08	0.56386E+07	-0.22079E+08	0.24152E+08	0.11186E+08	-0.99503E+08	77.06
1	L-I	-0.81497E+08	-0.68197E+07	-0.22079E+08	-0.40852E+08	0.11186E+08	-0.99503E+08	-56.21
1	J-K	-0.81549E+08	-0.67680E+07	-0.22079E+08	0.40804E+08	0.11186E+08	-0.99503E+08	66.25
1	I-J	0.56386E+07	-0.93955E+08	-0.22079E+08	-0.24152E+08	0.11186E+08	-0.99503E+08	-12.94

ELEMENT (56)

LOAD	LOC	S11	S22	S33	S12	S-MAX	S-MIN	ANGLE
1	CEN	-0.84318E+08	-0.41163E+07	-0.22109E+08	0.27064E+08	0.41621E+07	-0.92597E+08	72.99
1	L-I	-0.84318E+08	-0.41163E+07	-0.22109E+08	0.27064E+08	0.41621E+07	-0.92597E+08	72.99
1	J-K	-0.41163E+07	-0.84318E+08	-0.22109E+08	-0.27064E+08	0.41621E+07	-0.92597E+08	-17.01
1	I-J	-0.81586E+08	-0.68492E+07	-0.22109E+08	-0.30728E+08	0.41621E+07	-0.92597E+08	-70.29

ELEMENT (57)

LOAD	LOC	S11	S22	S33	S12	S-MAX	S-MIN	ANGLE
1	CEN	-0.86246E+08	-0.98985E+07	-0.24036E+08	0.31766E+08	0.15895E+07	-0.97734E+08	70.12
1	L-I	-0.97513E+08	0.13683E+07	-0.24036E+08	-0.46819E+07	0.15895E+07	-0.97734E+08	-87.30
1	J-K	-0.59842E+08	-0.36303E+08	-0.24036E+08	0.48247E+08	0.15895E+07	-0.97734E+08	51.85
1	I-J	-0.98985E+07	-0.86246E+08	-0.24036E+08	-0.31766E+08	0.15895E+07	-0.97734E+08	-19.88

ELEMENT (58)

LOAD	LOC	S11	S22	S33	S12	S-MAX	S-MIN	ANGLE
1	CEN	-0.65143E+08	-0.69671E+07	-0.18028E+08	0.32324E+08	0.74303E+07	-0.79541E+08	65.99
1	L-I	-0.65143E+08	-0.69671E+07	-0.18028E+08	0.32324E+08	0.74303E+07	-0.79541E+08	65.99
1	J-K	-0.69671E+07	-0.65143E+08	-0.18028E+08	-0.32324E+08	0.74303E+07	-0.79541E+08	-24.01
1	I-J	-0.79487E+08	0.73768E+07	-0.18028E+08	0.21562E+07	0.74303E+07	-0.79541E+08	88.58

ELEMENT (59)

LOAD	LOC	S11	S22	S33	S12	S-MAX	S-MIN	ANGLE
1	CEN	-0.23152E+08	0.14280E+09	0.14384E+09	-0.28236E+08	0.14748E+09	-0.27824E+08	-80.60
1	L-I	-0.23660E+08	0.14331E+09	0.14384E+09	0.26697E+08	0.14748E+09	-0.27824E+08	81.13
1	J-K	0.14280E+09	-0.23152E+08	0.14384E+09	0.28236E+08	0.14748E+09	-0.27824E+08	9.40
1	I-J	0.38065E+06	0.11927E+09	0.14384E+09	-0.64411E+08	0.14748E+09	-0.27824E+08	-66.35

ELEMENT (60)

LOAD	LOC	S11	S22	S33	S12	S-MAX	S-MIN	ANGLE
1	CEN	-0.68751E+08	-0.17790E+08	-0.21635E+08	0.47219E+08	0.10385E+08	-0.96926E+08	59.18
1	L-I	-0.61723E+08	-0.24817E+08	-0.21635E+08	0.50382E+08	0.10385E+08	-0.96926E+08	55.06
1	J-K	-0.21727E+08	-0.64813E+08	-0.21635E+08	0.49140E+08	0.10385E+08	-0.96926E+08	33.16
1	I-J	-0.17790E+08	-0.68751E+08	-0.21635E+08	-0.47219E+08	0.10385E+08	-0.96926E+08	-30.82

ELEMENT (61)

LOAD	LOC	S11	S22	S33	S12	S-MAX	S-MIN	ANGLE
1	CEN	-0.44916E+08	0.10238E+09	0.12207E+09	-0.27463E+08	0.10734E+09	-0.49869E+08	-79.78
1	L-I	0.16464E+08	0.41004E+08	0.12207E+09	-0.77640E+08	0.10734E+09	-0.49869E+08	-49.49
1	J-K	-0.44916E+08	0.10238E+09	0.12207E+09	-0.27463E+08	0.10734E+09	-0.49869E+08	-79.78
1	I-J	0.10238E+09	-0.44916E+08	0.12207E+09	0.27463E+08	0.10734E+09	-0.49869E+08	10.22

ELEMENT (62)

LOAD	LOC	S11	S22	S33	S12	S-MAX	S-MIN	ANGLE
1	CEN	0.20205E+08	0.15191E+09	0.16220E+09	-0.42819E+08	0.16461E+09	0.75086E+07	-73.48
1	L-I	0.11785E+08	0.16033E+09	0.16220E+09	0.25563E+08	0.16461E+09	0.75086E+07	80.50
1	J-K	0.15191E+09	0.20205E+08	0.16220E+09	0.42819E+08	0.16461E+09	0.75086E+07	16.52
1	I-J	0.90994E+08	0.81123E+08	0.16220E+09	-0.78394E+08	0.16461E+09	0.75086E+07	-43.20

ELEMENT (63)

LOAD	LOC	S11	S22	S33	S12	S-MAX	S-MIN	ANGLE
1	CEN	-0.99855E+07	0.95843E+08	0.13201E+09	-0.31725E+08	0.10462E+09	-0.18767E+08	-74.53
1	L-I	0.78250E+08	0.76073E+07	0.13201E+09	-0.50584E+08	0.10462E+09	-0.18767E+08	-27.54
1	J-K	-0.99855E+07	0.95843E+08	0.13201E+09	-0.31725E+08	0.10462E+09	-0.18767E+08	-74.53
1	I-J	0.95843E+08	-0.99855E+07	0.13201E+09	0.31725E+08	0.10462E+09	-0.18767E+08	15.47

ELEMENT (64)

LOAD	LOC	S11	S22	S33	S12	S-MAX	S-MIN	ANGLE
1	CEN	0.48956E+08	0.12506E+09	0.16286E+09	-0.46023E+08	0.14672E+09	0.27291E+08	-64.79
1	L-I	0.55942E+08	0.11807E+09	0.16286E+09	-0.51000E+08	0.14672E+09	0.27291E+08	-60.67
1	J-K	0.12506E+09	0.48956E+08	0.16286E+09	0.46023E+08	0.14672E+09	0.27291E+08	25.21
1	I-J	0.13556E+09	0.38454E+08	0.16286E+09	-0.34765E+08	0.14672E+09	0.27291E+08	-17.80

ELEMENT (65)

LOAD	LOC	S11	S22	S33	S12	S-MAX	S-MIN	ANGLE
1	CEN	0.25963E+08	0.82358E+08	0.13987E+09	-0.25123E+08	0.91926E+08	0.16394E+08	-69.15
1	L-I	0.79283E+08	0.29037E+08	0.13987E+09	-0.28197E+08	0.91926E+08	0.16394E+08	-24.15
1	J-K	0.25963E+08	0.82358E+08	0.13987E+09	-0.25123E+08	0.91926E+08	0.16394E+08	-69.15
1	I-J	0.82358E+08	0.25963E+08	0.13987E+09	0.25123E+08	0.91926E+08	0.16394E+08	20.85

ELEMENT (66)

LOAD	LOC	S11	S22	S33	S12	S-MAX	S-MIN	ANGLE
1	CEN	0.63114E+08	0.10178E+09	0.15967E+09	-0.33613E+08	0.12122E+09	0.43670E+08	-59.95
1	L-I	0.63114E+08	0.10178E+09	0.15967E+09	-0.33613E+08	0.12122E+09	0.43670E+08	-59.95
1	J-K	0.10178E+09	0.63114E+08	0.15967E+09	0.33613E+08	0.12122E+09	0.43670E+08	30.05
1	I-J	0.11606E+09	0.48832E+08	0.15967E+09	-0.19331E+08	0.12122E+09	0.43670E+08	-14.95

ELEMENT (67)

LOAD	LOC	S11	S22	S33	S12	S-MAX	S-MIN	ANGLE
1	CEN	0.47698E+08	0.73146E+08	0.14425E+09	-0.19258E+08	0.83504E+08	0.37340E+08	-61.73
1	L-I	0.79680E+08	0.41163E+08	0.14425E+09	-0.12724E+08	0.83504E+08	0.37340E+08	-16.73
1	J-K	0.47698E+08	0.73146E+08	0.14425E+09	-0.19258E+08	0.83504E+08	0.37340E+08	-61.73
1	I-J	0.73146E+08	0.47698E+08	0.14425E+09	0.19258E+08	0.83504E+08	0.37340E+08	28.27

ELEMENT (68)

LOAD	LOC	S11	S22	S33	S12	S-MAX	S-MIN	ANGLE
1	CEN	0.69919E+08	0.80079E+08	0.15446E+09	-0.23634E+08	0.99173E+08	0.50825E+08	-51.07
1	L-I	0.69919E+08	0.80079E+08	0.15446E+09	-0.23634E+08	0.99173E+08	0.50825E+08	-51.07
1	J-K	0.80079E+08	0.69919E+08	0.15446E+09	0.23634E+08	0.99173E+08	0.50825E+08	38.93
1	I-J	0.98633E+08	0.51365E+08	0.15446E+09	-0.50802E+07	0.99173E+08	0.50825E+08	-6.07

ELEMENT (69)

LOAD	LOC	S11	S22	S33	S12	S-MAX	S-MIN	ANGLE
1	CEN	0.63568E+08	0.68284E+08	0.14811E+09	-0.12383E+08	0.78532E+08	0.53320E+08	-50.39
1	L-I	0.78310E+08	0.53543E+08	0.14811E+09	-0.23583E+07	0.78532E+08	0.53320E+08	-5.39
1	J-K	0.63568E+08	0.68284E+08	0.14811E+09	-0.12383E+08	0.78532E+08	0.53320E+08	-50.39
1	I-J	0.68284E+08	0.63568E+08	0.14811E+09	0.12383E+08	0.78532E+08	0.53320E+08	39.61

ELEMENT (70)

LOAD	LOC	S11	S22	S33	S12	S-MAX	S-MIN	ANGLE
1	CEN	0.62774E+08	0.64621E+08	0.14655E+09	-0.29219E+07	0.66762E+08	0.60633E+08	-53.77
1	L-I	0.66619E+08	0.60775E+08	0.14655E+09	-0.92378E+06	0.66762E+08	0.60633E+08	-8.77
1	J-K	0.62774E+08	0.64621E+08	0.14655E+09	-0.29219E+07	0.66762E+08	0.60633E+08	-53.77
1	I-J	0.64621E+08	0.62774E+08	0.14655E+09	0.29219E+07	0.66762E+08	0.60633E+08	36.23

ELEMENT (71)

LOAD	LOC	S11	S22	S33	S12	S-MAX	S-MIN	ANGLE
1	CEN	0.65227E+08	0.69178E+08	0.14900E+09	-0.69350E+07	0.74414E+08	0.59992E+08	-52.95
1	L-I	0.65227E+08	0.69178E+08	0.14900E+09	-0.69350E+07	0.74414E+08	0.59992E+08	-52.95
1	J-K	0.69178E+08	0.65227E+08	0.14900E+09	0.69350E+07	0.74414E+08	0.59992E+08	37.05
1	I-J	0.74138E+08	0.60268E+08	0.14900E+09	-0.19754E+07	0.74414E+08	0.59992E+08	-7.95

ELEMENT (72)

LOAD	LOC	S11	S22	S33	S12	S-MAX	S-MIN	ANGLE
1	CEN	0.56133E+08	0.66727E+08	0.14496E+09	-0.52023E+07	0.68855E+08	0.54006E+08	-67.76
1	L-I	0.66633E+08	0.56228E+08	0.14496E+09	-0.52971E+07	0.68855E+08	0.54006E+08	-22.76
1	J-K	0.56133E+08	0.66727E+08	0.14496E+09	-0.52023E+07	0.68855E+08	0.54006E+08	-67.76
1	I-J	0.66727E+08	0.56133E+08	0.14496E+09	0.52023E+07	0.68855E+08	0.54006E+08	22.24

ELEMENT (73)

LOAD	LOC	S11	S22	S33	S12	S-MAX	S-MIN	ANGLE
1	CEN	0.64445E+08	0.82163E+08	0.15327E+09	-0.12969E+08	0.89010E+08	0.57598E+08	-62.17
1	L-I	0.64445E+08	0.82163E+08	0.15327E+09	-0.12969E+08	0.89010E+08	0.57598E+08	-62.17
1	J-K	0.82163E+08	0.64445E+08	0.15327E+09	0.12969E+08	0.89010E+08	0.57598E+08	27.83
1	I-J	0.86273E+08	0.60335E+08	0.15327E+09	-0.88592E+07	0.89010E+08	0.57598E+08	-17.17

ELEMENT (74)

LOAD	LOC	S11	S22	S33	S12	S-MAX	S-MIN	ANGLE
1	CEN	0.41785E+08	0.70326E+08	0.14120E+09	-0.77916E+07	0.72315E+08	0.39797E+08	-75.68
1	L-I	0.63847E+08	0.48264E+08	0.14120E+09	-0.14271E+08	0.72315E+08	0.39797E+08	-30.68
1	J-K	0.41785E+08	0.70326E+08	0.14120E+09	-0.77916E+07	0.72315E+08	0.39797E+08	-75.68
1	I-J	0.70326E+08	0.41785E+08	0.14120E+09	0.77916E+07	0.72315E+08	0.39797E+08	14.32

ELEMENT (75)

LOAD	LOC	S11	S22	S33	S12	S-MAX	S-MIN	ANGLE
1	CEN	0.57370E+08	0.99269E+08	0.15678E+09	-0.18762E+08	0.10644E+09	0.50197E+08	-69.08
1	L-I	0.57370E+08	0.99269E+08	0.15678E+09	-0.18762E+08	0.10644E+09	0.50197E+08	-69.08
1	J-K	0.99269E+08	0.57370E+08	0.15678E+09	0.18762E+08	0.10644E+09	0.50197E+08	20.92
1	I-J	0.97081E+08	0.59558E+08	0.15678E+09	-0.20950E+08	0.10644E+09	0.50197E+08	-24.08

ELEMENT (76)

LOAD	LOC	S11	S22	S33	S12	S-MAX	S-MIN	ANGLE
1	CEN	0.18783E+08	0.76094E+08	0.13517E+09	-0.94919E+07	0.77625E+08	0.17252E+08	-80.84
1	L-I	0.56930E+08	0.37947E+08	0.13517E+09	-0.28656E+08	0.77625E+08	0.17252E+08	-35.84
1	J-K	0.18783E+08	0.76094E+08	0.13517E+09	-0.94919E+07	0.77625E+08	0.17252E+08	-80.84
1	I-J	0.76094E+08	0.18783E+08	0.13517E+09	0.94919E+07	0.77625E+08	0.17252E+08	9.16

ELEMENT (77)

LOAD	LOC	S11	S22	S33	S12	S-MAX	S-MIN	ANGLE
1	CEN	0.45506E+08	0.12572E+09	0.16189E+09	-0.23819E+08	0.13226E+09	0.38966E+08	-74.65
1	L-I	0.45506E+08	0.12572E+09	0.16189E+09	-0.23819E+08	0.13226E+09	0.38966E+08	-74.65
1	J-K	0.12572E+09	0.45506E+08	0.16189E+09	0.23819E+08	0.13226E+09	0.38966E+08	15.35
1	I-J	0.10943E+09	0.61795E+08	0.16189E+09	-0.40108E+08	0.13226E+09	0.38966E+08	-29.65

ELEMENT (78)

LOAD	LOC	S11	S22	S33	S12	S-MAX	S-MIN	ANGLE
1	CEN	-0.10373E+08	0.84028E+08	0.12774E+09	-0.91747E+07	0.84911E+08	-0.11257E+08	-84.50
1	L-I	0.46002E+08	0.27653E+08	0.12774E+09	-0.47200E+08	0.84911E+08	-0.11257E+08	-39.50
1	J-K	-0.10373E+08	0.84028E+08	0.12774E+09	-0.91747E+07	0.84911E+08	-0.11257E+08	-84.50
1	I-J	0.84028E+08	-0.10373E+08	0.12774E+09	0.91747E+07	0.84911E+08	-0.11257E+08	5.50

ELEMENT (79)

LOAD	LOC	S11	S22	S33	S12	S-MAX	S-MIN	ANGLE
1	CEN	0.17652E+08	0.13607E+09	0.15576E+09	-0.23836E+08	0.14069E+09	0.13034E+08	-79.04
1	L-I	0.13607E+09	0.17652E+08	0.15576E+09	0.23836E+08	0.14069E+09	0.13034E+08	10.96
1	J-K	0.10070E+09	0.53026E+08	0.15576E+09	-0.59211E+08	0.14069E+09	0.13034E+08	-34.04
1	I-J	0.17652E+08	0.13607E+09	0.15576E+09	-0.23836E+08	0.14069E+09	0.13034E+08	-79.04

ELEMENT (80)

LOAD	LOC	S11	S22	S33	S12	S-MAX	S-MIN	ANGLE
1	CEN	-0.45017E+08	0.92712E+08	0.11865E+09	-0.79223E+07	0.93166E+08	-0.45471E+08	-86.72
1	L-I	0.31770E+08	0.15925E+08	0.11865E+09	-0.68864E+08	0.93166E+08	-0.45471E+08	-41.72
1	J-K	-0.45017E+08	0.92712E+08	0.11865E+09	-0.79223E+07	0.93166E+08	-0.45471E+08	-86.72
1	I-J	0.92712E+08	-0.45017E+08	0.11865E+09	0.79223E+07	0.93166E+08	-0.45471E+08	3.28

ELEMENT (81)

LOAD	LOC	S11	S22	S33	S12	S-MAX	S-MIN	ANGLE
1	CEN	-0.19960E+08	0.13925E+09	0.14371E+09	-0.21904E+08	0.14220E+09	-0.22919E+08	-82.31
1	L-I	0.14099E+06	0.11914E+09	0.14371E+09	-0.57236E+08	0.14220E+09	-0.22919E+08	-68.06
1	J-K	0.13925E+09	-0.19960E+08	0.14371E+09	0.21904E+08	0.14220E+09	-0.22919E+08	7.69
1	I-J	0.98712E+08	0.20573E+08	0.14371E+09	-0.72732E+08	0.14220E+09	-0.22919E+08	-30.88

ELEMENT (82)

LOAD	LOC	S11	S22	S33	S12	S-MAX	S-MIN	ANGLE
1	CEN	-0.73101E+08	0.10716E+09	0.11388E+09	-0.63785E+07	0.10739E+09	-0.73327E+08	-87.98
1	L-I	0.43308E+08	-0.92470E+07	0.11388E+09	-0.86452E+08	0.10739E+09	-0.73327E+08	-36.55
1	J-K	-0.73101E+08	0.10716E+09	0.11388E+09	-0.63785E+07	0.10739E+09	-0.73327E+08	-87.98
1	I-J	0.10716E+09	-0.73101E+08	0.11388E+09	0.63785E+07	0.10739E+09	-0.73327E+08	2.02

ELEMENT (83)

LOAD	LOC	S11	S22	S33	S12	S-MAX	S-MIN	ANGLE
1	CEN	-0.61429E+08	0.12884E+09	0.12555E+09	-0.11077E+08	0.12948E+09	-0.62071E+08	-86.68
1	L-I	0.12884E+09	-0.61429E+08	0.12555E+09	0.11077E+08	0.12948E+09	-0.62071E+08	3.32
1	J-K	0.50566E+08	0.16844E+08	0.12555E+09	-0.94281E+08	0.12948E+09	-0.62071E+08	-39.93
1	I-J	-0.58814E+08	0.12622E+09	0.12555E+09	0.24765E+08	0.12948E+09	-0.62071E+08	82.51

ELEMENT (84)

LOAD	LOC	S11	S22	S33	S12	S-MAX	S-MIN	ANGLE
1	CEN	-0.92656E+08	0.11456E+09	0.10962E+09	-0.37152E+07	0.11462E+09	-0.92722E+08	-88.97
1	L-I	0.20981E+08	0.92037E+06	0.10962E+09	-0.10319E+09	0.11462E+09	-0.92722E+08	-42.22
1	J-K	-0.92656E+08	0.11456E+09	0.10962E+09	-0.37152E+07	0.11462E+09	-0.92722E+08	-88.97
1	I-J	0.11456E+09	-0.92656E+08	0.10962E+09	0.37152E+07	0.11462E+09	-0.92722E+08	1.03

ELEMENT (85)

LOAD	LOC	S11	S22	S33	S12	S-MAX	S-MIN	ANGLE
1	CEN	-0.95815E+08	0.10869E+09	0.10647E+09	-0.10039E+07	0.10870E+09	-0.95820E+08	-89.72
1	L-I	0.10869E+09	-0.95815E+08	0.10647E+09	0.10039E+07	0.10870E+09	-0.95820E+08	0.28
1	J-K	0.74418E+07	0.54341E+07	0.10647E+09	-0.10225E+09	0.10870E+09	-0.95820E+08	-44.72
1	I-J	-0.95132E+08	0.10801E+09	0.10647E+09	0.11837E+08	0.10870E+09	-0.95820E+08	86.68

ELEMENT (86)

LOAD	LOC	S11	S22	S33	S12	S-MAX	S-MIN	ANGLE
1	CEN	-0.10192E+09	0.12068E+09	0.10853E+09	-0.18870E+07	0.12070E+09	-0.10194E+09	-89.51
1	L-I	0.11267E+08	0.74931E+07	0.10853E+09	-0.11130E+09	0.12070E+09	-0.10194E+09	-44.51
1	J-K	-0.10192E+09	0.12068E+09	0.10853E+09	-0.18870E+07	0.12070E+09	-0.10194E+09	-89.51
1	I-J	0.12068E+09	-0.10192E+09	0.10853E+09	0.18870E+07	0.12070E+09	-0.10194E+09	0.49

ELEMENT (87)

LOAD	LOC	S11	S22	S33	S12	S-MAX	S-MIN	ANGLE
1	CEN	-0.97311E+08	0.12059E+09	0.11011E+09	-0.30321E+01	0.12059E+09	-0.97311E+08	-90.00
1	L-I	0.11640E+08	0.11640E+08	0.11011E+09	-0.10895E+09	0.12059E+09	-0.97311E+08	-45.00
1	J-K	-0.97311E+08	0.12059E+09	0.11011E+09	-0.30321E+01	0.12059E+09	-0.97311E+08	-90.00
1	I-J	0.12059E+09	-0.97311E+08	0.11011E+09	0.30321E+01	0.12059E+09	-0.97311E+08	0.00

ELEMENT (88)

LOAD	LOC	S11	S22	S33	S12	S-MAX	S-MIN	ANGLE
1	CEN	-0.87188E+08	0.12862E+09	0.11646E+09	-0.27238E+07	0.12865E+09	-0.87222E+08	-89.28
1	L-I	-0.87188E+08	0.12862E+09	0.11646E+09	-0.27238E+07	0.12865E+09	-0.87222E+08	-89.28
1	J-K	0.12862E+09	-0.87188E+08	0.11646E+09	0.27238E+07	0.12865E+09	-0.87222E+08	0.72
1	I-J	0.23438E+08	0.17991E+08	0.11646E+09	-0.10790E+09	0.12865E+09	-0.87222E+08	-44.28

ELEMENT (89)

LOAD	LOC	S11	S22	S33	S12	S-MAX	S-MIN	ANGLE
1	CEN	-0.93426E+08	0.11703E+09	0.11022E+09	-0.83679E+06	0.11703E+09	-0.93429E+08	-89.77
1	L-I	0.12640E+08	0.10966E+08	0.11022E+09	-0.10523E+09	0.11703E+09	-0.93429E+08	-44.77
1	J-K	-0.93426E+08	0.11703E+09	0.11022E+09	-0.83679E+06	0.11703E+09	-0.93429E+08	-89.77
1	I-J	0.11703E+09	-0.93426E+08	0.11022E+09	0.83679E+06	0.11703E+09	-0.93429E+08	0.23

ELEMENT (90)

LOAD	LOC	S11	S22	S33	S12	S-MAX	S-MIN	ANGLE
1	CEN	-0.58007E+08	0.13321E+09	0.12828E+09	-0.85816E+07	0.13360E+09	-0.58391E+08	-87.44
1	L-I	0.13321E+09	-0.58007E+08	0.12828E+09	0.85816E+07	0.13360E+09	-0.58391E+08	2.56
1	J-K	0.46185E+08	0.29022E+08	0.12828E+09	-0.95610E+08	0.13360E+09	-0.58391E+08	-42.44
1	I-J	-0.58007E+08	0.13321E+09	0.12828E+09	-0.85816E+07	0.13360E+09	-0.58391E+08	-87.44

ELEMENT (91)

LOAD	LOC	S11	S22	S33	S12	S-MAX	S-MIN	ANGLE
1	CEN	-0.71286E+08	0.10855E+09	0.11500E+09	0.10278E+06	0.10855E+09	-0.71286E+08	89.97
1	L-I	0.18531E+08	0.18736E+08	0.11500E+09	-0.89919E+08	0.10855E+09	-0.71286E+08	-45.03
1	J-K	-0.71286E+08	0.10855E+09	0.11500E+09	0.10278E+06	0.10855E+09	-0.71286E+08	89.97
1	I-J	0.10855E+09	-0.71286E+08	0.11500E+09	-0.10278E+06	0.10855E+09	-0.71286E+08	-0.03

ELEMENT (92)

LOAD	LOC	S11	S22	S33	S12	S-MAX	S-MIN	ANGLE
1	CEN	-0.19100E+08	0.13624E+09	0.14296E+09	-0.11885E+08	0.13714E+09	-0.20004E+08	-85.65
1	L-I	0.13624E+09	-0.19100E+08	0.14296E+09	0.11885E+08	0.13714E+09	-0.20004E+08	4.35
1	J-K	0.70455E+08	0.46684E+08	0.14296E+09	-0.77670E+08	0.13714E+09	-0.20004E+08	-40.65
1	I-J	-0.19100E+08	0.13624E+09	0.14296E+09	-0.11885E+08	0.13714E+09	-0.20004E+08	-85.65

ELEMENT (93)

LOAD	LOC	S11	S22	S33	S12	S-MAX	S-MIN	ANGLE
1	CEN	-0.40280E+08	0.96905E+08	0.12178E+09	0.23722E+06	0.96905E+08	-0.40281E+08	89.90
1	L-I	0.28075E+08	0.28550E+08	0.12178E+09	-0.68593E+08	0.96905E+08	-0.40281E+08	-45.10
1	J-K	-0.40280E+08	0.96905E+08	0.12178E+09	0.23722E+06	0.96905E+08	-0.40281E+08	89.90
1	I-J	0.96905E+08	-0.40280E+08	0.12178E+09	-0.23722E+06	0.96905E+08	-0.40281E+08	-0.10

ELEMENT (94)

LOAD	LOC	S11	S22	S33	S12	S-MAX	S-MIN	ANGLE
1	CEN	0.13763E+08	0.12436E+09	0.15030E+09	-0.11995E+08	0.12565E+09	0.12477E+08	-83.88
1	L-I	0.12436E+09	0.13763E+08	0.15030E+09	0.11995E+08	0.12565E+09	0.12477E+08	6.12
1	J-K	0.81058E+08	0.57067E+08	0.15030E+09	-0.55300E+08	0.12565E+09	0.12477E+08	-38.88
1	I-J	0.13763E+08	0.12436E+09	0.15030E+09	-0.11995E+08	0.12565E+09	0.12477E+08	-83.88

ELEMENT (95)

LOAD	LOC	S11	S22	S33	S12	S-MAX	S-MIN	ANGLE
1	CEN	-0.70656E+07	0.85681E+08	0.12947E+09	0.77138E+06	0.85688E+08	-0.70720E+07	89.52
1	L-I	0.38536E+08	0.40079E+08	0.12947E+09	-0.46373E+08	0.85688E+08	-0.70720E+07	-45.48
1	J-K	-0.70656E+07	0.85681E+08	0.12947E+09	0.77138E+06	0.85688E+08	-0.70720E+07	89.52
1	I-J	0.85681E+08	-0.70656E+07	0.12947E+09	-0.77138E+06	0.85688E+08	-0.70720E+07	-0.48

ELEMENT (96)

LOAD	LOC	S11	S22	S33	S12	S-MAX	S-MIN	ANGLE
1	CEN	0.40199E+08	0.11126E+09	0.15497E+09	-0.10161E+08	0.11268E+09	0.38775E+08	-82.02
1	L-I	0.11126E+09	0.40199E+08	0.15497E+09	0.10161E+08	0.11268E+09	0.38775E+08	7.98
1	J-K	0.85891E+08	0.65568E+08	0.15497E+09	-0.35530E+08	0.11268E+09	0.38775E+08	-37.02
1	I-J	0.40199E+08	0.11126E+09	0.15497E+09	-0.10161E+08	0.11268E+09	0.38775E+08	-82.02

ELEMENT (97)

LOAD	LOC	S11	S22	S33	S12	S-MAX	S-MIN	ANGLE
1	CEN	0.21348E+08	0.76250E+08	0.13612E+09	0.72991E+06	0.76259E+08	0.21338E+08	89.24
1	L-I	0.48069E+08	0.49529E+08	0.13612E+09	-0.27451E+08	0.76259E+08	0.21338E+08	-45.76
1	J-K	0.21348E+08	0.76250E+08	0.13612E+09	0.72991E+06	0.76259E+08	0.21338E+08	89.24
1	I-J	0.76250E+08	0.21348E+08	0.13612E+09	-0.72991E+06	0.76259E+08	0.21338E+08	-0.76

ELEMENT (98)

LOAD	LOC	S11	S22	S33	S12	S-MAX	S-MIN	ANGLE
1	CEN	0.54474E+08	0.95313E+08	0.15438E+09	-0.71030E+07	0.96513E+08	0.53274E+08	-80.41
1	L-I	0.95313E+08	0.54474E+08	0.15438E+09	0.71030E+07	0.96513E+08	0.53274E+08	9.59
1	J-K	0.81996E+08	0.67790E+08	0.15438E+09	-0.20419E+08	0.96513E+08	0.53274E+08	-35.41
1	I-J	0.54474E+08	0.95313E+08	0.15438E+09	-0.71030E+07	0.96513E+08	0.53274E+08	-80.41

ELEMENT (99)

LOAD	LOC	S11	S22	S33	S12	S-MAX	S-MIN	ANGLE
1	CEN	0.40563E+08	0.69478E+08	0.14047E+09	0.33125E+06	0.69482E+08	0.40559E+08	89.34
1	L-I	0.54689E+08	0.55352E+08	0.14047E+09	-0.14458E+08	0.69482E+08	0.40559E+08	-45.66
1	J-K	0.40563E+08	0.69478E+08	0.14047E+09	0.33125E+06	0.69482E+08	0.40559E+08	89.34
1	I-J	0.69478E+08	0.40563E+08	0.14047E+09	-0.33125E+06	0.69482E+08	0.40559E+08	-0.66

ELEMENT (100)

LOAD	LOC	S11	S22	S33	S12	S-MAX	S-MIN	ANGLE
1	CEN	0.62164E+08	0.81299E+08	0.15217E+09	-0.46850E+07	0.82385E+08	0.61078E+08	-76.96
1	L-I	0.81299E+08	0.62164E+08	0.15217E+09	0.46850E+07	0.82385E+08	0.61078E+08	13.04
1	J-K	0.76417E+08	0.67046E+08	0.15217E+09	-0.95678E+07	0.82385E+08	0.61078E+08	-31.96
1	I-J	0.62164E+08	0.81299E+08	0.15217E+09	-0.46850E+07	0.82385E+08	0.61078E+08	-76.96

ELEMENT (101)

LOAD	LOC	S11	S22	S33	S12	S-MAX	S-MIN	ANGLE
1	CEN	0.53421E+08	0.65062E+08	0.14343E+09	0.26941E+06	0.65069E+08	0.53414E+08	88.68
1	L-I	0.58972E+08	0.59511E+08	0.14343E+09	-0.58208E+07	0.65069E+08	0.53414E+08	-46.33
1	J-K	0.53421E+08	0.65062E+08	0.14343E+09	0.26941E+06	0.65069E+08	0.53414E+08	88.68
1	I-J	0.65062E+08	0.53421E+08	0.14343E+09	-0.26941E+06	0.65069E+08	0.53414E+08	-1.32

ELEMENT (102)

LOAD	LOC	S11	S22	S33	S12	S-MAX	S-MIN	ANGLE
1	CEN	0.64332E+08	0.71142E+08	0.14938E+09	-0.22808E+07	0.71836E+08	0.63639E+08	-73.09
1	L-I	0.71142E+08	0.64332E+08	0.14938E+09	0.22808E+07	0.71836E+08	0.63639E+08	16.91
1	J-K	0.70018E+08	0.65456E+08	0.14939E+09	-0.34050E+07	0.71836E+08	0.63639E+08	-28.09
1	I-J	0.64332E+08	0.71142E+08	0.14938E+09	-0.22808E+07	0.71836E+08	0.63639E+08	-73.09

ELEMENT (103)

LOAD	LOC	S11	S22	S33	S12	S-MAX	S-MIN	ANGLE
1	CEN	0.59939E+08	0.62984E+08	0.14498E+09	0.20288E+06	0.62998E+08	0.59926E+08	86.21
1	L-I	0.61259E+08	0.61665E+08	0.14498E+09	-0.15224E+07	0.62998E+08	0.59926E+08	-48.80
1	J-K	0.59939E+08	0.62984E+08	0.14498E+09	0.20288E+06	0.62998E+08	0.59926E+08	86.21
1	I-J	0.62984E+08	0.59939E+08	0.14498E+09	-0.20288E+06	0.62998E+08	0.59926E+08	-3.80

ELEMENT (104)

LOAD	LOC	S11	S22	S33	S12	S-MAX	S-MIN	ANGLE
1	CEN	0.64349E+08	0.65470E+08	0.14740E+09	-0.83194E+06	0.65912E+08	0.63906E+08	-61.98
1	L-I	0.65470E+08	0.64349E+08	0.14740E+09	0.83194E+06	0.65912E+08	0.63906E+08	28.02
1	J-K	0.65741E+08	0.64077E+08	0.14740E+09	-0.56022E+06	0.65912E+08	0.63906E+08	-16.98
1	I-J	0.64349E+08	0.65470E+08	0.14740E+09	-0.83194E+06	0.65912E+08	0.63906E+08	-61.98

ELEMENT (105)

LOAD	LOC	S11	S22	S33	S12	S-MAX	S-MIN	ANGLE
1	CEN	0.62653E+08	0.62319E+08	0.14570E+09	0.16688E+06	0.62722E+08	0.62250E+08	22.51
1	L-I	0.62319E+08	0.62653E+08	0.14570E+09	0.16675E+06	0.62722E+08	0.62250E+08	67.51
1	J-K	0.62653E+08	0.62319E+08	0.14570E+09	0.16688E+06	0.62722E+08	0.62250E+08	22.51
1	I-J	0.62319E+08	0.62653E+08	0.14570E+09	-0.16688E+06	0.62722E+08	0.62250E+08	-67.49

B O U N D A R Y E L E M E N T F O R C E S / M O M E N T S

ELEMENT NUMBER	LOAD CASE	FORCE	MOMENT
1	1	0.20643E+08	0.00000E+00
2	1	-0.14106E+06	0.00000E+00
3	1	0.40843E+08	0.00000E+00
4	1	0.62499E+08	0.00000E+00
5	1	0.73016E+08	0.00000E+00
6	1	0.38059E+08	0.00000E+00
7	1	0.32928E+08	0.00000E+00
8	1	0.81997E+08	0.00000E+00
9	1	0.90791E+08	0.00000E+00
10	1	0.26975E+08	0.00000E+00

11	1	0.19259E+08	0.00000E+00
12	1	0.79550E+08	0.00000E+00
13	1	-0.89617E+07	0.00000E+00
14	1	0.86113E+07	0.00000E+00
15	1	-0.32294E+07	0.00000E+00
16	1	-0.11838E+09	0.00000E+00
17	1	-0.13800E+09	0.00000E+00
18	1	-0.10417E+09	0.00000E+00
19	1	-0.61186E+08	0.00000E+00
20	1	-0.12559E+09	0.00000E+00
21	1	-0.92458E+08	0.00000E+00
22	1	-0.17170E+16	0.00000E+00

23	1	-0.17170E+16	0.00000E+00
24	1	-0.17170E+16	0.00000E+00
25	1	-0.17170E+16	0.00000E+00
26	1	-0.17170E+16	0.00000E+00
27	1	-0.17170E+16	0.00000E+00
28	1	-0.17170E+16	0.00000E+00
29	1	-0.17170E+16	0.00000E+00
30	1	-0.17170E+16	0.00000E+00
31	1	-0.17170E+16	0.00000E+00
32	1	-0.17170E+16	0.00000E+00
33	1	-0.17170E+16	0.00000E+00
34	1	-0.60296E+08	0.00000E+00

S T A T I C S O L U T I O N T I M E L O G

EQUATION SOLUTION	=	0.09
DISPLACEMENT OUTPUT	=	0.06
STRESS RECOVERY	=	0.56

O V E R A L L T I M E L O G

NODAL POINT INPUT	=	0.17
ELEMENT STIFFNESS FORMATION	=	0.99
NODAL LOAD INPUT	=	0.02
TOTAL STIFFNESS FORMATION	=	0.28
STATIC ANALYSIS	=	0.70
EIGENVALUE EXTRACTION	=	0.00
FORCED RESPONSE ANALYSIS	=	0.00
RESPONSE SPECTRUM ANALYSIS	=	0.00
STEP-BY-STEP INTEGRATION	=	0.00
TOTAL SOLUTION TIME	=	2.16

Appendix D: Thermal Analogy Program Descriptions, Listings, and Outputs

Three different programs were used to execute the thermal analogy of Section 3.3. The three programs are as follows:

1. Superlam, a proprietary software package which performs plane stress analyses of flat plate and cylindrical composite laminates using Classical Lamination Theory. The assumptions disscussed in connection with CLT in the body of the thesis apply to this program as well. (Osborne, 1986ii)

2. CYLAN, an analysis program for composite cylinders developed at the University of Delaware Research Center for Composites Manufacturing Science and Engineering. The program uses Vlasov-Ambartsumyan shell theory. Some of the assumptions used include constant shell thickness, small displacements and small in-plane strains, negligble transverse shear strains, constant mid-plane radius, transverse normal strains independent of the laminate through-thickness coordinate, and Hookean behavior. (Whitney et al., 1987)

3. ELAS2, a generalized plane strain elasticity solution for cylindrical composite shells. The standard small strain and linear elastic material behavior assumptions apply.

Physical data used in ELAS2 are temperature-independent. (Rousseau et al., 1987)

Pertinent results from the thermal analogy runs using the first two programs are presented in the body of the thesis. Listings of INPUT (a module used to calculate lamina properties for input to ELAS2), ELAS2, the ELAS2 data files, and the ELAS2 outputs for the thermal analogy runs follow.

```
C       PROGRAM INPUT
C
C       THIS INPUT MODULE IS USED TO CALCULATE THE AVERAGED
C       THREE-DIMENSIONAL MECHANICAL PROPERTIES REQUIRED BY THE
C       PROGRAM "ELAS2" WRITTEN BY HYER ET AL.
C
C
C
C
      DOUBLE PRECISION Q(6,6),QB(6,6),QRAN(6,6)
      DOUBLE PRECISION ET(6)
      DOUBLE PRECISION E1,E2,G12,P12,EF,PF,AF,WF,VF,GF
      DOUBLE PRECISION EM,PM,AM,WM,VM,GM
      DOUBLE PRECISION A1,A2,F1,F2
      DOUBLE PRECISION T,TR,C,C2,C4,SI,SI2,SI4,H1,H2,DT
      DOUBLE PRECISION DEN,Z,Z1
      DOUBLE PRECISION DD,SS1,SS2,SS,ERAN,GRAN,NURAN,E3RAN
      DOUBLE PRECISION ERAN2,GRAN2,NURAN2,DD2,DD1,CC,ARAN
      DOUBLE PRECISION N1,N2,N3,NUTRAN,NUR,NURT,KF,KM,KT
C
C
C
C       DESCRIPTION OF VARIABLES AND ARRAYS
C
C       Q - STIFFNESS MATRIX OF A LAMINA (6 BY 6)
C       QB - TRANSFORMED STIFFNESS MATRIX OF A LAMINA (6 BY 6)
C       QRAN - STIFFNESS MATRIX OF A RANDOM 1-2 PLANE LAMINA
C              (6 BY 6)
C       EF - FIBER YOUNG'S MODULUS (PSI OR Pa)
C       PF - FIBER POISSON'S RATIO
C       AF - FIBER COEFFICIENT OF THERMAL EXPANSION
C            (in/in/degree F OR m/m/degree C)
C       WF - FIBER WEIGHT FRACTION IN A PARTICULAR LAMINA
C       VF - FIBER VOLUME FRACTION IN A PARTICULAR LAMINA
C       GF - FIBER SHEAR MODULUS (PSI OF Pa)
C       EM - MATRIX YOUNG'S MODULUS (PSI OR Pa)
C       PM - MATRIX POISSON'S RATIO
C       AM - MATRIX COEFFICIENT OF THERMAL EXPANSION
C            (in/in/degree F OR m/m/degree C)
C       WM - MATRIX WEIGHT FRACTION IN A PARTICULAR LAMINA
C       VM - MATRIX VOLUME FRACTION IN A PARTICULAR LAMINA
C       GM - MATRIX SHEAR MODULUS (PSI OR Pa)
C       E1 - LONGITUDINAL YOUNG'S MODULUS OF A LAMINA
C            (PSI OR Pa)
C       E2 - TRANSVERSE YOUNG'S MODULUS OF A LAMINA
C            (PSI OR Pa)
C       P12 - PRINCIPAL POISSON'S RATIO OF A LAMINA
C       PRAN - 1-2 RANDOM PLANE POISSON'S RATIO OF A LAMINA
C              PRAN=P12=P21
C       G12 - PRINCIPAL SHEAR MODULUS OF A LAMINA (PSI OR Pa)
C       GRAN - 1-2 RANDOM PLANE SHEAR MODULUS OF A LAMINA
C       A1 - LONGITUDINAL COEFFICIENT OF THERMAL EXPANSION OF
C            A LAMINA (in/in/degree F OR m/m/degree C)
C       A2 - TRANSVERSE COEFFICIENT OF THERMAL EXPANSION OF A
C            LAMINA (in/in/degree F OR m/m/degree C)
```

```
C       A3 - THROUGH THE THICKNESS COEFFICIENT OF THERMAL
C            EXPANSION
C       ARAN - 1-2 RANDOM PLANE COEFFICIENT OF THERMAL EXPANSION
C              ARAN=A1=A2
C       T - ANGLE, THETA, OF REINFORCEMENT OF A LAMINA, DEGREES
C       TR - ANGLE, THETA, OF REINFORCEMENT OF A LAMINA, RADIANS
C       C,C2,C4 - COS(T), COS(T)**2, COS(T)**4
C       SI,SI2,SI4 - SIN(T), SIN(T)**2, SIN(T)**4
C       H1,H2 - SMALLER AND LARGER POSITION VALUE OF LAMINA
C               (in OR m)
C       DT - CHANGE IN TEMPERATURE ACROSS THE LAMINATE
C       M - TOTAL NUMBER OF LAMINAE IN LAMINATE
C       K - LAMINA NUMBER
C
C       SUMMARY OF ORIENTED LAMINA SYMBOLS:
C
C           YOUNG'S MODULI: E1,E2,E3
C           SHEAR MODULI: G12,G13,G23
C           POISSON'S RATIOS: P12,P21,P13,P31,P23,P32
C           CTE'S: A1,A2,A3,ET(1),ET(2),ET(3),ET(6)
C           SUB-SYMBOLS: KF,KM,GF,GM,ETA6,ETA4,ETAK,D1,
C                        N1,D2,N2,D3,N3,KT,ZM
C
C       SUMMARY OF RANDOM 1-2 PLANE LAMINA SYMBOLS:
C
C           YOUNG'S MODULI: ERAN,E3RAN,ERAN2
C           SHEAR MODULI: GRAN,GRAN2,G13RAN,G23RAN
C           POISSON'S RATIOS: NURAN,NUTRAN,NURAN2
C           CTE'S: ARAN,ARAN3
C           SUB-SYMBOLS: DD,SS1,SS2,SS,DD2,DD1,CC
C
C
        READ(7,1) M,DT
 1      FORMAT (I2,D10.2)
C
        DO 200 II=1,M
C
C
        READ(7,2) K
 2      FORMAT (I5)
C
C
        DO 4 I=1,6
           DO 3 J=1,6
              Q(I,J)=0
              QB(I,J)=0
              QRAN(I,J)=0
 3         CONTINUE
              ET(I)=0
 4      CONTINUE
C
C
        READ(7,5) H1,H2
```

```
  5      FORMAT (2D10.5)
         READ(7,10) EF,PF,AF,VF
 10      FORMAT (D14.3,D5.3,D11.9,D5.3,D5.3)
         READ(7,20) EM,PM,AM,VM
 20      FORMAT (D14.3,D5.3,D11.9,D5.3,D5.3)
         READ(7,30) T
 30      FORMAT(D10.5)
C
C
         TR=0.017453*T
         C=DCOS(TR)
         C2=C**2
         C4=C2**2
         SI=DSIN(TR)
         SI2=SI**2
         SI4=SI2**2
C
C
         WRITE(8,89)
 89      FORMAT('1','ORIENTED LAMINA PROPERTIES')
C
C        MOST OF THE FORMULAE FOR THE THREE-DIMENSIONAL
C        MECHANICAL PROPERTIES OF UNIDIRECTIONAL LAMINAE
C        COME FROM THE BOOK "The Behavior of Structures
C        Composed of Composite Materials" BY VINSON AND
C        SIERAKOWSKI, pp. 39-40. **THE EXPRESSION FOR
C        POISSON'S RATIO 23 FOR A UNIDIRECTIONAL LAMINA
C        IS TAKEN FROM 'Engineer's Guide to Composite
C        Materials', pp. 3-12 **
C
C
         KF=EF/(2.*(1.-PF))
         KM=EM/(2.*(1.-PM))
         GF=EF/(2.*(1.+PF))
         GM=EM/(2.*(1.+PM))
         ETA6=(1.+(GM/GF))/2.
         ETA4=(3.-4*PM+(GM/GF))/(4.*(1-PM))
         ETAK=(1.+(1.-2.*PF)*(GM/GF))/(2.*(1.-PM))
         E1=(VF*EF)+(EM*VM)
         P12=(PF*VF)+(PM*VM)
         P13=P12
         D1=VF+ETA6*VM
         N1=(1./GF)*VF+(ETA6*(1./GM)*VM)
         G12=D1/N1
         G13=G12
         D2=VF+ETA4*VM
         N2=(1./GF)*VF+(ETA4*(1./GM)*VM)
         G23=D2/N2
         D3=VF+ETAK*VM
         N3=(1./KF)*VF+(ETAK*(1./KM)*VM)
         KT=D3/N3
         ZM=1.+(4.*KT*P12*P12)/E1
         E2=(4.*KT*G23)/(KT+ZM*G23)
         E3=E2
```

```
      P21=P12*E2/E1
      P23=VF*PF+VM*(2*PM-P21)
      P31=P13*E3/E1
      P32=P23*E3/E2
      A1=(AF*EF*VF+AM*EM*VM)/E1
      A2=(1+PF)*AF*VF+(1+PM)*AM*VM-A1*P12
      A3=A2
      ET(1)=C2*A1+SI2*A2
      ET(2)=SI2*A1+C2*A2
      ET(3)=A3
      ET(6)=2*SI*C*A1-2*SI*C*A2
      WRITE(8,31)
31    FORMAT('0',2X,'LAYER',6X,'E1',9X,'E2',9X,'E3',9X,'G12',
     + 9X,'G13',9X,'G23')
      WRITE(8,32) K,E1,E2,E3,G12,G13,G23
32    FORMAT('0',6X,I2,3X,6(D10.5,1X))
      WRITE(8,33)
33    FORMAT('0',4X,'P12',7X,'P21',7X,'P13',7X,'P31',7X,'P23',
     + 7X,'P32',9X,'A1',9X,'A2',9X,'A3')
      WRITE(8,34) P12,P21,P13,P31,P23,P32,A1,A2,A3
34    FORMAT('0',2X,6(D9.4,1X),3(D10.5,1X))
C
      WRITE(8,90)
90    FORMAT('4','RANDOM LAMINA PROPERTIES')
C
C     THE MICROMECHANICAL EQUATIONS FOR THE MECHANICAL
C     PROPERTIES OF A RANDON 1-2 PLANE LAMINA COME FROM
C     HULL (1981), PAGES 79-100 EXCEPT FOR THE FORMULA FOR
C     POISSON'S RATIO 23 WHICH IS AN ADAPTATION OF THE
C     FORMULA GIVEN BY CHAMIS (SEE ABOVE).
C
      DD=1-(P12*P21)
      SS1=E1+E2+(2*P12*E2)
      SS2=E1+E2-(2*P12*E2)
      SS=E1+E2
      ERAN=(SS1/DD)*((SS2+4*DD*G12)/(2*SS+SS1+4*DD*G12))
      GRAN=(SS2/(8*DD))+G12/2.
      NURAN=(ERAN/(2*GRAN))-1.
      NUTRAN=VF*PF+VM*(2*PM-NURAN)
      E3RAN=1./(VF/EF+(VM/EM))
      ERAN2=0.375*E1+0.625*E2
      ERAN3=0.375*EF*VF+0.625*EM*VM
      GRAN2=(E1/8.)+(E2/4.)
      NURAN2=(ERAN2/(2*GRAN2))-1.
      DD2=0.5*(E1-E2)*(A1-A2)
      DD1=E1+(1+2*P12)*E2
      CC=DD2/DD1
      ARAN=0.5*(A1+A2)+CC
      ARAN3=A3
      WRITE(8,35)
35    FORMAT('0',2X,'LAYER',7X,'ERAN',6X,'E3RAN',
     + 6X,'GRAN',6X,'G13RAN',6X,'G23RAN')
      G13RAN=0.5*(G23+G13)
      G23RAN=G13RAN
```

```
      WRITE(8,36)  K,ERAN,E3RAN,GRAN,G13RAN,G23RAN
36    FORMAT('0',6X,I2,3X,5(D10.5,1X))
      WRITE(8,37)
37    FORMAT('0',4X,'PRAN',7X,'P23RAN',7X,
     + 'ARAN',7X,'ARAN3')
      WRITE(8,38)  NURAN,NUTRAN,ARAN,ARAN3
38    FORMAT('0',2X,4(D10.5,1X))
      WRITE(8,39)
39    FORMAT('0',4X,'ERAN2',7X,'GRAN2',8X,'NURAN2',8X,'ERAN3')
      WRITE(8,40)  ERAN2,GRAN2,NURAN2,ERAN3
40    FORMAT('0',1X,2(D10.5,3X),D12.6,3X,D10.5)
C
C
C
      DEN=1.-P12*P21-P23*P32-P31*P13-2*P21*P32*P13
      Q(1,1)=E1*(1.-P23*P32)/DEN
      Q(1,2)=E1*(P21+P31*P23)/DEN
      Q(1,3)=E1*(P31+P21*P32)/DEN
      Q(2,1)=Q(1,2)
      Q(2,2)=E2*(1.-P31*P13)/DEN
      Q(2,3)=E2*(P32+P12*P31)/DEN
      Q(3,1)=Q(1,3)
      Q(3,2)=Q(2,3)
      Q(3,3)=E3*(1.-P12*P21)/DEN
      Q(4,4)=G23
      Q(5,5)=G13
      Q(6,6)=G12
C
      ER=E3RAN/ERAN
      NUR=NURAN*NURAN
      NURT=NUTRAN*NUTRAN
      DENR=1.-NUR-2*NURT-2*NURAN*NURT*ER
      QRAN(1,1)=ERAN*(1.-NURT*ER)/DENR
      QRAN(1,2)=ERAN*(NURAN+NURT*ER)/DENR
      QRAN(1,3)=ERAN*(NUTRAN*ER+NURAN*NUTRAN*ER)/DENR
      QRAN(2,1)=QRAN(1,2)
      QRAN(2,2)=ERAN*(1.-NURT*ER)/DENR
      QRAN(2,3)=ERAN*(NUTRAN*ER+NURAN*NUTRAN*ER)/DENR
      QRAN(3,1)=QRAN(1,3)
      QRAN(3,2)=QRAN(2,3)
      QRAN(3,3)=E3*(1.-NURAN**2)/DENR
      QRAN(4,4)=0.5*(G23+G13)
      QRAN(5,5)=QRAN(4,4)
      QRAN(6,6)=GRAN
C
      QB(1,1)=Q(1,1)*C4+2*(Q(1,2)+2*Q(6,6))*C2*SI2+Q(2,2)*SI4
      QB(1,2)=(Q(1,1)+Q(2,2)-4*Q(6,6))*C2*SI2+Q(1,2)*(C4+SI4)
      QB(1,3)=Q(1,3)*C2+Q(2,3)*SI2
      ZZ=SI*C*(C2-SI2)*(Q(1,2)+2*Q(6,6))
      QB(1,6)=-C*SI2*SI*Q(2,2)+C2*C*SI*Q(1,1)-ZZ
      QB(2,2)=Q(1,1)*SI4+2*(Q(1,2)+2*Q(6,6))*SI2*C2+Q(2,2)*C4
      QB(2,3)=SI2*Q(1,3)+C2*Q(2,3)
      QB(3,3)=Q(3,3)
      QB(2,1)=QB(1,2)
```

```
            QB(3,1)=QB(1,3)
            QB(6,1)=QB(1,6)
            QB(3,2)=QB(2,3)
            QB(2,6)=-C*C2*SI*Q(2,2)+C*SI2*SI*Q(1,1)+ZZ
            QB(6,2)=QB(2,6)
            QB(3,6)=(Q(1,3)-Q(2,3))*C*SI
            QB(6,3)=QB(3,6)
            QB(4,4)=Q(4,4)*C2+Q(5,5)*SI2
            QB(4,5)=(Q(5,5)-Q(4,4))*C*SI
            QB(5,4)=QB(4,5)
            QB(5,5)=Q(5,5)*C2+Q(4,4)*SI2
            ZZZ=(C2-SI2)*(C2-SI2)
            QB(6,6)=(Q(1,1)+Q(2,2)-2*Q(1,2))*C2*SI2+Q(6,6)*ZZZ
C
C
            WRITE(8,45) K,T
45          FORMAT('1','LAYER NUMBER ',I2,3X,'AT ANGLE ',D12.6)
            WRITE(8,46)
46          FORMAT('0',1X,' I ',' J ',6X,'Q(PSI)',14X,'QBAR(PSI)',
           + 11X,'QRAN(PSI)')
            DO 60 I=1,6
                DO 50 J=1,6
                   WRITE(8,70) I,J,Q(I,J),QB(I,J),QRAN(I,J)
50              CONTINUE
60          CONTINUE
C
C
70          FORMAT ('0',2I3,3D20.10)
C
C
200     CONTINUE
C
C           ENDFILE (UNIT=8)
C
            STOP
            END
```

```
      PROGRAM ELAS2
C     ELASTICITY SOLUTION FOR AN ANGLE-PLY TUBE W/THERMAL
C     AND MECHANICAL LOADS
C
C     CARL ROUSSEAU AND DR. MIKE HYER
C     ESM DEPT.
C     VIRGINIA TECH
C
      IMPLICIT REAL*8 (A-H), REAL*8 (M-Z)
      COMMON /IN/ANGLE(15),T(15),CB11(15),CB12(15),CB13(15),
     +       CB16(15),CB22(15),CB23(15),CB26(15),CB33(15),CB36(15),
     +       CB66(15),RO(15),RI(15),ALPAX(15),ALPAO(15),ALPAR(15),
     +       ALPAXO(15),DT,P,TW,J,JMAT
      COMMON /SOLN/BC(32,32),ET(32,1),V(15),V1(15),V2(15),V3(15),
     +       V4(15),Z1(15),Z2(15),Z3(15),Z4(15),Z5(15),Z6(15),Z7(15)
      COMMON /OUT/R(150),EPSX(10,15),EPSO(10,15),EPSR(10,15),
     +       GAMXO(10,15),SIGX(10,15),SIGO(10,15),SIGR(10,15),
     +       TAUXO(10,15),EPS1(10,15),EPS2(10,15),EPS3(10,15),
     +       GAM12(10,15),SIG1(10,15),SIG2(10,15),SIG3(10,15),
     +       TAU12(10,15),RR(10,15)
      DIMENSION SIGB(15),ZZ(15)
      PI=3.1415927
C
C
      CALL INPUT
C
C
      DO 10 I=1,J
C
        SIGB(I)=((CB23(I) - CB22(I))*ALPAO(I) + (CB33(I) -
     +      CB23(I))*ALPAR(I) + (CB13(I) - CB12(I))*ALPAX(I) +
     +      (CB36(I) - CB26(I))*ALPAXO(I)) * DT
        V(I)=DSQRT(CB22(I)/CB33(I))
        V1(I)=1. + V(I)
        V2(I)=1. - V(I)
        V3(I)=2. + V(I)
        V4(I)=2. - V(I)
        ZZ(I)=CB33(I) - CB22(I)
        Z1(I)=(CB12(I) - CB13(I)) / ZZ(I)
        Z2(I)=(CB26(I) - 2*CB36(I)) / (3*CB33(I)+ZZ(I))
        Z3(I)=SIGB(I) / ZZ(I)
        Z4(I)=CB12(I) + CB13(I)
        Z5(I)=CB26(I) + CB36(I)
        Z6(I)=CB23(I) + CB33(I)
10      Z7(I)=CB22(I) + CB23(I)
C
C
      BC(1,1)=CB13(1) + Z6(1)*Z1(1)
      BC(1,2)=((Z6(1) + CB33(1))*Z2(1) + CB36(1))*RI(1)
      BC(1,3)=(CB23(1) + V(1)*CB33(1)) * RI(1)**(-V2(1))
      BC(1,4)=(CB23(1) - V(1)*CB33(1)) * RI(1)**(-V1(1))
      ET(1,1)=(CB13(1)*ALPAX(1) + CB23(1)*ALPAO(1) + CB33(1)*
     +    ALPAR(1) + CB36(1)*ALPAXO(1))*DT -Z6(1)*Z3(1)
C
```

```
C
      DO 12 I1=5,2*J+2
C
        BC(1,I1) = 0.
        BC(2,1) = CB13(J) + Z6(J)*Z1(J)
        BC(2,2) = ((Z6(J) + CB33(J))*Z2(J) + CB36(J))*RO(J)
12    BC(2,(I1-2)) = 0.
      BC(2,(2*J+1)) = (CB23(J) + V(J)*CB33(J)) * RO(J)**(-V2(J))
      BC(2,(2*J+2)) = (CB23(J) - V(J)*CB33(J)) * RO(J)**(-V1(J))
      ET(2,1) = (CB13(J)*ALPAX(J) + CB23(J)*ALPAO(J) + CB33(J)*
     +    ALPAR(J) + CB36(J)*ALPAXO(J))*DT - Z6(J)*Z3(J)
      BC(3,1) = 0.
      BC(3,2) = 0.
      BC(4,1) = 0.
      BC(4,2) = 0.
      ET(3,1) = P/ 2/ PI
      ET(4,1) = TW/ 2/ PI
C
C
      DO 30 I=1,J
C
        BC(3,1) = BC(3,1) + (CB11(I) + Z1(I)*Z4(I)) * (RO(I)**2 -
     +      RI(I)**2) /2.
        BC(3,2) = BC(3,2) + ((CB13(I) + Z4(I))* Z2(I) +CB16(I))*
     +      (RO(I)**3 - RI(I)**3) / 3.
        BC(3,(1+2*I)) = (CB12(I) + V(I)*CB13(I)) * (RO(I)**V1(I) -
     +      RI(I)**V1(I)) / V1(I)
        BC(3,(2+2*I)) = (CB12(I) - V(I)*CB13(I)) * (RO(I)**V2(I) -
     +      RI(I)**V2(I)) / V2(I)
        ET(3,1) = ET(3,1) + (DT*(CB11(I)*ALPAX(I) + CB12(I)*
     +      ALPAO(I) + CB13(I)*ALPAR(I) + CB16(I)*ALPAXO(I)) -
     +      Z3(I)*Z4(I))*(RO(I)**2 - RI(I)**2) / 2.
        BC(4,1) = BC(4,1) + (CB16(I) + Z1(I)*Z5(I)) * (RO(I)**3 -
     +      RI(I)**3) / 3.
        BC(4,2) = BC(4,2) + (CB66(I) + Z2(I)* (Z5(I) + CB36(I)))*
     +      (RO(I)**4 - RI(I)**4) / 4.
        BC(4,(1+2*I)) = (CB26(I) + V(I) * CB36(I)) * (RO(I)**V3(I)
     +      - RI(I)**V3(I)) / V3(I)
        BC(4,(2+2*I)) = (CB26(I) - V(I) * CB36(I)) * (RO(I)**V4(I)
     +      - RI(I)**V4(I)) / V4(I)
30    ET(4,1) = ET(4,1) + (DT*(CB16(I)*ALPAX(I) + CB26(I)*
     +      ALPAO(I) + CB36(I)*ALPAR(I) + CB66(I)*ALPAXO(I)) -
     +      Z3(I)*Z5(I)) * (RO(I)**3 - RI(I)**3) / 3.
C
C
      DO 34 KK=5,2*J+2
      DO 34 LL=1,2*J+2
34    BC(KK,LL) = 0.
C
C
      DO 40 K=1,J-1
C
        BC((4+K),1) = (Z1(K) - Z1(K+1)) * RO(K)
        BC((4+K),2) = (Z2(K) - Z2(K+1)) * RO(K)**2
```

```
      BC((4+K),(1+2*K)) = RO(K)**V(K)
      BC((4+K),(2+2*K)) = RO(K)**(-V(K))
      BC((4+K),(3+2*K)) = -RO(K)**V(K+1)
      BC((4+K),(4+2*K)) = -RO(K)**(-V(K+1))
      ET((4+K),1) = (Z3(K+1) - Z3(K)) * RO(K)
      BC((3+J+K),1) = CB13(K) + Z6(K) * Z1(K) - CB13(K+1) -
     +     Z6(K+1) * Z1(K+1)
      BC((3+J+K),2) = ((Z6(K) + CB33(K)) * Z2(K) + CB36(K) -
     +     (Z6(K+1) + CB33(K+1)) * Z2(K+1) - CB36(K+1)) * RO(K)
      BC((3+J+K),(1+2*K)) = (CB23(K) + V(K)*CB33(K)) *
     +     RO(K)**(-V2(K))
      BC((3+J+K),(2+2*K)) = (CB23(K) - V(K)*CB33(K)) *
     +     RO(K)**(-V1(K))
      BC((3+J+K),(3+2*K)) = -(CB23(K+1) + V(K+1) * CB33(K+1)) *
     +     RO(K)**(-V2(K+1))
      BC((3+J+K),(4+2*K)) = -(CB23(K+1) - V(K+1) * CB33(K+1)) *
     +     RO(K)**(-V1(K+1))
40    ET((3+J+K),1) = DT * (CB13(K) * ALPAX(K) - CB13(K+1) *
     +     ALPAX(K+1) + CB23(K) * ALPAO(K) - CB23(K+1) * ALPAO(K+1)
     +     + CB33(K) * ALPAR(K) - CB33(K+1) * ALPAR(K+1) +
     +     CB36(K) * ALPAXO(K) - CB36(K+1) * ALPAXO(K+1)) -
     +     Z6(K) * Z3(K) + Z6(K+1) * Z3(K+1)
C
C
      WRITE(6,19)
19    FORMAT('PLY      LAMBDA'/)
C
C
      DO 52 I=1,J
        WRITE(6,20) I,V(I)
52    CONTINUE
20    FORMAT(I2,D16.8)
C
C
      WRITE(6,22)
22    FORMAT(//'BC(I,J)     EPS-O     GAM-O     A(1 THRU 2J)'/)
C
C
      DO 35 K9 = 1,2*J+2
        WRITE(6,45) (BC(K9,L9),L9=1,(2*J+2))
35    CONTINUE
45    FORMAT(6D16.8)
C
C
      WRITE(6,32)
32    FORMAT(//'ET(I,1)'/)
      WRITE(6,42) (ET(K8,1),K8=1,(2*J+2))
42    FORMAT(D16.8)
C
C
C     SOLVE BC*X=ET USING GASJON (REDDY)
C
C
      CALL GASJON (2*J+2,BC,32,ET,32)
```

```
C
      CALL OUTPUT
C
      CALL RESLTN
C
C
C     **SUBROUTINE FAIL ONLY WORKS FOR LAMINATES OF ONE MATERIAL
C
C     READ FLAG   0=NO FAILURE CRITERION; 1=TSAI-WU
C     INPUT FI AND FIJ
C
C
          READ(5,*) FL
          PRINT*, FL
          IF(FL.EQ.0) GOTO 101
          CALL FAIL (FL,J)
101       CONTINUE
C
C
      STOP
      END
C
C
C
      SUBROUTINE INPUT
C
C
      IMPLICIT REAL*8 (A-H), REAL*8 (M-Z)
      COMMON /IN/ANGLE(15),T(15),CB11(15),CB12(15),CB13(15),
     +          CB16(15),CB22(15),CB23(15),CB26(15),CB33(15),
     +          CB36(15),CB66(15),RO(15),RI(15),ALPAX(15),ALPAO(15),
     +          ALPAR(15),ALPAXO(15),DT,P,TW,J,JMAT
      DIMENSION E1(15),E2(15),E3(15),G12(15),NU23(15),NU32(15),
     +          NU13(15),NU31(15),NU12(15),NU21(15),ALPA1(15),
     +          ALPA2(15),ALPA3(15),C11(15),C12(15),C13(15),C22(15),
     +          C23(15),C33(15),C66(15),B11(15),B12(15),B13(15),
     +          B22(15),B23(15),B33(15),B66(15),
     +          THETA(15),ALFA1(15),ALFA2(15),ALFA3(15),KMAT(15)
      PI=3.14159265
C
C     MATERIAL PROPERTIES
C
      READ(5,*) J,JMAT,RI(1),DT,P,TW
      WRITE(6,15)
15    FORMAT(////'MATERIAL PROPERTIES'//'MATL',6X,'E1',10X,
     +     'E2',10X,'E3',10X,'G12',5X,'NU23',4X,'NU13',4X,'NU12',
     +     4X,'ALPHA 1',5X,'ALPHA 2',5X,'ALPHA 3'/)
30    FORMAT(I3,4D12.4,3F8.4,3D12.4)
      DO 20 I=1,JMAT
         READ(5,*) E1(I),E2(I),E3(I),G12(I),NU23(I),NU13(I),NU12(I),
     +        ALPA1(I),ALPA2(I),ALPA3(I)
         WRITE(6,30) I,E1(I),E2(I),E3(I),G12(I),NU23(I),NU13(I),
     +        NU12(I),ALPA1(I),ALPA2(I),ALPA3(I)
C
```

```
      NU32(I) = NU23(I) * E3(I)/E2(I)
      NU31(I) = NU13(I) * E3(I)/E1(I)
      NU21(I) = NU12(I) * E2(I)/E1(I)
      Z1 = (1. - NU23(I)*NU32(I) - NU13(I)*NU31(I) -
     +     NU12(I)*NU21(I) - 2*NU32(I)*NU13(I)*NU21(I))/
     +     (E1(I)*E2(I)*E3(I))
      C11(I) = (1. - NU23(I)*NU32(I)) / (E2(I)*E3(I)*Z1)
      C12(I) = (NU12(I) + NU32(I)*NU13(I)) / (E1(I)*E3(I)*Z1)
      C13(I) = (NU13(I) + NU12(I)*NU23(I)) / (E1(I)*E2(I)*Z1)
      C22(I) = (1. - NU13(I)*NU31(I)) / (E1(I)*E3(I)*Z1)
      C23(I) = (NU23(I)+ NU21(I)*NU13(I)) / (E1(I)*E2(I)*Z1)
      C33(I) = (1. - NU12(I)*NU21(I)) / (E1(I)*E2(I)*Z1)
20    C66(I) = G12(I)
C
      DO 22 K=1,JMAT
      WRITE(6,23) K,C11(K),C12(K),C13(K),C22(K),C23(K),C33(K),
     +     C66(K)
22    CONTINUE
23    FORMAT(/'C MATRIX FOR MATL',I2//3D16.8/16X,2D16.8/32X,D16.8/
     +  48X,D16.8/)
C
      WRITE(6,25)
25    FORMAT('LAYER PROPERTIES'//'PLY MATL PHI THICKNESS   RI',6X,
     +  'RO'/)
C
      DO 21 I=1,J
      READ(5,*) KMAT(I),T(I),ANGLE(I)
      PRINT*, KMAT(I),T(I),ANGLE(I)
      IF(I.EQ.1) GOTO 40
      RI(I) = RO(I-1)
40    RO(I) = RI(I) + T(I)
      B11(I) = C11(KMAT(I))
      B12(I) = C12(KMAT(I))
      B13(I) = C13(KMAT(I))
      B22(I) = C22(KMAT(I))
      B23(I) = C23(KMAT(I))
      B33(I) = C33(KMAT(I))
      B66(I) = C66(KMAT(I))
      ALFA1(I) = ALPA1(KMAT(I))
      ALFA2(I) = ALPA2(KMAT(I))
      ALFA3(I) = ALPA3(KMAT(I))
      THETA(I) = ANGLE(I) * PI / 180.
      TAYTA = THETA(I)
      M = DCOS(TAYTA)
      N = DSIN(TAYTA)
      Z2 = B12(I)+ 2*B66(I)
      CB11(I) = B11(I)*M**4 + 2*M**2*N**2*Z2 + B22(I)*N**4
      CB12(I) = (B11(I) + B22(I) - 4*B66(I))*M**2*N**2 +
     +     (N**4 + M**4) * B12(I)
      CB13(I) = M**2*B13(I) + N**2*B23(I)
      CB22(I) = B11(I)*N**4 + 2*M**2*N**2*Z2 + B22(I)*M**4
      CB23(I) = B13(I)*N**2 + B23(I)*M**2
      CB33(I) = B33(I)
      CB16(I) = ((B11(I) - Z2)*M**2 + (Z2 - B22(I))*N**2)*M*N
```

```
            CB26(I) = ((B11(I) - Z2)*N**2 + (Z2 - B22(I))*M**2)*M*N
            CB36(I) = (B13(I) - B23(I))*M*N
            CB66(I) = M**2*N**2*(B11(I) - 2*B12(I) + B22(I)) +
     +          B66(I)*(M*M-N*N)**2
            ALPAX(I) = ALFA1(I)*M**2 + ALFA2(I)*N**2
            ALPAO(I) = ALFA1(I)*N**2 + ALFA2(I)*M**2
            ALPAR(I) = ALFA3(I)
            ALPAXO(I) = 2*N*M*(ALFA1(I) - ALFA2(I))
            WRITE(6,45) I,KMAT(I),ANGLE(I),T(I),RI(I),RO(I)
21      CONTINUE
45      FORMAT(I2,I5,F7.0,2X,3F8.5)
         WRITE(6,46)
46      FORMAT(//'PLY',26X,'CBAR  MATRIX'//)
C
         DO 32 I=1,J
            WRITE(6,50) I,CB11(I),CB12(I),CB13(I),CB16(I),CB22(I),
     +          CB23(I),CB26(I),CB33(I),CB36(I),CB66(I)
32      CONTINUE
50      FORMAT(I2,3X,4D16.8/21X,3D16.8/37X,2D16.8/53X,D16.8/)
         WRITE(6,52)
52      FORMAT(/'PLY',5X,'ALPHA-X',7X,'ALPHA-THETA',7X,'ALPHA-R',
     +      5X,'ALPHA-X,THETA'/)
C
         DO 33 I=1,J
            WRITE(6,51) I,ALPAX(I),ALPAO(I),ALPAR(I),ALPAXO(I)
33      CONTINUE
51      FORMAT(I2,4D16.8)
         WRITE(6,60) DT,P,TW
60      FORMAT(/'DELTA-TEMPERATURE LOAD =',D16.8,' F'//'AXIAL '
     +      ,'LOAD=',D16.8,' LB'//'TORSION =',D16.8,' IN-LB'/)
C
         RETURN
         END
C
C
C
         SUBROUTINE OUTPUT
C
         IMPLICIT REAL*8 (A-H), REAL*8 (M-Z)
         COMMON /IN/ ANGLE(15),T(15),CB11(15),CB12(15),CB13(15),
     +      CB16(15),CB22(15),CB23(15),CB26(15),CB33(15),CB36(15),
     +      CB66(15),RO(15),RI(15),ALPAX(15),ALPAO(15),ALPAR(15),
     +      ALPAXO(15),DT,P,TW,J
         COMMON /SOLN/ BC(32,32),ET(32,1),V(15),V1(15),V2(15),
     +      V3(15),V4(15),Z1(15),Z2(15),Z3(15),Z4(15),Z5(15),
     +      Z6(15),Z7(15)
         COMMON /OUT/ R(150),EPSX(10,15),EPSO(10,15),EPSR(10,15),
     +      GAMXO(10,15),SIGX(10,15),SIGO(10,15),SIGR(10,15),
     +      TAUXO(10,15),EPS1(10,15),EPS2(10,15),EPS3(10,15),
     +      GAM12(10,15),SIG1(10,15),SIG2(10,15),SIG3(10,15),
     +      TAU12(10,15),RR(10,15)
         DIMENSION EMX(10,15),EMO(10,15),EMR(10,15),EMXO(10,15)
         PI=3.14159265
         WRITE(6,10) (ET(I1,1),I1=1,(2*J+2))
```

```
10      FORMAT(//'ELASTICITY CONSTANTS'//
     +     'EPSILON-O = ',D14.8,//'GAMMA-O = ',D14.8//
     +     7X,'A1',16X,'A2'/8(2D16.8/))
        DO 20 L=1,J
           TAYTA = ANGLE(L) * PI /180.
           M = DCOS(TAYTA)
           N = DSIN(TAYTA)
           T9 = T(L)/9
        DO 20 K=1,10
           R(K) = RI(L) + (K-1)*T9
           EPSX(K,L) = ET(1,1)
           EPSO(K,L) = Z1(L)*ET(1,1) + Z2(L)*ET(2,1)*R(K) + Z3(L) +
     +          ET((1+2*L),1)*R(K)**(-V2(L)) + ET((2+2*L),1)*
     +          R(K)**(-V1(L))
           EPSR(K,L) = Z1(L)*ET(1,1) + 2*Z2(L)*ET(2,1)*R(K) +
     +          Z3(L) + ET((1+2*L),1)*V(L)*R(K)**(-V2(L)) -
     +          ET((2+2*L),1)*V(L)*R(K)**(-V1(L))
           GAMXO(K,L) = ET(2,1)*R(K)
           EA1 = ET(1,1) - ALPAX(L)*DT
           EA2 = EPSO(K,L) - ALPAO(L)*DT
           EA3 = EPSR(K,L) - ALPAR(L)*DT
           EA4 = GAMXO(K,L) - ALPAXO(L)*DT
           EMX(K,L) = EA1
           EMO(K,L) = EA2
           EMR(K,L) = EA3
           EMXO(K,L) = EA4
           SIGX(K,L) = CB11(L)*EA1+CB12(L)*EA2+CB13(L)*EA3+CB16(L)*EA4
           SIGO(K,L) = CB12(L)*EA1+CB22(L)*EA2+CB23(L)*EA3+CB26(L)*EA4
           SIGR(K,L) = CB13(L)*EA1+CB23(L)*EA2+CB33(L)*EA3+CB36(L)*EA4
           TAUXO(K,L)= CB16(L)*EA1+CB26(L)*EA2+CB36(L)*EA3+CB66(L)*EA4
           EPS1(K,L) = EPSX(K,L)*M*M + EPSO(K,L)*N*N + GAMXO(K,L)*M*N
           EPS2(K,L) = EPSX(K,L)*N*N + EPSO(K,L)*M*M - GAMXO(K,L)*M*N
           EPS3(K,L) = EPSR(K,L)
           GAM12(K,L)= -EPSX(K,L)*2*M*N + EPSO(K,L)*2*M*N + GAMXO(K,L)
     +          *(M*M - N*N)
           SIG1(K,L) = SIGX(K,L)*M*M + SIGO(K,L)*N*N + TAUXO(K,L)
     +          *2*M*N
           SIG2(K,L) = SIGX(K,L)*N*N + SIGO(K,L)*M*M - TAUXO(K,L)
     +          *2*M*N
           SIG3(K,L) = SIGR(K,L)
           TAU12(K,L)= -SIGX(K,L)*M*N + SIGO(K,L)*M*N + TAUXO(K,L)
     +          *(M*M - N*N)
20      CONTINUE
        WRITE(6,30)
30      FORMAT(//'TOTAL STRAINS IN X-Y SYSTEM...LAYER...PHI...R/R...'
     +       ,'EPS-X...EPS-THETA...EPS-R...GAMMA-X,THETA'//)
50      FORMAT(I2,F5.0,F8.5,4D16.8)
C
        DO 40 L=1,J
        DO 40 K=1,10
           R(K) = RI(L) + (K-1)*T(L)/9
           RR(K,L) = (R(K)-RI(1))/(RO(J)-RI(1))
           WRITE(6,50) L,ANGLE(L),RR(K,L),EPSX(K,L),EPSO(K,L),
     +          EPSR(K,L),GAMXO(K,L)
```

```
 40     CONTINUE
         WRITE(6,31)
 31     FORMAT(//'MECHANICAL STRAINS IN X-Y SYSTEM...LAYER...PHI...'
        +     ,'R/R...EPS-X...EPS-THETA...EPS-R...GAMMA-X,THETA'//)
         DO 41 L=1,J
         DO 41 K=1,10
            R(K) = RI(L) + (K-1)*T(L)/9
            RR(K,L) = (R(K)-RI(1))/(RO(J)-RI(1))
            WRITE(6,50) L,ANGLE(L),RR(K,L),EMX(K,L),EMO(K,L),EMR(K,L),
        +        EMXO(K,L)
 41     CONTINUE
         WRITE(6,60)
 60     FORMAT(//'STRESSES IN X-Y SYSTEM...LAYER...PHI...R/R...',
        +      'SIG-X...SIG-THETA...SIG-R...TAU-X,THETA'//)
         DO 70 L=1,J
         DO 70 K=1,10
            WRITE(6,50) L,ANGLE(L),RR(K,L),SIGX(K,L),SIGO(K,L),
        +        SIGR(K,L),TAUXO(K,L)
 70     CONTINUE
         WRITE(6,90)
 90     FORMAT(//'TOTAL STRAINS IN 1-2 SYSTEM...LAYER...PHI...R/R',
        +      'EPS-1...EPS-2...EPS-3...GAMMA-1,2'//)
         DO 100 L=1,J
         DO 100 K=1,10
         WRITE(6,50) L,ANGLE(L),RR(K,L),EPS1(K,L),EPS2(K,L),EPS3(K,L),
        +     GAM12(K,L)
100     CONTINUE
         WRITE(6,120)
120     FORMAT(//'STRESSES IN 1-2 SYSTEM...LAYER...PHI...R/R...',
        +      'SIG-1...SIG-2...SIG-3...TAU-1,2'//)
         DO 130 L=1,J
         DO 130 K=1,10
            WRITE(6,50) L,ANGLE(L),RR(K,L),SIG1(K,L),SIG2(K,L),
        +        SIG3(K,L),TAU12(K,L)
130     CONTINUE
C
C
         RETURN
         END
C
C
C
         SUBROUTINE GASJON(N,A,NRMAX,B,NBMAX)
C
         IMPLICIT REAL*8(A-H), REAL*8 (O-Z)
         DIMENSION A(NRMAX,NRMAX),B(NBMAX,1),INDEX(32,2),IPVOT(32)
C
         M=1
         MM=1
1        DET=1.
         DO 2 J=1,N
2           IPVOT(J)=0.
         DO 14 I=1,N
            T=0.
```

```
      DO 5 J=1,N
         IF(IPVOT(J).EQ.1) GOTO 5
      DO 4 K=1,N
         IF(IPVOT(K)-1)3,4,17
3        IF(DABS(T).GE.DABS(A(J,K))) GOTO 4
         IROW=J
         ICOL=K
         T=A(J,K)
4     CONTINUE
5     CONTINUE
      IPVOT(ICOL) = IPVOT(ICOL) + 1
      IF(IROW.EQ.ICOL) GOTO 8
      DET = -DET
      DO 6 L=1,N
         T = A(IROW,L)
         A(IROW,L) = A(ICOL,L)
6        A(ICOL,L) = T
      IF(MM.LE.0) GOTO 8
      DO 7 L=1,M
         T = B(IROW,L)
         B(IROW,L) = B(ICOL,L)
7     B(ICOL,L) = T
8     INDEX(I,1) = IROW
      INDEX(I,2) = ICOL
      PIVOT = A(ICOL,ICOL)
      DET = DET*PIVOT
      A(ICOL,ICOL) = 1.
      DO 9 L=1,N
9     A(ICOL,L) = A(ICOL,L)/PIVOT
      IF(MM.LE.0) GOTO 11
      DO 10 L=1,M
10       B(ICOL,L) = B(ICOL,L)/PIVOT
11    DO 14 LI=1,N
         IF(LI.EQ.ICOL) GOTO 14
         T=A(LI,ICOL)
         A(LI,ICOL) = 0.
      DO 12 L=1,N
12       A(LI,L) = A(LI,L) - A(ICOL,L)*T
         IF(MM.LE.0) GOTO 14
      DO 13 L=1,M
13       B(LI,L) = B(LI,L) - B(ICOL,L)*T
14    CONTINUE
      IF(MM.EQ.1) RETURN
      DO 16 I=1,N
         L = N-I+1
         IF(INDEX(L,1).EQ.INDEX(L,2)) GOTO 16
         JROW=INDEX(L,1)
         JCOL=INDEX(L,2)
      DO 15 K=1,N
         T = A(K,JROW)
         A(K,JROW) = A(K,JCOL)
         A(K,JCOL) = T
15    CONTINUE
16    CONTINUE
```

```
 17      RETURN
 C
         END
 C
 C
 C
         SUBROUTINE FAIL(FL,J)
 C
         IMPLICIT REAL*8 (A-H), REAL*8 (M-Z)
         COMMON /OUT/ R(150),EPSX(10,15),EPSO(10,15),EPSR(10,15),
        +     GAMXO(10,15),SIGX(10,15),SIGO(10,15),SIGR(10,15),
        +     TAUXO(10,15),EPS1(10,15),EPS2(10,15),EPS3(10,15),
        +     GAM12(10,15),SIG1(10,15),SIG2(10,15),SIG3(10,15),
        +     TAU12(10,15),RR(10,15)
         DIMENSION TS(15),F1S1(15),F2S2(15),F2S3(15),F11S1(15),
        +     F22S2(15),F22S3(15),F66S6(15),F12S12(15),F12S13(15),
        +     F23S23(15)
 C
         READ(5,*) F1,F2,F11,F22,F66,F12,F23
         WRITE(6,45)
 45      FORMAT(//'TSAI-WU'//)
 30      DO 40 I=1,J
             F1S1(I) = F1 * SIG1(5,I)
             F2S2(I) = F2 * SIG2(5,I)
             F2S3(I) = F2 * SIG3(5,I)
             F11S1(I) = F11 * SIG1(5,I)**2
             F22S2(I) = F22 * SIG2(5,I)**2
             F22S3(I) = F22 * SIG3(5,I)**2
             F66S6(I) = F66 * TAU12(5,I)**2
             F12S12(I) = F12 * SIG1(5,I)*SIG2(5,I)
             F12S13(I) = F12 * SIG1(5,I)*SIG3(5,I)
             F23S23(I) = F23 * SIG2(5,I)*SIG3(5,I)
 40          TS(I) = F1S1(I) + F2S2(I) +F2S3(I) + F11S1(I) +
        +          F22S2(I) + F22S3(I) + F66S6(I) + F12S12(I) +
        +          F12S13(I) + F23S23(I)
             WRITE(6,50) F1,F2,F11,F22,F66,F12,F23
 50          FORMAT(7X,'F1',14X,'F2',13X,'F11',13X,'F22',13X,
        +          'F12',13X,'F23'/7D16.8)
             WRITE(6,65)
 65          FORMAT(//'PLY',6X,'F1S1',12X,'F2S2',12X,'F2S3'/)
         DO 80 I=1,J
 80          WRITE(6,60) I,F1S1(I),F2S2(I),F2S3(I)
         WRITE(6,110)
 110     FORMAT(//'PLY',4X,'F11S1S1',9X,'F22S2S2',9X,'F22S3S3',9X,
        +     'F66S6S6',9X,'F12S1S2',9X,'F12S1S3',9X,'F23S2S3'/)
         DO 90 I=1,J
 90          WRITE(6,60) I,F11S1(I),F22S2(I),F22S3(I),F66S6(I),
        +          F12S12(I),F12S13(I),F23S23(I)
         WRITE(6,120)
 120     FORMAT(//'PLY...FAILURE FRACTION,TS'/)
         DO 100 I=1,J
 100        WRITE(6,60) I,TS(I)
 60      FORMAT(I2,7D16.8)
 C
```

```
      RETURN
      END
C
C
C
      SUBROUTINE RESLTN
C
C     THIS S/R CALCULATES THE STRESS RESULTANTS
C         NX, NO, NXO; MX, MO, MXO
C
      IMPLICIT REAL*8 (A-H), REAL*8 (M-Z)
      COMMON /IN/ ANGLE(15),T(15),CB11(15),CB12(15),CB13(15),
     +     CB16(15),CB22(15),CB23(15),CB26(15),CB33(15),CB36(15),
     +     CB66(15),RO(15),RI(15),ALPAX(15),ALPAO(15),ALPAR(15),
     +     ALPAXO(15),DT,P,TW,J
      COMMON /SOLN/ BC(32,32),ET(32,1),V(15),V1(15),V2(15),
     +     V3(15),V4(15),Z1(15),Z2(15),Z3(15),Z4(15),Z5(15),
     +     Z6(15),Z7(15)
C
      PI = 3.1415927
      NX1 = 0.
      NX2 = 0.
      NX3 = 0.
      NX4 = 0.
      NX5 = 0.
      NO1 = 0.
      NO2 = 0.
      NO3 = 0.
      NO4 = 0.
      NO5 = 0.
      NXO1 = 0.
      NXO2 = 0.
      NXO3 = 0.
      NXO4 = 0.
      NXO5 = 0.
      MX1 = 0.
      MX2 = 0.
      MX3 = 0.
      MX4 = 0.
      MX5 = 0.
      MO1 = 0.
      MO2 = 0.
      MO3 = 0.
      MO4 = 0.
      MO5 = 0.
      MXO1 = 0.
      MXO2 = 0.
      MXO3 = 0.
      MXO4 = 0.
      MXO5 = 0.
      RM = (RO(J) + RI(1))/2.
C
      DO 107 I=1,J
          NX1 = NX1 + (CB11(I) + Z1(I)*Z4(I))*(RO(I)**2 -
```

```
     +        RI(I)**2)/2.
              NX2 = NX2 + ((CB13(I) + Z4(I))*Z2(I) + CB16(I))*
     +        (RO(I)**3 - RI(I)**3)/3.
              NX3 = NX3 + (CB12(I) + V(I)*CB13(I))*(RO(I)**V1(I) -
     +        RI(I)**V1(I)) * ET(2*I+1,1)/V1(I)
              NX4 = NX4 + (CB12(I) - V(I)*CB13(I))*(RO(I)**V2(I) -
     +        RI(I)**V2(I)) * ET(2*I+2,1)/V2(I)
              NX5 = NX5 + (DT*(CB11(I)*ALPAX(I) + CB12(I)*ALPAO(I) +
     +        CB13(I)*ALPAR(I) + CB16(I)*ALPAXO(I)) - Z3(I)*Z4(I))*
     +        (RO(I)**2 -RI(I)**2)/2.
              NO1 = NO1 + (CB12(I) + Z7(I)*Z1(I))*(RO(I)-RI(I))
              NO2 = NO2 + ((CB23(I) + Z7(I))*Z2(I) + CB26(I))*
     +        (RO(I)**2 - RI(I)**2)/2.
              NO3 = NO3 + (CB22(I) + V(I)*CB23(I))*(RO(I)**V(I) -
     +        RI(I)**V(I))*ET(2*I+1,1)/V(I)
              NO4 = NO4 + (CB22(I) - V(I)*CB23(I))*(RO(I)**(-V(I)) -
     +        RI(I)**(-V(I)))*ET(2*I+2,1)/(-V(I))
              NO5 = NO5 + (DT*(CB12(I)*ALPAX(I) + CB22(I)*ALPAO(I) +
     +        CB23(I)*ALPAR(I) + CB26(I)*ALPAXO(I)) -
     +        Z3(I)*Z7(I))*(RO(I) - RI(I))
              NXO1 = NXO1 + (CB16(I) + Z5(I)*Z1(I))*(RO(I)**2 -
     +        RI(I)**2)/2.
              NXO2 = NXO2 + ((CB36(I) + Z5(I))*Z2(I) + CB66(I))*
     +        (RO(I)**3 - RI(I)**3)/3.
              NXO3 = NXO3 + (CB26(I) + V(I)*CB36(I))*(RO(I)**V1(I) -
     +        RI(I)**V1(I))*ET(2*I+1,1)/V1(I)
              NXO4 = NXO4 + (CB26(I) - V(I)*CB36(I))*(RO(I)**V2(I) -
     +        RI(I)**V2(I))*ET(2*I+2,1)/V2(I)
              NXO5 = NXO5 + (DT*(CB16(I)*ALPAX(I) + CB26(I)*ALPAO(I) +
     +        CB36(I)*ALPAR(I) + CB66(I)*ALPAXO(I)) - Z3(I)*Z5(I))*
     +        (RO(I)**2 - RI(I)**2)/2.
              MX1 = MX1 + (CB11(I) + Z4(I)*Z1(I))*(RO(I)**3 -
     +        RI(I)**3)/3.
              MX2 = MX2 + ((CB13(I) + Z4(I))*Z2(I) + CB16(I))*(RO(I)**4
     +        - RI(I)**4)/4.
              MX3 = MX3 + (CB12(I) + V(I)*CB13(I))*(RO(I)**V3(I) -
     +        RI(I)**V3(I))*ET(2*I+1,1)/V3(I)
              MX4 = MX4 + (CB12(I) - V(I)*CB13(I))*(RO(I)**V4(I) -
     +        RI(I)**V4(I))*ET(2*I+2,1)/V4(I)
              MX5 = MX5 + (DT*(CB11(I)*ALPAX(I) + CB12(I)*ALPAO(I) +
     +        CB13(I)*ALPAR(I) + CB16(I)*ALPAXO(I)) - Z3(I)*
     +        Z4(I))*(RO(I)**3 - RI(I)**3)/3.
              MO1 = MO1 + (CB12(I) + Z7(I)*Z1(I))*(RO(I)**2 -
     +        RI(I)**2)/2.
              MO2 = MO2 + ((CB23(I) + Z7(I))*Z2(I) + CB26(I))*
     +        (RO(I)**3 - RI(I)**3)/3.
              MO3 = MO3 + (CB22(I) + V(I)*CB23(I))*(RO(I)**V1(I)
     +        - RI(I)**V1(I))*ET(2*I+1,1)/V1(I)
              MO4 = MO4 + (CB22(I) - V(I)*CB23(I))*(RO(I)**V2(I)
     +        - RI(I)**V2(I))*ET(2*I+2,1)/V2(I)
              MO5 = MO5 + (DT*(CB12(I)*ALPAX(I) + CB22(I)*ALPAO(I) +
     +        CB23(I)*ALPAR(I) + CB26(I)*ALPAXO(I)) -
     +        Z3(I)*Z7(I))*(RO(I)**2 - RI(I)**2)/2.
              MXO1 = MXO1 + (CB16(I) + Z5(I)*Z1(I))*(RO(I)**3 -
```

```
     +        RI(I)**3)/3.
              MXO2 = MXO2 + ((CB36(I) + Z5(I))*Z2(I) + CB66(I))*
     +        (RO(I)**4 - RI(I)**4)/4.
              MXO3 = MXO3 + (CB26(I) + V(I)*CB36(I))*(RO(I)**V3(I) -
     +        RI(I)**V3(I))*ET(2*I+1,1)/V3(I)
              MXO4 = MXO4 + (CB26(I) - V(I)*CB36(I))*(RO(I)**V4(I) -
     +        RI(I)**V4(I))*ET(2*I+2,1)/V4(I)
107           MXO5 = MXO5 + (DT*(CB16(I)*ALPAX(I) + CB26(I)*ALPAO(I) +
     +        CB36(I)*ALPAR(I) + CB66(I)*ALPAXO(I)) - Z3(I)*Z5(I))*
     +        (RO(I)**3 - RI(I)**3)/3.
        NX = (NX1*ET(1,1) + NX2*ET(2,1) + NX3 + NX4 - NX5)/RM
        NO = (NO1*ET(1,1) + NO2*ET(2,1) + NO3 + NO4 - NO5)
        NXO = (NXO1*ET(1,1) + NXO2*ET(2,1) + NXO3 + NXO4 - NXO5)/RM
        MX = (MX1*ET(1,1) + MX2*ET(2,1) + MX3 + MX4 - MX5)/RM - NX*RM
        MO = (MO1*ET(1,1) + MO2*ET(2,1) + MO3 + MO4 - MO5) - NO*RM
        MXO = (MXO1*ET(1,1)+MXO2*ET(2,1)+MXO3+MXO4-MXO5)/RM - NXO*RM
C
        WRITE(6,106)
106   FORMAT(//'STRESS RESULTANTS'/)
        WRITE(6,108) NX,NO,NXO,MX,MO,MXO
108   FORMAT(7X,'NX',14X,'NO',14X,'NXO'/3D16.8/3D16.8/
     +      7X,'MX',14X,'MO',14X,'MXO'//)
C
        RETURN
        END
```

Data File for Thermal Analogy

0.3-inch Thick Fiberglass Tube, 50 v/o Reinforcement

```
2.............number of plies
2.............number of different materials
1.951.........internal radius (inches)
-857..........temperature difference (°F)
0.0
0.0
9800000.......aluminum properties
9800000.
8820000.
3684211.
0.33
0.33
0.33
0.............CTE's of aluminum set to zero
0.
0.
5500000.......composite properties
1133900.
1020500.
497870.
0.444
0.30
0.30
0.00000159....thermal analogy CTE's of fiberglass
0.00002315                    (in/in/°F)
0.00002315
1
0.049.........thickness of aluminum mandrel (inches)
0.
2
0.300.........thickness of composite layer (inches)
90............orientation of reinforcement (degrees)
0.0
0.0
0.0
0.0
0.0
0.0
0.0
0.0
```

Data File for Thermal Analogy

0.3-inch Thick Polyester Tube, 0 v/o Reinforcement

```
2.............number of plies
2.............number of different materials
1.951.........internal radius (inches)
-857..........temperature difference (°F)
0.0
0.0
9800000.......aluminum properties
9800000.
8820000.
3684211.
0.33
0.33
0.33
0.............CTE's of aluminum set to zero
0.
0.
500000........polyester properties
500000.
450000.
185185.
0.35
0.35
0.35
0.000035......CTE's of polyester (in/in/°F)
0.000035
0.000035
1
0.049.........thickness of aluminum mandrel (inches)
0.
2
0.300.........thickness of polyester layer (inches)
0.
0.0
0.0
0.0
0.0
0.0
0.0
0.0
0.0
```

Thermal Analogy Output from Program ELAS2

For a 0.3-inch Thick Fiberglass Tube, 50 v/o Reinforcement

LAYER PROPERTIES

PLY	MATL	PHI	THICKNESS	RI	RO
1	1	0.	0.04900	1.95100	2.00000
2	2	90.	0.30000	2.00000	2.30000

PLY	CBAR MATRIX			
1	0.14022199E+08	0.66537784E+07	0.61407654E+07	0.00000000E+00
		0.14022199E+08	0.61407654E+07	0.00000000E+00
			0.12467615E+08	0.00000000E+00
				0.36842110E+07
2	0.14433264E+07	0.61631407E+06	0.61105385E+06	-0.27489230E-01
		0.58565767E+07	0.57227505E+06	-0.69152052E+00
			0.12965296E+07	0.63178691E-02
				0.49787000E+06

PLY	ALPHA-X	ALPHA-THETA	ALPHA-R	ALPHA-X,THETA
1	0.00000000E+00	0.00000000E+00	0.00000000E+00	0.00000000E+00
2	0.23150000E-04	0.15900000E-05	0.23150000E-04	0.70251397E-11

DELTA-TEMPERATURE LOAD = -0.85700000E+03 F
AXIAL LOAD= 0.00000000E+00 LB
TORSION = 0.00000000E+00 IN-LB

```
PLY     LAMBDA

 1   0.10605139E+01
 2   0.21253512E+01


BC(I,J)    EPS-0    GAM-0    A(1 THRU 2J)

  0.23283E-08  0.00000E+00  0.20162E+08 -0.17866E+07  0.00000E+00  0.00000E+00
  0.60889E+06  0.76607E+01  0.00000E+00  0.00000E+00  0.84964E+07 -0.16165E+06
  0.18786E+07  0.26437E+01  0.13280E+07  0.33661E+04  0.29287E+07 -0.40453E+05
 -0.37084E-01  0.28836E+07  0.00000E+00  0.00000E+00 -0.22373E+01 -0.89539E-01
 -0.65769E+00 -0.42010E-05  0.20856E+01  0.47946E+00 -0.43630E+01 -0.22919E+00
 -0.60889E+06 -0.66614E+01  0.20192E+08 -0.16976E+07 -0.72598E+07  0.25020E+06


ET(I,1)

  0.00000000E+00
 -0.41520366E+05
 -0.28056923E+05
 -0.79684585E-03
  0.30982034E-02
  0.41520366E+05


ELASTICITY CONSTANTS

EPSILON-0 = -.82274524E-02
GAMMA-0 = -.12890242E-08

       A1                  A2
-0.60307970E-03 -0.68057156E-02
-0.32891649E-02  0.52980864E-01
```

TOTAL STRAINS IN X-Y SYSTEM;LAYER;PHI;R/R;EPS-X;EPS-THETA;EPS-R;GAMMA-X,THETA

1	0.	0.00000	-0.82274524E-02	0.36999241E-03	0.38700923E-02	-0.25148863E-08
1	0.	0.01560	-0.82274524E-02	0.37971789E-03	0.38595536E-02	-0.25219043E-08
1	0.	0.03120	-0.82274524E-02	0.38936028E-03	0.38491037E-02	-0.25289223E-08
1	0.	0.04680	-0.82274524E-02	0.39892049E-03	0.38387415E-02	-0.25359403E-08
1	0.	0.06240	-0.82274524E-02	0.40839947E-03	0.38284660E-02	-0.25429583E-08
1	0.	0.07800	-0.82274524E-02	0.41779810E-03	0.38182763E-02	-0.25499764E-08
1	0.	0.09360	-0.82274524E-02	0.42711729E-03	0.38081715E-02	-0.25569944E-08
1	0.	0.10920	-0.82274524E-02	0.43635792E-03	0.37981505E-02	-0.25640124E-08
1	0.	0.12480	-0.82274524E-02	0.44552087E-03	0.37882125E-02	-0.25710304E-08
1	0.	0.14040	-0.82274524E-02	0.45460698E-03	0.37783565E-02	-0.25780484E-08
2	90.	0.14040	-0.82274524E-02	0.45460698E-03	-0.26595820E-01	-0.25780484E-08
2	90.	0.23591	-0.82274524E-02	0.14197078E-04	-0.26232457E-01	-0.26210159E-08
2	90.	0.33142	-0.82274524E-02	-0.40649759E-03	-0.25912174E-01	-0.26639834E-08
2	90.	0.42693	-0.82274524E-02	-0.80907216E-03	-0.25631563E-01	-0.27069509E-08
2	90.	0.52245	-0.82274524E-02	-0.11949714E-02	-0.25387539E-01	-0.27499183E-08
2	90.	0.61796	-0.82274524E-02	-0.15655059E-02	-0.25177300E-01	-0.27928858E-08
2	90.	0.71347	-0.82274524E-02	-0.19218664E-02	-0.24998300E-01	-0.28358533E-08
2	90.	0.80898	-0.82274524E-02	-0.22651362E-02	-0.24848223E-01	-0.28788208E-08
2	90.	0.90449	-0.82274524E-02	-0.25963024E-02	-0.24724954E-01	-0.29217882E-08
2	90.	1.00000	-0.82274524E-02	-0.29162656E-02	-0.24626567E-01	-0.29647557E-08

MECH STRAINS IN X-Y SYSTEM;LAYER;PHI;R/R;EPS-X;EPS-THETA;EPS-R;GAMMA-X,THETA

1	0.	0.00000	-0.82274524E-02	0.36999241E-03	0.38700923E-02	-0.25148863E-08
1	0.	0.01560	-0.82274524E-02	0.37971789E-03	0.38595536E-02	-0.25219043E-08
1	0.	0.03120	-0.82274524E-02	0.38936028E-03	0.38491037E-02	-0.25289223E-08
1	0.	0.04680	-0.82274524E-02	0.39892049E-03	0.38387415E-02	-0.25359403E-08
1	0.	0.06240	-0.82274524E-02	0.40839947E-03	0.38284660E-02	-0.25429583E-08
1	0.	0.07800	-0.82274524E-02	0.41779810E-03	0.38182763E-02	-0.25499764E-08
1	0.	0.09360	-0.82274524E-02	0.42711729E-03	0.38081715E-02	-0.25569944E-08
1	0.	0.10920	-0.82274524E-02	0.43635792E-03	0.37981505E-02	-0.25640124E-08
1	0.	0.12480	-0.82274524E-02	0.44552087E-03	0.37882125E-02	-0.25710304E-08
1	0.	0.14040	-0.82274524E-02	0.45460698E-03	0.37783565E-02	-0.25780484E-08
2	90.	0.14040	0.11612098E-01	0.18172370E-02	-0.67562699E-02	0.34424963E-08
2	90.	0.23591	0.11612098E-01	0.13768271E-02	-0.63929066E-02	0.33995288E-08
2	90.	0.33142	0.11612098E-01	0.95613241E-03	-0.60726236E-02	0.33565613E-08
2	90.	0.42693	0.11612098E-01	0.55355784E-03	-0.57920133E-02	0.33135939E-08
2	90.	0.52245	0.11612098E-01	0.16765860E-03	-0.55479893E-02	0.32706264E-08
2	90.	0.61796	0.11612098E-01	-0.20287590E-03	-0.53377503E-02	0.32276589E-08
2	90.	0.71347	0.11612098E-01	-0.55923637E-03	-0.51587505E-02	0.31846914E-08
2	90.	0.80898	0.11612098E-01	-0.90250616E-03	-0.50086725E-02	0.31417240E-08
2	90.	0.90449	0.11612098E-01	-0.12336724E-02	-0.48854042E-02	0.30987565E-08
2	90.	1.00000	0.11612098E-01	-0.15536356E-02	-0.47870175E-02	0.30557890E-08

STRESSES IN X-Y SYSTEM;LAYER;PHI;R/R;SIG-X;SIG-THETA;SIG-R;TAU-X,THETA

1	0.	0.00000	-0.89139803E+05	-0.25790209E+05	0.00000000E+00	-0.92653716E-02
1	0.	0.01560	-0.89139807E+05	-0.25718552E+05	-0.71669815E+02	-0.92912275E-02
1	0.	0.03120	-0.89139819E+05	-0.25647515E+05	-0.14274385E+03	-0.93170834E-02
1	0.	0.04680	-0.89139840E+05	-0.25577092E+05	-0.21322877E+03	-0.93429392E-02
1	0.	0.06240	-0.89139868E+05	-0.25507275E+05	-0.28313113E+03	-0.93687951E-02
1	0.	0.07800	-0.89139904E+05	-0.25438058E+05	-0.35245739E+03	-0.93946510E-02
1	0.	0.09360	-0.89139948E+05	-0.25369434E+05	-0.42121394E+03	-0.94205068E-02
1	0.	0.10920	-0.89139999E+05	-0.25301396E+05	-0.48940708E+03	-0.94463627E-02
1	0.	0.12480	-0.89140058E+05	-0.25233939E+05	-0.55704300E+03	-0.94722186E-02
1	0.	0.14040	-0.89140124E+05	-0.25167055E+05	-0.62412782E+03	-0.94980744E-02
2	90.	0.14040	0.13751591E+05	0.13933042E+05	-0.62412782E+03	0.95366110E-04
2	90.	0.23591	0.13702194E+05	0.11561691E+05	-0.40505243E+03	0.38082206E-03
2	90.	0.33142	0.13638624E+05	0.92811510E+04	-0.23054879E+03	0.65237234E-03
2	90.	0.42693	0.13561980E+05	0.70840283E+04	-0.97112666E+02	0.91114156E-03
2	90.	0.52245	0.13473257E+05	0.49636287E+04	-0.15687654E+01	0.11581483E-02
2	90.	0.61796	0.13373359E+05	0.29138795E+04	0.58964669E+02	0.13943166E-02
2	90.	0.71347	0.13263107E+05	0.92926419E+03	0.87107027E+02	0.16204858E-02
2	90.	0.80898	0.13143251E+05	-0.99523583E+03	0.85242766E+02	0.18374199E-02
2	90.	0.90449	0.13014472E+05	-0.28641927E+04	0.55545619E+02	0.20458147E-02
2	90.	1.00000	0.12877394E+05	-0.46817774E+04	0.17487086E-10	0.22463052E-02

TOTAL STRAINS IN 1-2 SYSTEM...LAYER...PHI...R/REPS-1...EPS-2...EPS-3...GAMMA-1,2

1	0.	0.00000	-0.82274524E-02	0.36999241E-03	0.38700923E-02	-0.25148863E-08
1	0.	0.01560	-0.82274524E-02	0.37971789E-03	0.38595536E-02	-0.25219043E-08
1	0.	0.03120	-0.82274524E-02	0.38936028E-03	0.38491037E-02	-0.25289223E-08
1	0.	0.04680	-0.82274524E-02	0.39892049E-03	0.38387415E-02	-0.25359403E-08
1	0.	0.06240	-0.82274524E-02	0.40839947E-03	0.38284660E-02	-0.25429583E-08
1	0.	0.07800	-0.82274524E-02	0.41779810E-03	0.38182763E-02	-0.25499764E-08
1	0.	0.09360	-0.82274524E-02	0.42711729E-03	0.38081715E-02	-0.25569944E-08
1	0.	0.10920	-0.82274524E-02	0.43635792E-03	0.37981505E-02	-0.25640124E-08
1	0.	0.12480	-0.82274524E-02	0.44552087E-03	0.37882125E-02	-0.25710304E-08
1	0.	0.14040	-0.82274524E-02	0.45460698E-03	0.37783565E-02	-0.25780484E-08
2	90.	0.14040	0.45460698E-03	-0.82274524E-02	-0.26595820E-01	-0.25092560E-09
2	90.	0.23591	0.14197078E-04	-0.82274524E-02	-0.26232457E-01	-0.64454362E-10
2	90.	0.33142	-0.40649759E-03	-0.82274524E-02	-0.25912174E-01	0.11559283E-09
2	90.	0.42693	-0.80907216E-03	-0.82274524E-02	-0.25631563E-01	0.28973575E-09
2	90.	0.52245	-0.11949714E-02	-0.82274524E-02	-0.25387539E-01	0.45844516E-09
2	90.	0.61796	-0.15655059E-02	-0.82274524E-02	-0.25177300E-01	0.62214810E-09
2	90.	0.71347	-0.19218664E-02	-0.82274524E-02	-0.24998300E-01	0.78123255E-09
2	90.	0.80898	-0.22651362E-02	-0.82274524E-02	-0.24848223E-01	0.93605152E-09
2	90.	0.90449	-0.25963024E-02	-0.82274524E-02	-0.24724954E-01	0.10869266E-08
2	90.	1.00000	-0.29162656E-02	-0.82274524E-02	-0.24626567E-01	0.12341514E-08

STRESSES IN 1-2 SYSTEM...LAYER...PHI...R/R...SIG-1...SIG-2...SIG-3...TAU-1,2

1	0.	0.00000	-0.89139803E+05	-0.25790209E+05	0.00000000E+00	-0.92653716E-02
1	0.	0.01560	-0.89139807E+05	-0.25718552E+05	-0.71669815E+02	-0.92912275E-02
1	0.	0.03120	-0.89139819E+05	-0.25647515E+05	-0.14274385E+03	-0.93170834E-02
1	0.	0.04680	-0.89139840E+05	-0.25577092E+05	-0.21322877E+03	-0.93429392E-02
1	0.	0.06240	-0.89139868E+05	-0.25507275E+05	-0.28313113E+03	-0.93687951E-02
1	0.	0.07800	-0.89139904E+05	-0.25438058E+05	-0.35245739E+03	-0.93946510E-02
1	0.	0.09360	-0.89139948E+05	-0.25369434E+05	-0.42121394E+03	-0.94205088E-02
1	0.	0.10920	-0.89139999E+05	-0.25301396E+05	-0.48940708E+03	-0.94463627E-02
1	0.	0.12480	-0.89140058E+05	-0.25233939E+05	-0.55704300E+03	-0.94722186E-02
1	0.	0.14040	-0.89140124E+05	-0.25167055E+05	-0.62412782E+03	-0.94980744E-02
2	90.	0.14040	0.13933042E+05	0.13751591E+05	-0.62412782E+03	-0.12492833E-03
2	90.	0.23591	0.11561691E+05	0.13702194E+05	-0.40505243E+03	-0.32089893E-04
2	90.	0.33142	0.92811510E+04	0.13638624E+05	-0.23054879E+03	0.57550205E-04
2	90.	0.42693	0.70840283E+04	0.13561980E+05	-0.97112666E+02	0.14425074E-03
2	90.	0.52245	0.49636287E+04	0.13473257E+05	-0.15687654E+01	0.22824609E-03
2	90.	0.61796	0.29138795E+04	0.13373359E+05	0.58964669E+02	0.30974887E-03
2	90.	0.71347	0.92926419E+03	0.13263107E+05	0.87107027E+02	0.38895225E-03
2	90.	0.80898	-0.99523583E+03	0.13143251E+05	0.85242766E+02	0.46603197E-03
2	90.	0.90449	-0.28641927E+04	0.13014472E+05	0.55545619E+02	0.54114817E-03
2	90.	1.00000	-0.46817774E+04	0.12877394E+05	0.17487086E-10	0.61444694E-03

STRESS RESULTANTS

NX	NO	NXO
0.17115873E-11	0.21827873E-10	-0.42790198E-04
0.71542296E+03	0.78843884E+02	0.90950566E-04
MX	MO	MXO

0.,

Thermal Analogy Output from Program ELAS2

0.3-inch Thick Resin Tube, 0 v/o Reinforcement

LAYER PROPERTIES

PLY	MATL	PHI	THICKNESS	RI	RO
1	1	0.	0.04900	1.95100	2.00000
2	2	0.	0.30000	2.00000	2.30000

CBAR MATRIX

PLY				
1	0.14022199E+08	0.66537784E+07	0.61407654E+07	0.00000000E+00
		0.14022199E+08	0.61407654E+07	0.00000000E+00
			0.12467615E+08	0.00000000E+00
				0.3684211OE+07
2	0.76725736E+06	0.39688699E+06	0.36670547E+06	0.00000000E+00
		0.76725736E+06	0.36670547E+06	0.00000000E+00
			0.68102445E+06	0.00000000E+00
				0.18518500E+06

PLY	ALPHA-X	ALPHA-THETA	ALPHA-R	ALPHA-X,THETA
1	0.00000000E+00	0.00000000E+00	0.00000000E+00	0.00000000E+00
2	0.35000000E-04	0.35000000E-04	0.35000000E-04	0.00000000E+00

DELTA-TEMPERATURE LOAD = -0.85700000E+03 F
AXIAL LOAD= 0.00000000E+00 LB
TORSION = 0.00000000E+00 IN-LB

```
PLY     LAMBDA

 1  0.10605139E+01
 2  0.10614247E+01


BC(I,J)    EPS-0    GAM-0    A(1 THRU 2J)

  0.23283E-08  0.00000E+00  0.20162E+08 -0.17866E+07  0.00000E+00  0.00000E+00
  0.14551E-10  0.00000E+00  0.00000E+00  0.00000E+00  0.11467E+07 -0.63967E+05
  0.12711E+07  0.00000E+00  0.13280E+07  0.33661E+04  0.53148E+06  0.10211E+04
  0.00000E+00  0.19468E+07  0.00000E+00  0.00000E+00  0.00000E+00  0.00000E+00
  0.40000E-01  0.00000E+00  0.20856E+01  0.47946E+00 -0.20869E+01 -0.47915E+00
  0.23137E-08  0.00000E+00  0.20192E+08 -0.16976E+07 -0.11369E+07  0.85326E+05


ET(I,1)

  0.00000000E+00
 -0.90949470E-12
 -0.96733875E+04
  0.00000000E+00
 -0.80986500E-01
  0.90949470E-12


ELASTICITY CONSTANTS

EPSILON-0 = -.77575028E-02
GAMMA-0 = 0.00000000E+00

       A1                A2
-0.22640646E-02 -0.25549824E-01
 0.59664933E-02  0.10696234E+00
```

TOTAL STRAINS IN X-Y SYSTEM;LAYER;PHI;R/R;EPS-X;EPS-THETA;EPS-R;GAMMA-X,THETA

1	0.	0.00000	-0.77575028E-02	-0.62438073E-02	0.68961677E-02	0.00000000E+00
1	0.	0.01560	-0.77575028E-02	-0.62072962E-02	0.68566038E-02	0.00000000E+00
1	0.	0.03120	-0.77575028E-02	-0.61710970E-02	0.68173730E-02	0.00000000E+00
1	0.	0.04680	-0.77575028E-02	-0.61352064E-02	0.67784715E-02	0.00000000E+00
1	0.	0.06240	-0.77575028E-02	-0.60996207E-02	0.67398957E-02	0.00000000E+00
1	0.	0.07800	-0.77575028E-02	-0.60643366E-02	0.67016418E-02	0.00000000E+00
1	0.	0.09360	-0.77575028E-02	-0.60293507E-02	0.66637065E-02	0.00000000E+00
1	0.	0.10920	-0.77575028E-02	-0.59946598E-02	0.66260860E-02	0.00000000E+00
1	0.	0.12480	-0.77575028E-02	-0.59602606E-02	0.65887770E-02	0.00000000E+00
1	0.	0.14040	-0.77575028E-02	-0.59261497E-02	0.65517759E-02	0.00000000E+00
2	0.	0.14040	-0.77575028E-02	-0.59261497E-02	-0.58369714E-01	0.00000000E+00
2	0.	0.23591	-0.77575028E-02	-0.67782933E-02	-0.57451802E-01	0.00000000E+00
2	0.	0.33142	-0.77575028E-02	-0.75885079E-02	-0.56578599E-01	0.00000000E+00
2	0.	0.42693	-0.77575028E-02	-0.83594768E-02	-0.55747251E-01	0.00000000E+00
2	0.	0.52245	-0.77575028E-02	-0.90936728E-02	-0.54955128E-01	0.00000000E+00
2	0.	0.61796	-0.77575028E-02	-0.97933778E-02	-0.54199801E-01	0.00000000E+00
2	0.	0.71347	-0.77575028E-02	-0.10460700E-01	-0.53479027E-01	0.00000000E+00
2	0.	0.80898	-0.77575028E-02	-0.11097589E-01	-0.52790732E-01	0.00000000E+00
2	0.	0.90449	-0.77575028E-02	-0.11705850E-01	-0.52132993E-01	0.00000000E+00
2	0.	1.00000	-0.77575028E-02	-0.12287160E-01	-0.51504028E-01	0.00000000E+00

MECH STRAINS IN X-Y SYSTEM;LAYER;PHI;R/R;EPS-X;EPS-THETA;EPS-R;GAMMA-X,THETA

1	0.	0.00000	-0.77575028E-02	-0.62438073E-02	0.68961677E-02	0.00000000E+00
1	0.	0.01560	-0.77575028E-02	-0.62072962E-02	0.68566038E-02	0.00000000E+00
1	0.	0.03120	-0.77575028E-02	-0.61710970E-02	0.68173730E-02	0.00000000E+00
1	0.	0.04680	-0.77575028E-02	-0.61352064E-02	0.67784715E-02	0.00000000E+00
1	0.	0.06240	-0.77575028E-02	-0.60996207E-02	0.67398957E-02	0.00000000E+00
1	0.	0.07800	-0.77575028E-02	-0.60643366E-02	0.67016418E-02	0.00000000E+00
1	0.	0.09360	-0.77575028E-02	-0.60293507E-02	0.66637065E-02	0.00000000E+00
1	0.	0.10920	-0.77575028E-02	-0.59946598E-02	0.66260860E-02	0.00000000E+00
1	0.	0.12480	-0.77575028E-02	-0.59602606E-02	0.65887770E-02	0.00000000E+00
1	0.	0.14040	-0.77575028E-02	-0.59261497E-02	0.65517759E-02	0.00000000E+00
2	0.	0.14040	0.22237497E-01	0.24068850E-01	-0.28374714E-01	0.00000000E+00
2	0.	0.23591	0.22237497E-01	0.23216707E-01	-0.27456802E-01	0.00000000E+00
2	0.	0.33142	0.22237497E-01	0.22406492E-01	-0.26583599E-01	0.00000000E+00
2	0.	0.42693	0.22237497E-01	0.21635523E-01	-0.25752251E-01	0.00000000E+00
2	0.	0.52245	0.22237497E-01	0.20901327E-01	-0.24960128E-01	0.00000000E+00
2	0.	0.61796	0.22237497E-01	0.20201622E-01	-0.24204801E-01	0.00000000E+00
2	0.	0.71347	0.22237497E-01	0.19534300E-01	-0.23484027E-01	0.00000000E+00
2	0.	0.80898	0.22237497E-01	0.18897411E-01	-0.22795732E-01	0.00000000E+00
2	0.	0.90449	0.22237497E-01	0.18289150E-01	-0.22137993E-01	0.00000000E+00
2	0.	1.00000	0.22237497E-01	0.17707840E-01	-0.21509028E-01	0.00000000E+00

STRESSES IN X-Y SYSTEM;LAYER;PHI;R/R;SIG-X;SIG-THETA;SIG-R;TAU-X,THETA

1	0.	0.00000	-0.10797441E+06	-0.96820869E+05	0.00000000E+00	0.00000000E+00
1	0.	0.01560	-0.10797443E+06	-0.96551855E+05	-0.26906078E+03	0.00000000E+00
1	0.	0.03120	-0.10797448E+06	-0.96285170E+05	-0.53588491E+03	0.00000000E+00
1	0.	0.04680	-0.10797455E+06	-0.96020789E+05	-0.80049737E+03	0.00000000E+00
1	0.	0.06240	-0.10797466E+06	-0.95759684E+05	-0.10629228E+04	0.00000000E+00
1	0.	0.07800	-0.10797479E+06	-0.95498832E+05	-0.13231855E+04	0.00000000E+00
1	0.	0.09360	-0.10797496E+06	-0.95241205E+05	-0.15813094E+04	0.00000000E+00
1	0.	0.10920	-0.10797515E+06	-0.94985781E+05	-0.18373181E+04	0.00000000E+00
1	0.	0.12480	-0.10797537E+06	-0.94732534E+05	-0.20912349E+04	0.00000000E+00
1	0.	0.14040	-0.10797562E+06	-0.94481439E+05	-0.23430829E+04	0.00000000E+00
2	0.	0.14040	0.16209334E+05	0.16887613E+05	-0.23430829E+04	0.00000000E+00
2	0.	0.23591	0.16207733E+05	0.16570403E+05	-0.20304479E+04	0.00000000E+00
2	0.	0.33142	0.16206377E+05	0.16268968E+05	-0.17328856E+04	0.00000000E+00
2	0.	0.42693	0.16205250E+05	0.15982296E+05	-0.14494360E+04	0.00000000E+00
2	0.	0.52245	0.16204333E+05	0.15709455E+05	-0.11792142E+04	0.00000000E+00
2	0.	0.61796	0.16203612E+05	0.15449584E+05	-0.92140360E+03	0.00000000E+00
2	0.	0.71347	0.16203072E+05	0.15201888E+05	-0.67524972E+03	0.00000000E+00
2	0.	0.80898	0.16202701E+05	0.14965632E+05	-0.44005441E+03	0.00000000E+00
2	0.	0.90449	0.16202486E+05	0.14740135E+05	-0.21517105E+03	0.00000000E+00
2	0.	1.00000	0.16202417E+05	0.14524766E+05	0.27284841E-11	0.00000000E+00

TOTAL STRAINS IN 1-2 SYSTEM...LAYER...PHI...R/REPS-1...EPS-2...EPS-3...GAMMA-1,2

1	0.	0.00000	-0.77575028E-02	-0.62438073E-02	0.68961677E-02	0.00000000E+00
1	0.	0.01560	-0.77575028E-02	-0.62072962E-02	0.68566038E-02	0.00000000E+00
1	0.	0.03120	-0.77575028E-02	-0.61710970E-02	0.68173730E-02	0.00000000E+00
1	0.	0.04680	-0.77575028E-02	-0.61352064E-02	0.67784715E-02	0.00000000E+00
1	0.	0.06240	-0.77575028E-02	-0.60996207E-02	0.67398957E-02	0.00000000E+00
1	0.	0.07800	-0.77575028E-02	-0.60643366E-02	0.67016418E-02	0.00000000E+00
1	0.	0.09360	-0.77575028E-02	-0.60293507E-02	0.66637065E-02	0.00000000E+00
1	0.	0.10920	-0.77575028E-02	-0.59946598E-02	0.66260860E-02	0.00000000E+00
1	0.	0.12480	-0.77575028E-02	-0.59602606E-02	0.65887770E-02	0.00000000E+00
1	0.	0.14040	-0.77575028E-02	-0.59261497E-02	0.65517759E-02	0.00000000E+00
2	0.	0.14040	-0.77575028E-02	-0.59261497E-02	-0.58369714E-01	0.00000000E+00
2	0.	0.23591	-0.77575028E-02	-0.67782933E-02	-0.57451802E-01	0.00000000E+00
2	0.	0.33142	-0.77575028E-02	-0.75885079E-02	-0.56578599E-01	0.00000000E+00
2	0.	0.42693	-0.77575028E-02	-0.83594768E-02	-0.55747251E-01	0.00000000E+00
2	0.	0.52245	-0.77575028E-02	-0.90936728E-02	-0.54955128E-01	0.00000000E+00
2	0.	0.61796	-0.77575028E-02	-0.97933778E-02	-0.54199801E-01	0.00000000E+00
2	0.	0.71347	-0.77575028E-02	-0.10460700E-01	-0.53479027E-01	0.00000000E+00
2	0.	0.80898	-0.77575028E-02	-0.11097589E-01	-0.52790732E-01	0.00000000E+00
2	0.	0.90449	-0.77575028E-02	-0.11705850E-01	-0.52132993E-01	0.00000000E+00
2	0.	1.00000	-0.77575028E-02	-0.12287160E-01	-0.51504028E-01	0.00000000E+00

STRESSES IN 1-2 SYSTEM...LAYER...PHI...R/R...SIG-1...SIG-2...SIG-3...TAU-1,2

1	0.	0.00000	-0.10797441E+06	-0.96820869E+05	0.00000000E+00	0.00000000E+00
1	0.	0.01560	-0.10797443E+06	-0.96551855E+05	-0.26906078E+03	0.00000000E+00
1	0.	0.03120	-0.10797448E+06	-0.96285170E+05	-0.53588491E+03	0.00000000E+00
1	0.	0.04680	-0.10797455E+06	-0.96020789E+05	-0.80049737E+03	0.00000000E+00
1	0.	0.06240	-0.10797466E+06	-0.95758684E+05	-0.10629228E+04	0.00000000E+00
1	0.	0.07800	-0.10797479E+06	-0.95498832E+05	-0.13231855E+04	0.00000000E+00
1	0.	0.09360	-0.10797496E+06	-0.95241205E+05	-0.15813094E+04	0.00000000E+00
1	0.	0.10920	-0 10797515E+06	-0.94985781E+05	-0.18373181E+04	0.00000000E+00
1	0.	0.12480	-0.10797537E+06	-0.94732534E+05	-0.20912349E+04	0.00000000E+00
1	0.	0.14040	-0.10797562E+06	-0.94481439E+05	-0.23430829E+04	0.00000000E+00
2	0.	0.14040	0.16209334E+05	0.16887613E+05	-0.23430829E+04	0.00000000E+00
2	0.	0.23591	0.16207733E+05	0.16570403E+05	-0.20304479E+04	0.00000000E+00
2	0.	0.33142	0.16206377E+05	0.16268968E+05	-0.17328856E+04	0.00000000E+00
2	0.	0.42693	0.16205250E+05	0.15982296E+05	-0.14494360E+04	0.00000000E+00
2	0.	0.52245	0.16204333E+05	0.15709455E+05	-0.11792142E+04	0.00000000E+00
2	0.	0.61796	0.16203612E+05	0.15449584E+05	-0.92140360E+03	0.00000000E+00
2	0.	0.71347	0.16203072E+05	0.15201888E+05	-0.67524972E+03	0.00000000E+00
2	0.	0.80898	0.16202701E+05	0.14965632E+05	-0.44005441E+03	0.00000000E+00
2	0.	0.90449	0.16202486E+05	0.14740135E+05	-0.21517105E+03	0.00000000E+00
2	0.	1.00000	0.16202417E+05	0.14524766E+05	0.27284841E-11	0.00000000E+00

STRESS RESULTANTS

NX	NO	NXO
0.85579365E-12	0.18894042E-10	0.00000000E+00
0.87468913E+03	0.80055574E+03	0.00000000E+00
MX	MO	MXO

0.,

Appendix E: Application of Strain Gages to an Aluminum Mandrel

The surface of the mandrel was prepared by sanding. Removal of the various sets of fresh scratches was time-consuming due to the softness of the metal. Sequential use of three grades of sand paper was necessary to achieve the desired surface finish. After sanding, the surface was wiped clean and guide lines were made using a ruler and a set square. Chlorothene SM was used to degrease the surface. Subsequently, metal A conditioner (an acidic cleaning agent) and Kleenex were used to clean the surface three times, after which the gage zone was neutralized (using an ammonia-based solution). Care was exercised in using the various chemicals, as a residue would cause poor adhesion of the strain gages. All of the supplies used were Intertechnology products.

Following surface preparation, the strain gages were carefully removed from their packaging using tweezers cleaned with neutralizer. A 4-inch long piece of thick adhesive tape placed over each gage aided in positioning the gage on the mandrel. After peeling the tape back on itself, catalyst was applied to the gage zone and left for one minute. Next, a drop of adhesive was applied and the tape was smoothed back, held under one finger for about a minute, and then peeled straight back over itself, leaving the gage in place.

In Experiment 1, 2 wires were soldered onto each gage. In subsequent experiments, 3 wires were applied per gage in the hope of minimizing spurious temperature effects. All lead wires for a given gage were of equal length. The end of each wire was stripped, an expansion hoop was formed, and the wire was tinned so as to give the strand additional physical strength. The tinned ends of the wires were soldered to the copper solder tabs on the strain gages. After using rosin solvent to clean flux from the gage area, an ohm meter was employed to check that the strain gage was electrically isolated from the mandrel. A resistance reading above 100 kΩ indicated sufficient isolation.

Due to the small diameter of the aluminum tube and the need to apply gages at the center of the tube on the inside surface, the various steps proved rather delicate. Careful measurement was required to align the gages accurately in the axial and hoop directions. As well, good soldering technique was imperative for successful application of the gages.

The lead wires were positioned in place and held with adhesive cured using an aerosol catalyst. Two applications of M coat A protective coating were used to cover the strain gages and the wires in the vicinity of the gages. Next, the lead wires were twisted together and labeled. The free ends were stripped, twisted together, and tinned. Finally, a multimeter was used to test the resistance of the gages against the manufacturer's specifications. Due to

contributions from the lead wires, the measured resistance tends to be slightly above the specified value.

Appendix F: Strain Calculations

Strain signals from the amplifier-conditioner unit were in millivolts. To convert these signals to strains, several steps were required, as outlined below.

1. For each voltage reading, the uncorrected strain was calculated as follows:

$$\epsilon_u = \frac{-4\Delta E_o/E_i}{K(T)(1+2\Delta E_o/E_i)} \quad \text{.....F.1}$$

ϵ_u = uncorrected strain

ΔE_o = voltage signal divided by amplifier gain

E_i = bridge voltage

$K(T)$ = gage factor at the test temperature

$$K(T) = K_o(1+\Delta K/100) \quad \text{.....F.2}$$

K_o = gage factor at 75°F (24°C)

$\Delta K(T)$ = gage factor correction, in %

$$\Delta K(T) = 0.02153(T-24)\ \%\ (T \text{ in } °C) \quad \text{.....F.3}$$

2. The uncorrected strain was corrected for temperature effects as follows:

$$\epsilon_t = \epsilon_u - \epsilon_{app}(T) \quad \text{.....F.4}$$

ϵ_t = strain corrected for temperature effects

$\epsilon_{app}(T)$ = the apparent strain at temperature T

Some data for Experiments 1 to 5 in Section 3.3 is provided in Table F.1, below.

Table F.1

Some Gage and Instrument Parameters

Exp't	E_i (volts)	K	Gain
1	2.80	2.13	-500
2	2.80	2.10	-500
3	2.90	2.10	-2100
4	3.25	2.10	-2100
5	3.25	2.10	-2100

For the CEA-13-125WT-350 (lot RM-A41AF20) gages used in Experiment 1, the formula for the apparent strain is as follows. Temperature is in °C.

$$\epsilon_{app} = -51.8+3.78T-0.073T^2+(4.18 \times 10^{-4})T^3-(4.99 \times 10^{-7})T^4$$

For the CEA-13-062UT-350 (lot R-A41BF13) gages used in Experiments 2 through 5, the formula for the apparent strain is as follows. Temperature is in °C.

$$\epsilon_{app} = -61.4+4.33T-0.0836T^2+(4.31 \times 10^{-4})T^3-(4.87 \times 10^{-7})T^4$$

Appendix G: Burn-off Tests and Resin Density Measurements

The required formulae and data needed to calculate the density of the resin within the composite tubes and also in the all-resin tubes produced is outlined first. The raw data is tabulated in Table G.1, following. As in the Archimedean density tests, which were performed in order to ascertain the amount of curing volume shrinkage, the technique of finding apparent masses was employed in taking the present resin density measurements. A Sartorius 2003 MP1 electronic balance was used. Composite samples were obtained by slicing rings from the composite tube using a band saw and then by dividing the rings into small pieces using a hack saw. Pure resin samples of an appropriate size were chosen from among the fragments which resulted due to the extensive cure cracks.

Firstly, the temperature of the water bath was measured and the water density determined. For samples 2-1 to 2-4, T_{water} = 23°C and ρ_{water} = 0.997538 g/cm^3 while for the remaining samples, T_{water} = 22°C and ρ_{water} = 0.99770 g/cm^3. The samples and the copper wire (ρ = 8.93 g/cm^3) used to suspend the samples in the water bath were weighed in air and then the sample plus wire was weighed in water. Several trials of each mass measurement were performed. The average values appear in Table G.1. Using the above mass measurements, the density of the composite plus wire (or, for samples from Experiments 3 to 5, the resin plus wire)

was determined using equation G.1.

$$\rho_{c+w} = \frac{\rho_{water}}{1 - (m_a/m)_{c+w}} \quad \text{.....G.1}$$

(c=composite, w=wire, r=resin, g=glass, m=mass, and a=apparent in formulae G.1 to G.4.) The density of the composite (or pure resin) without the wire was determined from equation G.2.

$$\rho_c = \frac{m_c}{m_{c+w}/\rho_{c+w} - m_w/\rho_w} \quad \text{.....G.2}$$

The next step involved burning off the resin from the composite samples. This was accomplished by holding the samples in a ventilated furnace at 600°C (1100°F) for several hours. The glass fibers remaining after this heat treatment were weighed in air and then the density of the resin within the composite could be determined from equation G.3.

$$\rho_r = (m_c - m_g) / (m_c/\rho_c - m_g/\rho_g) \quad \text{.....G.3}$$

The mass fraction of reinforcement in the composite samples was calculated by dividing the mass of the glass by that of the composite sample and the volume fraction of reinforcement was calculated using equation G.4.

$$V_f = m_g\rho_c / m_c\rho_g \quad \text{.....G.4}$$

Table G.1

Resin Density Measurement Data

#	mass (g) c	mass (g) w	mass (g) c + w	ρ (g/cm^3) c + w	mass (g) g + w	ρ (g/cm^3) c	ρ (g/cm^3) r	% g	V_f
1-1	8.5911	0.0333	4.3451	2.011	6.1745	2.005	1.267	71.5	54.9
1-2	8.8525	0.0334	4.4615	2.004	6.3508	1.998	1.261	71.4	54.6
1-3	8.2188	0.0334	4.1814	2.023	5.9654	2.016	1.268	72.2	55.8
1-4	8.2271	0.0337	4.1508	2.005	5.9155	1.999	1.259	71.5	54.8
2-1	7.8843	0.0312	3.8131	1.925	5.4237	1.919	1.220	68.4	50.3
2-2	8.1367	0.0381	4.0072	1.957	5.6446	1.950	1.250	68.9	51.5
2-3	8.5048	0.0424	4.1699	1.948	5.8909	1.940	1.239	68.8	51.1
2-4	13.5760	0.0338	6.5962	1.936	9.2680	1.932	1.244	68.0	50.3
3-1	10.2744	0.0604	1.8680	1.218			1.212		
3-2	20.3254	0.0425	3.6033	1.212			1.210		
4-1	32.5483	0.0755	5.7500	1.210			1.208		
4-2	32.5510	0.0755	5.8110	1.214			1.212		
4-3	32.4441	0.0437	5.7625	1.213			1.211		
5-1	6.3557	0.0475	1.1670	1.220			1.212		
5-2	12.9059	0.0433	2.3123	1.215			1.211		
5-3	5.4474	0.0346	1.0015	1.221			1.214		

Appendix H: The Technique of Impulse Viscoelasticity for Characterizing Mechanical Properties and Time-Dependent Curing Behavior of Thermosetting Polymers

Vratsanos and Farris (1986) used the technique of impulse viscoelasticity to monitor changes in the mechanical properties of DEGBA epoxy resin during curing. A rubber membrane held, between trials, at a constant strain was used to contain the resin. Each trial involved applying a box-strain deformation to the system. During a curing cycle, 100 to 150 such trials were performed, and the way in which the system recovered from the applied deformation allowed Vratsanos and Farris to establish such properties as the gel point, the equilibrium tensile modulus, and the residual stress state of the epoxy. The basic assumptions used in obtaining this data include incrementally linear elastic behavior, material isotropy, time dependent elastic moduli, and short impulse duration compared with the time scale of the "aging process" of curing.

Vratsanos and Farris suggest that the technique of impulse viscoelasticity could be used to find optimum cure cycles for thermosetting resins. The parameters they perturbed were the cure temperature and the ratio of hardener (a polyamide curing agent) to epoxy. An important observation from their work is that gelation occurring prior attainment of the isothermal cure temperature leads to sigmoidal tensile modulus versus time curves. The modulus

curve presented in Figure 9 is modelled after this result. Gelation prior to the cure temperature was also found to lead to significant thermal curing stresses. Samples which gelled subsequent to reaching their cure temperature showed much smaller residual stresses and irregular (but monotonically increasing) modulus versus time curves. impulse viscoelasticity to monitor changes in the mechanical properties of DEGBA epoxy resin during curing. A rubber membrane held, between trials, at a constant strain was used to contain the resin. Each trial involved applying a box-strain deformation to the system. During a curing cycle, 100 to 150 such trials were performed, and the way in which the system recovered from the applied deformation allowed Vratsanos and Farris to establish such properties as the gel point, the equilibrium tensile modulus, and the residual stress state of the epoxy. The basic assumptions used in obtaining this data include incrementally linear elastic behavior, material isotropy, time dependent elastic moduli, and short impulse duration compared with the time scale of the "aging process" of curing.

Vratsanos and Farris suggest that the technique of impulse viscoelasticity could be used to find optimum cure cycles for thermosetting resins. The parameters they perturbed were the cure temperature and the ratio of hardener (a polyamide curing agent) to epoxy. An important observation from their work is that gelation occurring prior attainment of the isothermal cure temperature leads to

sigmoidal tensile modulus versus time curves. The modulus curve presented in Figure 9.c is modelled after this result. Gelation prior to the cure temperature was also found to lead to significant thermal curing stresses. Samples which gelled subsequent to reaching their cure temperature showed much smaller residual stresses and irregular (but monotonically increasing) modulus versus time curves.

Appendix I: Material Properties

E glass

ν.....0.25	0.25
E.....72 GPa	1.05×10^7 psi
G.....28.8 GPa	4.2×10^6 psi
ρ.....2,600 kg/m^3	0.09432 lb/in^3
α.....5 x 10^{-6} /K	2.8 x 10^{-6} /°F

Vibrin 1029

ν.....0.35	0.35
E.....3.4 GPa	5×10^5 psi
G.....1.26 GPa	1.85×10^5 psi
ρ.....1,200 kg/m^3	0.0432 lb/in^3
α.....63 x 10^{-6} /K	35 x 10^{-6} /°F

Aluminum

ν.....0.33	0.33
E.....67 GPa	9.8×10^6 psi
G.....25.2 GPa	3.6[illegible] 10^6 psi
ρ.....2,700 kg/m^3	0.098 lb/in^3
α.....23 x 10^{-6} /K	13 x 10^{-6} /°F

Vibrin/Glass Unidirectional Lamina (50 v/o glass)

(From program INPUT; for use in programs CYLAN and ELAS2*)

E_1.....5.5 x 10^6 psi

E_2.....1.13 x 10^6 psi

E_3.....1.13 x 10^6 psi

G_{12}.....0.498 x 10^6 psi

ν_{12}.....0.300

ν_{23}.....0.444

α_1.....4.26 x 10^{-6} /°F

α_2.....24.1 x 10^{-6} /°F

f_1.....1.59 x 10^{-6} /°F

f_2.....23.2 x 10^{-6} /°F

* In program ELAS2, some terms within the analysis contain the difference (E_3 - E_2) in the denominator. Thus, the authors of the program have suggested that, in cases where these properties take on the same value, E_3 should be set equal to $0.9*E_2$.